STUDIES ON ADVANCED MEANS OF BIOMASS TORREFACTION

by

Daya Ram Nhuchhen

Submitted in partial fulfilment of the requirements

for the degree of Doctor of Philosophy

at

Dalhousie University

Halifax, Nova Scotia

April 2016

To My

Parents: Krishna Bahadur Nhuchhen and Punya Swori Nhuchhen

And

All loved ones

Table of Contents

LIST OF TABLES

LIST OF FIGURES

ABSTRACT

Biomass is a carbon neutral primary energy source that could be used as a sustainable energy resource in solid, liquid, and gaseous forms. Despite all its potential benefits, because of several shortcomings, biomass faces some challenges in its wide scale use in energy conversion systems. Torrefaction process can help biomass to overcome its limitations to a great extent. This is a mild roasting process that produces an upgraded biomass fuel, improving the technical viability of biomass use for co-firing with coal in power plants. This thesis examines two new novel techniques of torrefaction using (i) pressurized batch reactor and (ii) continuous rotary reactor. These techniques could eliminate the need for expensive nitrogen gas for torrefaction while producing more uniform and better quality products.

The first part of this work investigated a mild pressure torrefaction in air and nitrogen medium. The energy density enhancement factor of its torrefaction products was 1.42 in air medium while it was only 1.34 in N_2. Minimum solid mass yield was 49% in pressurized air torrefaction while it was 56% in N_2. Torrefaction in this reactor also gave higher fuel ratio, similar energy yield, but a reduced mass yield compared to those in pressurized N_2. This confirms that N_2 can indeed be eliminated in the mild pressure reactor.

The second part of the work studied continuous two-stage torrefaction in an indirectly heated inclined rotary torrefier (TIR). This reactor was studied in details examining a) solids motion in TIR reactor, b) heat transfer from wall to solids in TIR reactor, and c) torrefaction of wood chips in TIR torrefier.

A cascaded motion of solid was deployed to study the kinematics of solids in inclined rotating reactor to develop a semi-empirical model for mean residence time. The model was validated against experimental data and those from published literature. Another expression for filling factor was also derived and validated with experimental data.

A mechanistic model for predicting overall heat transfer coefficient in the externally heated TIR reactor was developed, and then verified experimentally. The model for effective wall to solids contact heat transfer was validated against published data.

To study the torrefaction capability of TIR torrefier, yellow poplar wood was torrefied in volatile gas medium. Energy density in products is comparatively low, but it gives higher mass yield. Thus this new torrefier retains greater part of the energy in the raw biomass while replacing nitrogen with its own volatile. This reactor also resulted in up to 26% improvement in energy yield over that from fixed bed reactor, and this improvement depended on torrefaction temperature and time.

LIST OF ABBREVIATIONS AND SYMBOLS USED

Notations

A_{cs}	Cross sectional area of solid in reactor, m^2
A_{csr}	Inner cross sectional area of reactor, m^2
A_{lsr}	Lateral surface area of the reactor, m^2
C_{pbs}	Specific heat capacity of brass particle, J/kgK
C_{pC}	Specific heat capacity of collector, J/kgK
C_{pw}	Specific heat capacity of water, J/kgK
BFR	Biomass flow rate, kg/min
d	Particle diameter, m
d_p	Effective particle diameter, m
D	Inner diameter of reactor, m
e_{bs}	Voidage factor of bulk brass particle
E_{eff}	Effective properties of solid
E_s	Thermal properties of solid
E_f	Thermal properties of gas
F	Solid flow rate per unit area of cross-section, kg/hr m^2
F_c	Centrifugal force, N
F_f	Filling factor, %
F_{ff}	Fraction of volume of the solid to volume of the reactor
$F_{ff,\ designated}$	Designated solid filling fraction
F_g	Gravity force, N
$F_{net,1}$	Net outward force on the particle, N
F_r	Froude number
g	Acceleration due to gravity, m/s^2
G	Gas flow rate per unit area of cross-section, kg/hr m^2
h_b	Bed height within the reactor, m
h_h	Horizontal distance, m
h_{hhc}	Critical horizontal distance, m
h_v	Vertical falling height, m
h_{ewb}	Effective wall to solid bed heat transfer coefficient, W/m^2K
h_o	Overall heat transfer coefficient of reactor, W/m^2K
h_{sb}	Heat transfer coefficient from solid surface to bed, W/m^2K
h_{wf}	Wall to gas heat transfer, W/m^2K
h_{ws}	Heat transfer coefficient from wall to solid surface, W/m^2K

I	Moment of inertial of spherical particle, kg m^2
k_{bs}	Thermal conductivity of solid (brass), W/mK
K_{ccFf}	Dimensional correction constant for filling factor
K_{ccRt}	Dimensional correction constant for mean residence time
k_f	Thermal conductivity of gas, W/mK
L_f	Width of flight, m
$LMTD$	Log mean temperature difference, °C
m	Mass of an ideal spherical particle, kg
m_b	Mass of collected brass particles in the container, kg
m_c	Mass of the container, kg
m_c	Mass of water in the container, kg
N	Angular speed of reactor, RPM
Pe	Peclet number
Pr_f	Prandtl Number of gas
Ra_D	Rayleigh Number
R_t	Mean residence time, min
t_c	Average solid contact time with hot surface per cascaded cycle, s
t_{cas}	Cascaded time per cycle, s
t_{cft}	Critical falling time, s
t_{cr}	Total critical time, s
T_e	Equilibrium temperature of fluid in the solid collector, °C
T_{ex}	Temperature of solid at exit of reactor, °C
t_f	Falling time, s
T_f	Mean temperature of fluid inside the reactor, °C
T_{fc}	Final temperature of collector, °C
T_{ic}	Initial temperature of collector, °C
T_{iw}	Initial temperature of water in the collector, °C
t_r	Rolling time, s
t_u	Uplifting time, s
T_w	Reactor wall temperature, °C
V_s	Volume of solid inside the reactor, m^3
V_{csr}	Effective volume of the reactor, m^3
$v_{s,h}$	Horizontal velocity, m/s
$v_{s,v}$	Vertical velocity component, m/s
y_s	Virtual solid bed height in the reactor at stationary condition, m

Symbols

α_f	Thermal diffusivity of gas, m^2/s

β	Inclination of the reactor, degree
δ	Angle of repose of material in dry condition, degree
δ	Fraction of area covered by solid on area of reactor stationary condition
δ_d	Average fraction of area covered by solid on area of reactor
γ	Angle subtended by bed at the center of the reactor, degree
$\mathcal{L}$	Reactor effective length, m
υ_f	Kinematic viscosity of gas at mean temperature of gas, m^2/s
μ_k	Rolling frictional coefficient
$\mu_{\theta s}$	Static frictional coefficient
Ω	Angle between flight and inclined solid bed surface, degree
ω	Angular speed of reactor, rad/s
$\emptyset$	Angular displacement of flight between the flight positions 1-1', degree
ϕ_s	Solid half-filling angle at stationary condition, degree
ρ_{bs}	Bulk density of solid, kg/m^3
ψ	Dimensionless virtual thickness of gas film
σ_r	Square root of the dimensionless relative variance
θ	Angular displacement of flight between the flight positions 1'-1''', degree
θ_1	Angle of inclination of flight just before completing cascaded cycle, degree
θ_2	Angle subtended by solid at flight to center at the end of cascaded cycle, degree
θ_{crf}	Critical angle defining flight location, degree
θ_{crp}	Critical angle defining particle location, degree
θ_d	Total angular displacement, degree
θ_f	Total angular displacement before particle take off the flight, degree
θ_{Pi}	Angle defining particle location at reactor surface, degree

ACKNOWLEDGEMENTS

I would like to express my deep gratitude and sincere thanks to my supervisor Dr. Prabir Basu for his invaluable role in my study. His constructive criticisms, guidance, and encouragement towards the completion of this thesis are always of my memory. The author would like to thank to the member of supervisory committee: Dr. Abdel E. Ghaly and Dr. Jiunn-Ming Chuang. Their constructive comments and valuable suggestions are always helpful to improve the quality of this thesis. Author would also like to extend his thanks to Dr. Dominic Groulx and Dr. Lukas Swan for accepting to be in the examining committee and for their suggestions. And, I would like to appreciate to Dr. Farid Chejne Jana of National University of Colombia who accepted to be an external examiner.

I would like to acknowledge to other staffs of Mechanical Engineering: Peter Jones, Jonathan MacDonald, and Mark MacDonald for their technical supports, and Ms. Selina Cajolais and Ms. Donna Laffin for administrative supports. I would also like to thank all to our research team member Dr. Bishnu Acharya for his technical supports in developing the experimental setup. And, my sincere thanks to Mr. Doug Armsworthy for his technical supports related to the experimental setup, and to Daniel Chevalier and Gerald Fraser from the Mineral Engineering Center for their supports.

My sincere thanks also goes to the National Science and Engineering Research Council (NSERC), Faculty of Graduate studies, and Faculty of Engineering (Bruce and Dorothy Rosetti Engineering Scholarships), for providing financial supports toward completing my study at Dalhousie University.

The author is very much grateful to Mrs. Rama Basu, for her parental care during my study at Dalhousie University. Finally, the author proudly acknowledges the continuous patience and encouragement of his beloved parents: Krishna Bahadur Nhuchhen and Punya Swori Nhuchhen, his caring wife Ms. Sarita Sibanjar, and all the loved ones in Nepal, who were always with me whenever I needed.

CHAPTER 1: INTRODUCTION

This chapter describes the background of this study, and presents objectives, scopes, and limitations of this thesis.

1.1. BACKGROUND

Fossil fuels have a dominant share of the global energy production market, contributing more than 80% of the total primary energy supply in 2012 (IEA, 2014). The carbon dioxide emissions (CO_2) have been doubled in 2012 compared to that in 1973. Global warming and climate change are two major consequences of the anthropogenic CO_2 emissions. Coal combustion is recognized as the main source of the anthropogenic carbon emission. Biomass being carbon neutral could replace coal in existing power plants to provide energy while reducing carbon emissions at affordable cost. Most importantly this technology is available right now. However, owing to large difference in chemical and physical properties between biomass and coal it is not possible to replace any more that 2-10% of coal with biomass. It has been shown in the Chapter 2 that torrefaction process could raise this share to about 50-60%. Thus, much interest has shown in this new option of biomass pretreatment.

Due to numerous benefits of the torrefaction process, different organizations, mainly from Europe and North American regions are extensively working on research and development of commercial torrefaction units and checking the technical and economical viability of overall systems. For instance, Topell Company from Netherland is using a multi-stage fixed bed reactor based torrefaction in which they burnt torgas – volatile gases from the torrefaction process – in a combustor to supply partial heat required for the process. They produce black pellets that can be co-fired up to 25% of one coal mill (Topell, 2014). Diacarbon Energy Incorporated in Canada is also working on biocoal production technology. They primarily work for replacing coal by biocoal and using biochar to mitigate energy related emissions. They developed a fully automated

technique of capacity 25,000 tons per year, which can avoid approximately 52,500 tons of CO_2 equivalent emissions (BCBN, 2014). Energy research Center for the Netherland (ECN) established BO2 technique – a moving bed reactor with direct heating – to test the torrefaction process. This technique includes three distinct processes: drying; torrefaction; and pelletization. They started their pilot test in 2008 and are able to produce 1-10 tons per hour (Kiel, 2011). More details of different organizations that are working on torrefaction technologies are reported in Nhuchhen et al. (2014) and explained in Chapter 2.

The present work aims to improve methods of torrefaction of biomass.

1.2. PROBLEM STATEMENT

Torrefaction, a pretreatment process, makes carbon neutral biomass to behave more like coal. So this process, which could increase share of biomass in co-firing power plants, could make important contribution in reducing greenhouse gas from coal-fired plants. This research focuses mainly on the technical issues of the torrefaction process and does not deal with the economic aspect of the process. A number of other studies (Batidzirai et al., 2013; Shah et al., 2011; Svanberg et al., 2013) showed economic aspect of the process.

Torrefaction has been in extensive use for roasting of coffee. Biomass torrefaction has one important difference from coffee roasting that the former requires inert atmosphere to maximize the carbon content of the product. This process is usually conducted at temperatures slightly above that for drying, and that below pyrolysis. So, torrefaction is often carried out in reactors used for drying or pyrolysis. Reactors for torrefaction include rotary drum, fluidized bed, moving bed, screw conveyor, microwave, and multiple hearth furnace (Acharya et al., 2012). Most of them except the microwave technology are technically proven, but they are still in the process of development.

One of the major operational difficulties of currently available torrefaction processes is provision of maintaining inert environment. Air infiltration, which is common in the fixed bed torrefiers, has the potential to add oxygen to the torrefaction medium that not only reduces the product quality, but also increases the risk of fire (Basu et al., 2013). The supply of the nitrogen as done in laboratory scale works can avoid that, but that is not economic in an industrial scale, as the cost of nitrogen will add to the total cost of torrefaction. To avoid this, flue gas that comprises significant amount of free nitrogen from the air could be used to replace pure nitrogen (Saadon et al., 2014). The flue gas is, therefore, used an alternative medium for some commercial torrefaction units. However, flue gas also includes other gases like oxygen, carbon dioxide, and steam, which may reduce the quality of torrefied biomass.

Some investigations of torrefaction process using carbon dioxide as a working medium have already been done; and its effect on torrefied products is known (Thanapal et al., 2014; Saadon et al., 2014). Steam is deployed in some biomass pretreatment processes – Steam Explosion – to hydrolyze hemicellulose, to depolymerize cellulose, and to soften and then depolymerize the lignin content of biomass (Iroba et al., 2014), but it is not conducive to production of torrefied biomass. Some studies (Lipinsky et al., 2002; Tooyserkani et al., 2013; Zakri et al., 2013) also used steam to torrefy biomass. Oxygen could easily ignite biomass at torrefaction temperature that is generally above the ignition temperature of most biomass. So presence of oxygen is undesirable anywhere in the torrefaction plant. Several studies investigated the influence of oxygen's presence on torrefied products (Basu et al., 2013; Rousset et al., 2012; Saadon et al., 2014; Uemura et al., 2011; Uemura et al., 2013; Wang et al., 2013). These researches found that the low oxygen concentration in the working media does not lead to ignition and it does not have any significant effect on either mass or energy yields at low temperature torrefaction (< 250°C) (Uemura et al., 2015). Rousset et al. (2012) have also reported that the presence of 6% oxygen in working media does not affect the torrefied product to a significant extent even when torrefaction is done at 280°C. But, the presence of oxygen greater than 6% in working medium may severely affect the operation of the system due the ignition of biomass fines. This effect is more severe in the fixed bed torrefiers because of their

poor particle mixing characteristics and non-uniform temperature distribution. The severity may further increase while a range of different particle sizes (from small to large) are to be torrefied. This problem could be avoided by preventing possible formation of hot spot or deposition of biomass fines at one specific location. The indirect heating method that avoids direct contact between hot flue gas and biomass fines could also reduce this problem.

Considering above discussions, one can list out some of the shortcomings of current designs of torrefiers as:

1. Difficulty in utilization of volatiles for providing energy for drying and torrefaction.
2. Non-uniform quality of torrefied products due to poor mixing of biomass in the fixed bed reactor.
3. Requirement of expensive nitrogen gas to provide inert ambience in the torrefier.
4. Inefficient transfer of heat from reactor wall to the biomass for indirectly heated torrefier or dryer.
5. Hotter biomass near the heated wall and cooler biomass in the interior resulting in a mixture of over torrefied and under torrefied or even raw biomass in the final product.

To address above issues, an innovative modified design of the torrefier is needed. Present work studies in two such designs.

Torrefaction involves two stages: drying and release of volatiles from the biomass. The steam released from the moist biomass dilutes the volatiles released from it during torrefaction, and thereby reduces its energy density of the gaseous volatile product. So, the utilization of the volatiles to provide the heat for torrefaction or drying becomes difficult. Most conventional torrefier are single stage design that uses single reactor for both drying and torrefaction. Above problem is naturally unavoidable in single stage

reactors, as the moisture released from the biomass during drying has to pass through the torrefied products along with the volatiles. This gave rise to shortcoming (1). This study proposes to use the multi-stage torrefaction that could separate the drying and devolatilization stages of the torrefaction. By conducting drying and torrefaction in two separate reactors, it would be feasible to get moisture free volatiles from later stage.

Many conventional torrefiers use moving bed reactor, which is characterized by rather poor mixing of biomass. To address the poor solid mixing limitation (2), this study also proposes to use rotary drum reactors (discussed more in Chapter 4). As rotary drum reactors have a high degree of particle mixing. Such mixing will provide uniform drying in drying section and avoid any formation of hot heat spots in the torrefaction section. One can further enhance particle mixing by using flights (lifters) along the inner wall of the reactors. Flights not only facilitate uniform heating and devolatilization reactions, but also enhance its loading capacity. As the operation of the rotary reactor system is limited to a solid filling factor up to 16%, one can expect more than 80% of the space filled with volatile gases during torrefaction when the reactor is heated externally without requiring a supply of any flue gas or inert gas. This will, thus, help in rationalizing the use of hot volatiles.

Nitrogen could very efficiently provide inert environment during torrefaction that offers good mass yield and at the same time avoid the risk of fire, but that brings in the shortcoming (3). To address this, this study proposes to use the gaseous products of torrefaction as a working medium instead of nitrogen. Since the major gaseous compositions in the gaseous products are steam and CO_2 (Stelte, 2012; Bates and Ghoniem, 2012), they may act as inert medium replacing nitrogen.

Rotary drum provides excellent contact between tumbling solids and the walls of the drum. This facilitates excellent heat transfer between the outer wall of the torrefied heated by external means and biomass tumbling inside. It would, thus, address the shortcoming (4).

Biomass being poor thermal conductor does not allows good conduction of heat from outer layer to inner layer of solids in the torrefier. This resulted in limitation (5). The large-scale mixing of solids in tumbling rotary reactor facilitated by flights in the present design easily overcomes the shortcomings of the conventional design.

In the proposed two-stage configuration of the torrefier there may have a small oxygen concentration in the working medium of the torrefaction, but that does not show significant effect on the torrefied biomass (Basu et al., 2013). In fact, the use of air as a working medium in an innovative way could be another means to avoid nitrogen or flue gas. To do that, we additionally developed a simpler batch reactor for torrefaction. It uses an externally heated mildly pressurized batch reactor. No additional equipment is needed for maintaining the high-pressure system unlike in the wet torrefaction.

The pressurized batch reactor comprises of biomass and mildly pressurized air. This does not require a high-pressure (<1 MPa). Pressure that builds up during torrefaction due to thermal expansion of gas and air in the reactor can be maintained by using pressure relief valve. Though air has an initial oxygen concentration of 21% by volume, it will gradually decrease due to release of steam and volatile gases from the biomass during heating inside the reactor. This entirely avoids nitrogen and utilizes the volatiles released during the process.

This study, thus, develops and investigates into the operational characteristics of two indirectly heated torrefaction reactors that could address many limitations of current designs. The first one is a mildly pressurized batch torrefier and the second one is an indirectly heated two-stage continuous rotary torrefier.

1.3. RESEARCH OBJECTIVES

This study contributes mainly to the development of indirectly heated torrefaction reactors and to the qualitative and quantitative characterization of the torrefied product

from such reactors. First part of the work involved a mildly pressurized batch reactor where experiments were conducted using air and nitrogen media and the product qualities were then compared. The second part involved a comprehensive assessment of a two-stage continuous indirectly heated rotary torrefier.

This research started with a comprehensive study of the current state of the art of torrefaction to identify knowledge or technology gaps. Based on that the work started to develop improved options for torrefaction with specific objectives as listed below:

i. To develop a deeper understanding of the biomass torrefaction process through a comprehensive review of the state of the art.
ii. To design and build an indirectly heated mildly pressurized batch reactor, which is different from the conventional high-pressure hydrothermal/wet torrefiers and to study the torrefaction of biomass in air and or nitrogen.
iii. To design and build an indirectly heated a two-stage continuous rotary reactor and to study the kinematics of particle motion in an inclined rotatory reactor.
iv. To examine the overall heat transfer coefficient of rotary reactor using cluster renewal model.
v. To study the effect of different design and operating parameters on the quality of torrefied biomass produced in the two-stage continuous rotary torrefaction system built in this work.

1.4. SCOPE AND LIMITATIONS

This research is carried out to advance the current torrefaction technologies. It investigates into two new techniques that overcome some of the limitations of currently available designs of torrefier.

Though torrefaction improves the thermochemical characteristics of biomass making it work more like coal, one could still argue about the net energy balance of the system. As

the torrefaction process is a thermal treatment process, it requires thermal energy to achieve an upgraded energy dense solid product. Only a preliminary work on the energy balance of the two-stage continuous indirectly heated rotary torrefier is conducted.

The specific scopes and limitations of individual objectives are explained below:

Task 1: This work provides a comprehensive review of biomass properties and its torrefaction. Published research papers were reviewed and different observations were presented to give an overall insight into the torrefaction process and its effects on biomass. This work, however, does not include the kinetics and modeling of torrefaction process. Another colleague in the Circulating Fluidized Bed (CFB) laboratory will develop a complete thermodynamic model later. In addition to this, only few works were published relating to energy return on investment and life cycle analysis of the torrefaction process at the time of this study, so they are not incorporated in this work.

Task 2: A laboratory scale batch type pressurized reactor (discussed more in Chapter 3) was developed and built to investigate into the mildly pressurized torrefaction process in nitrogen and air media. The test was also extended to atmospheric pressure condition and then the characteristics of solid products were compared with that obtained in the mildly pressurized reactor. It should be noted that this work avoids torrefaction in high-pressure water as practiced in the hydrothermal torrefaction process. This test used a bubbling bed heater to maintain the desired temperature inside the reactor. A single large sample was kept inside the reactor with the help of thermocouple, where it gets torrefied. As this study only aims to compare the solid products of torrefaction, this study excluded analysis of volatiles products released during the process.

Task 3: A laboratory scale two-stage continuous indirectly heated rotary torrefier with flights was developed and built. The cascaded motion of solids was studied to develop theoretical model of mean residence time of an ideal spherical particle. The model shows the effect of operating and geometrical parameters on the mean residence time of the

rotary reactor. Cold tests at a constant feed rate were conducted at different operating parameters to measure mean residence time and filling factor, which gave a correction factor for the above model. The model with the correction factor was used to estimate and validate the mean residence time of multi-particle flow system. Assuming plug flow of solid, a semi-empirical expression for filling factor was also established. The developed semi-empirical expression, however, does not account for axial distance covered by particle due to particle-particle interaction in multi-particle flow system.

Task 4: An expression for the effective wall to particle heat transfer coefficient was established using the concept of cluster renewal theory. It is then combined with the wall to gas heat transfer coefficient to estimate the overall heat transfer coefficient. An indirect method of finding the solid exit temperature from the rotary reactor was deployed using an insulated collector with known amount of water. While the model of effective wall to particle heat transfer coefficient was validated using the published experimental data, the model for the overall heat transfer coefficient was simulated and validated experimentally using brass particles. However, the developed expression is valid for a steady and plug flow of solid with negligible changes in solid bed height along the axial direction.

Task 5: A two-stage continuous indirectly heated rotary torrefier with flights was tested. Biomass was torrefied in an environment of the released volatiles alone. Steady temperature of the externally heated reactor was obtained before feeding the biomass sample, and then biomass was fed at a steady rate. Torrefied biomass was collected only after 120 minutes from initial feeding of the biomass. At steady state condition, the reactor is assumed to be full of volatiles gases and torrefaction occurs in the volatiles medium. Tests were carried out changing temperature, angular speed, and inclination of the torrefier. Additional experiments, keeping the same level of mean residence time, were also conducted in inert medium by supplying N_2 and then the characteristics of solid product obtained were compared with that from the fixed bed reactor. Overall energy balance of the system was calculated at selected conditions. System efficiencies

of the torrefaction process were determined. However, this work is limited to constant dryer operation conditions. Drying temperature, angular speed, and inclination of dryer was kept constant throughout this work.

1.5. CONTRIBUTION OF THIS DISSERTATION

This study laid foundation for the development of two new innovative torrefaction technologies, which could overcome the limitations of previously available torrefaction technologies. This thesis also provides a better understanding of torrefaction process where the volatile gas released serves as working media. Followings are some scientific contributions of this thesis:

- Mildly pressurized reactor could be a less expensive option for batch torrefaction
- Air could be used as working medium for the torrefaction in mildly pressurized reactor without degrading the product quality compared that produced in N_2 medium.
- Mild pressure does not affect the product quality irrespective of different operating temperature.
- In rotary reactor, consideration of the cascaded motion of particles could help developing semi-empirical models to predict mean residence time and filling factor in the flighted reactors of different geometry and operating conditions.
- A mechanistic model is developed for prediction of effective wall to particle heat transfer coefficient that has a good predictive power than the existing models.
- Torrefaction in rotary reactor can eliminate continuous supply of N_2 gas without any adverse effects on the quality of the torrefied product.

1.6. AUTHORSHIP OF PEER REVIEW PUBLICATIONS

Table 1.1**Table 1.1** presents the research outcomes that have been published after peer review and are under the process of peer review. Co-author's list as appeared in the journal shows that Nhuchhen is first author of all the listed publications.

Table 1.1: List of publications of this research

SN	Title	Author	Journal and Reference
1	A Comprehensive Review on Biomass Torrefaction	**Nhuchhen, D. R.,** Basu, P., and Acharya, B.	International Journal of Renewable Energy and Biofuel, 2014, 2014, 1-56.
2	Experimental Investigation of Mildly Pressurized Torrefaction in Air and Nitrogen	**Nhuchhen, D. R.** and Basu, P.	Energy and Fuels, 2014,28,3110-3121.
3	Investigation into Mean Residence Time and Filling Factor in Flighted Rotary Torrefier	**Nhuchhen, D. R.,** Basu, P., and Acharya, B.	Canadian Journal of Chemical Engineering, Accepted in November 2015
4	Investigation into the Overall Heat Transfer Coefficient in Indirectly Heated Rotary Torrefier	**Nhuchhen, D. R.,** Basu, P., and Acharya, B.	International Journal of Heat and Mass Transfer, Revision Submitted, March 2016
5	Torrefaction of Poplar in Continuous Two-stage Indirectly Heated Rotary Torrefier	**Nhuchhen, D. R**., Basu, P., and Acharya, B.	Energy and Fuels, 2016, 30(2), 1027-1038.

1.7. ORGANIZATION OF THESIS

The thesis comprises seven chapters whose relationship is shown in Figure 1.1. An outline of individual chapters is also provided below:

Chapter 1: This chapter provides an introduction to this study. It describes the motive of work and outlines its research objectives. Scope and limitations of the work are then explained for individual works. Finally, this chapter presents the list of publications that resulted from this work and summarizes the organization of the thesis.

Chapter 2: This chapter presents a broad review of the topic of biomass torrefaction. It discusses an overview of biomass and its shortcomings. It then presents an introduction of different modes of biomass pretreatment. A detailed discussion of dry torrefaction or simply called 'torrefaction' and its principles is presented in this chapter. Effects of different operating parameters of torrefaction on its product quality are also discussed. Changes in densification, gasification, and combustion properties due to torrefaction are reviewed and summarized. This section also provides the current status of torrefaction technologies developed in North American and Europe.

Chapter 3: This chapter examines batch torrefaction under low/mild pressure. It starts with an overview of the mild pressurized batch torrefaction process and its potential benefits. A small-scale mildly pressurized batch reactor is built to conduct experiments on torrefaction of biomass. Characteristics of solid product under air and nitrogen media at different pressures, temperatures, and residence times were studied and it also examined the effect of operating parameters.

Chapter 4: This chapter examines the cascaded motion of biomass in rotary reactor and provides experimental and theoretical results of mean residence time and filling factor in rotary reactors. This chapter deals mainly with the mean residence time and filling factor of rotary reactor. A cascaded motion of single particle model is developed for finding the

mean residence time. It is extended to use for multi-particle flow system with a correction factor. A steady plug flow motions of solid in the reactor was assumed to develop the semi-empirical expression for estimating the filling factor. Experiments in cold test rig were conducted at different operating conditions and measured mean residence time and filling factor in the dryer and torrefier. Effect of angular speed and inclination on the mean residence time and filling factor is then examined.

Chapter 5: This chapter presents a model for the overall heat transfer coefficient of an indirectly heated rotary reactor combining wall to particle and wall to gas heat transfer coefficients. Effective wall to particle heat transfer coefficient was developed using a simplified particle renewal approach. The reactor is assumed to be operated at steady plug flow mode at a constant solid feed rate and have uniform solid filling fraction throughout the reactor. The model for the effective wall to particle heat transfer coefficient is validated using the published experimental data. The model for the overall heat transfer coefficient is simulated and validated experimentally using brass particles. Effects of operating parameters on the overall heat transfer coefficient are also discussed.

Chapter 6: This chapter presents the experimental investigation of biomass torrefaction in a two-stage continuous indirectly heated rotary torrefier. A laboratory scale two-stage continuous rotary torrefier was developed and built. Experiments were conducted at different angular speeds, inclinations, and temperatures using volatiles as a working medium. Physical and chemical characteristics of solid products were examined to analyze the effect of operating parameters. Mass yields, energy density enhancement, and energy yields were also determined. Additional experiments using nitrogen as working medium were also conducted in the fixed bed and rotary reactors keeping same mean residence time. Overall process energy balance was then established to determine the system and net system efficiencies of torrefaction process at three operating temperatures.

Chapter 7: This chapter presents the overall conclusions from the present studies and recommendation for future works.

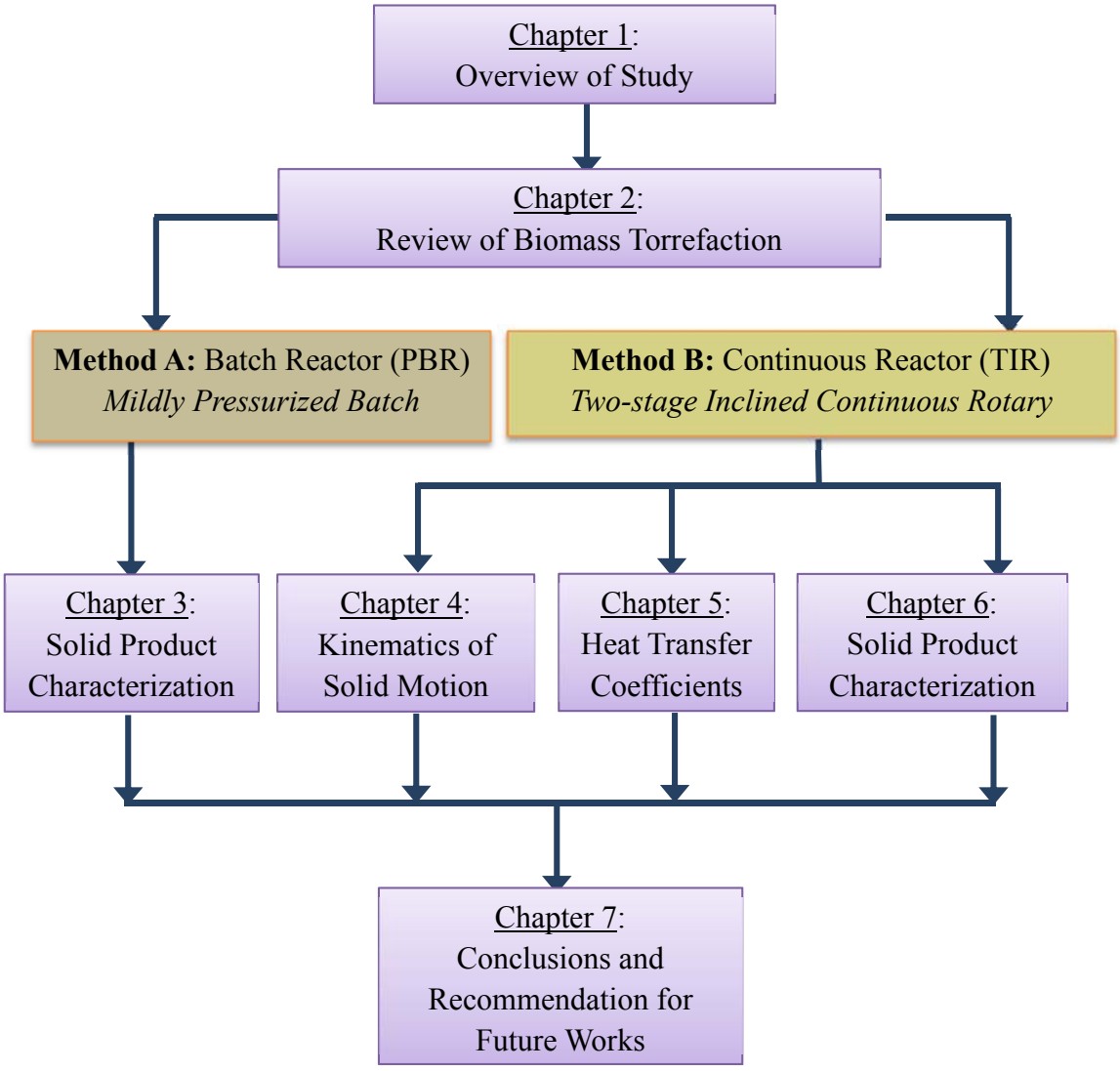

Figure 1.1: Summary of the study

CHAPTER 2: A COMPREHENSIVE REVIEW ON BIOMASS TORREFACTION*

Chapter 2 presents the background of this study by reviewing the present body of the knowledge of biomass torrefaction. As the present study concerns on the pretreatment of biomass using torrefaction process, it is important to understand the basics of biomass. So, this chapter starts out with a discussion on basics of biomass and follows that with its pretreatment methods. A review of biomass torrefaction is then presented to show the knowledge gap that the present study could fill in.

2.1. BACKGROUND

World primary energy demand, reported as 505 quadrillion BTU in 2008, is expected to increase by 53% in 2035 (IEO, 2011). Energy security and environmental sustainability are major emerging issues in the world that can only be addressed through diversification in energy resources and clean fuels. Promotion of indigenous renewable energy sources and low carbon fuels could be a win-win solution while addressing issues of the global warming and climate change. Kyoto Protocol, legally binding EU 20-20-20 targets, and volatility of oil prices have encouraged global community to reduce dependence on oil and replace it with clean and renewable energy resources (Deutmeyer et al., 2012). Biomass energy – a renewable energy – could be good candidate for replacement of fossil fuels. It can be used in three forms such as solid (briquette, pellet, char), liquid (ethanol, biodiesel), and gaseous (producer gas, biogas) (Koh and Hoi, 2003).

* This chapter is modified form of the paper published by the candidate: Nhuchhen, DR. Basu, P. and Acharya, B. (2014), "A comprehensive review on biomass torrefaction," *International Journal of Renewable Energy and Biofuel*, 2014, 1-56.

A blanket use of any type of biomass may not be good for a sustainable source. For example, rapid increase in food-based fuel has strained food supplies in some countries. Lignocellulose biomass on the other hand free from this problem is an alternative source of bioenergy. The use of lignocellulosic biomass has increased significantly in producing bio-oil and synthetics chemicals. The lignocellulosic biomass, in spite of all its positive attributes, associates with the different shortcomings like structural heterogeneity, non-uniform physical properties, low energy density, hygroscopic nature, and low bulk density. These limitations create difficulties in transportation, handling, storage, and conversion processes (Arias et al., 2008; Phanphanich and Mani, 2011; Medic et al., 2011; Uemura et al., 2011; Wannapeera et al., 2011). These properties limit the use of biomass to replace fossil fuels for energy production. Therefore, biomass needs to be pretreated before it can be used in any thermochemical conversions processes. Torrefaction is emerging as such pretreatment method that removes many of the above limitations associated with raw biomass.

2.2. OVERVIEW OF BIOMASS

Biomass is any organic materials derived from plants or animals, excluding materials that take millions of years to produce such as coal or petroleum (Basu, 2010). The energy produced from biomass does not contribute acid rain gases due to the negligible sulfur and nitrogen contents of biomass (Demirbas, 2008). Biomass stores sun's energy through photosynthesis process. Human being extract the stored energy with the help of different conversions routes as shown in Figure 2.1. It is noted that biomass can be used directly for energy conversion or upgraded into superior energy carriers such as bio-char, producer gas, and bio-oil through different routes like pyrolysis, gasification, fermentation, transesterification, and anaerobic digestion.

According to the Energy Statistics of International Energy Agency 2009, biomass energy contributed around 10% of the world's total primary energy supply (IEA, 2009). Biomass can be used as feedstock for liquid or gaseous fuel for the transport sector

through thermochemical and biological routes, and is therefore considered as a promising renewable energy resource (Demirbas, 2008). Table 2.1 presents a classification of biomass types by their sources. Forestry and agriculture sector are two main resources as the primary source of biomass. Industry and waste are secondary sources as these are derived from biomass from primary source.

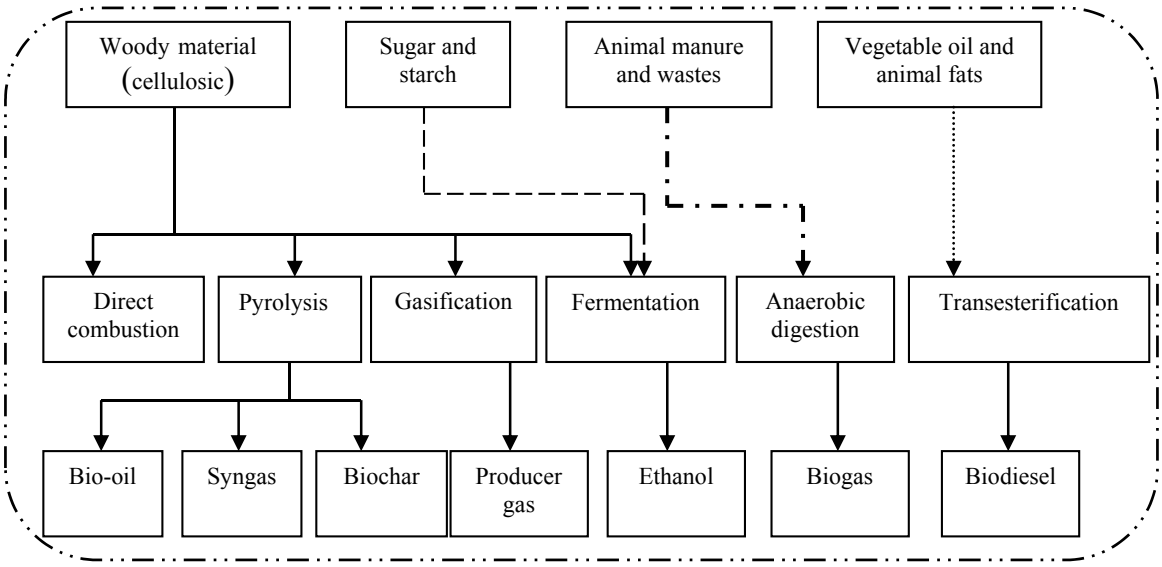

Figure 2.1: Biomass energy conversion routes

Traditional use of biomass has been limited to cooking and heating purpose, which has caused adverse impacts such as land degradation and desertification. However, modern use of biomass – a high quality energy carrier converted from raw biomass – for electricity and heat production can substantially reduce emissions from the conventional power plants (Hoogwijk et al., 2005). This ability to convert raw biomass into convenient energy carriers increases the interest on biomass use for energy purpose, especially the lignocellulosic biomass.

2.2.1 Structure of Lignocellulosic Biomass

Biomass can be lignocellulosic or non-lignocellulosic materials. The lignocellulosic material is non-starch and fibrous part of plants that consists mainly of cellulose,

hemicellulose, and lignin (Basu, 2010). The non-lignocellulosic material, on the other hand, is non-cellulosic organic material, which is used mainly for nutritional purpose. Sugar, starch, protein, and fat content of any crops are the non-lignocellulosic materials. These materials can be easily hydrolyzed to produce upgraded bioethanol (Doelle, 2012.).

Table 2.1: General classification of biomass resources

Supply sector	Type	Examples
Forestry	Dedicated forestry	Short rotation plantations (Willow, poplar and eucalyptus)
	Forestry by products	Wood blocks and wood chips from thinning
Agriculture	Dry lingo-cellulosic energy crops	Herbaceous crops (Miscanthus, reed canary grass and giant reed)
	Oil, sugar and starch energy crops	Oil seeds for methyl esters (Rape seed and sunflowers)
		Sugar crops for ethanol (Sugarcane and sweet sorghum)
		Starch crops for ethanol (Maize and wheat)
	Agriculture residues	Straw, prunings from vineyards and fruit trees
	Livestock	Wet and dry manure
Industry	Industrial residues	Industrial waste wood, sawdust from sawmills
		Fibrous vegetable waste from paper industries
Waste	Dry lingo-cellulosic	Residues from parks and gardens (Prunings and grasses)
	Contaminated waste	Demolition wood
		Organic fraction of municipal solid waste
		Biodegradable landfill waste, landfill gas
		Sewage sludge

Source: Adapted from EUBIA (2007)

An efficient conversion of lignocellulosic biomass needs better understanding of the cell wall structure and their compositions. Plant's cell wall, which consists of four major macro components namely primary wall, secondary wall, plasma membrane, and middle lamella, are made of cellulose, hemicellulose, lignin, and some extractives as shown in Figure 2.2. Such plants are referred as the lignocellulosic material (Foster et al., 2010).

These polymers give a rigid structure to the plant. Table 2.2 presents a comparison of range of these polymer constituents for some principal type of lignocellulosic materials. Here we note that biomass from animal waste is rather poor in these three polymers. As such their classification under lingo-cellulose biomass is questionable. A brief introduction to the polymeric constituents of the plant cell is presented here.

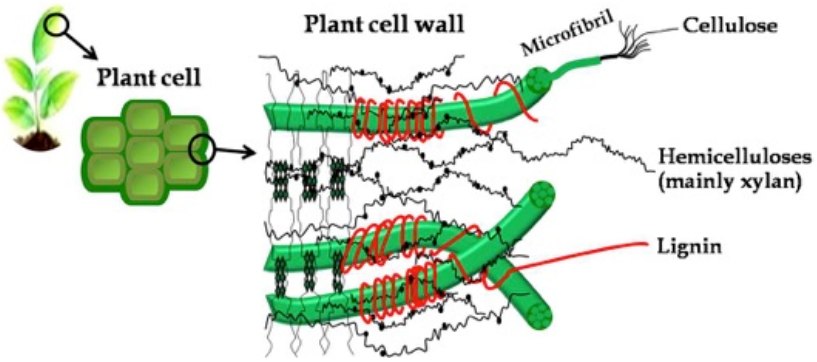

Figure 2.2: Structure of primary cell wall of plant cell
(Source: Adapted from Tomme et al., 1995)

2.2.1.1 Lignin

Lignin is a three-dimensional polymer made up of predominantly C-O-C and C-C linkages (Rowell, 2005). Lignin could be of different types such as: (i) lignin of hardwood (angiosperms); (ii) lignin of softwood (gymnosperms); and (iii) lignin of grasses (non-woody or herbaceous crops) (Buranov and Mazza, 2008).

Lignin is the generic term for a large group of aromatic polymers (Vanholme et al., 2010) Lignin is a co-polymer of three phenyl propane monomer units (monolignols) such as para-coumaryl alcohol, coniferyl alcohol, and sinapyl alcohol (Figure 2.3) β-O-4-aryl ether bonds are the most common coupling linkages in the polymerization process of lignin monomers (Pandey and Kim, 2011). Lignin thermally decomposes over a broad temperature range, because various oxygen functional groups from its structure have different thermal stabilities, their scission occurring at different temperatures (Brebu and Vasile, 2009). The lignin is thermally stable over a wide temperature range from 100 °C

to 900 °C (Yang et al., 2007). Thus, in torrefaction process, lignin remains less modified and a biomass with higher lignin content yields more solid products.

Table 2.2: Polymeric constituents of different biomass sources

Lignocellulosic materials	Cellulose (%)	Hemicellulose (%)	Lignin (%)
Hardwood stems	40-55	24-40	18-25
Softwood stems	45-50	25-35	25-35
Nut shells	25-30	25-30	30-40
Corn cobs	45	35	15
Grasses	25-40	35-50	10-30
Paper	85-99	0	0-15
Wheat straw	30	50	15
Sorted refuse	60	20	20
Leaves	15-20	80-85	0
Cotton seed hairs	80-95	5-20	0
Newspaper	40-55	25-40	18-30
Waste papers from chemical pulps	60-70	10-20	5-10
Primary wastewater solids	8-15	NA	24-29
Swine waste	6	28	NA
Solid cattle manure	1.6-4.7	1.4-3.3	2.7-5.7
Coastal Bermuda grass	25	35.7	6.4
Switch grass	45	31.4	12

Source: Adapted from Sun and Cheng (2002)

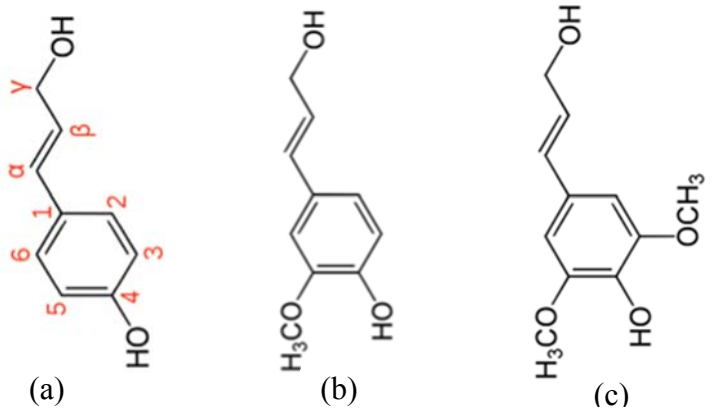

Figure 2.3: Three major monomers of lignin: (a) Paracoumaryl alcohol; (b) Coniferyl alcohol; and (c) Sinapyl alcohol

2.2.1.2 Cellulose

Cellulose is a long chain polymer of glucose that can establish intra-molecular and inter-molecular hydrogen bonds. Cellulose $(C_6H_{10}O_5)_n$ is characterized by its large molecular weights of 500,000 units monomers (Basu, 2010). D-glucoses are the major constituents of cellulose, which are linked by β- (1→ 4)-glucosidic bonds (Rowell, 2005). Structure of cellulose is crystalline in nature that has higher packing density that helps to increase the strength of biomass structure. Figure 2.4 shows the typical chemical structure of cellulose, showing different hydroxyl groups in the chain. The hydroxyl group increases its ability of forming hydrogen bonds that is responsible for hygroscopic behavior of raw biomass. The hygroscopic nature of cellulose increases the gap between cellulose chains, resulting in swelling of biomass. Thus, during thermal treatment period, the solid product undergoes the shrinkage phenomena, causing dimensional variations.

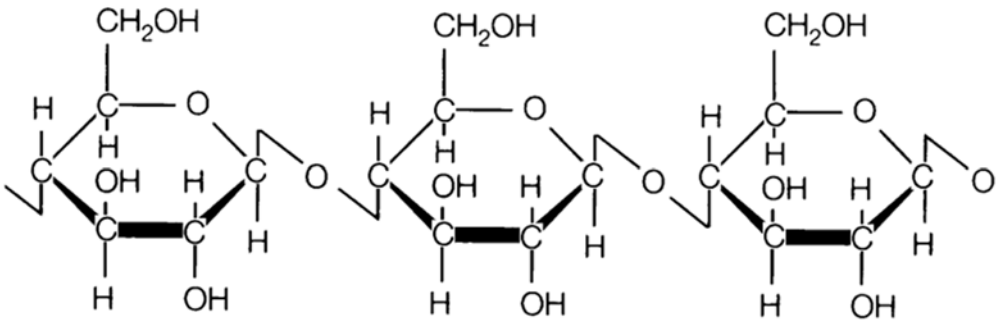

Figure 2.4: Structure of cellulose compositions

2.2.1.3 Hemicellulose

Hemicelluloses are composed mainly of heteropolysaccharides such as hexoses (glucose, mannose, and galactose) and pentoses (xylose and arabinose) (Pollex et al., 2012). Hemicelluloses are polysaccharides of plant walls, which strengthen the primary cell walls. Xyloglucans, xylans, mannans, gulcomannans and β - (1→3, 1→4) – glucans are important constituents in the hemicellulose (Scheller and Ulvskov, 2010). It has random amorphous structure, and is the weakest constituent of biomass cells (Basu, 2010).

Hemicellulose is made predominantly of acetyl- and methyl- substituted groups (Rowell, 2005). These groups are responsible for releasing light volatiles gases such as CO_2 and CO, upon low temperature thermal pretreatment. Hemicellulose, which has a lower degree of polymerization compared to cellulose, undergoes to substantial thermal degradation and has significant effect on mass yield in the torrefaction process. Figure 2.5 shows the structure of hemicellulose in a hardwood.

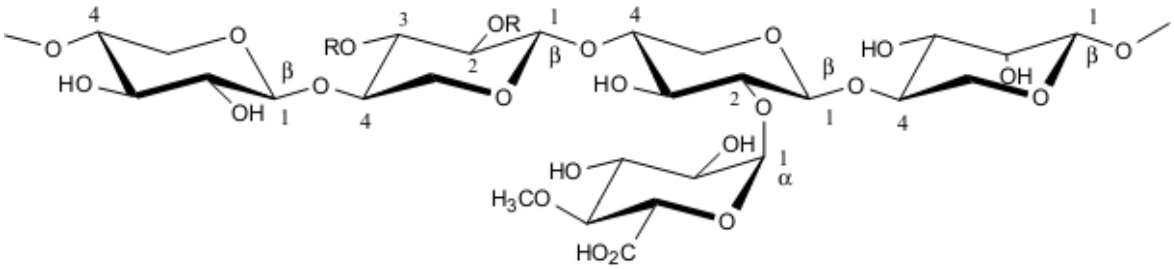

Figure 2.5: Structure of hemicelluloses (xylan)

2.2.2 Biomass for Energy Generation

With growing energy demand and emerging environmental issues, new and clean energy sources are being explored to avoid possible damages from global warming and climate change. Biomass is widely distributed around the world, and it often available at relatively low price. It could therefore become world's important renewable energy resource. Biomass can help replace fossil fuels in transportation and power generation sector because it has the ability of producing biofuels such as biodiesel, methanol, and hydrogen through the Fisher-Tropsch Synthesis process (Ptasinski, 2008). However, some of its inherent limitations like low energy density, fibrous nature, and hygroscopic nature, use of biomass for energy generation have so far been restricted. Currently, co-firing technology has gained wide acceptance for reducing fossil fuel consumption and corresponding emission in thermal power plants by replacing a part of fossil fuel with biomass. But the share of biomass in the mix has been limited to 5-10%. Higher percentage is not economically feasible unless the properties of biomass are upgraded.

2.2.2.1 Shortcomings of Biomass as Energy Source

Despite all its advantages biomass has some shortcomings that often create difficulties in its wide scale use as an energy source. Compared to other fuels like coal, biomass has higher oxygen content, lower calorific value, lower bulk density, higher hygroscopic nature, and higher moisture content. Thus biomass faces some technical challenges in energy conversion systems (van der Stelt et al., 2011).

Low bulk density of raw biomass causes storage and handling problems. It also reduces the energy density of biomass that in turn increases the volume of biomass feed into a conversion system to produce a given amount of power. The low bulk density of biomass also increases the cost associated with storage, transportation, and handling of materials at the conversion plant (Arias et al., 2008; Tumuluru et al., 2011).

Higher oxygen content reduces the heating value and thereby makes it a lower-grade fuel. Higher oxygen content is responsible for producing large volume of flue gas during combustion (van der Stelt et al., 2011) that requires much bigger size of plants and auxiliary equipment.

Higher moisture content (45-60%) of raw biomass has significant negative impact on the bioenergy production and its consumption chain (Ratte et al., 2011). Though moisture adds some benefits in biological conversion methods, it remains as one of the major obstacles for thermochemical conversion. A modest amount of moisture, however, shows some benefits in the gasification process in which steam produced from the moisture assists in increasing hydrogen concentration in the producer gas (Acharjee et al., 2011). At the same time, higher moisture also decreases the overall gasification temperature, resulting in a lower gasification efficiency and higher tar formation. Moist biomass on the other hand also shows a greater tendency to undergo the natural decomposition. This alters the physical, chemical, and microbiological properties and,

degrades the fuel quality (Tumuluru et al., 2011). A wet biomass, when stored could lose some solid mass due to microbial decaying process (Medic et al., 2011).

Hygroscopic nature is another major drawback of biomass. Though, biomass can be dried before its use, the hygroscopic nature makes it to reabsorb the moisture from surrounding atmosphere even if it is stored indoors.

Fibrous nature of biomass increases difficulties in pulverizing it into fine powder as required for co-firing in pulverized coal fired boiler. This results in higher grinding costs or reduces the generation capacity of the plant (Ratte et al., 2011; Wannapeera et al., 2011). The fibrous nature of biomass not only increases its grinding cost, but is also responsible for inconsistency in particle sizes (Tumuluru et al., 2011). Pulverized particles from raw biomass are coarse and slender in nature (100-10 mm) with low sphericity values (Phanphanich and Mani, 2011). Such lower sphericity reduces its flowability, reducing the performance of the entrained flow gasifier (Melkior et al., 2011).

2.2.3 Biomass Pretreatment Methods

Above limitations of biomass are hindering the wide-scale use of biomass. This limitation can be reduced to some extent by pretreatment. Pretreatment alters the biomass such that enzymatic hydrolysis of cellulose and hemicellulose can be achieved more rapidly and with greater yield (Harmsen et al., 2010). Pretreatment also enhance its physical properties making it suitable for use in existing energy conversion systems. However, for such process to be commercially viable, the technology should be well developed and economical feasible. Biomass pretreatment methods are classified into five categories: a) Chemical b) Mechanical, c) Thermal, (d) Hydrothermal (wet), and (e) Biological. These pretreatment methods facilitate biomass conversion process, increasing the economical and environmental viability of biomass use (Almeida et al., 2010; Harmsen et al., 2010). The study on the chemical, mechanical, and hydrothermal

pretreatment of biomass is beyond the scope of this work; only a short discussion on them is presented here.

2.2.3.1 Chemical or Hydrolysis

The primary goal of chemical pretreatment is to improve the biodegradability of cellulose in biomass by removing the lignin and hemicellulose (Zheng et. al. 2009). Common chemical pretreatment techniques are catalyzed steam-explosion, acid, alkaline, ammonia fiber/freeze explosion, organosolv, pH-controlled liquid hot water, and ionic liquids pretreatments. In ethanol production, chemical pretreatment separates lignin and hemicellulose, and enhances the hydrolysis of cellulose, increasing ethanol production (Sun and Cheng, 2002). Chemical pretreatment also changes the morphological structure as well as arrangement of different functional groups. For example, an alkali based chemical pretreatment reduces degree of polymerization, disturbs lignin structure, and breaks the linkages in different cell compositions (Agbor et al., 2011).

2.2.3.2 Mechanical

Mechanical pretreatment brings about only physical change of biomass. Milling, extrusion, and grinding are major mechanical pretreatment methods (Harmsen et al., 2010). Milling of biomass increases the accessible surface area of biomass for it conversion processes. A comparative study of sugar yield of two mechanically pretreated biomass namely extrusion and grinding, found that extrusion treated biomass shows higher sugar yield compared to the grinding for wheat bran (Lamsal et al., 2010). Similarly, in the screw press pretreatment method, an increase in pressure and temperature improves the extent of softening of biomass and, reduces the moisture level. However, mechanically pretreated biomass does not increase the hydrophobicity of biomass. One very popular pretreatment method is pelletization, but it does not necessarily increase the surface area. During pelletization, ground biomass is compressed

with at specified temperature into regular shape. Such regular greatly increases the handling ease of biomass but it does not have ability to avoid moisture reabsorption capacity.

2.2.3.3 Biological Pretreatment

Biological pretreatment uses microorganism to modify chemical composition and structure of the lignocellulose biomass for making it suitable for enzymatic digestion. The microorganisms used are white and brown soft-rot fungi, and bacteria (Zheng et al., 2009). The white-rot fungi, a major degrader of wood in the forest ecosystems, are the most effective microorganisms for the biological pretreatment of lignocellulose biomass (Akin et al., 1995; Chaturvedi and Verma, 2013). The biological treatment process seems to be a promising technology, as it avoids the use of chemicals, consumes less energy, produces minimal byproducts, works at mild operating conditions, and does not harm environmental (Wingreini et al., 2005). However, the biological pretreatment process is very slow and it requires large space and controlled environment for the effective pretreatment, which makes the process costly compared to other pretreatment methods (Zheng et al., 2009).

2.2.3.4 Hydrothermal

Hydrothermal carbonization may be defined as a thermochemical conversion process in which biomass is kept with water under high pressure at moderate temperatures (180–230°C) (Roman et al., 2012). Hydrothermal or wet torrefaction uses either compressed water in liquid form (Yan et al., 2010) or water mixed with acetic acid and lithium chloride (Lynman et al., 2011). Hydrothermal (wet) torrefier is an innovative reactor that could be used for treating a wet biomass such as animal manures, human waste, sewage sledges, municipal solid waste, aquaculture residues and microalgae. This overcomes the major limitation of dry torrefaction where the moisture content is limited to 15% (Koppejan et al., 2012).

Hydrothermal torrefaction is usually carried out in an autoclave or specially made custom steel reactor. Hydrothermal torrefaction of biomass is mainly characterized by its ability to bring instability in the structure of lignocellulosic biomass, initializing the decomposition reactions at a low temperature. Hydrolysis is the primary reaction that alters physical structure of biomass in the hydrothermal torrefaction. Decarboxylation, dehydration, condensation, and aromatization are four major reactions of the hydrothermal torrefaction (Funke and Ziegler, 2010).

Hydrothermal torrefaction can increase the higher heating value of biomass by up to 36% above that for raw biomass (Yan et al., 2010). Though hydrothermal torrefaction adds more steps such as filtration and drying process compared to the dry torrefaction, its ability to treat wet biomass increases the fuel flexibility making it more commercially attractive. For example, hydrothermal torrefaction can pretreat digested sludge from the anaerobic digester, increasing waste to energy recovery from agriculture residue (Oliveira et al., 2013). An aqueous waste stream from hydrothermal torrefaction contains substantial level of potentially valuable organic chemicals, such as sugars, furans, furfurals, and organic acids. The solution can also be used as a nutritional product that is applicable in growing algae (Jena et al., 2011). One potential major attraction of hydrothermal torrefaction is that it could lead to reduction in corrosion and agglomeration causing elements in biomass. Preliminary work of Dutta (2013) found evidence of major reduction in sodium and potassium content in the torrefied biomass.

Other major advantage of hydrothermal torrefaction is its ability to produce an energy dense product in a relatively short period (5 minutes) of residence time (Coronella et al., 2012), while that for dry torrefaction it is between 30-60 minutes. The heat transfer rate in aqueous media is very high (Hoekman et al., 2013). This reduces the residence time of the hydrothermal torrefaction compared to the dry torrefaction. For instance, Yan et al. (2010) able to perform the wet torrefaction of loblolly pine only within 5 minutes of residence time. In addition to this, the high working pressure around 20 bar reduces the carbon loss during the pretreatment (Libra et al., 2011). The solid product yield further

enhanced by re-condensation reactions in aqueous solution. The re-condensation of liquid increases the carbon content in torrefied biomass under the hydrothermal torrefaction. Thus, a hydrothermal torrefaction could produce higher solid yield. The carbon loss per unit mass of feedstock increases with the amount of water mixed in the hydrothermal torrefaction, causing to a low net energy yield (Libra et al., 2011). For instance, a typical study on hydrothermal (wet) torrefaction results 10% reduction in energy yield compared with that of a dry method under the similar operating conditions (Chen et al., 2012).

To widen the range of moisture in feedstock for torrefaction technology, the PCS biofuels of Canada developed a hydrothermal polymerization process. This system consists of a reactor with liquid catalyst in which biomass is kept under moderately high pressure at temperature around 250ºC for a certain period of time. Biomass inside the reactor undergoes series of chemical reactions, forming water, carbon dioxide, and solid biofuels. Depending upon the type of catalyst used, different compositions of biomass, which are soluble in the liquid catalyst, are liberated out. In addition to this, the ability to recycle the liquid catalyst using cascaded reactor systems could reduce thermal energy required for the process. Using an appropriate and hazards free catalyst also helps to use an aqueous solution of catalyst as a natural nutritional fertilizer for growing crops (PCSB, 2013).

2.2.3.5 Thermal

Thermal pretreatment is a slow heating process in which biomass releases its volatiles. This process modifies the physical, structural, and chemical properties of biomass. Torrefaction, which is a thermal pretreatment method, produces a carbon rich solid product. This process is different from drying because in addition to removal of moisture it involves some chemical transformations within the polymer constituents of the cell wall. These transformations reduce the mechanical strength of biomass, and produce more brittle and less fibrous products. Thermal pretreatment also increases

biodegradability of waste biomass in biological conversion process. For instance, thermally pretreated biomass at 70°C and 90°C increased the anaerobic biodegradability in a methane production process by 24% and 48%, respectively when compared with raw biomass (Gonzalez-Fernandez et al., 2012). Thermal treatment enhances the fuel flexibility making wide range of fuels suitable for firing in pulverized coal fired plant. For example, microalgae produced using flue gas from a thermal power plant can be made suitable for co-firing in a PC boiler by the torrefaction process (Wu et al., 2012).

Thermal pretreatment, which mainly refers to the torrefaction process, can be divided into dry and wet (hydrothermal) torrefaction (Yan et al., 2009). Table 2.3 presents different characteristics of wet and dry torrefaction.

Table 2.3: Characteristics of thermal pretreatment methods

Thermal pretreatment methods	Characteristics
Wet torrefaction	Temperature ranges: 200-260°C Media: hot compressed water Pressure range: 13.79-48.26 bar Biomass sample size: 2 g Residence time: 5 min Cooling process: rapidly immersion in an ice bath to avoid further degradation of the product Need filtration and evaporation process Higher energy density than dry torrefaction
Dry torrefaction	Temperature ranges: 250-300°C Media: inert gas (Nitrogen) Pressure: atmospheric pressure Biomass sample: 5 g Residence time: 80 min Cooling process: flowing nitrogen/indirect water cooling

Source: Adapted from Yan et al. (2009)

2.3. GHG EMISSIONS AND BIOMASS TORREFACTION

The most talked about means of reduction of the GHG emissions from coal-fired power plant is Carbons capture and storage (CCS), which involves capturing, separating, transporting, and storing of CO_2 into the safe area. This approach seems an ideal method that helps to get rid of the issues related to the CO_2 emissions. However, the low concentration of CO_2 (4-14%) in power-plants' flue gas requires a large volume of gas to be handled, leading to large equipment sizes and high capital costs (Olajire, 2010). For this reason, oxy-fuel combustion and chemical looping combustion technologies are the favorable methods for CCS. CCS, however, could add huge expenses for electricity production. Hoffmann et al. (2009) reported the additional cost of \$29/tCO_2 for pre-combustion capture system using advanced combined cycle gas turbine plants fueled by natural gas. Apart from the economical aspects, some capture processes have technical issues such as efficiency decrease and corrosion problems in the oxy-fuel combustion techniques and inadequate large scale operation experience in the chemical looping combustion process (Leung et al., 2014). Another important challenge for deploying a large scale CCS is the economic CO_2 separation technologies, which require more research and development. Most of all, the life cycle GHG assessment has to be conducted for the CCS technologies to determine whether the CCS is a net CO_2 emission sink or source. Though some studies (Odeh and Cokerill, 2008; Pehnt and Henkel, 2009) showed positive results, CCS requires many years (no specific limits) to be implemented as a safe storage of CO_2 because the leakage may completely impair the effectiveness of the CO_2 capture. This, therefore, requires CO_2 leakage monitoring of the storage sites, as a leakage rate above 0.1% will undermine the use of CCS in the global warming control (Enting et al., 2008). Considering these facts, CCS, though it can be good methods to eliminate the CO_2 emissions, may only be a good solution in future.

2.3.1 Biomass Co-firing

Biomass co-firing is a transition step towards a carbon free electricity production (Lempp, 2013). Biomass co-firing only requires minor modifications in the conventional coal power plants without adding significant investment (Basu et al., 2011). Biomass co-firing is one of the most attractive methods and readily available means for immediate CO_2 reduction compared to the carbon capture and storage method. Canadian Clean Power Coalition reported that co-firing, which can replace some portion of coal with a carbon neutral fuel – Biomass, could replace 20-30% of coal (CCPC, 2011). Co-firing technique not only reduces the emission, but also enhances the rational use of biomass by avoiding intermediate conversion steps unlike in the ethanol production process (Aravindhakshan et al., 2010). Typically, the emission intensity of coal-fired power plants decreases from 830 to 550 gCO_2/kWh_e when they were upgraded to biomass co-firing plants (CG, 2011). In addition to this, co-firing power plant also reduces the cost of power generation compared that to 100% biomass based power generation (IRENA, 2013). Cost of the electricity generation from the pulverized coal power plant reduces once it is co-fired with biomass. For example, the electricity production cost in a typical fluidized bed power plant of 15MW is reported to be 5.41cent/kWh and 5.24cent/kWh without and with co-firing facilities, respectively (FEMP, 2004). The payback period for the invested capital of co-firing could be less than a year (FEMP, 2004). However, the electricity production cost may be different for the specific power plants and their locations. For instance, the cost of electricity production in a pulverized coal power plant of capacity 100MW is 3.26cent/kWh and 3.15cent/kWh without and with the co-firing facilities, respectively (FEMP, 2004). The use of biomass in co-firing also avoids landfills and their associated costs, and reduces sulfur dioxide and nitrogen oxide emissions (FEMP, 2004). The blending of biomass with coal will also diversify the energy source, improving the energy security indicator. Since the biomass feedstock, which includes forestry and agricultural waste, industrial waste (sawdust), and dedicated energy crops, depends on the locally available resources, biomass co-firing could increase the employment opportunities to the local people and help to improve their economic status. Biomass co-firing is, therefore, considered as one of the feasible short-

term technology to integrate the renewable energy resource in the power generating industries (Agbor et al., 2014).

Co-firing technique may be classified as: (i) Direct co-firing; (ii) Indirect co-firing; and (iii) Parallel co-firing (EUBIONET, 2003). Fluidized bed boilers due to their ability to adopt variations in fuel quality and moisture usually deploy direct co-firing. On the other hand, indirect co-firing technique uses a clean producer gas obtained from the gasification of biomass in a separate reactor. This technique helps to reduce effective emission as the gasification removes the chlorine content and heavy metals (EUBIONET, 2003). In the parallel co-firing method, two boilers, one for coal and another for biomass combustion are used. This increases the cost of electricity production.

Biomass co-firing, however, is not free from its limitations. Some of the major technical problems in co-fired power plants are: handling of biomass; grinding difficulties; changing ash deposition behavior (Madrali, 2008); a large volume of the flue gas; unstable flame propagation; non-uniform heat distribution; big feeding system (Nhuchhen et al., 2014); higher flue gas exit temperature; shorter soot blowing interval; bed material agglomeration; and higher rate of cleaning heat transfer areas (EUBIONET, 2003). Though the combustion efficiency of the co-firing plant is higher than direct biomass-fired power plants, the overall generation efficiency of a co-firing plant decreases compared that of the standalone coal-fired power plant (Belosevic, 2010). The limitation of co-firing also depends greatly on the type of biomass. For instance, straw has a major limitation because of its low bulk density, and high chlorine and potassium content (EUBIONET, 2003). High alkali content in biomass that reduces the agglomeration temperature always leads to operational difficulties. Some of the other problems in co-firing plant that arise due to differences in fuel characteristics are shorter soot blowing interval, higher cleaning requirement for the heat transfer surfaces, and higher flue gas exit temperature compared that of the conventional coal-fired power plants (EUBIONET, 2003). However, this could be avoided by limiting blending ratio

and finding optimum blending ratio. Despite this, the separate feed system for firing biomass because of its low energy density is often necessary if a higher fraction of biomass co-firing was desired (Belosevic, 2010). On the other hand, the biomass fuel quality can also be upgraded before feeding them to the coal-fired power plants. Pretreatment of biomass using torrefaction process could reduce the intrinsic difference between coal and biomass elevating the share of biomass use and emission savings in the coal fired power plant.

2.3.2 Overview of Torrefaction

Torrefaction is a partial pyrolysis of biomass which is carried out under atmospheric pressure in a narrow temperature range of 200-300°C and under an inert environment (Acharya et al., 2012; Agar and Wihersaari, 2012; Basu et al., 2013; Bergman, 2005; Bergman et al., 2005; Bourgois and Guyonnet, 1988; Chew and Doshi, 2011; Clausen et al., 2010; GuiJun et al., 2011; Klinger et al., 2014; Lu and Chen, 2014; Lu et al., 2012; Medic et al., 2011; Pach et al., 2002; Prins et al., 2006; Qing et al., 2011; Saadon et al., 2014; Sun et al., 2011; Tapasvi et al., 2013; Thanapal et al., 2014; Yan et al., 2009). It produces three major products such as dark color solid products, yellowish color acidic aqueous products, and non-condensable gaseous products. Torrefaction, a French word for roasting, changes the chemical and physical properties of raw biomass making it similar to those of char. Torrefaction is usually performed at a low heating rate, which gives higher yield of solid product (Deng et al., 2009). Unlike pyrolysis, the major motivation of torrefaction is maximization of solid yield. Decomposition, devolatilization and depolymerization are three major reactions that occur during the torrefaction process. This process releases condensable hydrocarbon, hydrogen, oxygen, and some carbon content from the biomass in the form of water, carbon monoxide, and carbon dioxide (Pach et al., 2002). During the torrefaction process, drying is considered to be more destructive as it breaks inter- and intra-molecular hydrogen, C-O, and C-H bonds (Tumuluru et al., 2011). This leads to emissions of hydrophilic and oxygenated compounds, forming a blackened hydrophobic energy dense product. This greatly helps

storage of biomass and thereby addresses the problem of seasonal availability of biomass.

2.3.3 Motivations for Torrefaction

The main motive of torrefaction is to upgrade the fuel quality of biomass to make it more suitable for thermo-chemical conversion. A torrefied biomass can be used in briquetting, pelletization, gasification, and co-firing thermal power plants (Bridgeman et al., 2010; Felfli et al., 2005; van der Stelt et al., 2011). Torrefaction of biomass destructs tenacity and fibrous structure of biomass, and also increases its energy density. Numerous studies concluded that torrefied biomass can avoid many limitations associated with the raw biomass because it produces moisture free hydrophobic solid products (Acharjee et al., 2011), decreases O/C ratio (Prins et al., 2006), reduces grinding energy (Repellin et al., 2010; Phanphanich and Mani, 2011), enhances energy density (Yan et al., 2009), increases bulk density and simplifies storage and transportation (Bergman, 2005; Phanphanich and Mani, 2011), improves particle size distribution (Phanphanich and Mani, 2011), intensifies combustion with less smoke (Pentananunt et al.,1990), shifts combustion zone to the high temperature zone in a gasifier (Ge et al., 2013), and increases resistance to biological decay (Chaouch et al., 2010). Many of these improvements make torrefied biomass more suitable than raw biomass for co-firing in the conventional coal power plants with minor modifications (Clausen et al., 2010).

The removal of volatiles (light gases) during torrefaction leads to a decreased in O/C ratio, and increased energy density of the biomass. Losses of carbonyl and carboxyl groups from cellulose, carboxyl group from hemicellulose, and aromatic ring and methoxyl groups from lignin are the major sources of mass loss during this thermal treatment of biomass (Yang et al., 2007). These components have less energy content than the biomass as a whole. Thus their loss increases the energy density of biomass after torrefaction. Increase in energy density in torrefied product may also be due to higher fraction of lignin (heating value of 25.0 MJ/kg) and reduced fraction of

hemicellulose and cellulose with heating value 18.6 MJ/kg (Gupta and Demirbas, 2010). Increase in the energy density of biomass helps in decreasing the volume of biomass to be fed in biomass co-firing plant to achieve a similar level of heat input compared that to if raw biomasses were to supply.

Hydroxyl group, which can establish ions and attract water molecules, is responsible for hydrophilic behavior of biomass. The hydrophilic nature of biomass decreases as torrefaction reduces the hydroxyl groups through decomposition reactions. The removal of hydroxyl groups also decreases the capability of forming hydrogen bonds that in turn reduces the moisture-absorbing capacity of biomass. This effect leads to the transformation of polar molecules into non-polar unsaturated molecules and produces a hydrophobic product.

Tenacious and fibrous nature of raw biomass established due to a complex structure of interlinked polymeric components increase the grinding cost of biomass. The heat applied during torrefaction process modifies the complex structures of interlinked polymeric components. It thus breaks down the hemicellulose matrix and depolymerizes the cellulose structure, resulting in a decrease in fiber length (Bergman and Kiel, 2005). Decomposition of hemicellulose matrix produces mainly light volatiles gases such as CO_2, CO, CH_4 and traces of H_2 (Prins et al., 2006a). The structural rearrangement and depolymerization of molecules during the torrefaction process, due to the mild heating phenomena, reduces fibrous and tenacious nature of the raw biomass (Wu et al., 2012), making more friable or brittle (Sun et al., 2011). This improves the Hardgrove Grindability Index (HGI) of biomass and then eventually increases the fineness of the ground powder of the biocoal (Shang et al., 2012; Wu et al., 2012).

Torrefaction also reduces the reactivity of biomass (Fisher et al., 2012; Jones et al., 2012). This allows more uniform combustion inside the co-fired plants, which in turn avoids non-uniform heat distribution along the flame direction and also reduces the flue gas exit temperature. The increase in fuel ratio of biomass comparable to coal after

torrefaction of biomass, which could be enhanced up to 1.44 (Nhuchhen and Basu, 2014), may considerably increase the share of renewable source in existing coal-fired power plants. This also avoids unnecessary additional secondary airports, otherwise may have to be installed for the combustion of volatiles released during co-firing of biomass.

2.3.4 Mechanism of Torrefaction

In torrefaction process, the major changes and transformation occurring inside biomass can be predicted mainly by understanding the behavior of three polymeric constituents. For example, hemicellulose – a highly reactive component – undergoes decomposition and devolatilization, and contributes a major part of mass loss in the torrefaction process. Therefore, biomass materials with high hemicellulose content have lower solid product yield compared with that of biomass with low hemicellulose. Acetic acid and methanol from acetoxy- and methoxy-groups are the major constituents of volatiles gases released during the thermal degradation of hemicellulose (Prins et al., 2006a). Although only a small portion of the cellulose degrades within the torrefaction temperature range (200-300°C), water vapor and acids released from hemicellulose may also enhance degradation of cellulose. Lignin that has more carbon than other two polymeric constituents of biomass (Table 2.4) is thermally more stable and takes a larger share in the final solid product. The solid product with higher carbon content produces an energy dense product after the torrefaction.

Table 2.4: Typical element analyses of lignin, cellulose, and hemicellulose

Constituents of biomass cells	Ultimate analysis (wt. %, dry basis)				
	C	H	O	N	S
Lignin	57.70	4.38	34.00	0.11	3.22
Cellulose	42.96	6.30	50.74	0.00	0.00
Hemicellulose (xylan)	43.25	6.20	49.90	0.00	0.00

Source: Pasangulapati et al. (2012)

Dry torrefaction comprises of four simple steps (Figure 2.6) such as:

(a) Drying, in which only surface (free) moisture is removed,

(b) Post – drying, in which bound moisture as well as some of light hydrocarbons are removed,

(c) Torrefaction – isothermal heating – in which supplied heat establishes depolymerization, partial devolatilization, and partial carbonization reactions

(d) Cooling process (ambient temperature, T_a).

The overall cycle time of the dry torrefaction process is the sum of the time taken by drying, post-drying, torrefaction and cooling process. As one can see from Figure 2.6, temperature remains unchanged during drying and torrefaction with an important distinction that energy used during drying is highest and that during torrefaction is much lower. As destructive torrefaction starts only above 200°C, the duration of torrefaction, known as residence time, is usually measured from the instant when the temperature of biomass exceeds that temperature (Basu, 2013).

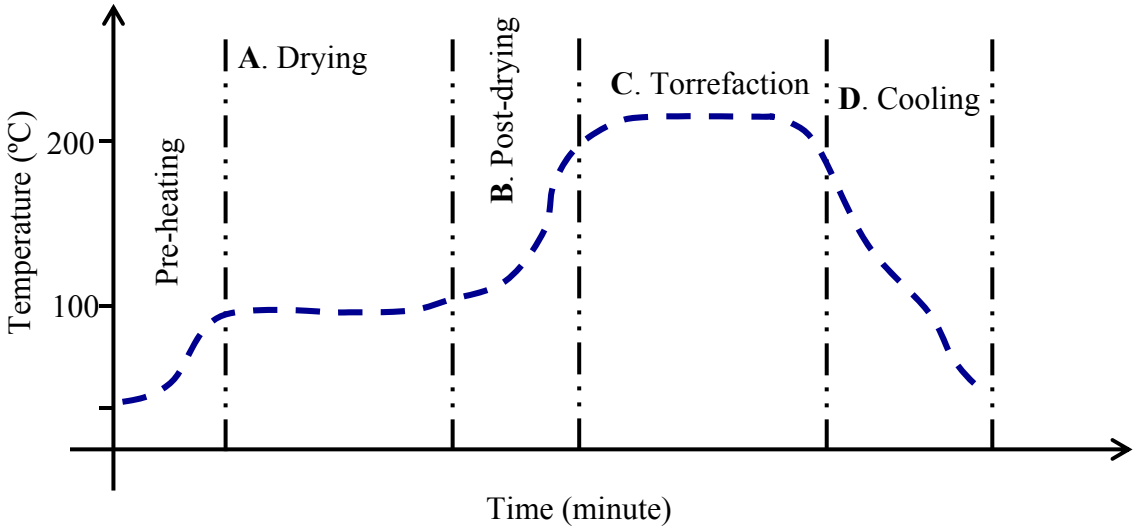

Figure 2.6: Stages of torrefaction process

While wet torrefaction uses the concept of solubility of different compositions of biomass in hot and aqueous solutions, dry torrefaction is characterized mainly by the thermal degradation of polymeric constituents of the biomass. Degradation of biomass

during dry torrefaction, therefore, can be explained through drying and devolatilization process.

2.3.4.1 Drying

Drying is a major and most energy intensive step in the torrefaction process. Drying process refers to the process of removing surface and bound water from the raw biomass. Drying is classified as a non-reacting and reactive process. Heating of biomass (at atmospheric pressure) in the temperature range of 50-150°C is known as non-reactive drying, when it mainly removes the surface water, resulting shrinkages in the product size (Tumuluru et al., 2011). The non-reactive drying is followed by the reactive drying in the temperature range of 150-200°C at which the breakage of hydrogen and carbon bonds occurs, emitting lipophilic extractives. This phase is characterized by permanent structural deformation. Reactive drying substantially removes bound water from the biomass.

2.3.4.2 Devolatilization

Devolatilization may be defined as a process of removing oxygen and volatile content of biomass. It generally occurs once temperature of the biomass is above 200°C at which volatiles (both gases and tar) start leaving the solid matrix of biomass (Basu and Kaushal, 2009; van de Weerdhof, 2010). It is also known as destructive drying process, which is characterized by devolatilization and carbonization of hemicellulose, depolymerization, devolatilization, and softening of lignin, and depolymerization and devolatilization of cellulose. However, it may be noted that devolatilization is rarely complete during torrefaction. The torrefied biomass always contains some volatile matters unlike the char produced from a pyrolysis process.

2.3.5 Effect of Design and Operating Parameters

2.3.5.1 Temperature

The mode of a torrefaction process may be classified as light, mild, and severe torrefaction based on the torrefaction temperature range around 230°C, 260°C, and 290°C, respectively (Chen and Kuo, 2010). Temperature shows a dominant influence on the product quality of torrefaction. Solid yield of torrefaction product depends on the temperature. For instance, in one case the solid yield decreased from 94% to 56% when torrefaction temperature increased from 220°C to 275°C (Felfli et al., 2005). On the other hand, Acharya (2013) in his study of torrefaction of Oats reported decrease in energy yield but increase in energy density when the temperature of torrefaction increased from 210°C to 300°C. The mass loss or solid yield at different torrefaction temperatures can be explained mainly through the impact of temperature on (i) polymeric compositions, and (ii) devolatilization rate.

Polymeric composition of lingo-cellulosic biomass to some extent influences the nature of torrefied products. Table 2.5 presents the temperature ranges over which thermal degradation of hemicellulose, cellulose, and lignin takes place during a pyrolysis process. It indicates that lignin decomposes over a wider temperature range than other two components. The stability of lignin is due to the thermal stability of its different functional groups containing oxygen (Brebu and Vasile, 2009). On the other hand, hemicellulose is highly sensitive in the narrow temperature range of torrefaction. The mass loss during torrefaction therefore depends highly on the devolatilization of hemicellulose. Hemicellulose shows significant effects in initiation and propagation of different pyrolysis reactions (Rousset et al., 2011). The composition of hemicellulose also affects the degradation rate of biomass. For example, biomass with higher xylan in hemicellulose is more temperature sensitive than one with mannan based hemicellulose (Basu, 2013). Celluloses are relatively stable to the temperature than hemicellulose because of the crystalline structured of cellulosic fibrils. Breakage of these crystalline

fibrils, which affects glucosidic bonds between glucose monomers, and inter and intra-molecular hydrogen bonds at higher torrefaction temperature reduces the strength of solid products (Emsley and Stevens, 1994). Table 2.6 presents typical mass loss percentages of hemicellulose, cellulose and lignin at different torrefaction temperatures.

Table 2.5: Temperature range for peak thermal degradation of hemicellulose, cellulose, and lignin

Degradation temperature range (°C)			Source
Hemicellulose	Cellulose	Lignin	
220-315	315-400	160-900	Yang et al. (2007)
225-325	305-375	250-500	Shafizadeh (1985)
200-400	275-400	200-500	Sorum et al. (2001)
250-350	300-430	250-550	Raveendran et al. (1996)
227-327	327-407	127-477	Giudicianni et al. (2013)

Note: Different temperature range is due to different techniques used in their studies.

Table 2.6: Weight losses in polymer components with temperatures

Torrefaction temperature (°C)	Hemicellulose (wt. %)	Cellulose (wt. %)	Lignin (wt. %)
230	2.7	1.1	1.5
260	38.0	4.4	3.1
290	58.3	44.8	7.0

Source: Adapted from Chen and Kuo (2011)

Devolatilization rate is defined as the rate of mass loss during thermal degradation of biomass and will be more at high temperature. A higher heating rate of biomass at higher operating temperature usually produces more volatile gases during the pyrolysis process, and increases the devolatilization rate. This reduces the solid product yield from the

process. Figure 2.7 shows the effect of the temperature in product distributions during the process of torrefaction of cotton stalk and wheat straw. Volatiles, which include both condensable as well as non-condensable product, increased at higher temperature torrefaction. In addition to this, higher heating rate also affects the morphological structure of the solid product. More round pores are formed during pyrolysis when the temperature increased from 600°C to 800°C (Guerrero et al., 2008). This establishes larger internal cavity and more open structures.

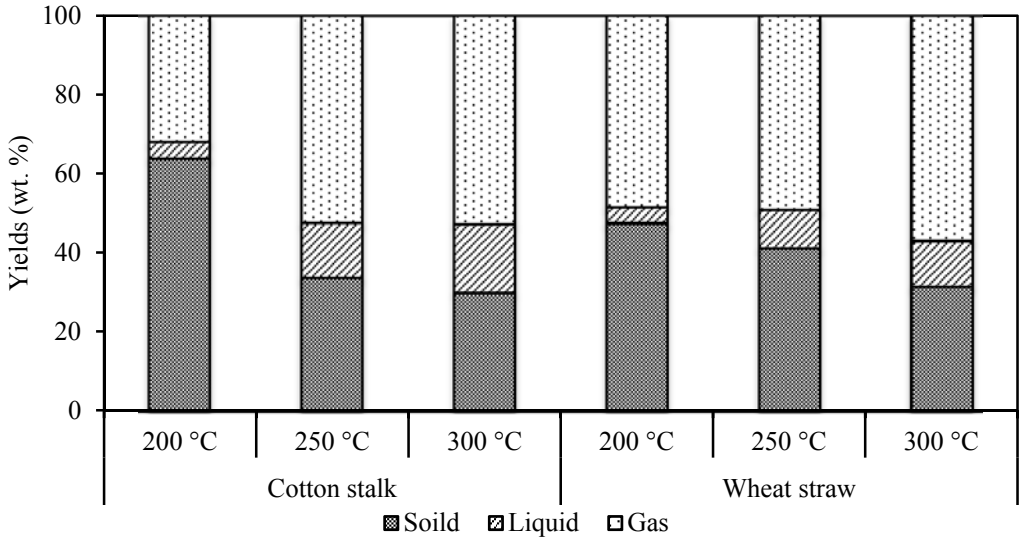

Figure 2.7: Effect of torrefaction temperature in product distribution of cotton stalk and wheat straw (residence time = 30 minutes)
Source: Adapted from Wang et al. (2011)

2.3.5.2 Residence Time

Residence time of the feedstock in the reactor is an important parameter for designing reactors. Compared to many other thermo-chemical conversion processes like combustion, gasification or pyrolysis, the reaction time for torrefaction is much longer (about an hour). It is nearly an order of magnitude longer than that for other processes. Such a long reaction time requires the biomass feed to reside within the reactor for very long time. This naturally increases the volume requirement of the reactor for a given

output. The residence time has thus a greater impact on the reactor size. For example, length and rotational speed of the screw in a screw type reactor and belt speed in conveyer belt reactor are mainly determined by the required residence time (Koppejan et al., 2012). The residence time also determines the solid space velocity and reactor height of a moving bed torrefier.

Although the net effect of residence time is not as prominent as that of temperature, residence time influences the torrefied product at longer residence time. Solid mass loss increases with residence time, resulting in lower solid product yield (Chen et al., 2011, Acharya et al., 2012). This is due to an increase in the extent of devolatilization (Prins et al., 2006a). Condensable product contributes significantly to the solid mass loss at higher residence time as it increases with time as shown in Figure 2.8. On the other hand, non-condensable product such as CO_2 and CO reaches the peak value at residence time of 10 minutes, and then starts declining (Bates and Ghoniem, 2012). The amount of methanol and lactic acid, which are produced during decomposition of acetoxy- and methoxy-groups (Tumuluru et al., 2012), increases up to 10 minutes and then remains unchanged (Bates and Ghoniem, 2012).

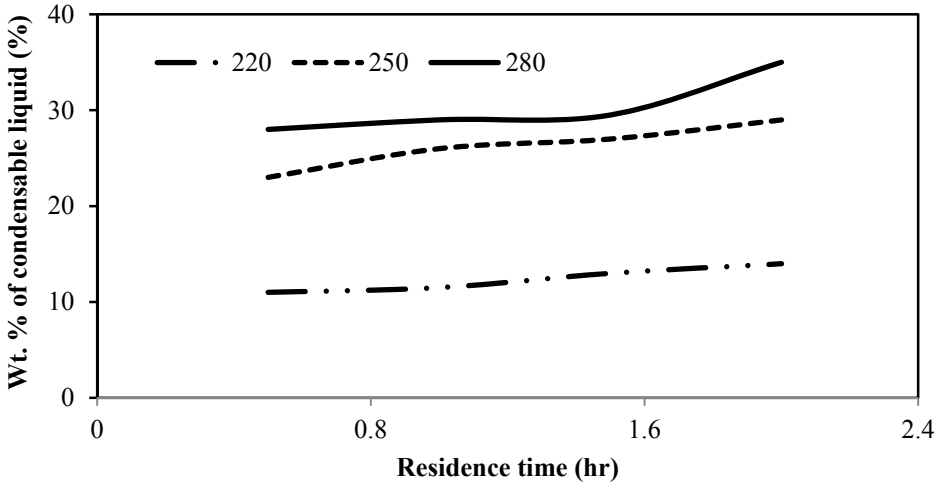

Figure 2.8: Variations in condensable liquid with torrefaction temperature (ºC)
Source: Adapted from Chen et al. (2011)

With increase in residence time one expects an increase in carbon content and a decrease in hydrogen and oxygen content of the torrefied product. For example, the carbon content of palm kernel shell increased from 55% to 58% at torrefaction temperature of 250°C when residence time was increased from 30 to 90 minutes (Felfli et al., 2005). At the same condition, oxygen content of the product was decreased from 31 to 29%. It is interesting that though the carbon content increases with residence time, the absolute value of carbon always decreases due to increase in the reaction of carbon dioxide and steam with the porous char (Prins et al., 2006a). They reported that a gradual decrease in CO_2 and an increase in CO composition were found in the non-condensable volatiles when residence time increased from 5 to 30 minutes. This suggests that the formation of CO increases in the secondary reactions occurring at longer residence time, which increases the energy content of the volatile gas and reduces overall torrefaction efficiency especially if volatiles were not utilized. The quantity of CO_2 and CO in volatile gases is significant only at higher torrefaction temperature (Deng et al., 2009). On other hand, relative amount of carbon loss with that of oxygen also increases with rise in residence time. For instance, Bates and Ghoniem (2012) found that the amount of carbon and oxygen losses was 11% and 40% in 15 minutes compared to 26% and 69% in fourty minutes, resulting more carbon loss per unit of oxygen loss (from 0.28 to 0.38). This suggests that the rate of de-oxygenation of biomass slows down at higher residence time, which increases the carbon content in the volatiles.

2.3.5.3 Oxygen Concentration

Presence of oxygen in torrefaction media increases the extent of combustion reactions, which converts carbon into flue gas instead of leaving it in solid form. Additionally, the combustion in the reactor could increase the temperature of the product endangering the safety of the unit. Therefore, oxygen is not desirable for safe and efficient operation of the torrefaction process. So, torrefaction would require either indirect heating or a continuous supply of hot inert gas. The latter option is not economically feasible. To minimize the energy cost, in a commercial torrefaction unit, flue gas could be used as

both heat source and working media. But flue gas form a combustion process is always associated with some free oxygen. To get more insight into the effect of this oxygen on torrefaction a brief review of this is presented below.

The solid product yield of torrefaction decreases when oxygen is present in the working media. Uemura et al. (2013) and Basu et al. (2013) noted appreciable effect of oxygen on solid yield at 250°C. The extent of this depends on the torrefaction temperature, but. Rousset et al. (2012) observed only negligible changes in the torrefied solid yield at around 250°C.

Presence of oxygen in the working media increases devolatilization reactions that have higher ability to remove the oxygen from the sample compared to that of nitrogen media. But Rousset et al. (2012) observed only a slight change in the values of O/C and H/C for eucalyptus wood under air and the nitrogen media. The O/C and H/C ratios decreased with rise in the oxygen concentration

However, some studies (Basu et al., 2013; Rousset et al., 2012; Uemura et al., 2013; Wang et al., 2012) found that oxidative media shows only minor effects on the heating value of the solid product. Tumuluru et al. (2011) noted some increase in heating value of willow, red canary grass and wheat straw with rise in torrefaction temperature in an inert medium. Lu et al. (2012) noted that heating value of oil palm fiber torrefied in nitrogen is higher than that in air, which agrees with the observation of Tumuluru, but that did not happen for eucalyptus, where oxygen had minor effect on HHV except above 300°C. Another differences between these two biomass is that HHV of air-torrefied oil palm fiber decreased steadily with torrefaction temperature while torrefaction temperature had minor effect on HHV of eucalyptus torrefied in air. The data point being limited it is not certain if this can be taken as an effect of the type of biomass.

Lu et al. (2012) made a comparative study of torrefaction using eucalyptus wood and oil palm fiber in nitrogen and air media. Both solid and energy yield were less in air media than that in nitrogen for both oil palm fiber and eucalyptus wood, but the yields decreased with torrefaction temperature for both types. Lu et al. (2012) used a new parameter (energy-mass co-benefit index to assess the effectiveness of a torrefaction process. Using this index, they concluded that the use of air is suitable for eucalyptus wood but not for oil palm fiber.

Torrefaction under the oxidative media, however, reduces to the torrefaction process time required for a given mass loss (Wang et al., 2012). Table 2.7 presents the torrefaction time required for a torrefaction process at 280°C with different oxygen concentration in the working media. In addition to the time saving, Wang et al. (2012) also proved that flue gas with oxygen could be used as a working media without any significant changes in the torrefaction process and the product. This reduction in torrefaction could have much practical significance as it might reduce the size of the torrefaction reactor and therefore the capital investment required.

Table 2.7: Reduction of process time for similar output in torrefaction process under oxidative environment at 280°C

Parameter	Oxygen concentration in working media (vol. %)				
	0	3	6	10	21
Time for 70% solid product yield (sec)	2640	1690	1540	1260	840
Solid product yield at 2640 sec (%)	70	61.4	56.8	48.6	42.4

Source: Adapted from Wang et al. (2012)

2.3.5.4 Particle Size

Heat source is required to preheat, dry, and devolatilize the biomass for torrefaction process. The amount of heat required depends on the size, shape, and biomass properties. These parameters affect both convective and conductive heat transfer rate from reactor to biomass and within the biomass, respectively. A larger piece of biomass will have less surface area per unit mass, reducing convective heat transfer rate. The larger particle may also have non-uniform heat distribution within the biomass due to anisotropic and heterogeneous properties of biomass. In addition to this, larger particle may face difficulties with volatile diffusion through it because of high mass transfer resistance. Thus, the quality of the torrefaction process may not be identical for all particle sizes. In this context, effect of particle size may be analyzed by estimating Biot and Pyrolysis number of the process.

Mass loss due to torrefaction in smaller particles (size varies from 0.23 to 0.81 mm) is higher than that in larger particles (Peng et al., 2012) due to both lower resistances to diffusion of volatiles and higher heat transfer rate in small particles. For example, Medic et al. (2011) noted a higher mass loss in ground corn Stover compared to that of whole Stover. Even in a bubbling bed reactor that is characterized by high heat transfer rate, Kokko et al. (2012) found higher mass loss in smaller particle compared to that of bigger particle. A finer particle size also increases mass losses in the microwave-assisted torrefaction process (Wang et al., 2012a). They observed mass reduction ratios of 65%, 69%, and 72%, when the particle sizes were in the range of 0.149-0.297 mm, 0.149-0.074 mm, and < 0.074 mm, respectively. Greater intra-particle effect and heat transfer area in the fine particles causes higher reaction temperature, enhancing devolatilization reactions. The effect of particle size on mass and energy yields in torrefaction at different temperature and time is shown in Figure 2.9 It shows a small but consistent increase in mass and energy yields.

On the other hand, a study on large cylindrical particle (size varies from 5 to 25 mm diameter with a constant length of 65 mm) observed lower solid product yield when the diameter of particle size increased (Basu et al., 2013a). They also found that in large particle size the core temperature of particle was greater than that of the furnace it was in, indicating the exothermicity of torrefaction process. This is due to higher heat transfer resistance in large particles compared with that of smaller particles.

2.3.5.5 Reactor Pressure

Biomass torrefaction usually deploys atmospheric pressure condition. Though there are few works (Mahinpey et al., 2009; Mok and Antal, 1983; Seebauer and Staudinger, 1997) of biomass pyrolysis under the pressurized condition, only limited research works (Wannapeera and Worasuwannarak, 2012) have conducted on torrefaction of biomass under elevated gas (nitrogen) pressure. The work of Wannapeera and Worasuwannarak (2012) concluded that the carbon content in torrefied biomass increases when the reactor pressure rises from 0.1 to 4 MPa. This then led to a higher HHV values when compared to that of the product produced at atmospheric pressure torrefaction. The use of elevated reactor pressure provides a good platform to torrefy biomass with high moisture. This is known as wet torrefaction or hydrothermal torrefaction (discussed more in Section 2.2.3.4). This replaces nitrogen by water, but the operating pressure has to be maintained very high. Despite such benefits, only a few works have been conducted so far. This may be due to the possible difficulties in scaling up and operation of the reactor in industrial standpoint.

On the other hand, torrefaction in vacuum pressure may be a good option to avoid the need of nitrogen to maintain the ambient environment. It may enhance the diffusion of volatile gasses and then reduce the residence time to achieve the same level of yield when torrefied at atmospheric pressure. However, it would also be very challenging to develop a large industrial scaled vacuum reactor with no air infiltration.

2.3.6 Effect of Torrefaction on Biomass Properties

Torrefaction process has significant effects on different properties of biomass such as proximate analyses, ultimate analyses, solid residue, heating values, hydrophobicity, grindability, and density and volume of the sample. In the following sub-sections, changes in these properties of biomass due to the torrefaction process are discussed.

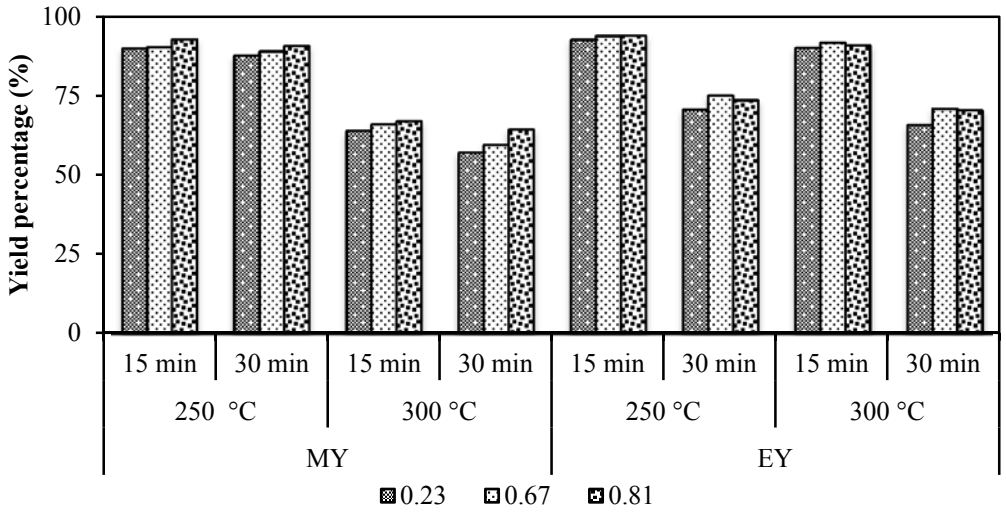

Figure 2.9: Effect of particle size (mm) on mass yield (MY) and energy yield (EY) at different temperature and time

Source: Adapted from Peng et al. (2012)

2.3.6.1 Proximate and Ultimate Analysis

Torrefaction process converts complex polymers of biomass into smaller monomers and then the smaller monomer into condensable and non-condensable volatile gases. This transformation alters both proximate and ultimate analyses of the biomass. Torrefaction drives away volatile matter as well as fixed carbon from a biomass due to decomposition and devolatilization reactions. Although the absolute amount of fixed carbon decreases after the torrefaction process, the fraction of fixed carbon in the torrefied biomass

increases. However, the fraction of ash, the inert and non-combustible material in biomass increases even more because none of it is driven away during torrefaction.

Decrease in volatiles along with the chemical transformation of remaining polymeric components produces a brittle carbonaceous coal like solid torrefied products. The torrefied product would, therefore, have a proximate and ultimate composition different from that of the parent biomass. The change in proximate composition of the torrefied biomass is influenced by both temperature and residence time of torrefaction. Increase in time and temperature reduces the volatile content of biomass (Arias et al., 2008). Typical proximate analyses of torrefied Pine chips, Laucaena, and Eucalyptus wood at different torrefaction temperature is shown in Figure 2.10.

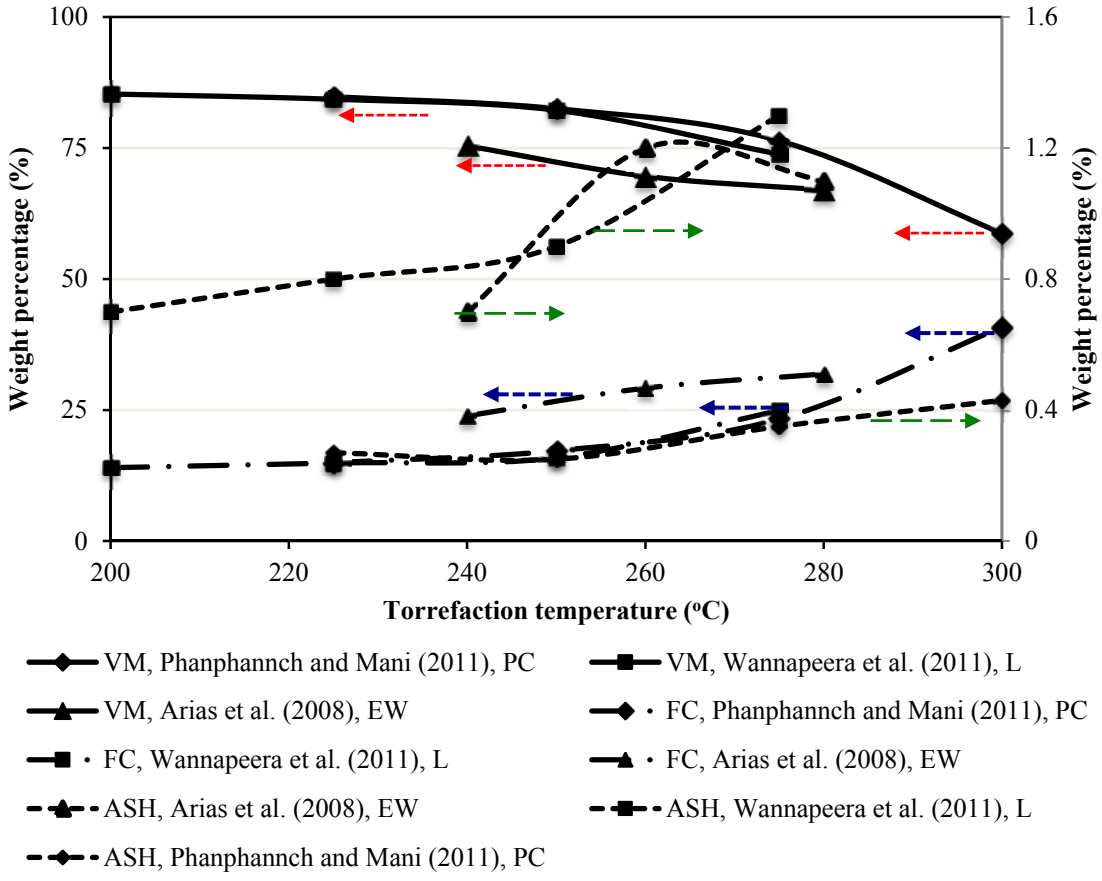

Figure 2.10: Volatile matter (VM), ash content (ASH), and fixed carbon (FC) content of biomass in wt. % dry basis with torrefaction temperature at a residence time of 30 min (PC=Pine chips, L=Laucaena, and EW=Eucalyptus wood)

Carbon usually contributes 60-85% of the total mass of coal composition whereas oxygen content ranges from 5-20% (Prins et al., 2007). Biomass on the other hand contains much lower carbon (50%) but much higher oxygen (45%). This indicates that O/C ratio of biomass is very high compared with that of coal. This significantly reduces the energy density of biomass. Therefore, torrefaction – a technology capable of reducing O/C in biomass – has a greater impact on the energy density of biomass.

Arias et al. (2008) found about 26% reduction in oxygen and 24% increment of carbon content in eucalyptus wood after it is torrefied at 280°C for 3 hours. These changes are in contrast with that of Chen et al. (2011) who observed around 45% less oxygen and 44% more carbon content in Lauan block after it is torrefied at 280°C in 2 hours. This indicates that longer residence time alone does not necessarily have a major effect on change with carbon and oxygen content in a biomass. Other than operating conditions, changes in the ultimate analyses also depend on particle size, type of materials, and method of torrefaction. The rate of increasing carbon content is higher in severe torrefaction condition. For instance, the carbon increment rate was found 0.88 wt. % of dry ash free carbon per hour at 220°C, while it was 1.55% and 3.66% per hour at 250°C and 280°C, respectively. While carbon content was increased in torrefied products, both oxygen and hydrogen were decreased (Bridgeman, et al., 2008; Felfli et al., 2005). A typical chemical composition of briquettes after torrefaction is shown in Figure 2.11. One easily notes here that while carbon percentage increases, the hydrogen decreases with both temperature and residence time.

2.3.6.2 Solid Product and Energy Yield

Solid product yield and energy yield are important quantitative and qualitative measures of a torrefaction process. Solid product yield is defined as a ratio of final mass of solid torrefied product to initial mass whereas energy yield is a ratio of final energy in solid product to initial energy content of raw biomass. Both solid product and energy yields are expressed in dry basis or in dry and ash free (daf) basis.

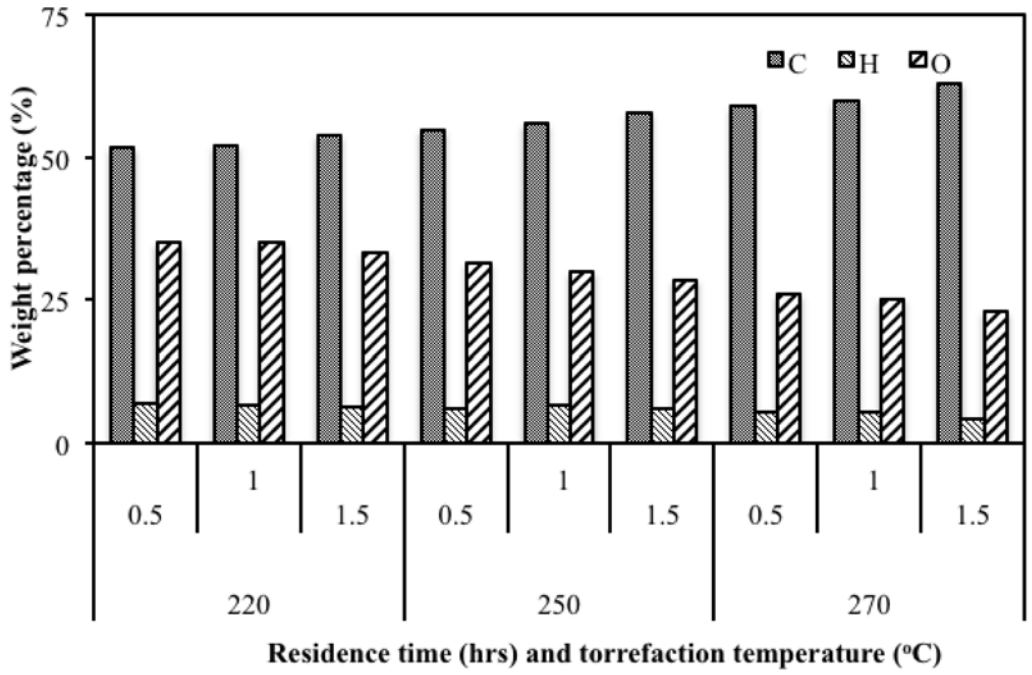

Figure 2.11: Chemical composition (in dry and ash free basis) of briquette at different torrefaction temperature and residence time
Source: Adapted from Felfli et al. (2005)

Solid Product Yield

The torrefaction process yields solid, condensable (liquid), and non-condensable products (light volatiles) among which solid is the desired product (Wang et al., 2011). The fractions of individual products vary with operating conditions. The solid product is made of original sugar structures, modified sugar structures, newly formed polymeric structures, and ash content whereas condensable products comprise mainly of water, organics (sugars, poly-sugars, acids, alcohols, furans, and ketones), and lipids (tarpenes, phenols, waxes, fatty acids, and tanins). The non-condensable product is a mixture of gases like CO_2, CO, CH_4, C_xH_y, toluene, and benzene (Bergman, et al., 2005a; Yang et al., 2007). The condensable product contains water vapor and heavy tars. This liquid fraction of the torrefaction product depends on process temperature and time. Figure 2.8

also shows how the fraction of condensable product changed with residence time and temperature in a typical case. This effect might be due to decomposition of molecules with hydroxyl groups, releasing more water vapor. For instance, an increase in water vapor from 7.6% to 17.8% was reported in Wannapeera et al. (2011) when the torrefaction temperature increased from 200°C to 275°C.

The fraction of solid product yields varies widely from 50% to 97% (Felfli et al., 2005) depending on the temperature and residence time. The solid yield also depends on the type of biomass materials (Prins et al., 2006a). Figure 2.12 shows how the solid product yield depends on the hemicellulose content of the biomass. It reveals that the lignocellulosic biomass with higher hemicellulose composition has lower solid product yield. For instance, the willow, which has the least hemicellulose content of 14% compared to 30% with that of reed canary grass and 31% with that of wheat straw, shows the highest solid product yield (Bridgeman et al., 2008). High-pressure like a pressurized torrefaction system could increase the solid product yield. This could be due to the possible trapping of heavy volatiles within the pores of biomass. However, the trapped heavy volatiles may devolatilize into light volatiles that easily escape from the biomass when the torrefaction temperature and the residence time are increased. For instance, Wannapeera and Worsauwannarak (2012) found an increase in the solid product yield from 88.2% to 89.9% at 200°C when reactor pressure increased from atmospheric condition (0.1 MPa) to 4 MPa. But they also observed a gradual decrease in the solid product yield with rise in temperature from 225°C to 250°C.

Energy Yield

Losses in quantitative measure (solid product yield) do not show any importance while selecting an operating condition of the torrefaction process. Higher mass loss could be desirable if the qualitative measure (energy yield) is within an acceptable range (Range depends on individual needs). Therefore, the quality of solid product, which is measured in term of the higher heating value of the torrefied biomass, is of greater importance.

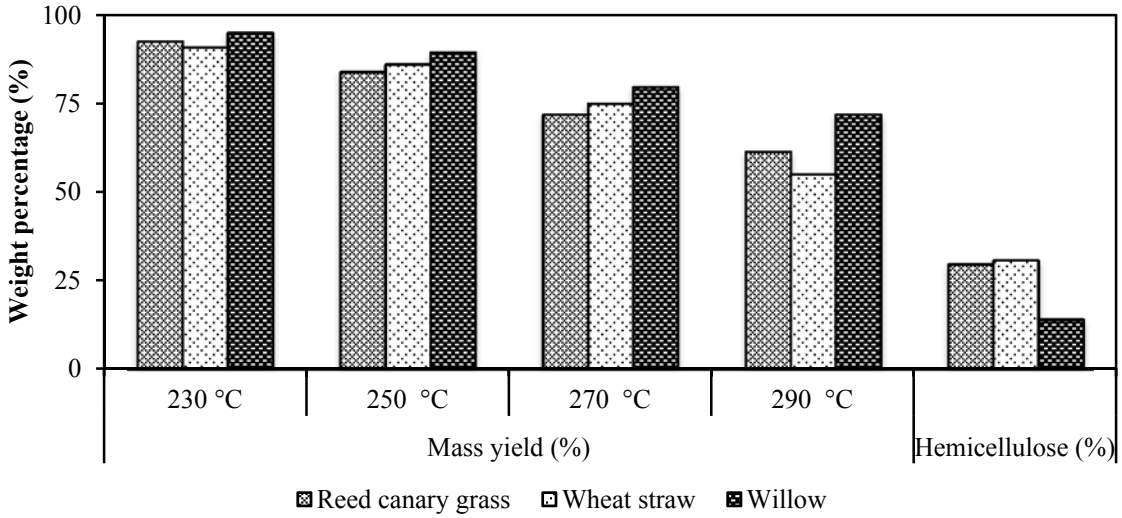

Figure 2.12: Energy yield and solid product yield (mass yield) in dry and ash free basis from the torrefaction of reed canary grass, willow and wheat straw (residence time of 30 minutes) showing effect of temperature and biomass type

Source: Adapted from Bridgeman et al. (2008)

Heating value of torrefied biomass increases because it has more C-C and C-H bonds with aromatic molecules (Ben and Ragauskas, 2012) with an ability to release more energy than O-H and C-O bonds in the raw biomass. Reduction in hydrogen and oxygen reduces the O/C and the H/C ratios of biomass. This moves the torrefied biomass towards the coal side in the Van Krevelen diagram (Figure 2.13). Higher torrefaction temperature and residence time decrease O/C and H/C ratios and move the torrefied product close to that of coal. This suggests that the formation of CO_2 and H_2O increases with temperature and residence time due to the release of oxygen from biomass. For example, at different residence time and temperature, O/C of deciduous wood decreases from 0.70 to 0.52 (Prins et al., 2006). Biomass with higher hemicellulose, which has the highest oxygen compositions, is more likely to produce an energy dense product. This indicates that the energy density of the solid product also depends on the type of biomass. But the question is how the energy density varies with the type of biomass. Higher the lignin content, the more energy will be extractable from the biomass. Thus the torrefied solid product from a biomass with higher lignin content becomes more

energy dense fuel compared to others with lower lignin content. Thus, a complete elimination of both cellulose and hemicellulose contents of wood produces a product that could have energy density similar with that of the coal. Ben and Ragauskas (2012) noted that the energy density of loblolly pine increased from 20.16 MJ/kg to 32.34 MJ/kg (dry basis) when the torrefaction was carried out at 300°C for 4 hours.

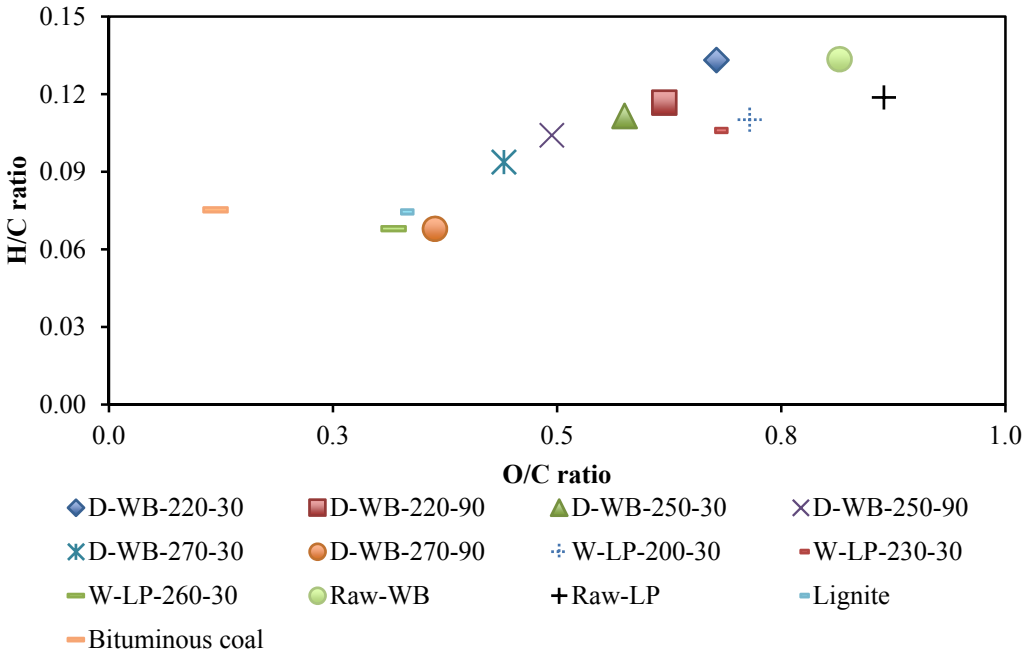

Figure 2.13: Van Krevelen diagram of different fuels (Notation: Type of torrefaction-biomass type-temperature-time; D=dry torrefaction; W=wet torrefaction; WB = briquette of wood (Felfli et al., 2005); LP= Loblolly Pine (Yan et al., 2010); and Lignite and bituminous (McKendry, 2002))

An increase in energy density of torrefied solid product could be expressed as energy enhancement factor (EDF), which is defined as a ratio of higher heating value of torrefied to that of raw biomass. This is different from energy yield, but could be used to determine it. The energy yield of a torrefaction process also varies with the type of biomass. The biomass with higher lignin content produces higher energy yield because they have higher solid product yield as well as higher energy density enhancement

factor. For instance, Bridgeman et al. (2008) observed energy yields of 77%, 78% and 86% for wheat straw (7.7% lignin), reed canary grass (7.6% lignin), and willow (20% lignin), respectively after they are torrefied at 270°C for 30 minutes. The willow with 20% initial lignin content attained the energy density enhancement factor of 1.196 compared to 1.095 by reed canary grass and 1.118 by wheat straw.

2.3.6.3 Hydrophobicity

Torrefaction substantially removes both free and bound moisture of biomass. The free moisture inside capillaries of fibers shows surface wetness whereas the bound moisture determines the hydrophilic or hygroscopic (affinity for water) nature of biomass. Though drying could remove the surface moisture as well as some of the bound moisture of biomass, its hydrophilic property makes it regain the moisture from the surrounding air when stored. Equilibrium moisture content (EMC) of raw biomass influences its hygroscopic nature. Lowering the EMC reduces the moisture absorbing capacity and thereby increases the hydrophobicity of biomass. The equilibrium moisture content also depends on the chemical composition and functional groups of biomass (Acharjee et al., 2011). The EMC highly varies with the relative humidity of air. Table 2.8 shows how a variation in EMC of a hydrothermally torrefied biomass is influenced by temperature and relative humidity of air in an atmospheric pressure. Torrefaction process has a positive effect on humidity uptake from the air. The torrefied pellets can be considered more hydrophobic than the reference biomass pellets. A higher torrefaction temperature also has a favorable influence on hydrophobicity. Wood and straw pellets are known to disintegrate quite rapidly when exposed to water. After 15 minutes of immersion water absorption in wood pellet is 76% while that of torrefied pellet reduces it to 55% (Torrent, 2011).

Table 2.8: Variation of the equilibrium moisture content (EMC) with hydrothermal torrefaction temperatures at different relative humidity

Materials	Torrefaction temperature (°C)	EMC (%) at relative humidity 11.3%	EMC (%) at relative humidity 83.6%
Raw biomass	-	3.5±0.5	15.6±0.9
Torrefied biomass	200	1.8±0.5	12.8±0.7
	230	0.9±0.3	8.2±0.7
	260	0.4±0.3	5.3±0.03

Note: $EMC=(W_e-W_{dry})/W_{dry}*100\%$; where W_e and W_{dry} refer to weight of sample at equilibrium condition and the weight of bone dry sample, respectively.

Source: Adapted from Acharjee et al. (2011)

The ability to resist bound moisture is known as hydrophobic nature of biomass. Hydrophobicity is also related to its ability to destruct hydrogen bonds. Decomposition of hydroxyl groups and lignin coating in biomass particles are believed to be the major causes of increasing hydrophobicity in torrefied biomass (Li et al., 2012). Torrefaction can reduce the EMC of biomass down to about 3% (Lipinsky et al., 2002). Equilibrium moisture content is directly related to moisture absorption capacity of biomass. Li et al. (2012) found a reduction in the moisture adsorption capacity from 20.7% wt. to 13.6% wt. in torrefied pellets. Similarly, Sule (2012) analyzed the effect of temperature on moisture absorption capacity and they found about 20% drop in moisture absorption when torrefaction temperature increased from 230°C to 270°C. Reduction in moisture reabsorption capacity of biomass is due to ability to break and remove carboxyl and hydroxyl groups during torrefaction. This type of pretreatment of biomass will be a good as it converts biomass into non-polar substances, which are less capable of forming hydrogen bonds. For instance, Shoulaifar et al. (2012) clearly noted a decrease in the EMC of torrefied spruce wood with destruction of carboxylic groups.

2.3.6.4 Grindability

Biomass possessing visco-elastic and plastic behaviors dissipates much energy before failure, increasing the energy cost of grinding (Repellin et al., 2010). The energy required for grinding process of any materials could be defined as its grindability. The main limitations in grinding of raw biomass are fibrous and tenacious natures, which create difficulties in grinding. Thus, the process that reduces fibrous and tenacious behavior of biomass enhances the overall performance of size reduction equipment.

Grindability is characterized by the nature of particle size distribution and sphericity of particles. Grindability is usually expressed by the Hardgrove Grindability Index (HGI) that measures the level of difficulty in grinding solid sample into powder form (Wu et al., 2012). The higher the value of HGI, more easily a solid fuel can be reduced to fine powder (Shang et al., 2012; Wu et al., 2012). The value of HGI of torrefied biomass increases with residence time and torrefaction temperature (Wu et al., 2012). This is due to harder and more brittle nature of torrefied product. Wu et al. (2012) speculate that rearrangement of structure and depolymerization of different molecules during thermal treatment is one of the reasons of producing such hard and brittle product. Shang et al. (2012), on the other hand, reported that removal of hemicellulose during the torrefaction process is the main reason of increasing the HGI value of torrefied product than raw biomass.

Decrease in fibrous nature of torrefied biomass produces more spherical and isolated particles when grinded. This improves in co-milling and blending of biomass with coal, and then increases the co-firing potential of biomass in coal-fired power plants (Bridgeman et al., 2010). An increase in the sphericity of particle or a decrease in slenderness of particle was also presented in Arias et al. (2008). Figure 2.14 shows the changes in the particle size distribution of biomass torrefied at different residence time and torrefaction temperature. It shows that the fraction of the finest particle size (< 75 μm) is maximum at torrefaction temperature of 280°C and residence of 30 minutes.

As discussed before, torrefaction with an ability to reduce fibrous nature in torrefied biomass, it significantly reduces the energy required for grinding wood (Bergman et al., 2005). For instance, Svoboda et al. (2009) reported a decrease in milling energy by 3-7 times than untreated biomass. However, it varies with operating conditions of the torrefaction. Repellin et al. (2010a) found that the grinding energy of torrefied spruce is reduced to around 200 kWh/tonne and 400 kWh/tonne at 280°C and 200°C, respectively compared with that of 750 kWh/tonne for raw spruce. The effect was more prominent in torrefied pine chips than in logging residues.

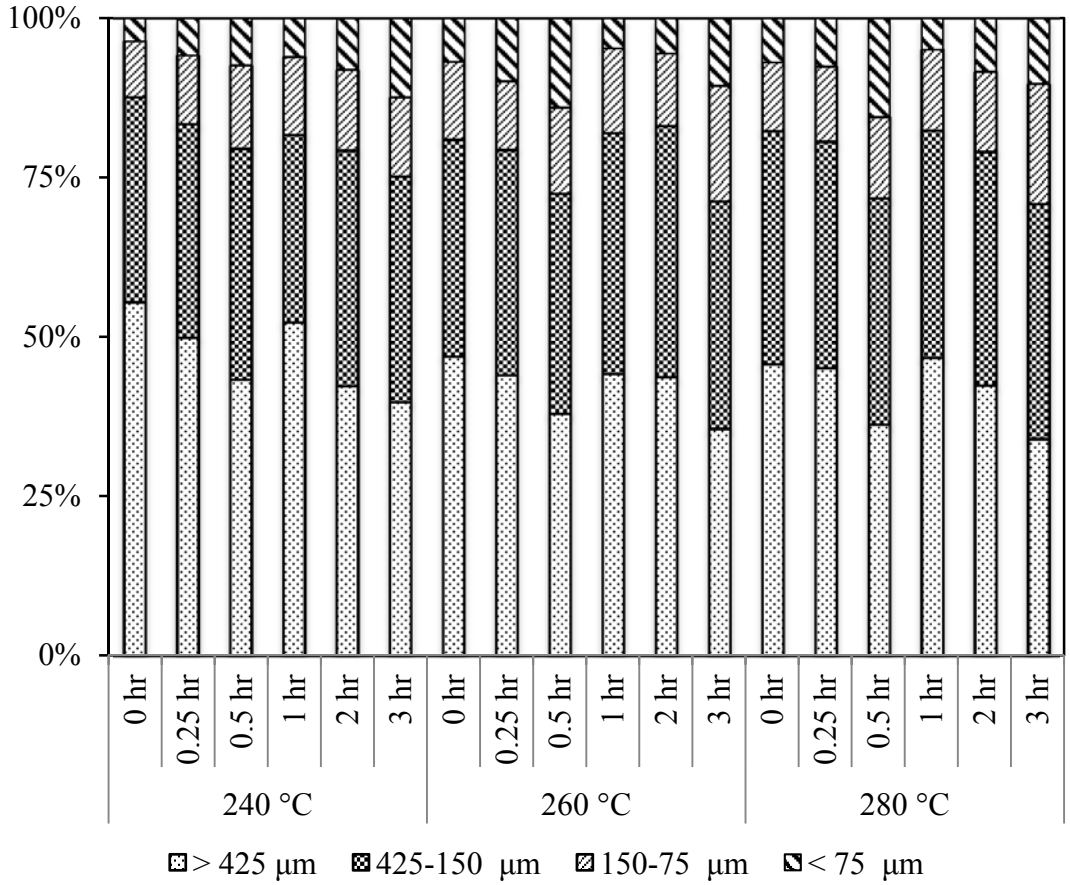

Figure 2.14: Distribution of particle size at different operating conditions of eucalyptus wood (particle distribution of raw eucalyptus wood 71% >425; 18.7%, 425-150; 4.7%, 150-75; and 5.4%, < 75)

Source: Adapted from Arias et al. (2008)

The energy required for grinding or milling also varies with the type of biomass, the level of moisture content, and the extent of fineness. A decrease in specific grinding energy by one-tenth (from 237.7 kWh/tonne to 23.9 kWh/tonne) for pine chips and one-sixth (from 236.7 kWh/tonne to 36.7 kWh/tonne) for logging residues was noted when the biomass was torrefied at 300°C for 30 minutes (Phanphanich and Mani, 2011). Similar results were also reported for rice straw and rape stalked in Deng et al. (2009). Figure 2.15 shows changes in the specific grinding energy consumption and mean particle diameter of pine chips and logging residues at different torrefaction temperatures. It shows that both mean particle size specific grinding energy consumption decreases with temperature. The effect was more prominent in torrefied pine chips than in logging residues.

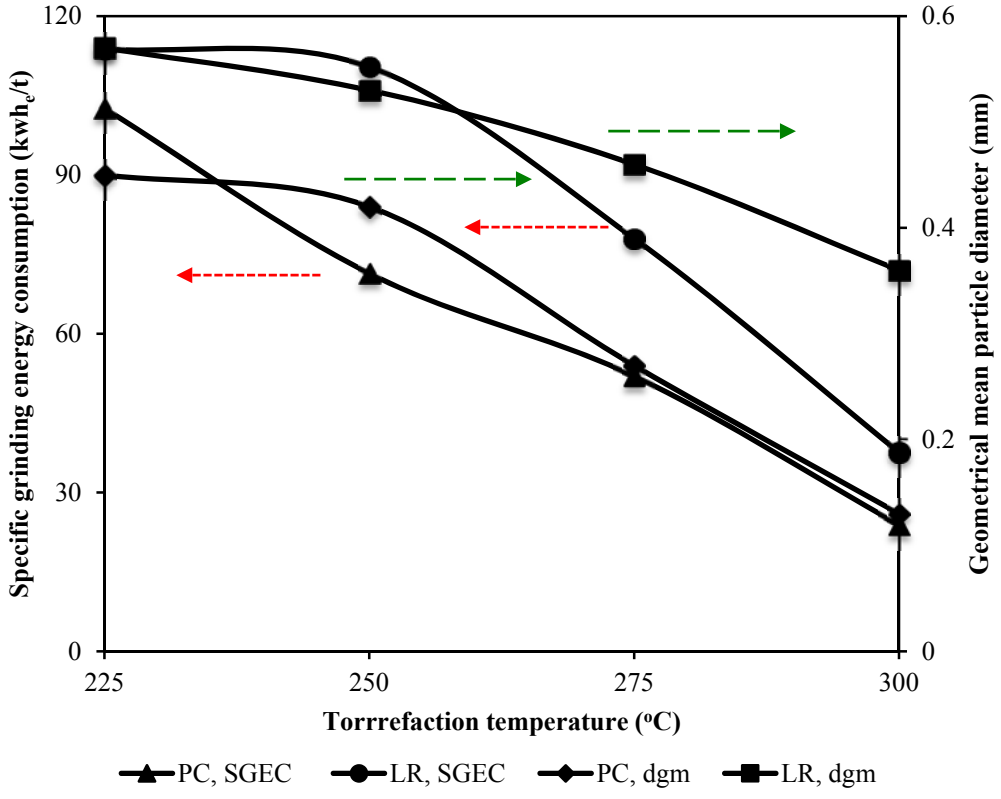

Figure 2.15: Temperature effect on specific grinding energy consumption in kWh per tonne and geometrical mean particle diameter of pine chips and logging residues
Source: Adapted from Phanphanich and Sudhagar (2011)

Along with the grinding energy, particle size distribution, sphericity and particle internal surface area also determine the flowability and combustion behavior in co-firing plants (Tumuluru et al., 2011). The mean particle size of ground torrefied biomass (as shown in the Figure 2.15) decreases with the torrefaction temperature (Deng et al., 2009; Phanphanich and Mani, 2011). The particle size distribution curve also skews more towards lower particle sizes at different torrefaction temperature compared to untreated biomass (Phanphanich and Mani, 2011; Repellin et al., 2010). Repellin et al. (2010) suggested a linear relationship between particle size and anhydrous weight loss during torrefaction. The fineness of particle after torrefaction of raw biomass not only depends on the operating condition but also varies with the type of biomass. For example, Phanphanich and Mani (2011) found the fineness fraction of particle 82% in pine chips and 51% in logging residues. This difference in the fineness of the particle, though solid product yields are similar for both pine chips and logging residues, is not well explained in literatures. Thus, torrefaction because of its potential to reduce the fibrous and tenacious nature, the net grinding energy, the slenderness ratio, and the particle size is being promoted as one of important biomass pretreatment methods.

2.3.6.5 Density and Volume of Particle

For design of biomass handling and transport systems, a good knowledge of its density and volume change after torrefaction is necessary. Devolatilization process creates voids due to escape of volatiles and thereby reduces density of the product. Shrinkage in the physical dimensions (length and diameter), which reduces volume of the product, also occurs during the biomass devolatilization process. It may reduce the extent of density reduction due to mass loss. The shrinkage of solid is due to loss of water, rearrangement of chemical bonds, and coalescence of graphite nuclei within the solid structure (Moghtaderi, 2006). The shrinkage of particle is significant at high temperature (1000-1300°C) pyrolysis and in thermally thick particles (Biot number > 10) (Moghtaderi, 2006), but it may also be observed at low temperature torrefaction. Only limited information is available on the impact of torrefaction in the shape and size of particle. A

preliminary study of Basu et al. (2013a) found that both volume and density of the cylindrical poplar are reduced after the torrefaction process. They found that decrease in diameter was higher compared with that of length of the product. They also reported that changes in dimension are due to drying process below the fiber saturation point and devolatilization reactions causing to damages in fibers. In addition to this, the density of torrefied product at a given torrefaction temperature was found higher in a slender particle with high length to diameter (*L/D)* ratio. This is due to higher solid product yield at higher *L/D* of the particle (Basu et al., 2013a).

Generally, raw biomass swells because of moisture. Swelling of biomass occurs when the water vapor diffuses into cell lumen and then from the cell lumen to the cell wall. Swelling of woody biomass is a reversible process that continues to swell until the moisture level reaches to the fiber saturation point, and starts shrinking once it loses the moisture below that point (Rowell, 2005). Water molecules attracted by hydroxyl groups of polymeric components of lignocellulosic biomass also occupy the space between the cell wall components (Homan et al., 2012). Torrefaction process not only removes the moisture but also increases the non-polar molecules in the wood through devolatilization and depolymerization reactions. This naturally brings some changes in the physical size of the particle.

Torrefaction reduces the bulk density of biomass though because of its less sharp shape one would expect higher packing density. Torrefaction however increases the porosity of biomass. Increase in porosity reduces the density of the torrefied product. Changes in density depend on operating parameters of torrefaction as well as type of biomass. Figure 2.16 shows the variation in reduction of bulk density of biomass after torrefaction at different temperature and residence time. The porous product becomes more brittle that significantly reduces the power required for size reduction compared to that of raw biomass. In addition to this, torrefaction reduces the slenderness of particle, increasing the sphericity of ground particles (Figure 2.15).

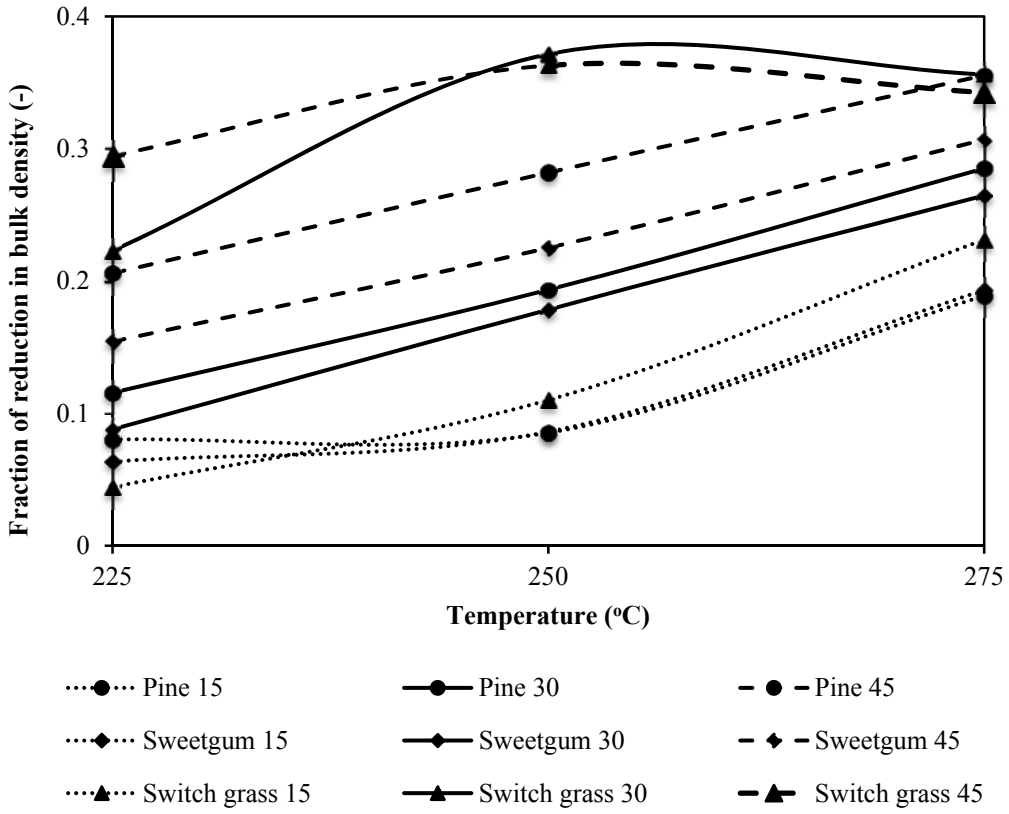

Figure 2.16: Variation in fractional reduction in bulk density after torrefaction (Bulk densities of raw pine, sweet gum and switch grass are 159.2, 182.1, and 117.1 kg/m^3, respectively)

Source: Adapted from Carter (2012)

2.3.6.6 Color of Torrefied Products

The color of biomass changes through torrefaction due to losses of surface (free) moisture, bound moisture, and light volatile gases at different stages of torrefaction. The color of the torrefied biomass depends on torrefaction conditions. For example, the color changes from brownish to dark when the treatment time and temperature are increased. Changes in wood color under the thermal treatment are mainly due to hydrolysis and oxidation reactions (Torres et al., 2010). The changes in color can also be used as an

indicator of the degree of conversion (Bourgois et al., 1991). The color of torrefied biomass also depends on the type of raw biomass (early wood or late wood) and their densities (Aydemir et al., 2010). They also found that the color of wood, which is affected by color of extractives, also changes due to variation in extractive compositions. Changes and transformation of hemicellulose and lignin under the thermal degradation, which depends on pH level, moisture content, heating medium, exposure period, and type of species, produce dark color in a product (White and Dietenberger, 2001). Sundqvist (2004) explained changes in color after the thermal treatment of biomass through absorption, reflection, or scattering phenomena of the visible light incident (380-800 nm) on the surface of wood. The grayish color of wood surface at normal temperature is due to the high concentration of hemicellulose and cellulose that have higher scattering ability of incident light. On the other hand, formation of different chromophoric groups such as carbonyls, hydroxyls, methoxyls, and phenolic compounds with an ability to absorb an incident light are also responsible for the dark color (Sundqvist, 2004). Color variations such as brown, purple, black, and red-orange may be observed in the heartwood of different species, depending upon the type of phenolic compounds formed during torrefaction viz. tannins, lignans, flavonoids, and quinones, respectively (Sundqvist, 2004). Chemical reactions forming aldehydes and phenols also change the color of products. Thus, depending upon time and temperature of thermal treatment, the color of product changes from light brown to dark brown (Aydemir et al., 2010). Figure 2.17 shows the effect of temperature on the color of torrefied pine chips.

Figure 2.17: Effect of temperature on the color of torrefied pine chips at (a) Raw, (b) 225 °C, (c) 250 °C, (d) 275 °C, and (e) 300 °C

Source: Phanphanich and Mani (2011)

Furthermore, during drying stage, movement of hydrophilic and lipophilic extractives towards the surface of wood produces a brown strain in softwoods (Torres et al., 2010). The color of surface of wood is also affected by the concentration of low-molecular-weight sugars, sugar alcohols, and nitrogenous compounds. An increase of the concentration of the low molecular weight sugars at the surface (0-3 mm) also influences the surface color (Terzie and Boutelje, 2007). The color response of wood under the hydrothermal treatment can be studied using color coordinates Lightness (L^*), Chroma (C_{ab}^*), hue (h), and color difference (ΔE_{ab}^*) (Sundqvist, 2004).

2.4. EFFECT OF TORREFACTION IN OTHER PROCESSES

2.4.1 Pelletization

Pelletization – a densification process that produces compacted products of desired shaped from biomass. It requires powdered biomass in designated particle sizes. This means a biomass easier to grind makes superior raw material for biomass pelletization. Though pelletization avoids some of major problems like transportation difficulties, low bulk density, low energy density, and handling complexity, normal wood pellets will have a strong affinity towards moisture and reabsorb humidity from surrounding air during storage period. Torrent (2011) shows photographs of raw biomass pellets and torrefied biomass pellets after both were soaked in water for 15 minutes. Owing to reabsorption of water raw biomass pellets nearly disintegrated, while torrefied biomass pellets still retained its shape. Reabsorption of moisture enhances physio-chemical degradation as well as microbial disintegration of biomass (Duncan et al., 2013). This limitation of the normal pellets is easily avoided by using a torrefied biomass as a feedstock.

Though one expects pelletization of torrefied wood to be easier because of increase percentage of lignin after torrefaction, in reality that does not necessary happens. Li et al. (2012) reported that pelletization of torrefied biomass is more energy intensive than raw

biomass. Due to the lack of sufficient hydrogen bonds in torrefied biomass, pelletization process consumes more compression energy (Li et al., 2012; Na et al., 2013; Stelte et al., 2011). The compression energy will thus increase while pelletizing dried biomass particles. The dried biomass materials are hard to plasticize, and possess a significant frictional resistance (Gilbert et al., 2009; Stelte et al., 2011). For example, the compression pressure in the pelletization process of torrefied spruce increased by approximately 7 times that required for pellets from raw spruce (Stelte et al., 2011). They also reported adverse effect of torrefaction temperature on the pellet quality.

One of the major advantages of producing pellet using torrefied biomass is its hydrophobic nature. Hydrophobicity of pellets increases with increasing the torrefaction temperature (Duncan et al., 2013; Li et al., 2012). The hydrophobicity of pellet increases when pellets are produced using smaller particle size (Duncan et al., 2013). On the other hand, pelletization followed by torrefaction process is more energy efficient than a conventional pelletization process. The TOP process of ECN for wet sawdust shows that the volume of pellets production could reduce drastically for the same energy output in the TOP method (Agar and Wihersaari, 2012). In the TOP method, thermal energy input decreases by 50% of the thermal energy requirement of the conventional method.

Due to the lack of hydroxyl groups of moisture and hemicellulose content, the bonds between individual particles in the torrefied pellet are also weaker compared to that for normal pellets (Na et al., 2013). Shang et al. (2012) noted that the strength of pellets from Scot Pine torrefied at 250°C was significantly reduced, and the pellets are brittle, uneven, and non-uniform in physical appearance. Brittle torrefied pellets are difficult to handle and transport because they are easily breakable, and produce dust (Gilbert et al., 2009). Durability of torrefied pellet is low, and it decreases even more at higher torrefaction temperature. Mass fraction of dust in pellets using torrefied biomass increases with the temperature (Gilbert et al., 2009).

2.4.2 Gasification

Biomass gasification is a clean and convenient option for biomass to energy conversion. Some characteristics of raw biomass could adversely affect the gasification process. For instance, fibrous nature of biomass causes difficulties in pulverizing and feeding to the entrained flow gasification system (Erlach et al., 2012).

Additionally, biomass generally has higher O/C ratio than that in coal. A feedstock with high O/C ratio increases the extent of oxidation reactions in a gasifier, resulting in low gasification efficiency (Prins et al., 2006) as well as higher exergy loss. For example, gasification of biomass having high O/C ratio of 0.6 shows more exergy loss than that with coal with low O/C of 0.3 (Prins et al., 2007). So, a reduction in oxygen content of a biomass through torrefaction pretreatment prevents potential of oxidation reactions, increasing the suitability of biomass for gasification process.

As torrefied biomass has low O/C ratio and lower moisture level, one expects less oxidation reaction to convert CO to CO_2. Solid fuels with low O/C and H/C ratios are also desirable in gasification process due to its higher energy content (Yusup et al., 2013). The quality of product gas depends highly on the chemical composition of the feedstock and the operating gasification temperature. For example, Prins et al. (2007) recommended an optimum gasification condition with O/C of 0.4 and 0.3 at gasification temperatures of 927°C and 1227°C respectively. Additionally, a higher temperature in the gasification zone could be achieved due to relatively low moisture content in torrefied biomass. This will enhance reforming reactions and increase H_2 and CO concentration in the product gas. So higher the torrefaction temperature, higher will be the H_2 and CO concentration in the product gas.

Figure 2.18 shows the effect of torrefaction condition on the gasification product of the torrefied biomass. One notes here a variation in the composition of the product gas obtained from gasification of torrefied sawdust at different torrefaction temperature. It is

also compared with that of producer gas composition produced from gasification of raw biomass. Though the cold gas efficiency of torrefied sawdust obtained at different torrefaction temperature is higher compared to that for raw sawdust, the torrefaction condition that produces the largest surface area or develops the smallest pore size within the biomass shows significant effects on gasification efficiency. For example, Qing et al. (2010) observed the highest cold gas efficiency from the torrefied sawdust at 250ºC. Interestingly, Prins et al. (2006) observed reduction in overall efficiency gasification for torrefied wood compared with that of raw biomass. Such reduction was even more significant when the gasification was carried using the torrefied biomass produced at higher temperature. This may be due to higher losses in volatiles at higher torrefaction temperature without adding their energy values in the product gas. Couhert et al. (2009) also observed poor performance in steam gasification at 1200ºC in a fixed bed reactor of torrefied wood compared with that of the gasification of the normal char. But, the quality of syngas, which is a ratio of sum of H_2 and CO to CO_2, improves significantly when the torrefied biomass produced at higher temperature was used as a feedstock.

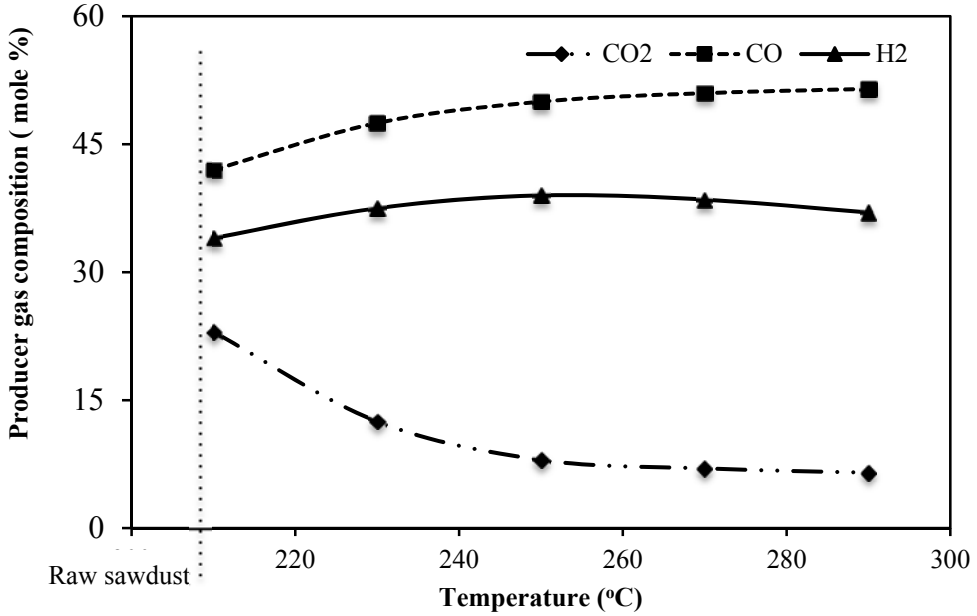

Figure 2.18: Producer gas composition of torrefied sawdust at different temperature (residence time 20 min)

Source: Adapted from Qing et al. (2010)

Exploratory work by Raut et al. (2013) showed that tar production from gasification of torrefied biomass is lower than that from gasification of the raw biomass. This is due to breakdown of tar producing cellulose in biomass. Phanphanich and Mani (2011) found that due to this high hemi-cellulose and lignin in the biomass produce more tar during the gasification. The torrefaction process reduces the lignocellulose structures of raw biomass and minimizes the tar content. Furthermore, Prins et al. (2006) suggested that the controlled or proper temperature of torrefaction would minimize pyrolysis of cellulose and avoid tar formation.

Torrefaction of biomass could enhance the gasification process. Because of its ability to produce more small size and spherical particles compared with that of raw biomass, the limitation of entrained flow gasification could be avoided and thereby increasing the performance of gasifier. For example, Tremel et al. (2012) found that the overall gasification efficiency and carbon conversion efficiency of the entrained flow gasifier was observed superior for smaller (80-160 μm) particles torrefied biomass compared with that of larger (160-250 μm) particles. This could help to use the torrefied biomass in the facility of the entrained flow coal gasification without any modifications.

Gasification rate, which varies with the local heterogeneous reaction between char and gasifying agent, depends on an intrinsic reaction rate (Mani et al., 2011). The reaction rate of char would depend mainly on the porosity of particle or internal surface area. Higher the internal surface area, easier it is to transport fluidizing media and heat into the particle core. It increases conversion rate of char in gasification process. Thus, torrefaction that alters specific surface area of pores inside biomass will have greater impact in the gasification rate. Changes in the specific surface and cold gasification efficiency with torrefaction temperature are therefore closely related (Figure 2.19). Figure 2.19 shows that torrefaction of biomass at 250ºC produces products with the maximum specific surface area and achieved the highest cold gas efficiency. Increase in internal surface area enhances heterogeneous reactions between char and CO_2/H_2O and

leads to higher char conversion rate. The higher char conversion rate increases the gasification temperature and thereby improves the quality of producer gas.

Gasification rate of char depends on how it was produced. A detailed study on gasification reactivity of char is examined by Fisher et al. (2012). They found that the gasification reactivity reduced after the torrefaction process. They also speculated that the char from torrefied biomass having less volatiles compared that in raw biomass may have low pore formation and thus reduce to lower surface area. A study by Raut (2014) reported that the formation of secondary char (more stable char than the primary char) in the torrefied biomass leads to a lower reactivity of char from the torrefied biomass.

Combination of torrefaction and gasification is similar to a two-stage pyrolysis and gasification (Qing et al., 2010). This follows the principle of two-stage gasification in which the first stage (pyrolysis zone) uses syngas from second stage (gasification zone) as a heat source and the second stage (gasification zone) uses the pyrolysis gas from first stage as a heat source for gasification reactions (Henrich et al., 2008). The combination of torrefaction and gasification minimizes the problem of integrating heat source for the torrefaction process. Figure 2.20 shows a typical coal co-gasification integrated with torrefaction system.

2.4.3 Combustion

Combustion is the most widely used conversion technique to release energy from a fuel. As the main motive of torrefaction is to increase the share of biomass in power production and to decrease the emission level by avoiding coal use, torrefied biomass should have combustion characteristics comparable to those for coal. This section presents a review of combustion issues of torrefied biomass.

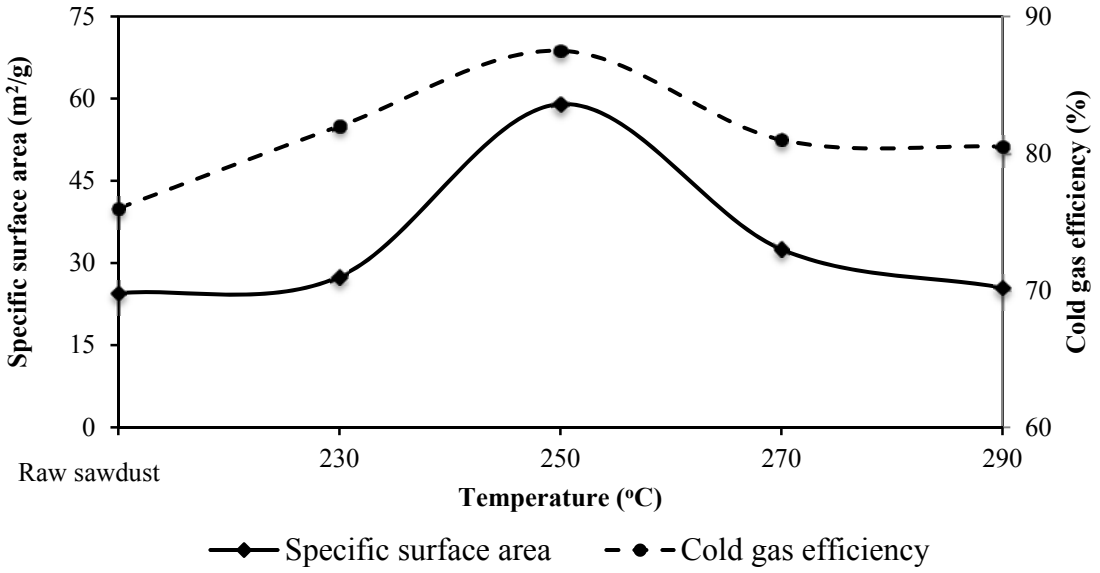

Figure 2.19: Effect of torrefaction temperature on cold gas efficiency and specific surface area of pores (residence time 30 min)

Source: Adapted from Qing et al. (2010)

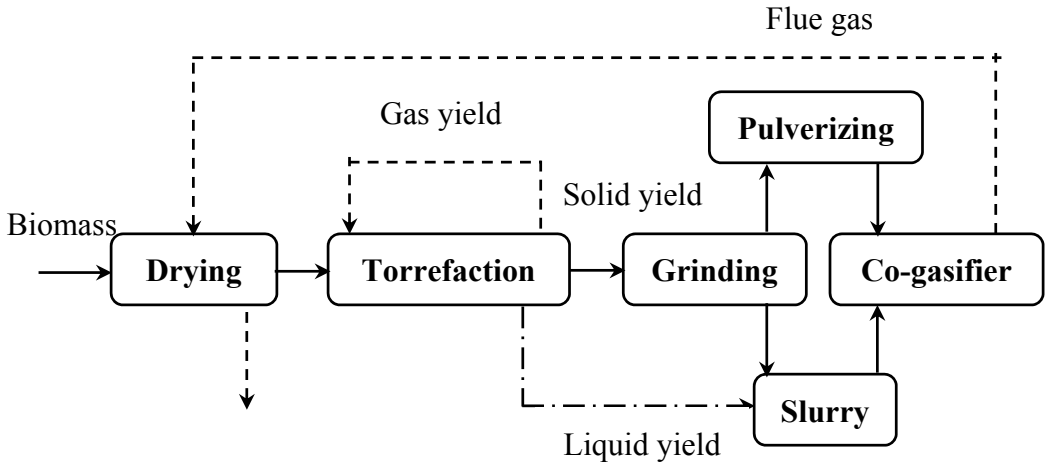

Figure 2.20: Typical an auto-thermal torrefaction integrated with coal co-gasification

Source: Adapted from Deng et al. (2009)

Torrefied biomass is thermally more stable than raw biomass and produces higher heat of reactions during combustion (Bridgeman et al., 2008). Decrease in the reactivity is also related with the increase in the fixed carbon content that has slower reaction rate

than the volatile matter of biomass. The exothermicity of torrefied sample is higher than that of raw biomass and it increases with the severity of torrefaction process. This is due to higher quality of the volatile and porous char in the torrefied product. In their TGA studies Arias et al. (2008) found two distinct peaks of mass loss rate, representing combustion of cellulose and lignin. The activation energy of the second stage combustion is not affected by the torrefaction condition as it is the combustion of the least reactive component – lignin. The activation energy of the first stage combustion increases with severity of torrefaction (temperature and residence time).

Burnout rate of biomass decreases after torrefaction because of low volatile content in torrefied biomass (Chen et al., 2012). Burning of torrefied biomass takes longer time for the above reason compared to that of raw biomass. This effect is more prominent in torrefied biomass at higher temperatures because of higher volatile reduction potential. The burn out time is, however, shorter than that of coal (Chen et al., 2012) because of its more porous structure and remaining volatile matter. Decrease in volatiles in torrefied biomass may delay ignition of fuel in a pulverized coal fired boiler when torrefied biomass is combusted with coal. This may lead to accumulation of un-burnt fuel inside the furnace.

Char reactivity in oxidation process decreases after the biomass is torrefied (Fisher et al., 2012; Jones et al., 2012). Decreased reactivity of torrefied biomass could be explained through the accumulation of ash (the mineral content of the biomass) over the char surface. The accumulation of ash reduces direct contact of oxidation media with the carbon and increases combustion time (Chan et al., 1999). Fisher et al. (2012) however reported that the char reactivity depends on how the volatile is removed from the original raw biomass.

Volatiles matter and porosity are two major factors affecting the reactivity of solid fuel. Since the volatile matter in torrefied biomass is higher than that in char from raw biomass, the torrefied biomass is more reactive. However, the reactivity of char and

torrefied biomass is higher than with that of coal. Reduction in an initial ignition temperature and an increment of burnout temperature of torrefied coal are presented in Ge et al. (2013). They observed the maximum mass loss band shifted towards high temperature zone. Typical combustion parameters of torrefied biomass produced by the hydrothermal torrefaction are also presented in Table 2.9.

Table 2.9: Combustion parameters of torrefied biomass under the hydrothermal torrefaction (residence time = 30 min)

Sample	Ignition Temperature, T_i (°C)	Temperature at the maximum weight loss rate, T_m (°C)	Burnout Temperature, T_b (°C)	Maximum weight loss, R_{max} (%/°C)	Ignition index, D_i (10^{-2})
Coconut fiber	273	295	326	2.39	1.48
C-220	295	450	472	1.64	0.59
C-250	372	436	472	1.71	0.49
C-300	400	458	478	1.67	0.42
C-350	410	451	512	0.94	0.24
C-375	393	505	580	0.47	0.11
Eucalyptus leaves	253	312	456	0.82	0.52
L-200	288	414	449	1.59	0.64
L-250	288	423	445	1.97	0.78
L-300	374	417	449	1.15	0.35
L-350	369	410	470	0.98	0.30
L-375	428	522	581	0.55	0.11

Note: Ignition index, $D_i=R_{max}/(t_{max}\times t_i)$

Source: Adapted from Liu et al. (2013)

2.5. EXPLOSIVITY OF TORREFIED BIOMASS

An explosion of fuel or dust is characterized by its rapid oxidation of combustible materials causing a sudden rise in temperature and pressure (Cashdollar, 2000) with resulting damage to lives and properties nearby. Dust explosion could be a major issue in handling torrefied biomass as because of its brittle nature can produce more dust than

raw biomass. Explosion potential depends on type of dust, concentration of dispersed dust particles, combustion media, area of suspension, and heat source for ignition. An explosion of dust is only possible if there is five essential elements namely fuel, heat, oxygen, suspension, and confinement (Stephan, 2012.). For the dispersed dust cloud to ignite, the ambience in the confinement must reach the minimum temperature of the dust cloud. Furthermore, for ignition to sustain, the cloud must have a minimum dust concentration. Thus, two parameters that give an assessment of the likelihood of a dust explosion are:

a) Minimum ignition temperature of a dispersed cloud (MIT), and
b) Minimum explosible concentration (MEC).

The severity of an explosion after it occurs is determined by the maximum rate of pressure rise (K_{st}) and the maximum explosion pressure (P_{max}) (Cashdollar and Harazberg, 1987).

At the time of writing no information on incidence of explosion in torrefied biomass plant was known to have occurred, but several incidence of biomass plant was known. For example, in June 2011 – explosion occurred at the world's largest pellet manufacturing facility in Georgia, USA (Renewables-International-Magazine 2011). Though large amount of information on explosion of coal dust is available (Abbasi and Abbasi, 2007), very little information on explosion in torrefied biomass dust is available in published literature. Andrej et al. (2013) and Huescar et al. (2013) compared the explosion potential of raw biomass with those of torrefied biomass and found that torrefaction do not necessarily increase the explosion potential of its dust.

Torrefaction appears to have limited effect on the explosivity of biomass-dust especially when particle sizes are below 150 μm. Though torrefaction temperature reduces the volatiles and makes biomass more brittle, Andrej et al. (2013) did not see much effect of this temperature on the explosion potential. The MIT increased from 410 to only 430°C

when torrefaction temperature rose from 200 to 300°C. Torrent (2011) measured the MIT of torrefied biomass dust as 460°C while that for wood dust is 420°C. The MEC values for raw and torrefied Poplar wood 50~60 g/m^3. This is in contrast with the MEC of coal dust reported by Liu et al. (2010) in the range of 120 g/m^3. This may be due to higher volatile matter in biomass compared with that in coal. Materials with higher volatiles will also produce more severe impact even at lower dust concentration. For instance, Li et al. (2012a) found that anthracite, lignin, and bituminous coal produced an extreme overpressure at dust concentration of 500 g/m^3, 250 g/m^3, and 125 g/m^3, respectively. This also suggests that anthracite with the lowest volatile matter requires the highest concentration of dust for explosion. The typical effect of volatile content of coal on severity of explosion is shown in Figure 2.21. Increase in volatile matter of fuel reduces the self-ignition temperature. For example, biomass with higher volatile content (80-85%) has the self-ignition temperature of 302ºC whereas torrefied biomass with less volatile content around 60-65% has 327-347ºC (ECPI, 2012). The self-ignition temperature further increases to the range of 727-827ºC for the carbonized biomass with volatile content of 10-12%.

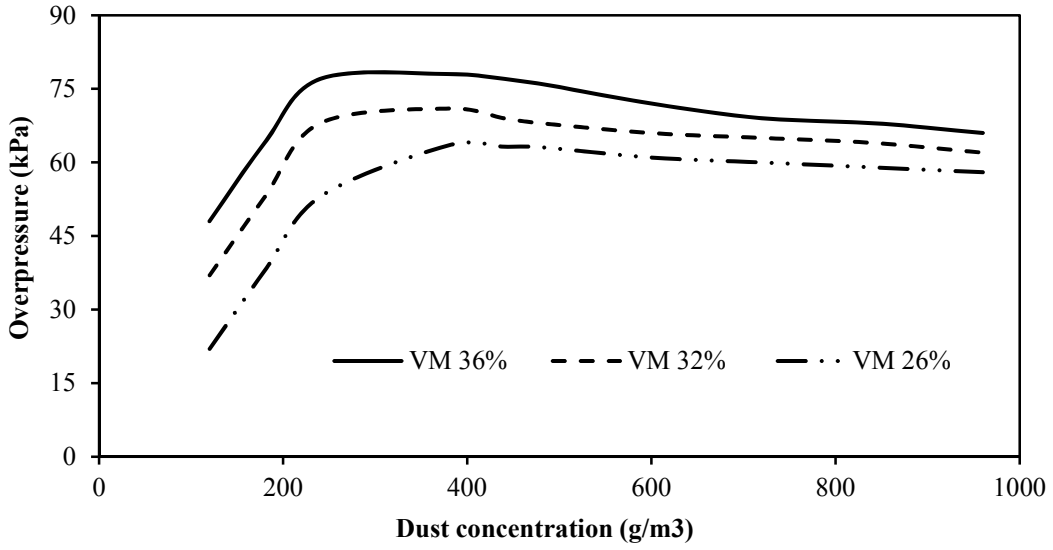

Figure 2.21: Effect of volatile content on overpressure in dust explosion (for a given suspension density and particle size)

Source: Adapted from Liu et al. (2010)

The MIT also depends on the nature of dust. Suspended dust as a cloud has higher MIT compared with that of the dust in layer form. For example, fuels with high volatile content have MIT of around 400ºC to the dust in cloud form compared to 160ºC that the dust in layer form (Stephan, 2012). Variation in the MIT of coal dust, biomass, and torrefied biomass dust in cloud and layer forms is presented in Table 2.10. Risk of explosion increases significantly with thickness of dust layers as they have higher heat holding capacity.

Table 2.10: Variation of the minimum ignition temperature of different type of coal in cloud and layer form

Fuel type	Minimum ignition temperature (ºC)	
	Cloud	Layer
Pocahontas seam bituminous	610	220
Wood dust	420	340
Torrefied wood dust	460	330
Pittsburgh seam bituminous	525-560	170
Sub-bituminous blend (as received)	475	-
Sub-bituminous blend (dried)	455	-
Lignite (as received)	450-600	-
Lignite (dried)	425-555	-
Rhode island (Cranston) anthracite	-	520
Illinois No. 7 bituminous	-	160

Source: Adapted from (Stephan, 2012)

Porosity and ability to produce finer dust of torrefied biomass than that of raw biomass may increase risk of dust explosion. For example, the fuel (lignite) with an ability to produce more pores by releasing volatiles has better explosive reactivity than the fuel (anthracite) with lower volatile matter (Li et al., 2012a). Very fine dust particles having high surface area to volume ratio are prone to dust explosion phenomenon. Decrease in dust particle size will reduce the MIT. Weigo et al. (2012) observed that the MIT for coal particle size range of 250-500 micron, 150-250 micron, 75-150 micron, 48-75 micron, and 25-48 micron is between 620-603°C, 590-600°C, 580-590°C, 560-570°C, and 520-

530°C, respectively. For sizes less than 75 microns, Huescar et al. (2013) however noted negligible effect of particle size, but they found that the MEC increased above 75 microns. Cashdollar (1996) noted a sharp rise in the MEC for coal dust when size exceeded 150 microns. This increase was higher for torrefied biomass and smaller for raw biomass.

Minimum Ignition Energy (MIE) is another important characteristic that influences the explosive potential of a dust cloud. The supply of minimum ignition energy (MIE) has much impact on the initiation of dust explosion. The role of the MIE is even more in the explosion of carbonaceous materials such as biomass and coals in which the explosion phenomenon influence greatly by the volatile content and its devolatilization rate (Kuai et al., 2013). MIE measured for torrefied wood dust was 160 mJ, which is of the same magnitude as that of other biomass dusts. Coal dust, on the other hand has a much higher MIE (greater than 1000 mJ).

Although research till date found torrefied biomass no worse than biomass for explosion, the work being limited more research is needed to settle this important question.

2.6. COMMERCIAL DEVELOPMENT

Torrefaction originated as a process for toasting of coffee beans, nuts, and seeds in Ethiopia by using hot air in the temperature range 190-280 ºC back in 1000 AD (Melin, 2011). Though thermal treatment of woods for improving quality of wooden furniture was established much earlier, its application to produce energy denser biofuels was introduced only in 1987 in France. Guyonnet and Bourgois (1988) recognized torrefied biomass as a good source for combustion and gasification process. Presently, significant amount of research and development on torrefaction is conducted as a thermal pretreatment method for upgrading biomass for energy applications (ecoTech Energy Group, 2010). Global interest on torrefaction is growing because of its potential for substituting coal with carbon neutral biomass in pulverized coal power plants.

Because of growing interest in torrefaction process and its potential benefits, many organizations are working on the commercial development of torrefaction. Many research centers, national governments and non-governmental organizations around the world are working on the development and commercialization of different torrefier system. Table 2.11 summarizes the major torrefaction reactors based on rotary drum, screw conveyor type, multiple heath furnace, torbed, microwave, compact moving, and oscillating belt conveyor reactors etc. developed by different organizations in Europe and North America. More details on the working principle and their diagrams are presented in Koppejan et al. (2012).

2.6.1 Torrefaction Reactor Technologies

Torrefier – based on the mode of heat transfer – is broadly classified into two types: (i) direct heating and, (ii) indirect heating (Dhungana et al., 2012). Most common reactors such as moving bed, augur, entrained bed, microwave, fluidized bed, hydrothermal, and rotary drum reactors fall within one of these two categories. Movement of biomass, the working media, and heat transfer mechanism are the most important distinguishing features of reactors. These features determine the nature of torrefied products as well as the total torrefaction time. For example, the rotational speed, length of the drum, and the tilt of the drum characterizes the rotary drum torrefier (Koppejan et al., 2012). The rotational speed determines the heat transfer rate whereas the drum length affects the residence time. In Torbed (fluidized bed) reactor, where the heat carrier fluids move at a relatively high velocity, is characterized by its intense heat transfer rate. This reactor can produce torrefied biomass at a very shorter residence time (around 80 sec) while using fine particles (Koppejan et al., 2012). The major advantages and disadvantages on different type of reactors are presented in Table 2.12.

Table 2.11: Summary of recent development on torrefaction reactors and their suppliers

SN	Developer	Name of reactor	Heating mode	Technology	Capacity (tons/hr)	Country
1	Agritech	Torre-tech	Indirect	Screw conveyor	5	USA
2	AIREX	CarbonFX technology	Direct	Cyclonic bed reactor	0.25	Canada
3	Allied Blower	-	Indirect	Augers	-	-
4	Alterna	Alterna	Direct	Tunnel	-	Canada
5	Atmoclear	Airless	Direct	Belt	5	UK
6	Biolake	ECN	Direct	Moving bed	5	Netherlands
7	BIO3D	BIO3D	Direct	Rotating drum	-	France
8	BTG	BTG	Indirect	Screw conveyor	5	Netherlands
9	Buhler	Buhler	Direct	Compact moving bed	-	USA
10	CanBiocoal	Rotawave	Direct	Microwave	12	UK
11	CDS	CDS	Direct	Rotating drum	-	UK
12	CMI-NESA	CMI-NESA	Direct	Multiple hearth	-	Belgium
13	EBES	ACB	Direct	Rotating drum	1.5	Germany
14	ECN	BO2	Direct	Moving bed	5	Netherlands
15	ETPC	BioEndev	Indirect	Rotary drum	4.3	Spain
16	Foxcoal	Foxcoal	Indirect	Screw conveyor	4.2	Netherlands
17	IDEMA	Thermya	Direct	Moving bed	2.5	France
18	Integro	Wyssmont	Direct	Multiple hearth	2	USA
19	New Earth	ECO-PYRO	Direct	Oscillating belt conveyor	2	USA
20	RFT	RFT	Indirect	Screw conveyor	5	USA
21	Stramproy	Stramproy	Direct	Oscillating belt conveyor	5	Netherlands
22	Terradybe		Direct	Not disclosed	-	Canada
23	Thermya	-	Direct	Moving bed	-	France
24	Topell	Torbed	Direct	Toroidal	8	Netherlands
25	Torr-coal	Torr-coal	Indirect	Rotary drum	4.5	Netherlands
26	Torrfuels	SVI	Direct	Rotary drum	-	Canada
27	Torrsys	Torrsys	-	-	5	USA
28	West Creek Energy	Konza	Direct	Rotary drum	10	USA
29	WPAC	WPAC	Unknown Technology	Unselected	5	Canada
30	4 Energy	Stramproy	Direct	Belt conveyor	5.5	Netherlands

Source: Adapted from Dhungana (2011)

Table 2.12: Advantages and limitations of different types of torrefaction reactors

Reactor type	Advantages	Limitations
Rotary drum	Proven relatively simple equipment Low pressure drop Possibility of both direct and indirect heating	Lower heat transfer (specially in indirect heating) Difficult to measure and control temperature Less plug flow compared with other reactors Bigger system size Necessary proper drum sealing Difficult in scaling up the system
Moving bed	Simple reactor and its construction Very good heat transfer High bed density	Significant pressure drop Difficult to control temperature
Screw type	Possibility for plug flow Mature technology for torrefaction	Indirect heating only Higher possibility of hot spots Lower heat transfer rate Scale up problem Require shaft sealing
Multiple heart furnace	Proven equipment design Higher possibility of scale up Close to plug flow Good temperature and residence time control Possibility of adding fines	Lower heat transfer rate compared with other direct reactors Limited volumetric capacity Relatively larger reactors Require shaft sealing
Fluidized bed	Excellent heat transfer rate Easily scalable	Require smaller particle size Necessary to have additional gas equipment to supply fluidizing fluids Possibility of attrition (fines formation) Difficult to get plug flow

Source: Adapted from Bi (2012)

Microwave torrefaction uses microwave irradiation as a heat source, which is characterized by its fast internal and uniform heating properties (Ren et al., 2012). Microwave heating can be achieved by two mechanisms viz. rotation of dipoles, and migration of ions (Huang et al., 2012). Microwave torrefaction requires moisture content less than 10% but it is not necessary the particle to be small (Wang et al., 2012a). Characteristics of microwave torrefaction depend on the type of materials and their ability in absorbing the microwave radiation. Since the microwave torrefaction is powered by microwave irradiation, torrefaction temperature and biomass-heating rate depend highly on the power of microwave. This alters both physio-chemical properties of torrefied product, especially in the morphological structure. Higher microwave power could achieve torrefaction temperature of biomass in the reactor in very short period of time, and thus significantly reduce processing time (Huang et al., 2012). However, in large particles there may be significant temperature gradient in the particle resulting in non-uniform torrefaction (Dhungana, 2011). Huang et al. (2012) did not notice this effect as they used small particles of average diameter 0.297 mm.

Figure 2.22 shows how the mass and energy yields decrease with the increase in microwave power. A significant loss in masses of rice husk and Pennisetum at higher microwave power is due to higher torrefaction temperature obtained at 25 minutes residence time. Temperature of biomass (7.0-7.6 gm) in the reactor rose well above 300°C at 25 minutes when the microwave power was in the range 250-350 W. Huang et al. (2012) also showed that biomass temperature increased with both time and microwave power. At higher microwave power, the torrefaction temperature exceeded 300°C within 10 minutes and such fast heating rate is known to reduce solid yield (Basu, 2010). Thus, being an energy efficient heating method and high potential to release volatiles in short time interval, microwave torrefaction has higher possibility of enhancing the porosity of products, and improves the combustion properties of biomass. Information on morphological changes in biomass with microwave power, and combustion and gasification characteristics of the solid product under the microwave torrefaction is still unavailable in literatures.

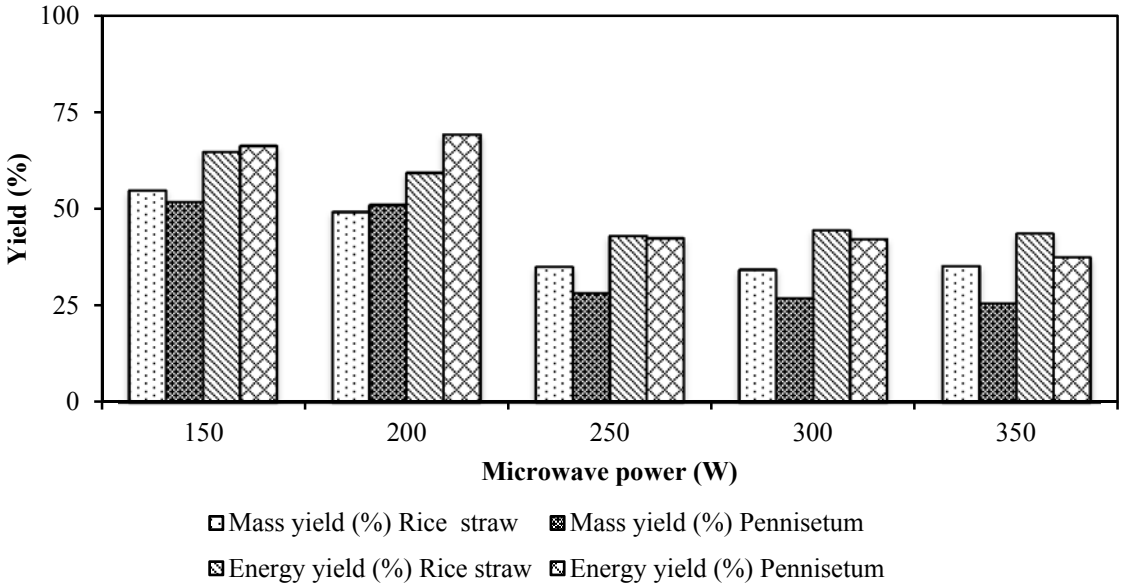

Figure 2. 22: Effect of microwave power in solid product (mass) and energy yields of rice straw and pennisetum under the microwave torrefaction at residence time of 25 minutes

Source: Adapted from Huang et al. (2012)

A comparative study between different reactors – keeping all other conditions same is presented by Dhungana et al. (2012) in which they observed that rotary drum reactor has lower solid product yield compared to that for convective reactor and fluidized bed reactor. This could be due to the differences in gas to particle heat transfer in the specific reactor type. In the rotary drum reactor, primary heat transfer to particle is through thermal conduction. Possibility of high heat transfer rate to the particle due to continuous tumbling action of particle with the rotational movement of the reactor may be one of the reasons for low solid product yield in the rotary drum reactor. Additionally, high heat transfer to surface of large particles could give higher temperature in the core. This may also increase the mass loss.

However, the major problems of currently used torrefier reactors include:

1. Use of nitrogen as a torrefaction medium added cost of torrefaction

2. Non-uniform products due to improper solid mixing and inefficient heat transfer
3. Volatiles released with moisture reducing the effectiveness of the use of volatiles

Thus, authors developed a batch type low-pressure batch torrefier (at CFB laboratory of Dalhousie University) to eliminate the first problem. In this inexpensive reactor torrefaction takes place in the mildly pressurized air instead of nitrogen. This method, however, could not address the other two shortcomings of existing reactors. Additionally, batch operation under pressure might face difficulties for large commercial unit. Authors, in collaboration with the Greenfield Research Incorporated of Halifax, therefore developed a two-stage continuous indirectly heated rotary torrefier with flights. This reactor splits drying and torrefaction in two in-line rotary reactors, allowing to obtain moisture free volatiles from the torrefier. Tumbling actions facilitated by the flights improves internal mixing of solid. This unit could also utilize the released volatiles as a torrefaction medium.

Above two technologies being in conceptual stage were not tested experimentally. The present study, therefore, aims to investigate them.

2.7. APPLICATION OF TORREFIED BIOMASS

A major application of torrefied biomass is in co-firing of biomass in coal-fired power plants. Torrefied wood could ideally increase the share of biomass feed up to 80% compared to 5-10% share of non-torrefied wood pellets (Topell, 2012). In addition to this, torrefied biomass can also be used in different sectors such as industrial furnace in a metallurgical process, as an activated carbon in water treatment, metal extraction process, gas and air filtration process, and chemical treatment plants (Rautiainen et al., 2012). Potential application of torrefied biomass in specific sectors and their requirements are presented in Table 2.13.

Table 2.13: Application of torrefied biomass

Target	Conversion process	Conversion equipment	Biofuel	Level of pretreatment requirement	Benefit of pretreatment	Level of market potential
Large-scale power production	Co-firing	Coal-fired boilers	Wood pellets	High	Higher co-firing rates	High
	Co-gasification	Entrained flow gasifier	Wood pellets	Very high	Size reduction, uniform particle distribution, C/H/O ratio, dry and hydrophobic	Limited
	Combustion*	Fluidized boilers	Wood chips	Moderate	Limited and relatively expensive	Small
Industrial heating	Combustion	Blast furnace	None	Moderate	Easy handling, lower C/H/O ratio, Energy Content	High
Residential/district heating	Combustion	Stoves/boilers	Wood pellets	High, decentralized	Transport savings	High

Note: * 'Combustion' implies 100% combustion of biomass

Source: Adapted from Koppejan et al. (2012)

In the area of biofuel production, the quality of bio-oil can be improved using torrefied biomass because of lower moisture and O/C ratio. Such feedstock has ability to produce a concentrated good quality bio-oil through a fast pyrolysis process (Meng et al., 2012). Prando et al. (2013) studied a combined heat and power (CHP) system using torrefied biomass in the gasification process. They found that the use of torrefied biomass in gasifier could increase the overall efficiency of the CHP system compared to that of using raw biomass.

Torrefied biomass can be used also as activated carbon – an adsorbent made from biomass, which is used to remove organic or inorganic substances from liquid and gases (Rautiainen et al., 2012). An activated carbon is a carbonaceous material with low volume pores. The low volume pore biomass with higher degree of micro-porosity possesses higher contact surface area. It increases the combustion rate in flame burning, process and enhances the adsorption capacity in a gas purification process. Since the porosity of torrefied biomass depends on the temperature of torrefaction, torrefied biomass obtained under a particular torrefaction condition at which the micro-porosity reaches to the maximum value alone would be suitable for production of activated carbon.

In metallurgical process like iron making process, biomass could be used as a reducing agent to replace the coking coal (Basu, 2013). To replace the coking coal or oil by biomass, the latter needs to have high heating value, low volatile content, low ash and free from harmful elements, and particle size in the range of 1-10 mm (Fick et al., 2012). These characteristics can be obtained by converting biomass into either charcoal or torrefied biomass. One of the major benefits of using charcoal or torrefied biomass over coke is their ability to prevent sulfur dioxide emissions (Rautiainen et al., 2012). Though lower volatile content in torrefied biomass increases its suitability over raw biomass, they are usually not preferable compared to the charcoal.

A comparison of properties of torrefied biomass and other biomass fuels are presented in Table 2.14. Higher volumetric energy density and bulk density, low volatile contents and moisture content, uniform particle size, and homogenous nature of torrefied biomass are important benefits in co-firing power plants. Major problems in co-firing raw biomass in coal-fired plants include large volume of flue gas, rapid homogeneous combustion of volatiles resulting an unstable flame propagation and non-uniform heat distribution, and low energy density of fuel requiring larger feeding system. Many of these can be greatly avoided after the torrefaction of biomass. In addition to this, co-firing with torrefied biomass requires fewer modifications in the existing facility. Thus it avoids major capital expenditures that otherwise need to be made for retrofitting if wood pellets are to be co-fired (Koppejan et al., 2012).

2.8. TORREFACTION IN THE SUSTAINABLE DEVELOPMENT

Growing energy demand, declining fossil fuel resources and their greenhouse gas emissions are major motivations for adopting sustainable development practice.

Bio-char could serve as long-term sink of atmospheric carbon dioxide (Glaser et al., 2002). Conversion of biomass-carbon to bio-char carbon leads to sequestration of about 50% of the initial carbon in the biomass, this is significantly higher than the low fraction of parent carbon retained after burning (<3%) and biological decomposition (<10-20% after 5-10 years) (Lehmann et al., 2006). The large scale slash and burn technique, though converts only small fraction (3%) of biomass carbon to bio-char carbon, is widely practiced in agricultural fields in many countries because it has added benefit of improving the soil property by retaining nutrients and enhancing soil physical and biological properties (Lehmann et al., 2006). This practice however is highly polluting regionally as it emits large amount of particulate and volatile organic compound.

Table 2.14: Comparison of properties of torrefied biomass and other solid fuels

Parameters	Wood	Wood pellet	Coal	Torrefied biomass (dry torrefaction)	Hydrochar (Hydrothermal torrefaction)	Hydrochar + coal fines (PCS hybrid biofuels)
Moisture (wt. %)	30-40	8-10	6-15	2-3	4-5	6-7
Higher heating values (MJ/kg)	9-12	16-19	18-30	20-25	24-34	24-27
Volatile content (wt. % db)	70-75	70-75	15-30	55-65	NA	NA
Fixed carbon (wt. % db)	20-25	20-25	50-55	28-35	NA	NA
Ash content (wt. % db)	< 5	< 5	6-15	NA	0.3-0.5	5-7
Bulk density (kg/m^3)	200-250	550-750	800-850	700-850	NA	NA
Volumetric energy density (GJ/m^3)	2-3	7.5-10.4	18.4-23.8	15-18.7	NA	NA
Explosibility	Average	Limited	Limited	Limited	NA	NA
Water resistant	Hydrophilic	Hydrophilic	Hydrophobic	Hydrophobic	Hydrophobic	Hydrophobic
Biological decay	Yes	Yes	No	No	No	No
Milling requirements	Special	Special	Classic	Classic	Classic	Classic
Handling of fuel	Special	Easy	Easy	Easy	Easy	Easy
Transportation cost	High	Average	Low	Low	Low	Low
Quality variability	High	Limited	Limited	Limited	NA	NA
Tar and cresol	Yes	Yes	Yes	No	No	Negligible
Heavy metals	No	No	Yes	No	No	Negligible
Sulfur	No	No	Yes	No	No	No

Source : Adapted from Acharya et al. (2012); Koppejan et al. (2012); PCSB (2011)

More than 80% of terrestrial organic carbon is stored in solids (IPCC, 2000). But soils show low potential for additional accumulation of carbon compared with that of growing forest can absorb (Schlesinger and Lichter, 2001). The next best option is conversion of biomass into bio-char for long-term sink in soil while simultaneously improving soil fertility and water retention capacity. This concept is not new. One can see evidences of such storage in the Amazon basin well before European arrived there. Storage density of organic carbon there is as high as 250 Mg/ha/m (Glaser et al., 2001).

Torrefaction, on the other hand, can provide a good alternative to the traditional means of bio-char production. First because of its low temperature (200-300°C), larger fraction of biomass char is retained in solid form. While nothing can be done about the non-condensable CO_2 emissions, the condensable hydrocarbon, and CH_4 can be burnt to provide energy for torrefaction. Present technology of torrefaction, however, is limited to smaller scale production. It could be developed further into large-scale production, which might be superior to carbon-capture-sequestration both in cost and reliability.

To promote torrefaction as a low emission technology, it needs to be established that the technology is a net emission sink. To do this, one needs to determine different sources of emissions along the way. The emission level from a torrefier can be assessed by careful examination of its volatiles (tar and gases) products. Although non-condensable gases could be used as an energy carrier, condensable gases need to be properly managed to avoid possible environmental issues. Some constituents of volatiles such as carbon monoxide, traces of hydrogen, and methane can be used as the source of energy, but volatiles like carbon dioxide adds to the GHG emissions. To minimize such emissions level, the University of Laval in Canada has recently investigated a study to capture CO_2 from torrefaction unit using mining waste. The study showed that CO_2 from the torrefaction unit could be successfully captured and stored in magnesium rich ultramafic mining waste in a carbonation reactor. The other option is to use the CO_2 rich low temperature flue gas in greenhouse farms for enhanced production of and heating.

The combustion of torrefied biomass may have higher CO_2 emission per unit energy release basis than that from raw biomass, because of the higher carbon fraction in torrefied biomass. This GHG emission can be better managed when torrefaction is integrated with co-firing plants. Torrefaction allows reduction in coal/biomass ratio that reduces the overall emissions from power plants on per unit energy produced basis. In addition to this, torrefaction process will also avoid the emission by natural decay of the raw biomass if left in the forest or so. Also, the transportation related emission decreases after torrefaction as it reduces the volume of materials to be transported for a given amount of energy transport.

However, the interest in torrefaction as pretreatment option for biomass has grown, only limited studies are available on emission related issues. More studies on technical and economical aspects of torrefaction are needed to analyze the effect of torrefaction on GHG emissions. Chiueh et al. (2012) found that torrefaction had only a limited savings (3 US Dollar per kg of heat released) on the transportation cost of raw biomass from source to the pretreatment plants, and then to the co-firing plants. However, such conclusion cannot be drawn based on one work.

The savings in CO_2 emission in some cases could be substantial with torrefaction. For example, Fick et al. (2012) found that 300 kg of CO_2 equivalent per tonne of pig iron could be avoided by replacing 20% of coke with the torrefied biomass. Total greenhouse gas emissions from different scenarios of fuel mix for producing one tonne of liquid iron are shown in Figure 2.23. Because of the higher solid product of torrefaction and lower operating temperature compared to that in conventional carbonization process, a switch to torrefaction process could be preferable for iron making without compromising the level of GHG emission savings obtained by the use of char.

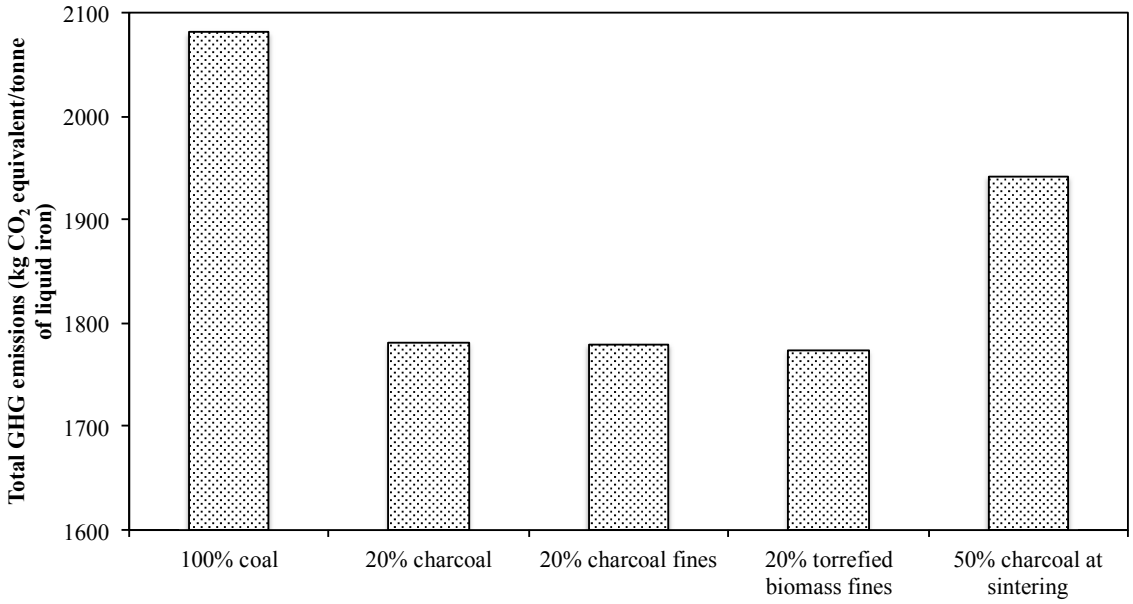

Figure 2.23: Different scenarios of GHG emissions in steel industry
Source: Adapted from Fick et al. (2012)

Torrefaction could make similar positive contribution in making use of biomass as fuel healthier in rural area of the developing countries. Many countries like Nepal depend greatly on biomass fuel in homes, but the resultant indoor air pollution remains a major issue. Increase in indoor air pollution due to inefficient use of biomass could increase the risk of respiratory tract infections, exacerbations of inflammatory lung conditions, cardiac events, stroke, eye disease, tuberculosis, and cancer (Fullerton et al., 2008). Though it is believed that high indoor air pollution results from inappropriate ventilation, poor design of stoves, and inefficient burning, higher volatile content in biomass is one that causes excessive smoke. Biochar, which can be burnt efficiently with less smoke, is often promoted as an effective practical solution to address issues of fuel, health, climate, agricultural production, soil depletion, and poverty in the rural communities (NSWDPI, 2013). But, torrefaction of biomass can also take this option on step further because of its higher mass and energy yield compared to traditional biochar or charcoal production methods.

The greatest contribution of torrefaction lies in its near term use in partially replacing coal in existing coal-fired power plants. This being commercially viable, technically proven it can bring about immediate reduction in GHG emissions from thousands of power plants around the world.

2.9. SUB-CONCLUSIONS

Despite the huge potential of biomass energy resource, it is not utilized as widely as it could be due to some of its inherent limitations such as low energy density, low bulk density, heterogeneity, hygroscopic behavior and fibrous nature, biomass. These limitations result in transportation difficulties, storage problem, and spontaneous decay of biomass. Such problems could be substantially avoided through the torrefaction process. Degradation of hemicellulose is considered to be the main benefit of the torrefaction process.

The most important immediate use of torrefaction lies in increasing the share of biomass in existing coal fired plants from current level of 3-10% to 40-60%. This could make GHG emissions reduction much more affordable. Torrefaction technologies are still in developmental stage with no clear winner. Mildly pressurized batch reactor and two-stage continuous indirectly heated rotary torrefier with flights are two novel reactor technologies. Although they appear to be improvements over presently used technologies no units are built let alone investigation into their effectiveness and process dynamics.

It is, thus, necessary to study above two reactor technologies in laboratory scale units for examining the effectiveness in the production of torrefied products, and develop a reasonable understanding of the basics of working of these reactors.

CHAPTER 3: EXPERIMENTAL INVESTIGATION OF MILDLY PRESSURIZED TORREFACTION IN AIR AND NITROGEN[†]

This chapter introduces a novel means of batch torrefaction of biomass in mild pressure without the need of expensive nitrogen as torrefaction medium. It also compares the characteristics of the solid torrefied products obtained under air and nitrogen medium in pressurized batch reactor

3.1. BACKGROUND

Dry torrefaction (commonly known as just 'torrefaction') is a slow heating process within a temperature range of 200-300°C in an inert environment at constant atmospheric pressure (Bergman, 2005; Bourgois and Guyonnet, 1988; Nhuchhen et al., 2014; Tapasvi et al., 2013; Thanapal et al., 2014). Nitrogen is the most commonly used inert medium used for torrefaction especially in laboratory units. Nitrogen being expensive its use in commercial units is not economic. Some investigators (Basu et al., 2013, Lu et al. 2012; Rousset et al., 2012; Uemura et al., 2013) replaced nitrogen with air at atmospheric pressure as the torrefaction medium and studied its impact on the product quality. Basu et al. (2013) noted reduction in mass yield when oxygen was used. Eseltine et al. (2013) and Thanapal et al. (2014) have examined the possibility of torrefaction using carbon dioxide as a non-oxidizing inert gas.

Wet torrefaction that deploys compressed water within a temperature range around 180-260°C (Acharjee et al., 2011; Bach et al., 2013; Yan et al., 2010), can avoid nitrogen. Wet torrefaction requires shorter residence time and lower temperature compared to that

[†] This chapter is taken from the paper published by the candidate: Nhuchhen, D. R., and Basu, P. (2014), " Experimental investigation of mildly pressurized torrefaction in Air and Nitrogen,"*Energy and Fuels*, 28, 3110-3121.

required for dry torrefaction. This process could add the potential benefit of using the volatiles dissolved in water.

Only limited information on dry pressurized torrefaction is available in the literature. A patent by Rawls et al. (2011) developed a continuous (feeding from top) reactor in which a non-oxidizing pressurized gas at 2000 kPa gauge pressure and 200°C is supplied from the bottom. The product obtained in a pressurized reactor system had a number of benefits. For instance, an increase in heating value from 21.9 to 25.8 MJ/kg was noted when the reactor pressure increased from atmospheric pressure to 4000 kPa (Wannapeera and Worasuwannarak, 2012). High-pressure pyrolysis could result in an increase in porosity in the char produced (Mahinpey et al., 2009). The pressurized process also helps in trapping volatiles especially heavier molecules tars that produce more char and CO_2 (Mok and Antal, 1983). One could also expect reduction in tar yield and slight increment in light gases with increasing pressure (Seebauer and Staudinger, 1997). However, Sun et al. (1997) observed that mild pressure has no effects in the total volatile yields. Zeng (2005) reported only a minor effect of pressure on the total volatiles yield in a low temperature pyrolysis process, but there still exists the possibility of trapping and depositing fraction of heavy tars with heating values 22-26 MJ/kg (Richard and Thumann, 2002) on the surface of torrefied biomass, which in turn could increase the energy density of the solid product.

The above works show positive effects of torrefaction at very high pressures in the range of MPa, but such high-pressure operation may create difficulties in operation and maintenance in large plants. Additionally, operation of continuous reactor high pressure greatly increases the cost owing to complex feeding and product withdrawal systems. So, from a practical and industrial standpoint torrefaction under mild pressures (< 1 MPa) could be a good alternative method of torrefaction provided it offers some attractive enough advantages. Very little or no work on mild pressure torrefaction is available in published literature. The present work develops a simple practical means of avoiding nitrogen use through batch torrefaction in closed vessel under mild pressure.

This chapter compares the torrefaction products produced in air and in nitrogen media in the closed reactor to examine if atmospheric pressure torrefaction in nitrogen can be replaced with torrefaction in air in a mildly pressurized batch type torrefier. To get baseline data, experiments at atmospheric pressure reactor in both air and nitrogen were conducted. These data were compared with those for mildly pressurized reactor.

Effects of pressure, temperature, and residence time on the solid product of mild pressure torrefaction are also analyzed. This work has also used the Response Surface Methodology (RSM) to develop correlations for the mass loss through torrefaction. Two other correlations for energy density enhancement and fuel ratio are then proposed. Finally, an attempt is made to characterize different modes of pressurized torrefaction using experimental results.

3.2. EXPERIMENTS

Following section describes experimental methods employed for torrefaction. All pressure indicated here are gauge value i.e., pressure above atmospheric.

3.2.1 Biomass Sample

Cylindrical shaped poplar wood samples of 50.5 mm length and 19 mm diameter were used for torrefaction. After the samples were cut, they were kept in a plastic bag to avoid change in initial moisture content of the raw biomass. For continuous accurate measurement of the temperature of the biomass sample during torrefaction, a hole was drilled in the center of the cylindrical sample and a K-type thermocouple was inserted it.

3.2.2 Procedures

Figure 3.1 shows a schematic of the experimental set up used. A stainless steel pipe of 304.8 mm length and 25.4 mm diameter with Swagelok fittings was used as the

pressurized reactor. This reactor (torrefier) is indirectly heated by immersing it in an electrically heated bubbling fluidized bed sand heater.

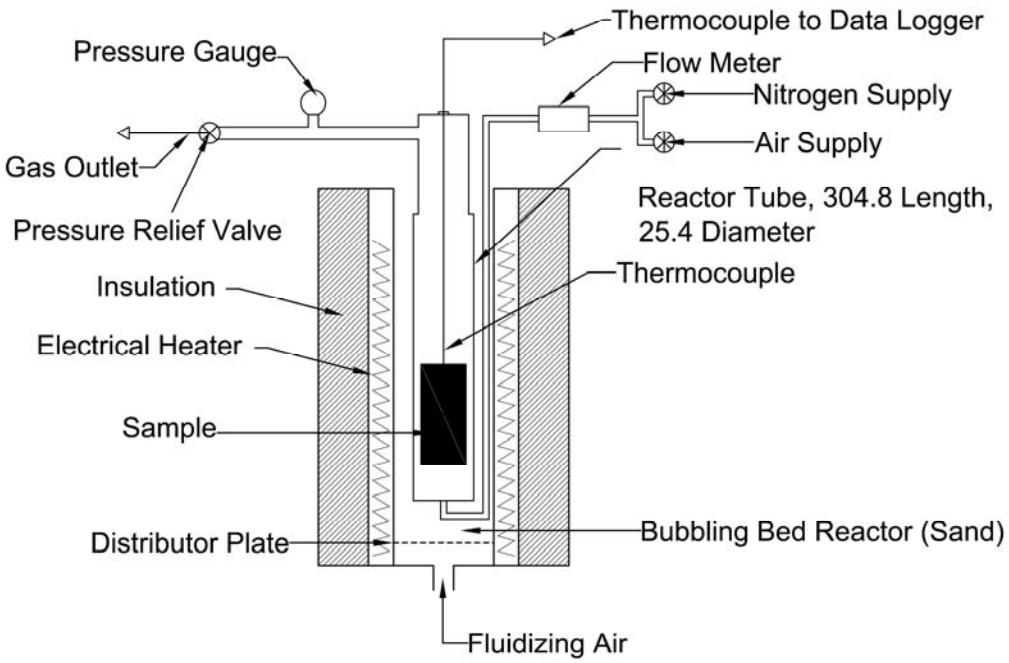

Figure 3.1: Schematic of the experimental set up used

Experiments were conducted at mild pressures (< 600 kPa gauges) in a reactor with (i) air and (ii) nitrogen separately. The reactor was first purged with N_2 before pressurizing it. Initial reactor pressure was kept slightly below the designated pressure because thermal expansion of gas will increase the pressure to the designated pressure. When the reactor is heated, the reactor pressure increases due to the thermal expansion, but a pressure relief valve maintains at the designated pressure. The torrefaction took place in an ambience of a mixture of air and released volatiles for air torrefaction, as well as in a mixture of nitrogen and released volatiles for nitrogen torrefaction.

In order to conduct the experiment at atmospheric pressure, the same set up was used, but with a slight modification. The reactor used for pressurized torrefaction was opened on the top and connected with a stainless tube at the bottom. The stainless tube was then connected to flow meter, flow control valves, nitrogen supply cylinder, and air supply

line as shown in Figure 3.1. The flow rate of nitrogen and air was maintained at the rate of 1.2 standard liters per minute in all atmospheric pressure torrefaction in air and nitrogen medium.

One may note an important characteristic of the series of tests with the atmospheric pressure reactor. During air torrefaction it was left open to atmosphere. As a result of that biomass had continuous access of oxygen. In pressurized air torrefaction the reactor was filled with air and then sealed. Once the oxygen was depleted no additional oxygen could reach the biomass in the pressurized reactor.

Experimental conditions involved four pressures, viz. 0, 200, 400, 600 kPa (gauge pressure), three residence times, viz. 15, 25, 35 min, and three temperatures, viz. 220, 260, 300°C. As the torrefaction process starts from 200°C, the residence time of torrefaction in all experiments was recorded after the sample reached this temperature. After the lapse of the chosen residence time, the reactor pressure was released except at atmospheric conditions, and the torrefied solid product was removed from the reactor and stored in a desiccator. The solid product being the main product of torrefaction was analyzed. Proximate analyses were conducted as per ASTM standard method (ASTM D1762-84) (ASTM, 2007). To measure the heating value (HHV) of the torrefaction products, a Compensated Jacket Calorimeter (model Parr-6100) was used.

3.2.3 Performance of Torrefaction

Mass yield (*MY*) is one of the main characteristics of the torrefied product. It is defined as the ratio of final mass of torrefied product to initial mass of raw biomass in dry and ash free basis (daf).

$$MY = \frac{M_{f,daf}}{M_{i,daf}} \times 100(\%) \tag{3.1}$$

To express the degree of increase in heating value of the solid product, we use the term energy density enhancement factor ($EDEF$) that is defined as the ratio of higher heating value of torrefied product (HHV_{tp}) to that of raw biomass (HHV_{raw}) in dry and ash free (*daf*) basis.

$$EDEF = \frac{HHV_{tp,daf}}{HHV_{raw,daf}} \tag{3.2}$$

The *EDEF* can also be expressed as an energy density enhancement (*EDE*) that shows the percentage increase in energy density of torrefied biomass compared to that for raw biomass.

$$EDE = \frac{HHV_{tp,daf} - HHV_{raw,daf}}{HHV_{raw,daf}} \times 100(\%) \tag{3.3}$$

Energy yield (*EY*) is a measure of energy recovered after torrefaction process. It can be related to *MY* and *EDEF* as:

$$EY = MY \times EDEF(\%) \tag{3.4}$$

3.3. RESULTS AND DISCUSSION

Table 3.1 presents the proximate analysis and the heating value of the raw biomass (Poplar) as measured for the sample biomass studied. The experiments were conducted mainly at mild pressures (200-600 kPa gauges). Temperatures of torrefaction selected were 220°C, 260°C, and 300°C, which correspond to light, mild, and severe mode of torrefaction respectively (Basu, 2013; Chen et al., 2011). To avoid excessive mass loss during the process, residence times were varied only up to 35 minutes. For base line

study experiments at atmospheric pressure (0 kPa gauge or 101.3 kPa absolute) were conducted at above range of torrefaction temperatures and residence times.

Table 3.1: Properties of raw cylindrical yellow poplar

Properties	Parameter	As received basis	Dry and ash free (daf)
Proximate components	Moisture, % wt.	4.75	-
	Volatile content, % wt.	85.37	89.73
	Ash content, % wt.	0.11	-
	Fixed carbon, % wt.	9.77	10.27
Heating value	Higher heating value, MJ/kg	18.48	19.43

3.3.1 Core Temperature vs. Time

Several earlier studies (Basu et al., 2013; Turner et al., 2010) showed that during torrefaction the temperatures in the core of a relatively large biomass piece could be higher than that of its surface. This may be due to the exothermic reactions in the core of the sample. The rise and growth rate of core temperature are two important parameters that can influence the properties of torrefied biomass significantly. These two parameters depend to some extent on the operating conditions of torrefaction. Figure 3.2 shows the core temperature history at different pressures in air and nitrogen torrefaction at 300ºC. The core temperature increased steadily in all cases to a value above the furnace or surface temperature, and thereafter it decreased slowly to a value slightly higher than the furnace temperature. It shows that the rate of rise in core temperature was faster and the peak core temperature though they also depend on other parameters was found higher in air compared with that in nitrogen media. Here, one notes a potential for greater mass loss at severe torrefaction (300°C) mode in pressurized air compared that in nitrogen. Therefore, in severe torrefaction using air, one could significantly reduce the residence time to achieve a given level of torrefaction. The trend of core temperature rise was similar for mild and medium torrefaction conditions (260°C and 220°C), but the above

effect was not significant at these conditions. It took longer time to reach the peak core temperature.

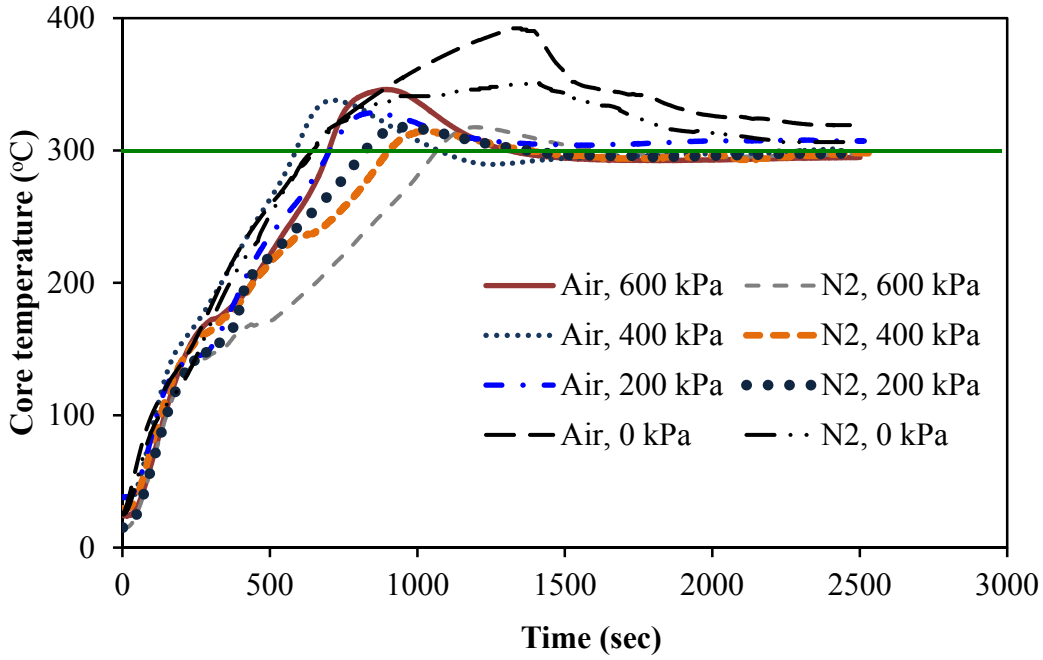

Figure 3.2: Temperature history of core temperature rise in air and nitrogen medium during torrefaction at 300 °C and reactor pressures of 0 kPa, 200 kPa, 400 kPa and 600 kPa (Note: 0 kPa means atmospheric pressure torrefaction having different torrefaction mechanism than pressurized torrefaction)

Exothermicity, which is usually measured in terms of core temperature overshoot (core temperature of sample – furnace temperature) (Turner et al., 2010) was observed higher (46°C) in pressurized air compared to that (17°C) in nitrogen medium. This is due to possible oxidation reactions in air media. One also notes an increase in the amount of temperature overshoot though small, with a rise in reactor pressure in air medium, but that was not significant in nitrogen. This may suggest a higher degree of heterogeneous exothermic reactions between char and volatile gases at higher pressure and in air. However, such exothermic reactions may be increased further if biomass is torrefied at atmospheric pressure with continuous air supply. Therefore, comparison of temperature overshoot in pressurized and atmospheric pressure torrefaction was excluded hereafter.

Figure 3.3 plots the temperature overshoot in pressurized torrefaction at 260 and 300°C at different pressures. The rise with pressure in air is clear, but that is not the case with nitrogen. As discussed in Dhungana (2011), both internal and external heat and mass transfer phenomena could affect the core temperature rise and degree of overshooting. At higher reactor pressure, either the decrease in convective heat transport by volatile gases or higher degree of exothermic devolatilization reactions may have occurred inside the biomass sample, resulting in an increase temperature overshoot. Though Figure 3.4 supports the latter cause, it does not necessarily rule out any effect of pressure on the convective heat transfer.

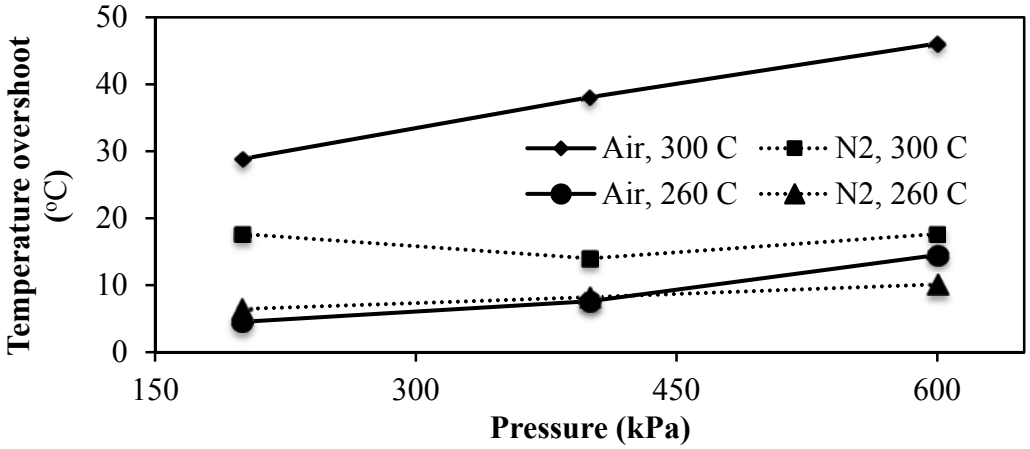

Figure 3.3: Effect of torrefaction temperature and pressure in temperature overshoot during torrefaction

3.3.2 Proximate Analyses

One of the motives of torrefaction is to upgrade the quality of biomass, making them more compatible with coals. Torrefaction reduces the volatile content and increases the fixed carbon content of biomass. Table 3.2 presents volatile matter (daf) and fixed carbon content (daf) of biomass torrefied at different operating conditions. A decrease in volatile matter and increase in fixed carbon content of torrefied solid product (Table 3.2) compared to those in the raw biomass (Table 3.1) was observed at different pressures, temperatures, and residence times, but the amount depends on the severity (higher temperature, longer residence time, and higher pressure) of the torrefaction.

Table 3.2: Volatile matter (%), fixed carbon content (%), HHV (MJ/kg) of torrefied biomass (dry and ash free basis)

Medium	Pressure (kPa)	Parameter	Temperature (°C)								
			220			260			300		
			Residence time (min)								
			35	25	15	35	25	15	35	25	15
Air	0	VM	86.57	88.50	89.40	58.5	69.84	79.81	41.03	47.38	56.99
		FC	13.43	11.50	10.60	41.50	30.16	20.19	58.97	52.62	43.01
		HHV	19.87	20.06	19.94	24.03	24.67	21.15	26.09	26.85	26.27
	200	VM	87.73	88.22	88.53	82.04	82.71	85.07	59.03	68.46	76.35
		FC	12.27	11.78	11.47	17.96	17.29	14.93	40.97	31.54	23.65
		HHV	19.62	19.56	19.44	21.87	21.53	20.98	26.75	24.59	22.52
	400	VM	87.59	88.01	88.14	81.48	82.04	83.96	54.22	59.90	65.43
		FC	12.41	11.99	11.86	18.52	17.96	16.04	45.78	40.10	34.57
		HHV	20.09	19.74	19.58	21.78	21.32	20.99	27.56	25.88	24.60
	600	VM	86.38	86.49	86.88	79.54	79.83	82.40	51.11	57.20	58.81
		FC	13.62	13.51	13.12	20.46	20.17	17.60	48.89	42.80	41.19
		HHV	20.40	20.19	19.61	21.83	21.70	21.38	27.12	26.65	25.63
Nitrogen	0	VM	88.01	88.23	89.47	79.87	81.78	84.18	61.64	65.77	67.98
		FC	11.99	11.77	10.53	20.13	18.22	15.82	38.36	34.23	32.02
		HHV	19.96	19.97	19.69	21.15	21.05	20.86	22.52	23.76	23.40
	200	VM	87.48	88.54	88.64	82.53	84.11	86.85	66.22	68.09	68.82
		FC	12.16	11.46	11.36	17.47	15.89	13.15	33.78	31.91	31.18
		HHV	19.96	19.79	19.83	21.06	20.49	19.50	24.71	24.64	23.58
	400	VM	87.70	88.17	88.17	81.22	82.64	84.53	62.07	66.41	68.23
		FC	12.30	11.83	11.83	18.78	17.36	15.47	37.93	33.59	31.77
		HHV	20.08	19.77	19.59	21.49	21.27	20.75	25.49	25.07	23.44
	600	VM	87.44	87.65	87.77	81.14	81.15	83.80	58.54	65.19	67.49
		FC	12.56	12.35	12.23	18.86	18.85	16.20	41.46	34.81	32.51
		HHV	19.83	19.47	19.50	21.39	21.20	20.63	26.00	25.54	23.50

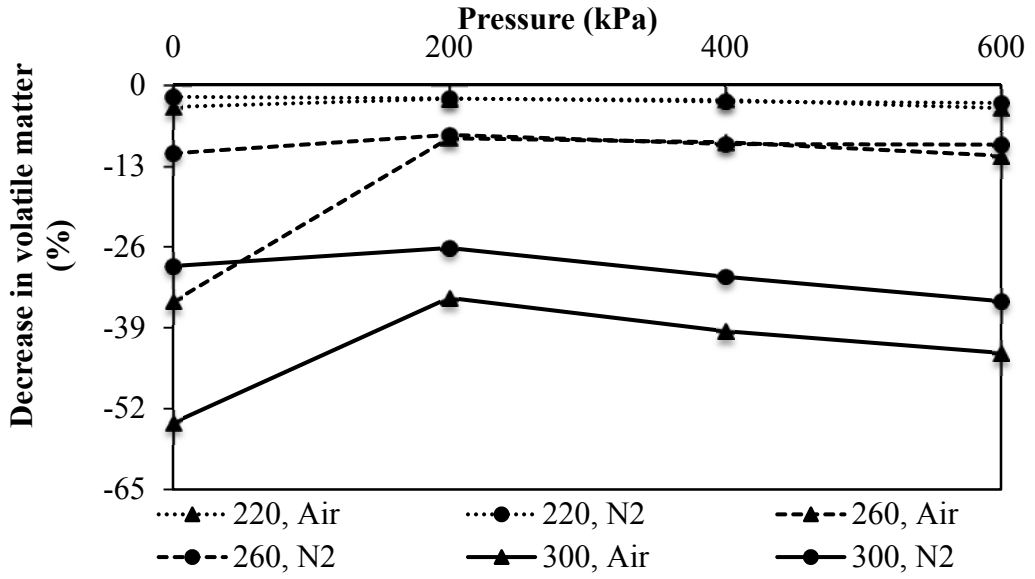

(a)

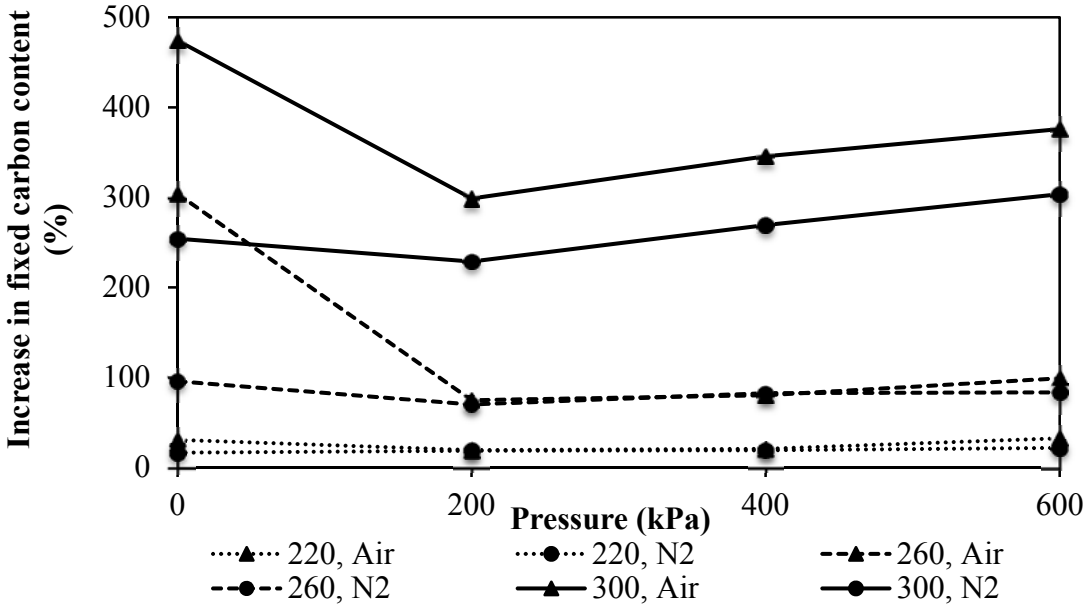

(b)

Figure 3.4: Variations in proximate components observed at residence time of 35 minutes; (a) Decrease in volatile contents; (b) Increase in fixed carbon contents (% of FC increase or VM decrease=(% before - % after)/ % before torrefaction (raw))

For all pressures excluding atmospheric pressure torrefaction, the decrease in volatile matter (VM) was within 4% in light (220°C), 12% in mild (260°C), and 44% in severe (300°C) torrefaction conditions (Figure 3.4a). Devolatilization of biomass in light and mild torrefaction temperature zone is limited only by the degradation of hemicellulose. In severe (300°C) torrefaction conditions, both cellulose and hemicellulose undergo major degradation, causing higher volatile losses.

An increase in residence time also enhances volatiles losses. For instance, the losses in volatile matter increased from 15 to 34% in pressurized air torrefaction when residence time increased from 15 to 35 min at 200 kPa and 300°C. However, decrease in volatile matter with increasing residence time is less at higher pressure even at severe torrefaction temperature (Table 3.2). This might be the effect of tapering off of devolatilization rate at higher-pressure.

While comparing the pressurized air and nitrogen torrefaction, the former has higher potential to remove volatiles from the biomass. This effect was however noticeable only at severe conditions (Figure 3.4a). For example, volatile matters of torrefied biomass at pressure 600 kPa and residence time of 35 min were 86% and 80% at 220°C and 260°C, respectively in air media, whereas they were 87% and 81% in nitrogen media; but at 300°C, the volatile matters were reduced to 51% and 59% respectively, in air and nitrogen media (Table 3.2).

Fixed carbon content (FC) of torrefied solid products increased with rise in residence time, pressure, and temperature (Table 3.2). It rose from 10% in raw biomass to 49% in torrefied product produced under the pressurized air torrefaction at 600 kPa, 300°C, and 35 min. A typical percentage increase in the FC with respect to raw biomass is shown in Figure 3.4(b). The maximum percentage increase in the FC was 376% under air medium at 300°C, 35 min, and 600 kPa, whereas it was only around 304% in nitrogen medium. Such dependency on the working media was not significant at light and mild torrefaction temperature, while a larger change was observed at severe torrefaction conditions.

Similar results were also presented in Rousset et al. (2012) at atmospheric pressure. This could be explained through an examination of the devolatilization and decomposition of hemicellulose and cellulose. The presence of oxygen in working media does not show any change in the temperature of devolatilization of hemicellulose, whereas the decomposition temperature ranges of cellulose decreases significantly from 335°C at 0% oxygen to 295°C at 20% oxygen (Chouchene et al, 2010). This temperature range lies in the temperature range for severe torrefaction, indicating a higher possibility of mass loss under severe condition.

Fixed carbon content of the torrefied product increased when pressure was increased from 200 to 600 kPa. Furthermore, it was higher in air compared to that in nitrogen. Both increases were distinct at 300°C but nearly imperceptible at 220°C and 260°C. For example, the increase in FC of the products from the torrefaction (35 min) in air media were 1.36%, 2.50%, and 7.92% at 220°C, 260°C, and 300°C, respectively, while it was around 0.41%, 1.39%, and 7.68% in the nitrogen media.

A comparison between pressurized and atmospheric pressure torrefaction under both working media shows that at lower torrefaction temperature the volatile and fixed carbon contents of torrefied biomass under both cases were close to each other, but at higher torrefaction temperature there is significant effect. For instance, volatile content was decreased to 59% at 260°C in atmospheric pressure air torrefaction conducted for 35 min compared that with 82%, 81%, and 80% at 200 kPa, 400 kPa, and 600 kPa respectively. The volatile content of torrefied product decreased up to 41% in atmospheric pressure air torrefaction conducted at severe conditions. Such significant decrease in the volatile content in atmospheric air (unpressurized) torrefaction could be due to a continuous supply of oxygen (air) that maintains the concentration of oxygen unchanged throughout the process, but in the pressurized reactor being closed, the oxygen concentration during pressurized torrefaction will progressively be reduced as the biomass is torrefied. For this reason, one can see a major reduction in the volatile content of torrefied biomass

produced under atmospheric pressure air torrefaction compared that with pressurized air torrefaction.

Fixed carbon content of torrefied biomass was found in the range of 11-59% in atmospheric pressure air torrefaction compared to that with 12-49% in pressurized air torrefaction. Increase in fixed carbon content under the atmospheric pressure air torrefaction was higher at higher torrefaction temperatures. The variation in percentage increase in fixed carbon content compared with that in raw biomass is shown in Figure 3.4(b).

3.3.3 Fuel Ratio

Fuel ratio (FC/VM) is defined as the ratio of fixed carbon and volatile matter content of a fuel. It is an important parameter in biomass co-firing. The lower the fuel ratio of biomass the more difficult it will be to maintain flame stability because of the different burning rates of volatiles and char. Volatiles burn much faster than the fixed carbon. So the fuel with a less fuel ratio is more prone to instability in the flame, causing operational difficulties and poor combustion efficiency in co-firing power plants (Lu et al., 2008). However, high volatile content in biomass could enhance ignition properties of low rank coal (Gani et al., 2005) and then increase the suitability of raw biomass in co-firing, but the high volatile content of biomass also creates non-uniform heat flux distribution inside the furnace and then reduces the extent of blending. Thus improving the fuel ratio of biomass comparable with that of coal, one can increase the share of biomass in the co-firing power plant.

Figure 3.5 shows fuel ratios of torrefied biomass produced at some selected operating conditions. The fuel ratio of torrefied biomass under air medium was generally higher than that in nitrogen, and it increased moderately with pressure. For instance, the fuel ratio of torrefied biomass produced at 600 kPa, 300°C, and 35 min in air media was 0.96 while that at 220°C it was only 0.15. Owing to the continuous presence of oxygen in

atmospheric pressure air torrefaction (at 300°C), authors note the fuel ratio to rise to 1.44. This value exceeds that for lignite and bituminous coal. Higher fuel ratio takes biomass closer to coal or lignite. So, the blending ratio of torrefied biomass with lignite and bituminous coal could be increased significantly in such cases. The fuel ratio in the case of nitrogen torrefaction is lower than that of air torrefaction in all cases due to the oxidation of volatile in oxygen.

Though an increase in the fuel ratio can be related with a decrease in reactivity of torrefied biomass, such decrease in reactivity may have occurred due to the condensation of the heavy volatiles with a more stable carbon compounds. Such condensation may clog the pores formed during torrefaction. This might reduces the reactivity of torrefied biomass obtained at high temperature torrefaction compared that at low temperature torrefaction. This supports a discussion on specific surface area presented in Chapter 2. So, a detailed analysis on the reactivity of the torrefied biomass is needed to answer this question and author has recommended this as a possible future work.

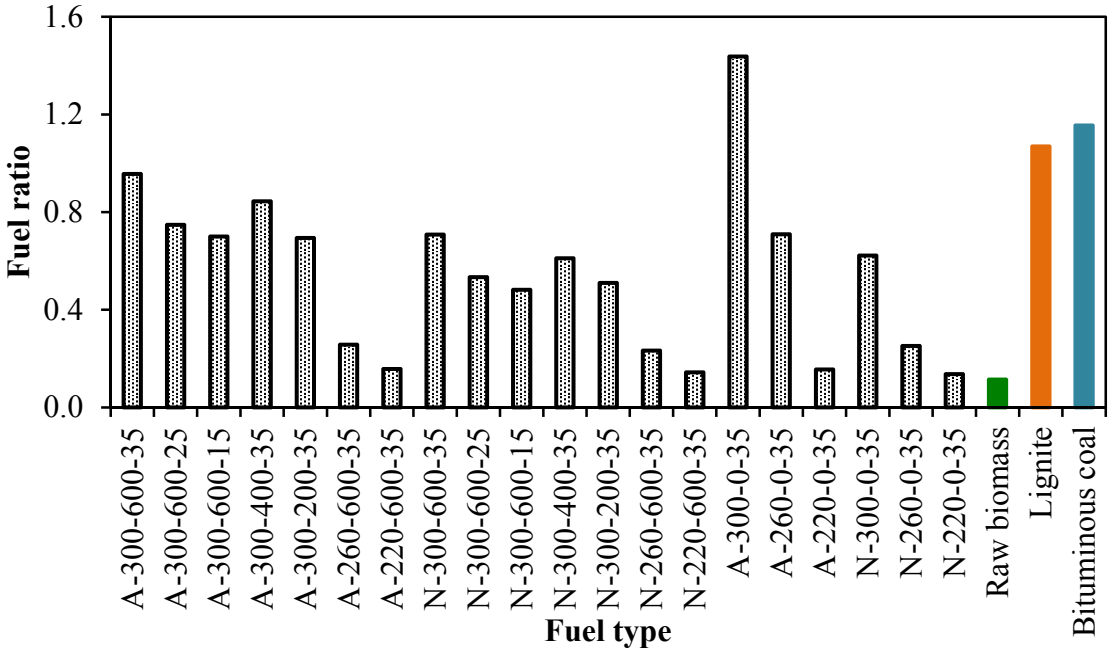

Figure 3.5: Fuel ratio of torrefied biomass, raw, and coal [A=Air 300 °C =Temperature 600 kPa=Pressure 35 min=Time]. Note: A=Air and N=Nitrogen

3.3.4 Mass Yield

Table 3.3 presents the result of mass yields of the torrefaction process at different operating conditions. From a comparison of the mass yield, one notes the lowest mass yield of 49% under pressurized air torrefaction at 300°C, 600kPa, and 35min. In nitrogen media it was around 56% under the same operating conditions. The effect of pressure and residence time on mass yield was minimal at a torrefaction temperature of 220°C under both air and nitrogen media. Similar results were also found in Fang et al. (2006). This suggests that air could be used as a working media without affecting any significant drop in mass yield compared with that of torrefaction using nitrogen if the torrefaction process were to carry out at low temperature condition.

Table 3.3: Mass yield (% weight dry and ash free basis) in torrefaction at different operating conditions

Working media	Pressure (kPa)	Temperature (°C)								
		220			260			300		
		Time (min)								
		35	25	15	35	25	15	35	25	15
Air	0	82.22	84.93	88.57	54.47	60.32	70.87	26.11	37.10	39.62
	200	89.78	89.84	90.37	77.40	79.68	83.12	50.54	56.09	61.62
	400	87.41	88.94	90.07	77.07	79.07	81.31	50.05	54.75	59.77
	600	86.46	87.54	88.86	76.20	77.69	79.45	49.08	51.91	58.59
Nitrogen	0	86.06	87.17	89.14	74.79	75.97	77.96	51.49	53.70	56.20
	200	89.93	91.30	92.33	79.45	82.16	84.97	57.05	59.32	62.45
	400	89.70	90.79	91.94	78.82	79.84	82.28	56.00	57.25	60.39
	600	89.43	90.29	91.61	77.75	78.56	81.20	55.55	56.44	59.43

Mass yields decreased with increase in residence time and reactor pressure at a higher torrefaction temperature. This could be due to cellulose degradation. The reactor pressure causes only minor changes (within the range of 4%) in the mass yield. Figure 3.6 shows the variation in mass yield with pressure under different operating conditions. When the reactor pressure was increased from 200 to 600 kPa, mass yield decreased from 90% to 87% in pressurized air torrefaction at 220°C (Figure 3.6). This effect was within the range of 1% in nitrogen media under identical conditions. Such a small

decrease in mass yields at higher pressure however may be due to a small increment in the formation of light gases such as CO_2 and CO (Rousset et al., 2012). This may be due to a decrease in diffusivity of gas products from the biomass. Such decrease in diffusivity of gas increases the residence time of volatile gases inside the sample, making it favorable to have more heterogenous reactions. So, a decrease in mass yield can be seen when the reactor pressure increases.

Mass yield in pressurized air torrefaction is less than that in nitrogen torrefaction (Table 3.3). At the torrefaction conditions of 600 kPa, 300°C, and 35 min, mass yields under air and nitrogen media were 49% and 56%, respectively. Such lower mass yield in an oxidative environment was also reported in Lu et al. (2012). This is due to the possibility of increased partial pressure of oxygen, causing more solid and oxygen reaction in the oxidative medium. However, mass yields were similar in both air and nitrogen media at lower temperature torrefaction. For example, at 220°C and 260°C, the mass yields were found around 89% and 79%, respectively. This may be due to an insufficient heat source to overcome the activation energy level required for the heterogeneous reactions.

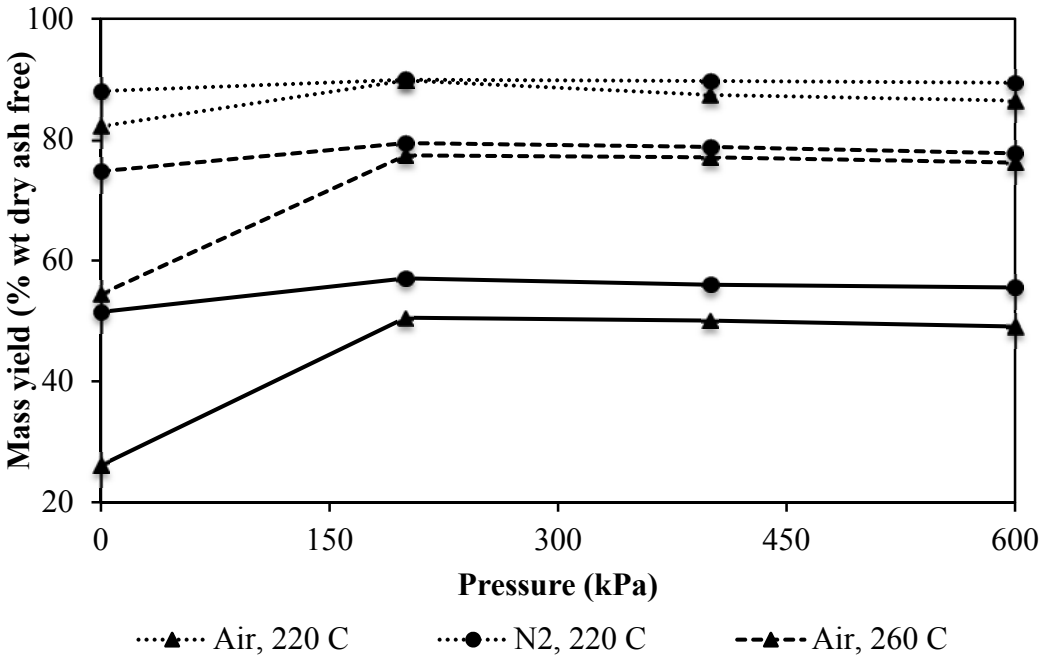

Figure 3.6: Effect of pressure in the mass yield (Residence time=35 minutes)

Mass yields under pressurized torrefaction also compared that with the atmospheric pressure torrefaction process in Figure 3.6. Mass yields were significantly lower in the atmospheric pressure air torrefaction than those with the pressurized torrefaction. For instance, the mass yield in atmospheric pressure reactor decreased to 26% at torrefaction temperature of 300°C and in 35 min of residence time. Under the similar conditions, pressurized nitrogen torrefaction yields around 50% solid mass (Table 3.3). Such a significant decrease in the mass yield in the atmospheric pressure air torrefaction is due to availability of free oxygen over entire operation.

In atmospheric pressure nitrogen torrefaction, mass yields were not significantly decreased compared those with pressurized nitrogen torrefaction. The lowest mass yield was found 52% in the atmospheric pressure torrefaction at severe conditions, i.e. 300°C and 35 min compared that with 56% in the pressurized torrefaction at 600 kPa, 300°C, and 35 min. However, the main advantage of pressurized torrefaction over atmospheric pressure nitrogen torrefaction would be the savings in the nitrogen gas. Though amount of savings of the nitrogen gas would be small in this study (small-scale reactor), the savings would be more significant in the industrial scale reactor.

3.3.5 Energy Density and Energy Yield

The loss of volatiles during torrefaction produces an excellent energy dense solid product that is suitable for co-firing, but an ideal torrefaction technology must retain a reasonable amount of original energy of the raw biomass. Table 3.2 shows the higher heating values of torrefied biomass obtained under different operating conditions. Table 3.4 presents energy density enhancement factor (EDEF) of the torrefied biomass. The maximum EDEF of 1.42 was found under the pressurized air torrefaction. Increases in heating values were 5%, 13%, and 42% at 220°C, 260°C, and 300°C, respectively at different pressures and residence times. Enhancement of energy density factor was more in the pressurized air torrefaction than that in nitrogen. For instance, the maximum value of EDEF was only around 1.34 in nitrogen media compared to 1.42 for air.

The EDEF increased when residence time was raised. The EDEF, for instance, increased from 16% at 15 min to 38% at 35 min at severe torrefaction conditions in air medium, but this effect was not significant at low temperature. The reactor pressure has only a minor effect on the EDEF and does not show any specific trend. However, authors had found that the surfaces of solid products were deposited with patches of dark color tars. This could be an evidence of cracking of tar on char surface. These patches were higher at a high reactor pressure. For this reason, the carbon content in the product under pressurized torrefaction increases with the reactor pressure, resulting in an increase in energy density. In atmospheric pressure air and nitrogen torrefaction, no such dark patches were found. Due to this, though the atmospheric pressure air torrefaction showed higher volatiles losses (more mass loss), energy densities of solid products are still lower than that from the pressurized air torrefaction especially at high pressure.

Table 3.4: Comparative values of energy density enhancement factor of torrefied biomass (-)

Working media	Pressure (kPa)	Temperature (°C)								
		220			260			300		
		Time (min)								
		35	25	15	35	25	15	35	25	15
Air	0	1.023	1.033	1.026	1.237	1.270	1.089	1.343	1.382	1.352
	200	1.010	1.007	1.001	1.126	1.108	1.080	1.377	1.266	1.159
	400	1.034	1.016	1.008	1.121	1.097	1.080	1.419	1.322	1.266
	600	1.050	1.039	1.009	1.123	1.117	1.100	1.396	1.372	1.319
Nitrogen	0	1.028	1.028	1.014	1.089	1.084	1.074	1.159	1.223	1.205
	200	1.028	1.019	1.021	1.084	1.055	1.004	1.272	1.268	1.214
	400	1.033	1.017	1.008	1.106	1.095	1.068	1.312	1.290	1.206
	600	1.021	1.002	1.003	1.101	1.091	1.062	1.338	1.315	1.210

Table 3.5 shows energy yields (in dry and ash free basis) of the torrefaction at different operating conditions. Energy yields reduced with temperature for both air and nitrogen, with slightly higher value for nitrogen than for air. This suggests that energy yields in air and nitrogen media are comparable though mass losses are higher in air medium. This is due to higher energy density of the torrefied product in air medium. Torrefaction temperature is the only major parameter with a significant effect on energy yield. The

energy yield is not affected much by the reactor pressure, which varies within the range of 2-3%. Residence time also does not show any significant changes in the energy yield.

Table 3.5: Energy yields from air and nitrogen torrefaction (% dry and ash free basis)

Working media	Pressure (kPa)	Temperature (°C)								
		220			260			300		
		Time (min)								
		35	25	15	35	25	15	35	25	15
Air	0	84.10	87.69	90.90	67.36	76.60	77.16	35.06	51.27	53.58
	200	90.68	90.46	90.44	87.13	88.29	89.78	69.59	71.00	71.44
	400	90.39	90.38	90.76	86.41	86.77	87.83	71.00	72.93	75.67
	600	90.79	90.97	89.67	85.61	86.78	87.43	68.51	71.21	77.30
Nitrogen	0	90.49	89.59	90.35	81.44	82.33	83.72	59.69	65.68	67.70
	200	92.41	93.02	94.24	86.13	86.66	85.27	72.55	75.24	75.79
	400	92.70	92.37	92.69	87.19	87.39	87.88	73.47	73.87	72.86
	600	91.30	90.47	91.92	85.62	85.72	86.23	74.34	74.19	71.89

Energy yields were also compared between pressurized and atmospheric pressure torrefaction. One can see (Table 3.5) that energy yields were decreased much faster in the atmospheric pressure air torrefaction compared that in the pressurized air torrefaction. The minimum energy yield was 35% in the atmospheric pressure air torrefaction, which is much lower than 70% in the pressurized air torrefaction. These results were also similar in the nitrogen medium though the extent of decrease in energy yields was not as low as in the air medium. Table 3.5 also reveals that the energy yield obtained at high temperature atmospheric pressure nitrogen torrefaction is lower than that in the pressurized reactor in air medium. This suggests that the pressurized air torrefaction is more useful over conventional atmospheric pressure nitrogen torrefaction.

3.3.6 Correlations for Mass Loss in Pressurized Torrefaction

Anhydrous mass loss during torrefaction could give a good indication of the changes in energy properties or fixed carbon in torrefied product. This loss is a function of operating parameters like residence time, temperature, pressure, and type of biomass (Vincent et al., 2010). In addition to this, the mass loss is also affected by type of reactors, particle

size, and working medium. So, while designing a torrefier system, it would be easy to find an optimum design point if the designer has an easier means for finding the effects of operating parameters on mass losses during torrefaction. Almeida et al. (2010) developed linear correlations between mass loss and other properties of torrefied solid product like fixed carbon, volatile matter, and energy density, but they were not able to relate mass loss with the operating parameter that influence this. Additionally, they did not study the effect of pressure and gas media. The present study therefore developed correlations, showing the effect of operating parameters like pressure, temperature, and time on the mass loss during torrefaction process. As this has not been reported so far in the open literature, it could greatly help in designing and developing commercial torrefaction units.

Two different correlations were proposed: one for air and another for nitrogen medium. Response surface methodology (RSM) principles were used to analyze the effect of operating parameters and to identify the factor with most influence on pressurized torrefaction. Correlations are developed using the RSM in Minitab (16) software. Tables 3.6 and 3.7 present the randomly developed Box-Behnken experimental designs for three factors (Pressure-*P* in kPa, Residence time-*Rt* in minutes, and Temperature-*T in* ºC) at three levels for pressurized air and nitrogen torrefaction. Predicted values of mass loss and their errors between predicted and measured values are also shown in the corresponding tables. The error levels were negligible in both correlations, indicating high accuracy of prediction. Correlations for mass loss in air ML_{air} and in nitrogen ML_{N2} are:

$$ML_{air} = 247.172 - 213.466 \times 10^{-2}T - 559.571 \times 10^{-5}P - 643.810 \times 10^{-3}Rt + 467.116 \times 10^{-5}T^2 + 638.374 \times 10^{-8}P^2 - 225.466 \times 10^{-5}Rt^2 + 589.618 \times 10^{-7}TP + 441.289 \times 10^{-5}TRt - 309.754 \times 10^{-6}PRt \quad (3.5)$$

$$ML_{N2} = 163.446 - 157.127 \times 10^{-2}T + 543.886 \times 10^{-5}P + 242.544 \times 10^{-3}Rt + 369.968 \times 10^{-5}T^2 - 103.732 \times 10^{-8}P^2 - 588.043 \times 10^{-5}Rt^2 + 584.744 \times 10^{-7}TP + 137.740 \times 10^{-5}TRt - 259.660 \times 10^{-6}PRt \quad (3.6)$$

Table 3.6: Randomly generated Box Behnken experimental design for pressurized air torrefaction by Minitab 16

Standard order	Run order	Factors			Experimental value of mass loss (% wt. daf), *E*	Predicted value of mass loss (% wt. daf), *P*	Error (*E*-*P*)	% Error (%)
		T (°C)	*P* (kPa)	R_t (min)				
2	1	300	200	25	43.91	43.89	0.01	0.1
12	2	260	600	35	23.80	24.43	-0.63	-2.7
7	3	220	400	35	12.59	11.95	0.64	5.1
3	4	220	600	25	12.46	12.47	-0.01	-0.1
13	5	260	400	25	20.93	20.93	0.00	0.0
1	6	220	200	25	10.16	10.58	-0.42	-4.1
10	7	260	600	15	20.55	20.33	0.23	1.1
5	8	220	400	15	9.93	10.14	-0.21	-2.1
6	9	300	400	15	40.23	40.87	-0.64	-1.6
8	10	300	400	35	49.95	49.74	0.21	0.4
15	11	260	400	25	20.93	20.93	0.00	0.0
14	12	260	400	25	20.93	20.93	0.00	0.0
4	13	300	600	25	48.09	47.68	0.42	0.9
9	14	260	200	15	16.88	16.25	0.63	3.7
11	15	260	200	35	22.60	22.83	-0.23	-1.0

Since the R^2 values for both correlations are well within the range of acceptable level, correlations are considered to be statistically significant. Results of statistical analysis are presented in Table 3.8. In the statistical analyses, different terms with p-values less than 0.05 are considered only as significant terms. The linear term of pressure, temperature, and time has a significant effect on the mass loss during torrefaction under both air and nitrogen media. Among the squared terms, only the temperature squared (T^2) term has significant effect in both working media. The effect of temperature is highly significant in both linear and quadratic terms compared to the other two factors. This suggests that temperature is the prime factor that affects the characteristics of pressurized torrefaction irrespective of working media or other operating parameters.

The combined effect of temperature and residence time has a positive effect on the mass loss, which indicates that larger mass loss occurs at higher temperature and longer residence time. The combined effect of temperature and residence time is, however, smaller in nitrogen than that in air media. This suggests that presence of oxygen in air medium could further increase mass loss at higher temperature and residence time.

Table 3.7: Randomly generated Box Behnken experimental design for pressurized nitrogen torrefaction by Minitab 16

Standard order	Run order	Factors			Experimental value of mass loss (% wt. daf), *E*	Predicted value of mass loss (% wt. daf), *P*	Error (*E*-*P*)	% Error (%)
		T (°C)	*P* (kPa)	R_t (min)				
13	1	260	400	25	20.16	20.16	0.00	0.0
6	2	300	400	15	39.61	39.39	0.22	0.7
4	3	300	600	25	43.56	43.69	-0.12	-0.3
1	4	220	200	25	8.70	8.58	0.12	1.4
2	5	300	200	25	40.68	40.41	0.27	0.7
14	6	260	400	25	20.16	20.16	0.00	0.0
15	7	260	400	25	20.16	20.16	0.00	0.0
8	8	300	400	35	44.00	44.37	-0.37	-0.8
7	9	220	400	35	10.30	10.52	-0.22	-2.1
5	10	220	400	15	8.06	7.70	0.37	4.5
12	11	260	600	35	22.25	21.76	0.49	2.2
9	12	260	200	15	15.03	15.52	-0.49	-3.3
10	13	260	600	15	18.80	18.90	-0.10	-0.5
11	14	260	200	35	20.55	20.46	0.10	0.4
3	15	220	600	25	9.71	9.98	-0.27	-2.8

To examine the applicability correlation over wider pressure ranges both below and above the operating pressure of the present study, the proposed correlation under nitrogen medium was validated with mass losses observed by Wannapeera and Worasuwannarak (2012) at different pressure and temperature. The main purpose of this validation with published data is only to check the data trend rather than the actual value as they depend on (i) biomass type, (ii) particle size, (iii) working media, and (iv) reactor type.

Table 3.8: Results of statistical analyses

Parameter	Air						Nitrogen					
	DF	Seq. SS	Adj. SS	Adj. MS	F values	P values	DF	Seq. SS	Adj. SS	Adj. MS	F values	P values
R^2	99.92						99.96					
Adjusted R^2	99.77						99.87					
RMS	0.6571						0.4569					
Regression	9	2644.32	2644.32	293.81	680.52	0.000	9	2328.29	23.28.19	258.69	1238.85	0.000
Linear	3	2420.55	2420.55	806.85	1868.80	0.000	3	2189.29	2189.29	729.76	3494.82	0.000
T	1	2347.44	2347.44	2347.44	5437.06	0.000	1	2147.91	2147.91	2147.91	10286.32	0.000
P	1	16.12	16.12	16.12	37.34	0.002	1	10.96	10.96	10.96	52.48	0.001
Rt	1	56.99	56.99	56.99	132.00	0.000	1	30.41	30.41	30.41	145.65	0.000
Square	3	208.88	208.88	69.63	161.27	0.000	3	135.79	135.79	45.26	216.76	0.000
T×T	1	208.42	206.25	206.25	477.70	0.000	1	134.00	129.38	129.38	619.60	0.000
P×P	1	0.28	0.24	0.24	0.56	**0.489**	1	0.51	0.64	0.64	3.04	**0.141**
Rt×Rt	1	56.99	56.99	56.99	132.00	**0.539**	1	1.28	1.28	1.28	6.11	**0.056**
Interaction	3	14.89	14.89	4.96	11.49	0.011	3	3.12	3.12	1.04	4.97	0.058
T×P	1	0.89	0.89	0.89	2.06	**0.211**	1	0.88	0.88	0.88	4.19	**0.096**
T×Rt	1	12.46	12.46	12.46	28.87	0.003	1	1.16	1.16	1.16	5.56	**0.065**
P×Rt	1	1.54	1.54	1.54	3.56	**0.118**	1	1.08	1.08	1.08	5.17	**0.072**
Residual error	5	2.16	2.16	0.43			5	1.04	1.04	0.21		
Lack of fit	3	2.16	2.16	0.72			3	1.04	1.04	0.35		
Pure error	2	0.00	0.00	0.00			2	0.00	0.00	0.00		
Total	14	2646.48					14	2329.23				

Note: Bolded P values (> 0.05-5.00% confident level) are considered to be statistically insignificant terms

Figure 3.7 shows the experimental mass loss measured by Wannapeera and Worasuwannarak (2012) and the model predicted mass loss (using Eq 3.6). The predicted mass losses were more close to the measured values at 1000 kPa compared to those with atmospheric pressure condition. The figure also reveals higher mass loss at 1000 kPa compared to those at atmospheric pressure. This indicates that the mass yield decreases when the reactor pressure increased. This supports the conclusion we drawn from Table 3.3.

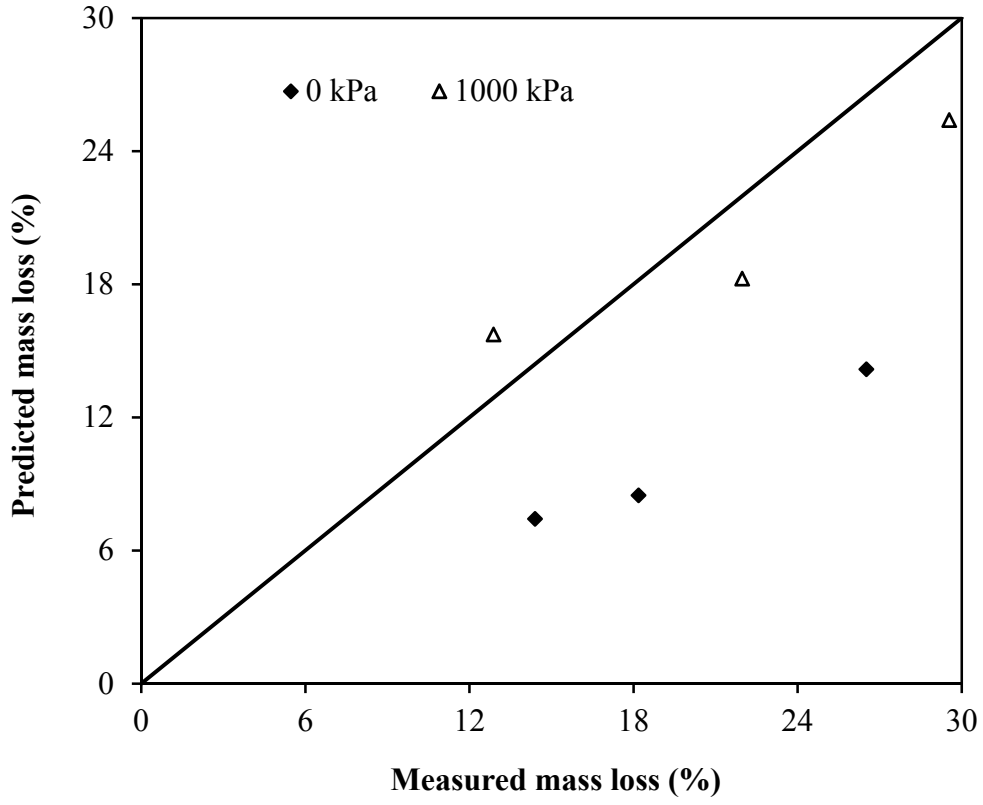

Figure 3.7: Verification of correlation trend with published experimental values

3.3.7 Correlations between Mass Loss and Other Properties

For a complete characterization of the torrefied product, one needs higher heating values as well as proximate analyses. To do that, bomb calorimeter is required to determine higher heating value of fuels, which is not only time-consuming but also expensive (Nhuchhen and Salam, 2012). Therefore, determination of the higher heating values for each different torrefied solid products at various operating conditions is not cost-effective. An empirical correlation to determine higher heating values thus could help in reducing expense and effort in analyzing the samples. Similarly, proximate analysis is also a tedious job that requires much time and experimental facilities. Though the proximate analysis is easier than ultimate and heating value analysis, it is still laborious especially when the number of samples is large.

Therefore, this study attempts to develop a correlation for fuel ratio (*FR*) and energy density enhancement (*EDE*) as a function of mass loss, which could facilitate in characterizing and analyzing the solid product of pressurized torrefaction.

Proposed correlation is a second order polynomial equation in the form as:

$$\theta = a + bML + cML^2 \tag{3.7}$$

Where θ represents different dependent variables such as energy density enhancement (*EDE*) and fuel ratio, and *ML* ((*ML* = 100 − *MY*) % daf) is the percent of mass loss during torrefaction process. All the parameters are expressed in dry and ash free basis.

To fit and develop the correlation, 27 data under pressurized air torrefaction at different operating conditions were used and then remaining 27 data under pressurized nitrogen torrefaction were used for validation. Correlations were developed using the principle of the least sum square error to fit the curve. The solver tool from the Microsoft Excel 2011 was used to iterate coefficients (a, b, and c) of the proposed equations. Table 3.9 shows

the correlations developed. The constant term of the correlation for the energy density enhancement is zero, indicating no energy density enhancement until there is any dry mass loss. The table also presents the sum of the least squares error and mean absolute error (MAE). The lower the value of MAE indicates that accuracy of the prediction is higher. Figure 3.8 plots experimentally measured against predicted values of energy density enhancement and fuel ratio. Most of the plotted points are closed toward the straight line; indicating only a small error between predicted and experimentally measured values.

Table 3.9: Correlations developed for the EDE and FR

Parameter	Correlation	Sum of the least square error	Mean absolute error
EDE (%)	$EDE = ML(0.17033 + 0.01214ML)$	175.7	1.47
Fuel Ratio-*FR* (*FC*/*VM*)	$FR = 0.08811 + 0.00074ML + 0.00026ML^2$	0.12	0.03

Note: Mean absolute error (MAE) =∑| (Predicted-Measured) |/*N*, and *N*=27. The unit of MAE is same as the parameter.

3.3.8 Characterization: Modes of Torrefaction

In the previous literature, the mode of torrefaction is defined mainly by the process parameter, torrefaction temperature. It would have been more useful if it could be characterized with product parameters such as mass yield, energy yield, proximate analyses, heating values, volatile generation rate, and level of energy consumption.

The authors thus offer a quantitative characterization of different modes of torrefaction. This characterization though use of the same modes (light, mild, and severe) is based on

the experimental results as presented in Table 3.10. It shows that average mass yields are around 90%, 80%, and 55% for light, mild, and severe torrefaction, respectively.

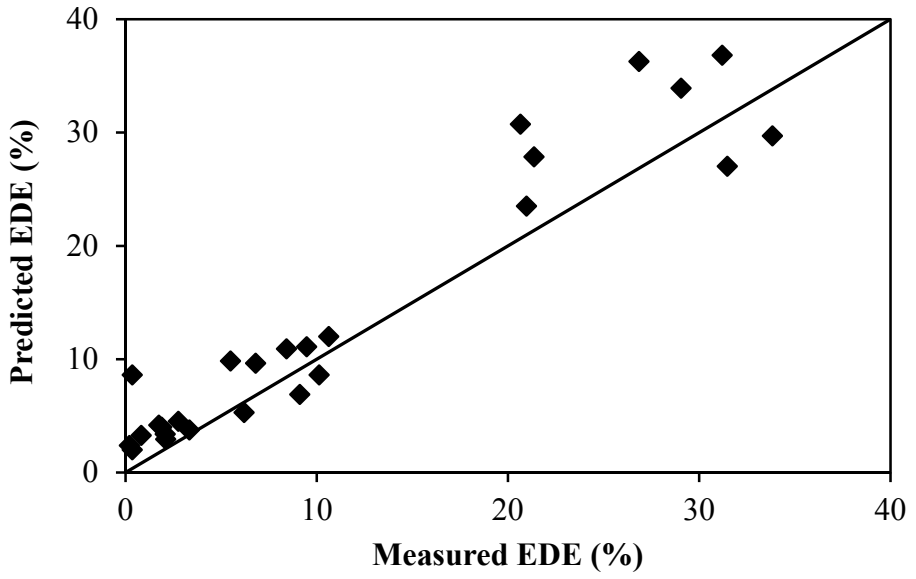

(a)

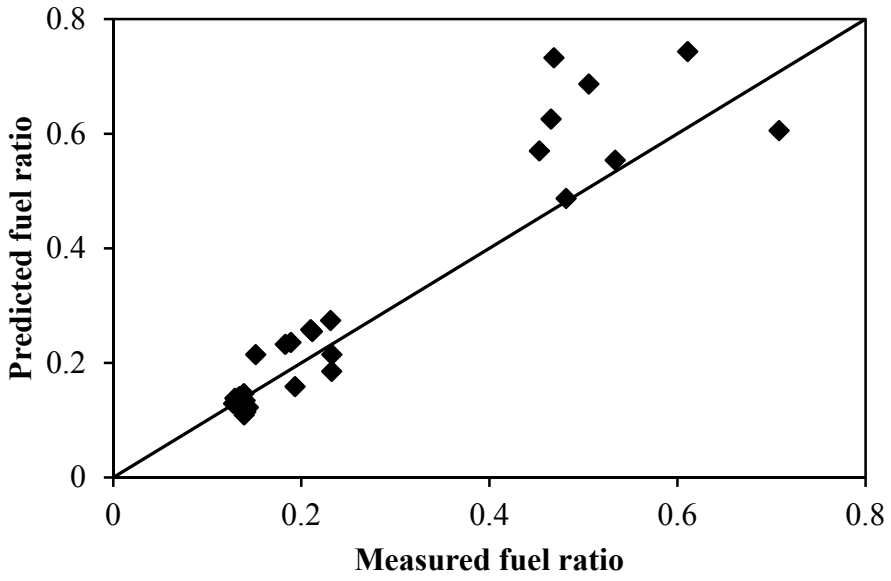

(b)

Figure 3.8: Validation of correlations: (a) energy density enhancement; and (b) fuel ratio

Table 3.10: Characterization of different modes of pressurized torrefaction

Parameter	Medium	Mode of torrefaction		
		Light (220°C)	Mild (260°C)	Severe (300°C)
Mass yield (% wt. daf)	Air	88.8	79.0	54.7
	Nitrogen	90.8	80.5	58.2
Energy yield (% wt. daf)	Air	90.5	87.3	72.1
	Nitrogen	92.4	86.4	73.8
Energy density enhancement (%)	Air	1.9	10.5	32.3
	Nitrogen	1.7	7.4	27.0
Fuel ratio (*FC*/*VM*)	Air	0.142	0.218	0.657
	Nitrogen	0.137	0.204	0.526

Such a table could be used in a decision-making process. For example, the selection of mode of torrefaction operation depends on the application of torrefied biomass and the location of end users. A supplier of torrefied biomass, who does not require a longer distance shipping, can operate the reactor in severe torrefaction mode because its low mass yield can reduce the transportation cost. Higher energy density in severe mode can compensate for the cost of the mass loss during the torrefaction process. Severe torrefaction has a higher fuel ratio (Table 3.10). So, the torrefied solid product from this would permit an increase of biomass in the coal blend ratio in co-firing power plants and save emission reduction cost compared to that for coal alone. Similarly, if the biomass cannot be torrefied at the source and it needs to be transported a long distance; the high transportation cost has already been incurred. So, a torrefied biomass at mild conditions may increase the utilization of biomass because of its higher mass yield compared with that at a severe torrefaction mode. Though the severe torrefaction produces a product of higher energy density, its lower mass yield may have a negative impact on the economic attractiveness of the overall torrefaction plant.

3.4 SUB-CONCLUSIONS

This work investigated mildly pressurized torrefaction of biomass in both air and nitrogen media. Effects of pressure, temperature, torrefaction time, and working media on a

torrefied solid product were studied. The effect of the above parameters was also analyzed using the response surface methodology (RSM) method, and a correlation was developed for prediction of mass loss due to torrefaction. Additional correlations between mass loss, energy density enhancement, and fuel ratio were also developed. The importance findings are listed below:

- The effect torrefaction temperature on mass yield is greater than those of torrefaction medium, residence time, and reactor pressure.
- The effect of torrefaction medium (air or nitrogen) is small at low torrefaction temperature, but it is significant at high temperature.
- The energy density enhancement factor (*EDEF*) is higher in mildly pressurized air reactor compared to that in nitrogen fed atmospheric pressure reactor.
- In a mildly pressurized reactor, the energy yields are similar in both air and nitrogen media due to higher energy density of solid product produced in pressurized air torrefaction. However, the energy yield in nitrogen medium at atmospheric pressure is lower than that in the pressurized reactor in air medium.

The above remarks suggest that nitrogen could be replaced by air in mildly pressurized torrefaction.

- Mass loss may be correlated with pressure, temperature, and residence time by eqs 3.5 and 3.6.
- Both energy density enhancement and fuel ratio may be correlated with the mass loss (*ML*) as
- $EDE = ML(0.17033 + 0.01214ML)$
- $FR = 0.08811 + 0.00074ML + 0.00026ML^2$

The above four correlations could give a complete product characterization of mildly pressurized torrefaction.

CHAPTER 4: INVESTIGATION INTO MEAN RESIDENCE TIME AND FILLING FACTOR IN FLIGHTED ROTARY TORREFIER[‡]

Remaining chapters of the thesis concern with a two–stage continuous indirectly heated rotary torrefier. Present chapter gives a brief introduction to different types of continuous torrefiers laying the background for the development of inclined rotary two stage torrefiers with flights. This chapter then deals with the kinematics of solid's motion through such reactor while chapter 5 explores the overall heat transfers in it, and chapter 6 reports the results of torrefaction in it.

4.1. INTRODUCTION

A number of different reactor technologies for torrefaction have been proposed and implemented (Batidzirai et al., 2013; Koppajan et al., 2015), but none of them work perfectly. Additionally, these technologies have also not been studied in depth, which is alarming since reactor types have significant effects on the solid products of the biomass torrefaction process. Depending upon the design of the reactor and the method of heat transfer, the quality of the torrefied solid products may also vary greatly. For instance, Dhungana et al. (2012) found that the rotating drum reactor produced the torrefied solid products with much higher energy yield, compared to other reactors such as the microwave, fluidized bed, and convective fixed bed reactors.

Several companies, such as FoxCoal (Netherlands), Agritech (USA), Biolake (Netherlands), and 4Energy Invest (Belgium), are currently working on developing an indirectly heated rotary torrefier. Some companies, like Earth Care Product Incorporation

[‡] This chapter is taken from the paper published by the candidate: Nhuchhen, D. R., Basu, P., Acharya, B. (2015), "Investigation into mean residence time and filling factor in flighted rotary torrefier," *The Canadian Journal of Chemical Engineering*, Paper under Editorial Office, November 2015.

and AIREX Energy, have established a system using two rotary reactors, enabling separation of the drying and devolatilization stages of the torrefaction process and allowing for separation of the water vapor and volatile gases that result from these respective stages. The moisture-free volatile gases can then be burnt in order to provide a portion of the total heat load needed for the overall process. This, in turn, may help to reduce auxiliary fuel consumption and enhance the net system efficiency. Krokida et al., (2006) report the virtues of inclined rotating rotor surrounded peripherally by a cylindrical shell where feedstock, fed from the upper end of the reactor, moves towards the lower end.

The CFB laboratory of Dalhousie and Greenfield Research Incorporated of Halifax improved the above design by adding flights and developed a two-stage continuous indirectly heated rotary torrefier. The flights in rotary reactors provide excellent solid mixing through tumbling motion, which enhances heat transfer to the solid. A detailed parametric study of such two-stage continuous indirectly heated torrefier is still lacking, precluding systematic design and optimization of the overall torrefaction process.

The overall design process requires information on how solid movement affects the mean residence time, as well as heat transfer and the quality of the torrefied solid products. A study on the solid movement within the rotary reactor is essential for estimation of the solid mean residence time and the solid filling factor in the reactor for any given set of operating conditions. Thus, the main objective of this chapter is to investigate the two important design parameters, mean residence time and filling factor, of rotating drum reactors of the developed torrefier. To accomplish this, authors develop semi-empirical expressions for mean residence time and filling factor, and then validate them against the experimental data.

4.1.1 Design parameters

The mean residence time (R_t) is defined as the average time spent by the particles in the rotary reactor while they advance towards the exit port during the course of the reactor's rotation. Mean residence time of particle, which depends on the type of particle, rotational speed has a major influence on the heat and mass transfer in a rotating drum reactor (Grajales et al., 2012; Li et al., 2002). Thus, mean residence time is considered to be one of the most important parameters in terms of the overall effectiveness of the process.

There are a number of ways to estimate the mean residence time of particles, including the residence time distribution (RTD) method (Li et al., 2002), the particle tracking method using a high magnification camera (Lebas et al., 1995), and measurement of the solid hold-up in the reactor (Shone and Bravo, 2007). This study, assuming the plug flow of the solids at a steady operating condition, has used the most practical method (Eq. 4.1), as presented in Shone and Bravo (2007).

$$R_t = \frac{Solid\ hold-up \text{ in } the\ reactor}{Steady\ state\ solid\ \ flow\ rate} \tag{4.1}$$

In the above equation, solid hold-up is the mass of solid inside the reactor at steady operating conditions, which depends mainly on the solid flow rate and the other operating conditions of the reactor.

The particle motion in the rotary drum reactor can be divided into its axial and transverse components (Boateng, 1993). The axial component determines the axial solid velocity along the axis of the reactor and, as a result, also the mean residence time, whereas the transverse component contributes to the transverse mixing of particles inside the reactor. However, in the case of an inclined rotary reactor with a Length/Diameter ratio greater than 5, the flow of solid in the transverse direction can be disregarded (Bensmann et al.,

2010). From the simplest Seaman model (Seaman, 1951) to a complex Descoins model (Descoins et al., 2005), much work has been done to predict the mean residence time in the rotary reactor (Chen et al., 2009; Li et al., 2002; Li et al., 2002a; Liu and Specht, 2006). Most of these works are for directly heated reactor systems, with or without the effect of the gas flowing through the reactor. Table 4.1 summarizes predictors of the mean residence time, as proposed by such studies.

Table 4.1: Correlations for estimating mean residence time of particles in rotary reactor

Correlation	Source
$R_t = \frac{7856d^{0.032}\rho^{0.002}}{\frac{\pi D^2 Fr}{4}(18.95S+1)} + \frac{1009d^{-0.0765}\rho^{0.002}}{(27.22S+1)} - \frac{0.108G^{0.5}}{(29.19S+1)}$ [s]	Alvarez and Shene (1994)
$R_t = \frac{10.58\mathcal{L}}{SN^{0.9}D}$ [s]	Friedman and Marshall (1949)
$R_t = \frac{10.58\mathcal{L}}{SN^{0.9}D} \pm \frac{608.3}{{d_p}^{0.5}}\frac{\mathcal{L}G}{F}$ [s]	Friedman and Marshall (1949)
$R_t = \frac{12.024\mathcal{L}}{NDsin\beta}$ [s]	Klose and Wiest (1999)
$R_t = \frac{13.8\mathcal{L}}{SN^{0.9}D} \pm \frac{590.6}{d^{0.5}}\frac{\mathcal{L}G}{F}$ [s]	Perry and Green (1984)
$R_t = \frac{{78912h_b}^{0.24}}{(tan^{-1}(S))^{1.02}N^{0.88}\left(\frac{\pi D^2 F}{4}\right)^{0.072}}$ [s] & $h_b = [1-\cos(\gamma/2)]D/2$	Sai et al. (1990)
$R_t = \frac{106.2\mathcal{L}\delta^{.5}}{tan^{-1}(S)ND}$ [s]	Sullivan et al. (1927)
$R_t = \frac{21\mathcal{L}}{SN^{0.9}D} \pm \frac{614.2}{d^{0.5}}\frac{\mathcal{L}G}{F}$ [s]	Renaud et al. (2000)

Notation: δ angle of repose of material in dry condition (degree), S dryer slope (m/m), β inclination of the reactor (degree), N angular speed of drum (RPM), D drum inner diameter (m), d particle diameter (m), Fr Froude number (w^2R/g-), $\mathcal{L}$ effective drum length (m), G gas flow rate per unit area of cross-section (kg/hr.m^2), F solid flow rate per unit area of cross-section (kg/hr.m^2), h_b bed height within reactor (m), γ Angle subtended by bed at the center of the reactor (rad), w is angular velocity, and R is radius of the reactor.

Filling factor, defined as the percentage of the solid volume occupied in the total volume of the reactor itself, is another of the rotary reactor's most important design parameters. Solids flowing through the drum of a rotary reactor rarely fill the drum entirely, and

occupy only a small fraction of the drum volume (m^3). This helps to maintain the tumbling motion of solid particles. It has been recommended that the filling factor, which determines the solid volume or bed load at a particular condition, should not exceed 16% (Konisia, 1984). Therefore, to avoid this limit and operate the reactor smoothly, the filling factor of a reactor operated under any operating conditions should be known. The following expression is used to determine the filling factor (%).

$$F_f = \frac{Volume\ of\ solids}{Volume\ of\ reactor} \times 100 \tag{4.2}$$

Equation (4.2) can be rewritten using the solid hold-up (kg) and the bulk density (kg/m^3) of solids, as follows.

$$F_f = \frac{Solid\ hold-up}{Bulk\ density\ of\ solids \times Volume\ of\ reactor} \times 100 \tag{4.3}$$

4.2. MODEL DEVELOPMENT

4.2.1 Solid Motions

Song (2003) discussed the four solid motions that determine the phenomenon of solid movement within rotary reactors:

a) Cascaded motion of solids using flights (Friedman and Marshall, 1949),
b) Rolling motion of solids at the top of the bulk bed surface inside the reactor (Kelly and O'Donnell, 1977),
c) Bouncing motion of solids at the cylinder wall or solid bed surface (Kelly and O'Donnell, 1968), and
d) Sinking motion of solids from the top of the solid bed surface to the reactor wall (Kelly and O'Donnell, 1968).

It is interesting that each mechanism can affect the motion of particles and, consequently, the overall process occurring inside the reactor. One of the mechanisms, the cascaded motion of particles, mainly describes the path of a particle in a rotary reactor installed with the flights (lifters). The forward motion of a particle during each cascaded cycle during the course of the rotation of the rotary reactor results in axial movement of the particle and alters the mean residence time. Figure 4.1 shows the developed torrefier system using such two rotary reactors with the flat axial flight (flights are not visible in this photograph).

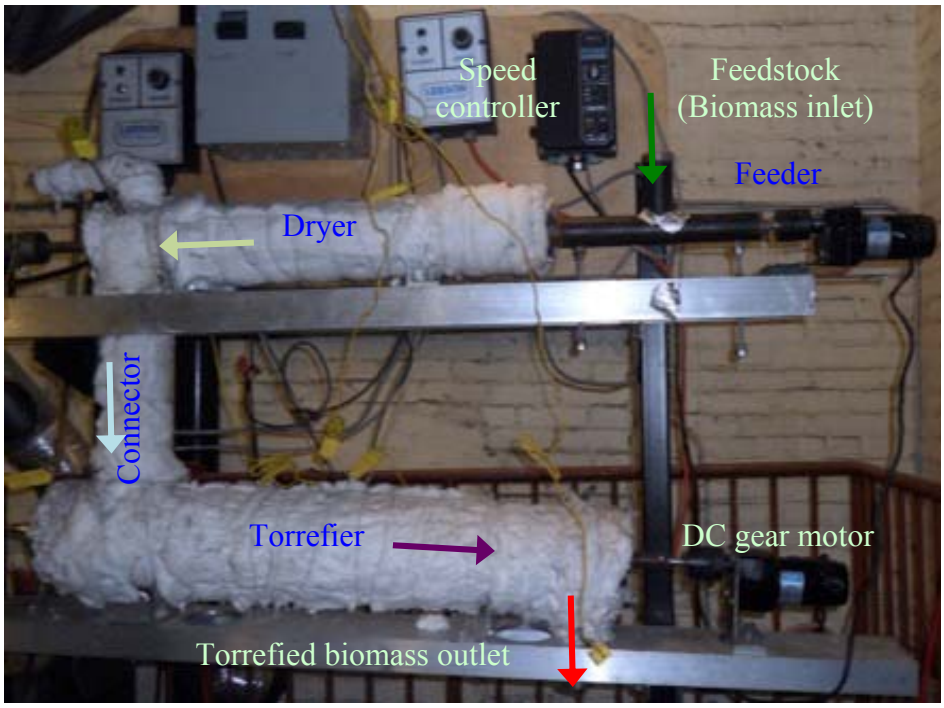

Figure 4.1: Experimental setup showing particle flow directions

4.2.2 Cascaded Motion of Particle

The cascaded movement (cycle) refers to an ideal pathway followed by a particle inside the reactor as it moves towards the exit port, as illustrated in Figure 4.2. In a cascaded cycle, the particle is lifted up by a flight (Figures 4.2a, 4.2b, and 4.2c). Beyond a certain

angle (θ), the particle starts rolling over the flight surface (Figure 4.2d), and then flies from the edge of the flight (Figure 4.2e) back to the bottom of the reactor. Finally, the particle is picked up by another flight and continues into the next cascaded cycle.

Owing to the small inclination of the reactor, the particle does not fall on the same radial plane, instead moving forward a certain axial distance (Figure 4.2f). This forward movement during each cascaded cycle, which is associated with four different times (uplifting time (t_u), rolling time (t_r), falling time (t_f), and pick-up time (t_{pu})), leads to the axial motion of the particle.

4.2.3 Mean Residence Time

Mean residence time of a particle can be estimated using the cascaded cycle time, the axial distance travelled by a particle per cycle, and the effective length of the reactor. Derivation of different components of the cascaded cycle times for an ideal spherical particle is presented in the appendix A. As the biomass particle displaces more than 30° before it starts rolling over the flight, Eq. A.23 can be used to determine the total cascaded cycle time. Neglecting the rolling and falling times, and using Eqs. (A.27) and (A.25), Eq. (A.23) can be further simplified as:

$$t_{cas} = \frac{4\pi}{3\omega} \tag{4.4}$$

In order to simplify the axial distance per cascaded cycle, it can be assumed that the particle will land very close to position 1. Thus, the angle α will be close to zero. So, the vertical falling height (Eq. (A. 8)) can be simplified as:

$$h_v = R + (R - L_f)\sin\theta \tag{4.5}$$

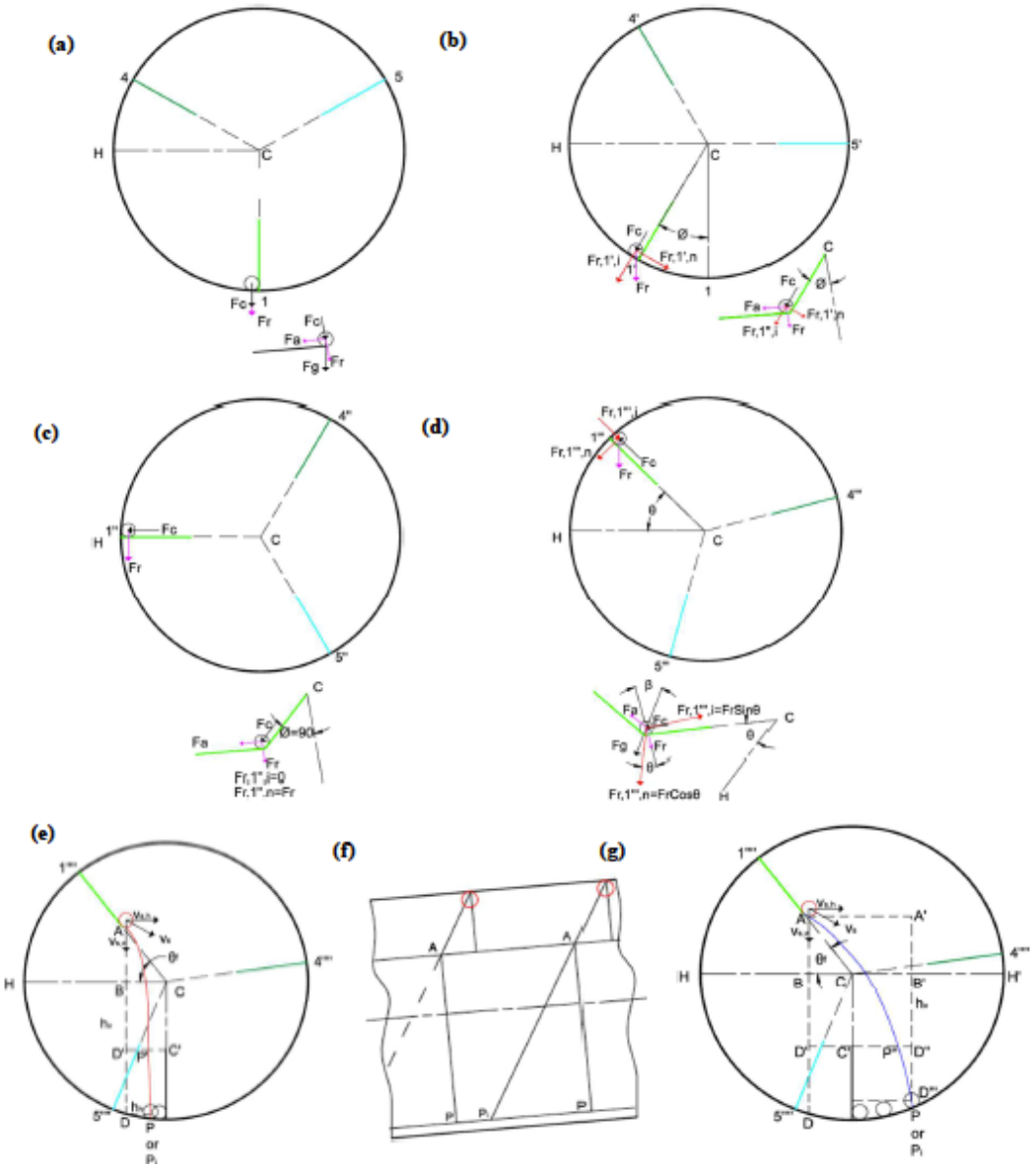

Figure 4.2: Schematic representation of the cascaded motion of a spherical particle through the inclined drum: (a) beginning of a cascaded cycle; (b) at any instant when particle moves up with flight; (c) at a instant when flight surface is horizontal; (d) at a instant when particle starts moving; (e) at a instant when particle leaves the flight edge and takes trajectory in red line; (f) axial movement in a cascaded cycle; and (g) at a instant when particle leaves the flight edge and takes trajectory in blue line.

Based on the geometry (Figure 4.2f), the total axial distance covered by the particle in one cascaded cycle may be estimated as:

$$x_{cas} = \left(R + (R - L_f)\sin\theta + L_f\right)\tan\beta \tag{4.6}$$

Using Eqs. (4.4) and (4.6), the mean residence time (in seconds) of the particle inside the reactor can be expressed as:

$$R_t = \frac{L}{\left(R + (R - L_f)\sin\theta + L_f\right)\tan\beta}\frac{4\pi}{3w}$$

$$R_t = \frac{8\pi}{3}\frac{L}{\omega D\tan\beta}\frac{1}{\left(1 + \frac{2L_f}{D} + \left(1 - \frac{2L_f}{D}\right)\sin\theta\right)}$$

It can also be written in minutes as:

$$R_t = 80\frac{L}{DN\tan\beta}\frac{1}{\left(1 + \frac{2L_f}{D} + \left(1 - \frac{2L_f}{D}\right)\sin\theta\right)} \tag{4.7}$$

Eq. 4.7 is based on an ideal single particle; a dimensionless correction constant is therefore introduced to incorporate possible differences in the axial movement of the particle caused by sliding and bumping motions of solid and inter-particle interaction effects in the continuously fed reactor. Therefore, Eq. 4.7 can be further rewritten as:

$$R_t = K_{ccRt}\frac{L}{DN\tan\beta}\frac{1}{\left(1 + \frac{2L_f}{D} + \left(1 - \frac{2L_f}{D}\right)\sin\theta\right)} \tag{4.8}$$

In the above equation, K_{ccRt} is the dimensionless correction constant. The experimental results for the mean residence times were then used to estimate the correction constant.

4.2.4 Filling Factor

The solid flow in the reactor, when operated at steady and plug flow conditions, can be assumed to have a constant axial velocity ($v_a = \mathcal{L}/R_t$) (Li et al., 2002a). Thus, one can approximate the biomass flow rate (BFR) as:

$$BFR \propto \rho_b A_{cs} v_a$$

Above, ρ_b is the bulk density of particles and A_{cs} is the virtual cross-section of solid that is assumed to remain constant throughout the reactor at steady plug flow operation (Herz et al., 2012). The above expression can then be simplified as:

$$BFR \propto \frac{\rho_b V_s v_a}{\mathcal{L}} \frac{V_{csr}}{V_{csr}}$$

$V_s = A_{cs}\mathcal{L}$ is the volume of solids inside the reactor, $V_{csr} = A_{csr}\mathcal{L}$ is the effective volume of reactor, and $A_{csr} = \pi D^2/4$ is the inner area of the cross section of the reactor. The solid filling fraction ($F_{ff} = V_s/V_{csr}$) in the reactor can be substituted as:

$$BFR \propto \rho_b F_{ff} v_a A_{csr}$$

$$F_{ff} \propto \frac{BFR}{\rho_b A_{csr}} \frac{R_t}{\mathcal{L}}$$

$$F_{ff} \propto \frac{BFR}{\rho_b A_{csr}} \frac{1}{DN\tan\beta} \frac{1}{\left(1 + \frac{2L_f}{D} + \left(1 - \frac{2L_f}{D}\right)\sin\theta\right)}$$

$$F_{ff} = K_{ccFf} \frac{BFR}{\rho_b} \frac{1}{D^3 N \tan\beta} \frac{1}{\left(1 + \frac{2L_f}{D} + \left(1 - \frac{2L_f}{D}\right)\sin\theta\right)} \tag{4.9}$$

The filling factor may also be expressed in percentage as:

$$F_f = K_{ccFf} \frac{BFR}{\rho_b} \frac{1}{D^3 N \tan\beta} \frac{1}{\left(1 + \frac{2L_f}{D} + \left(1 - \frac{2L_f}{D}\right)\sin\theta\right)} \times 100(\%) \tag{4.10}$$

Where, K_{ccFf} is the dimensionless correction constant for the filling factor.

4.3. EXPERIMENTAL SECTION

This section describes the test unit, materials, and methodology adopted for the cold experiments conducted in order to measure the mean residence time and the filling factor in the rotary torrefier and dryer at different operating conditions.

4.3.1 Test Setup

The present experiment was conducted on a two-stage continuous indirectly heated rotary torrefier. This unit comprises two laboratory scale rotary drums (dryer and torrefier) connected in series, as shown in Figure 4.1. Both the dryer and torrefier are rigidly mounted on aluminum bases, which in turn are fastened to a mild steel structure that is equipped with slots for changing the inclination of the reactor. Three different DC motors with adjustable speed controllers are used to maintain the rotating speed of the dryer, the torrefier, and the screw feeder.

The drum (reactor) has three flights mounted at equally spaced intervals of 120° on the inner surface. The geometry of both the dryer and torrefier are presented in Table 4.2.

Flights are aligned axially along the reactor axis on the inner surface of the drum. A screw type biomass feeder is connected at the inlet of the dryer. The outlet of the dryer is a hole of diameter 50.8 mm, which is connected to the inlet of the torrefier using a flexible aluminum pipe (Figure 4.1). Biomass entering the torrefier moves along the reactor and then exits through an outlet of 50.8 mm diameter at the other end of the torrefier. The effective length of the torrefier is the distance between the centers of the inlet and outlet holes of the torrefier, whereas the effective length of the dryer is the distance between the center of the dryer exit hole and the exit of the screw-feeder.

Table 4.2: Geometrical dimensions of two rotary reactors (dryer and torrefier)

Parameter	Dryer	Torrefier
Internal diameter (D), mm	64.0	100.0
Effective particle travel length ($\mathcal{L}$), mm	609.6	762.0
Flight width (L_f), mm	16.0	25.0

4.3.2 Materials

Yellow cylindrical poplar (dowels) was chopped into small pieces (of sizes 3-8 mm), and the chopped materials were stored in the plastic bags. Experiments were then conducted using the chopped poplar biomass. The bulk density of solids, measured using the ASTM (E-873-06) standard (ASTM, 2013), was found to be 245.85 kg/m^3.

4.3.3 Procedures

For a given set of operating parameters, there is a maximum flow rate of solids through the reactor. While feeding solids at a rate higher than the maximum flow rate of solids risked jamming up the reactor, feeding solids at a relatively lower rate ensured the smooth flow of solids in the reactor. Use of a higher feeding rate may also lower the tumbling motion of particles, reducing the benefits of having the rotary reactor. Taking this into consideration, a biomass flow rate of 2.54 g/min was maintained for all the

experiments to prevent overloading of solids inside the small reactor. The designated biomass flow rate was maintained by the calibrated screw-feeder installed at the inlet of the dryer.

Experiments were initially performed at three different angular speeds (4, 6, and 8 RPM) and three inclinations (1, 2, and 3°). Additional experiments were conducted at speeds of 4.5, 5.0, 5.5, and 7 RPM and inclinations of 1° and 3° in order to investigate further the effect of angular speed. An adjustable DC motor coupled with a drum shaft was used to vary the angular speed, while inclination of the drum axis was maintained by changing the vertical position of the drum.

4.3.4 Measurements

Experimental mean residence time (in minutes) can be determined using Eq. 4.1. Solid flow rate and solid hold-up were measured experimentally. Solid hold up is the mass of solid inside the reactor at a steady operating condition. At steady state operation, the feeder is stopped to collect and then measure the amount of solid in the reactor (Nasr-EI-Din et al., 1996). Equation (4.3) is then used to determine the filling factor (in %) of the reactor.

The solid flow rate, which is the inflow to the reactor, is known from the calibration of the feeder. At steady state condition, the outflow of solid from the reactor is also measured directly by collecting and weighing the amount of the solid over a known period. Ideally, during steady operation of the reactor (in cold conditions without chemical reactions), the inlet and the outlet solid flow rates should be the same. From initial operation of the reactor onwards, a ±2.5% difference between inlet and outlet solid flows is noted as an indication of having a steady operation condition. This is achieved within 30-60 minutes following initial operation.

It should be noted, however, that the mean residence time obtained using Eq. 4.1 only gives the statistical average of the residence time. Individual particles may exhibit a wide range of residence times. To establish a typical distribution of mean residence times, a set of experiments using 15 colored individual particles was conducted at angular speed 6 RPM and inclination 2°. Distribution of the tracer concentration with the time interval is presented later.

4.4. RESULTS AND DISCUSSION

While the pitch of the spiral path guides the movement of a particle in a reactor via the spiral flights, the particle does not necessarily follow the exact same pathway within the reactor installed with flat flight. As the particle is lifted up by a flight, it remains stationary until the flight moves to the position 1'' (Figure 4.2c). The particle moves forward in the axial direction when it starts rolling down over the flight surface and flies from the edge of the flight. A simple analytical model, incorporating the geometrical displacement per cascaded cycle (Figure 4.2f) and the total cascaded cycle time of a single spherical particle, was therefore developed to represent the effect of design and operating parameters of the rotary reactor on the mean residence time. This model, purely based on the cascaded motion, leads to an underestimation of the axial distance travel per cycle. As a consequence, the experimentally measured mean residence times were found to be smaller than the values predicted from Eq. 4.7. The possible reasons behind this overestimation of the mean residence time include failure to incorporate the axial displacements of the particle that may have caused by the bumping and sliding motions of particles and the inter-particle collision of particles. Because of the complexity in incorporating such axial movements of the particle, a dimensionless correction factor is introduced, and the mean residence time is expressed as in the Eq. 4.8.

4.4.1 Mean Residence Time

Table 4.3 presents the mean residence time of particles in two rotary reactors of different diameters measured under steady operation conditions. The measured mean residence time of particles was found in the range of 5.8-27.5 minutes and 4.7-21.4 minutes at different operating conditions of the dryer and the torrefier, respectively. As discussed before, a dimensionless correction constant was calculated for the individual measured mean residence times. Though the introduced correction factor is different for various operating conditions, it was found to be only in a narrow range of 0.346-0.515. Thus, an average value of all the dimensionless correction factors is introduced in Eq. 4.8. Thus, the expression for the mean residence time (min) can be rewritten as:

$$R_t = 0.435 \frac{L}{DN \tan\beta} \frac{1}{\left(1 + \frac{2L_f}{D} + \left(1 - \frac{2L_f}{D}\right)\sin\theta\right)} \tag{4.11}$$

The accuracy of the proposed semi-empirical expression (Eq. 4.11) can be established by plotting the experimental and predicted mean residence times, as shown in Figure 4.3. The predicted values are close to the straight line, indicating the accuracy of the developed expression. Furthermore, the proposed expression was also compared with the other published correlations by Klose and Wiest (1999), who provide mean residence time for a rotary reactor system of diameter 0.13 m and length 1.15 m operated at different angular speeds, and by Friedman and Marshall (1949). Comparison shows that the present work predicts mean residence time more accurately in the range of 5-17 minutes compared to the other expressions.

Table 4.3: Measured residence time of solid in dryer and torrefier

Angular rotation (RPM)	Mean residence time (Minutes)					
	Dryer			Torrefier		
	1°	2°	3°	1°	2°	3°
4.0	27.49	15.96	11.54	21.36	11.33	8.72
4.5	24.99	-	10.64	19.25	-	8.03
5.0	23.14	-	9.99	17.51	-	7.52
5.5	21.20	-	9.02	16.01	-	6.95
6.0	19.81	11.15	8.00	15.07	8.08	6.48
7.0	16.11	-	6.61	13.24	-	5.54
8.0	12.59	7.01	5.75	11.86	6.90	4.72

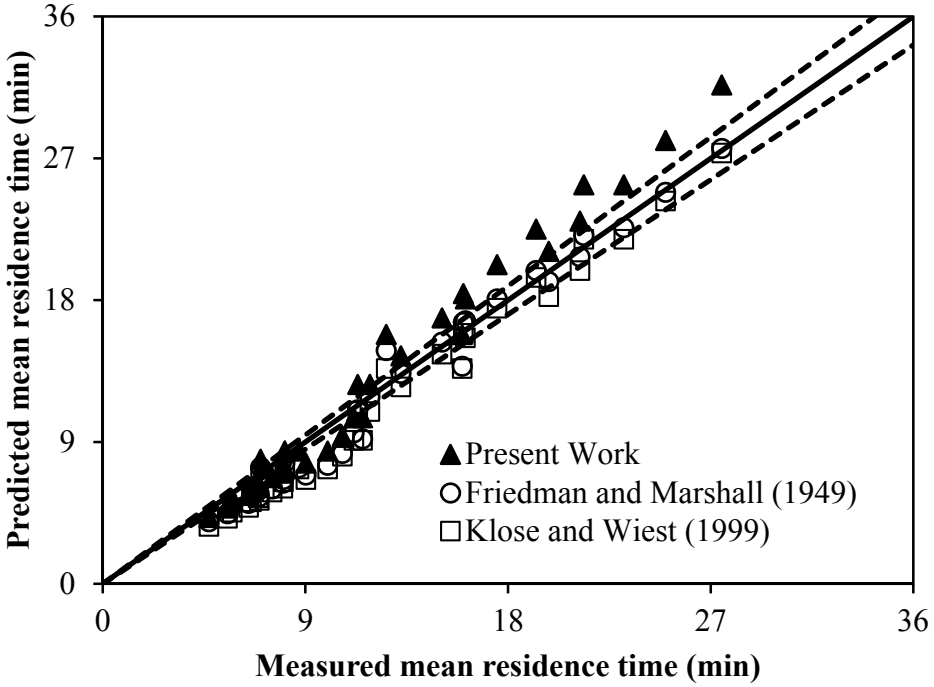

Figure 4.3: Validation of semi-empirical expression with experimental results and comparison with the expression of other authors (dot lines represent error level of ±5% of center solid line)

The mean residence time, as it is presented in the Eq. (4.8), should be independent of the solid supply rate. To validate this, experiments changing the solid supply rate were carried out for a dryer at angular speed 6 RPM and inclination 2°. As summarized in Table 4.4, authors confirmed that mean residence time is nearly independent of solid supply rate.

Table 4.4: Effect of biomass feed rate on mean residence time and dimensionless correction constant

Solid flow rate (g/min)	Solid hold up (g)	Mean residence time (min)	Dimensionless correction constant
2.49	28.29	11.36	0.47
2.82	31.40	11.14	0.46
4.11	44.13	10.73	0.44
5.28	62.43	11.82	0.49
6.26	68.89	11.01	0.45

Though the mean residence time gives a range of practically acceptable residence times, rotary reactor will have a wider distribution of particle residence times. Figure 4.4 shows a typical tracer output signal plotted between normalized tracer concentration and time interval. The average residence time, the variance of the residence time, and the dimensionless relative variance ($\sigma_r{}^2$) (Li et al., 2002) were found to be 12.1 min, 5.7 min^2, and 0.039, respectively. The measured mean residence time and the average residence time using the residence time distribution (RTD) curve are in an acceptable range. Such small dimensionless relative variance indicates that the residence time distribution has a narrow shape, with only small deviation from a normal distribution. In addition to this, the small value of the dimensionless relative variance, which results in a high Peclet number (ratio of convective flow to dispersive flow in an axial direction), validates the former assumption of the plug flow behavior for the solids in the rotary reactor. The high values of the Peclet number in the rotary reactors can be approximated (Tscheng, 1978) as $Pe \approx 2/\sigma_r{}^2$. This expression resulted in a Peclet number of 51, which

is high enough for the axial solid flow in the rotary reactor to be of a plug flow nature (negligible axial diffusion) (Tscheng, 1978).

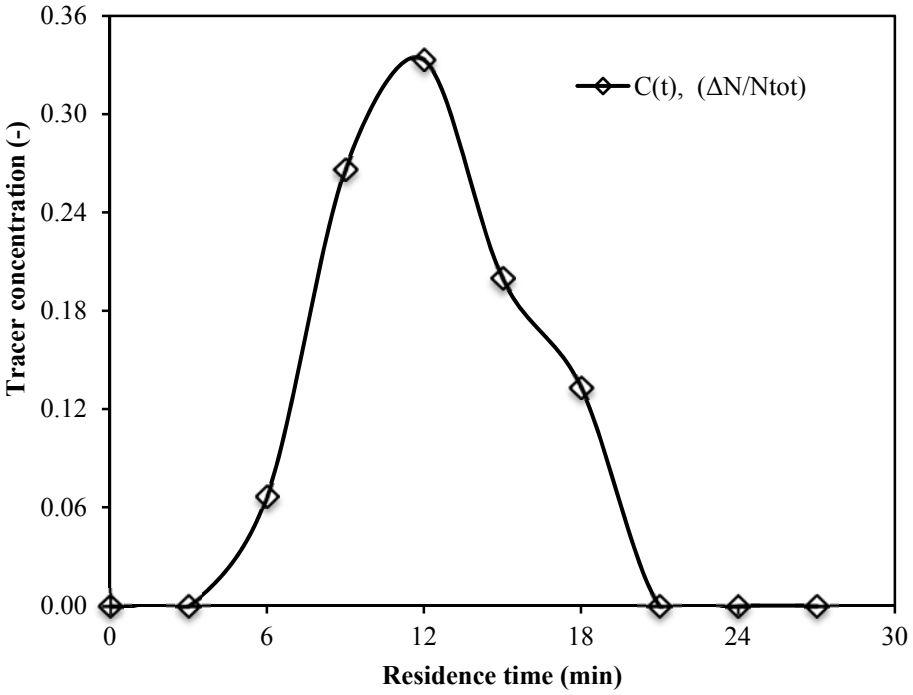

Figure 4.4: Typical tracer distribution curve in a rotary reactor of diameter 64 mm operated at angular speed 6 RPM and inclination 2º

4.4.1.1 Effect of Inclination

Figure 4.5 shows the effect of inclination on the mean residence time of particles in the dryer. It also shows the effect of rotation or angular speed of the reactor. Because the construction of the reactor allows only discrete angles of inclination, only three data points for the inclination of the reactor were studied. However, within this range, it was clear that the mean residence time decreases with a rise in angle of inclination of the reactor. One of the possible explanations for this could be an increase in axial movement of the particle in each cascaded cycle. It is also evident that variation in mean residence time with increasing angular speed is more significant at small inclination than at high

inclination. While the axial displacement will be less at the small inclination of the reactor, the time to travel such a small distance will be significantly more at the low angular speed of the reactor. Following from this, the mean residence time of the particle was found to be very high at low inclination and angular speed of the reactor. A large increase in the mean residence time at 4 RPM and 1° compared to 8 RPM and 1° was therefore caused mainly by the increase in the cascaded cycle time. At high inclination (e.g., 3°), increased mean residence time is not significant although the angular speed increases. This indicates that sliding may have had a more prominent effect on axial movement of particles at high inclination compared to the increase in the cascaded cycle time at low angular speed. However, it is interesting to note that decreased mean residence time does not vary linearly with the inclination of the reactor.

Figure 4.5 also compares the predicted and measured values of mean residence time. The strong correlation between predicted and experimentally measured residence times at different inclination angles and angular speeds shows that the proposed expression can accurately predict the influence of inclination.

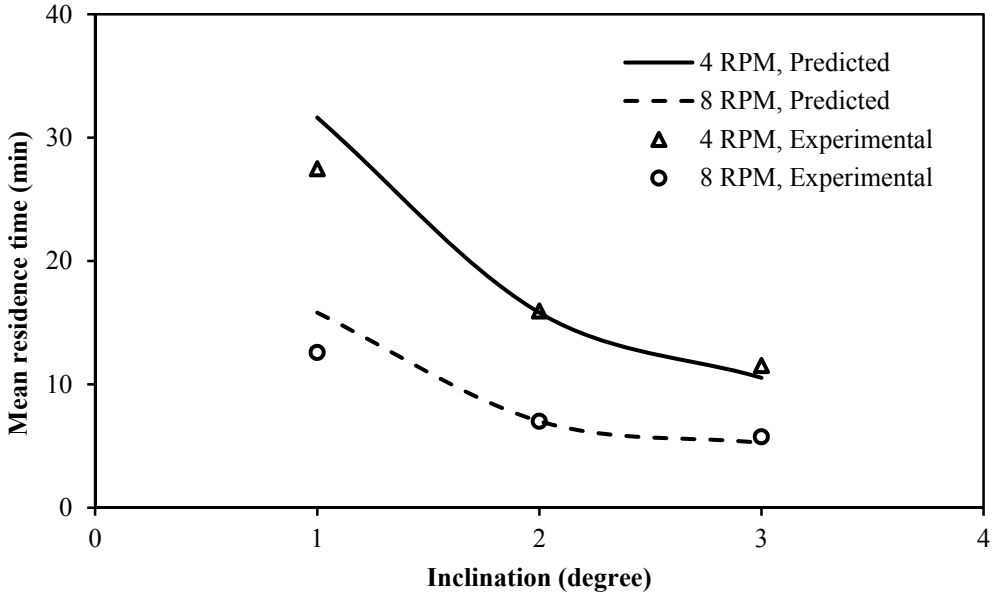

Figure 4.5: Effect of inclination on the mean residence time (D=64 mm)

4.4.1.2 Effect of Angular Speed

Figure 4.6 shows how measured and predicted mean residence times vary with the angular speed of the dryer. Since the angular speed of the reactor is relatively low (4-8 RPM), the particle will not experience any significant centrifugal force. Particles thus fall freely from the flight to the bottom of the reactor, forming the cascaded movement. At low angular speed, the lifting time (t_u) is significantly longer than at high angular speed. As a result, a particle will take longer time to complete one cascaded cycle, regardless of the inclination of the reactor, which would naturally increase the mean residence time of the particle in the reactor when the reactor is operated at low RPM. For instance, the mean residence time of particles in the dryer tilted at 1° was decreased from 27.5 min to 12.6 min when the angular speed was increased from 4 RPM to 8 RPM. Authors noted a similar observation at inclination of 3°. Therefore, the angular speed of the reactor should be chosen very carefully in order to achieve residence time that is sufficient for the biomass drying and devolatilization processes.

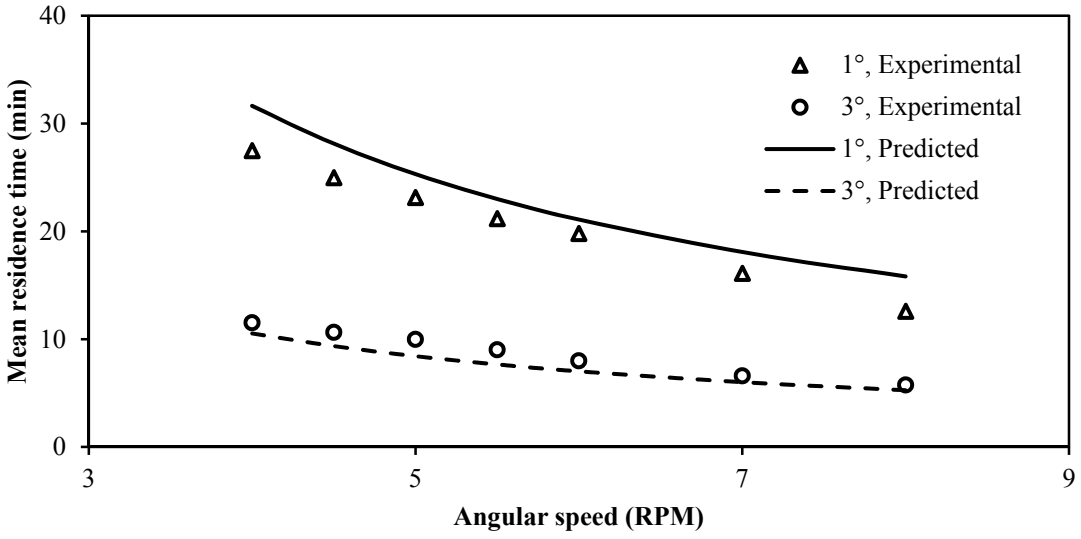

Figure 4.6: Effect of angular speed on mean residence time (*D*=64 mm)

4.4.1.3 Effect of Reactor Diameter

Equation (4.11) indicates an inverse relation between mean residence time and the diameter of reactor, which is confirmed by the experimental results presented in Table 4.3. Figure 4.7 illustrates the effect of reactor diameter on mean residence time at different angular speeds and inclinations of the reactor. Regardless of the angular speed and inclination of the reactor, the mean residence time was observed to be lower in the reactor of larger diameter. For example, at 4 RPM and 1°, the mean residence time was found to be 21.4 min and 27.5 min in reactors of 100 mm and 64 mm diameters, respectively. A decrease in the axial distance travelled by the particle per cascaded cycle (as represented by Eq. 4.6) is one of the possible reasons of having high mean residence in the small reactor. Also of relevance, the filling factor will be lesser in a large reactor than in a small reactor when they are operated at a fixed biomass supply rate, as will be discussed later. Such a decrease in filling factor represents that the amount of solid hold-up in the larger reactor will be less. As a result, the mean residence time is lower in a larger reactor operated at a fixed biomass flow rate (Eq. 4.1). Though an increase in reactor diameter can raise the volumetric solid loading capacity, it will decrease the filling factor of the reactor operated at a fixed biomass supply rate condition. Such a decrease in the filling factor will reduce the effective heat transfer area between the reactor wall and solids, thus decreasing the heat transfer rate. Therefore, attention should be paid to the designated volumetric solid loading, the filling factor, and the level of mean residence time necessary for the torrefaction process when selecting a reactor diameter.

4.4.2 Filling Factor

Filling factor, defined in Eq. 4.3, may affect the heat transfer rate to the solid and is therefore another important parameter to consider in designing the rotary torrefier. For a given solid flow rate, the total solid inventory in the reactor is lower at high angular speed because the volumetric solid flux rate increases with the rise in the angular speed.

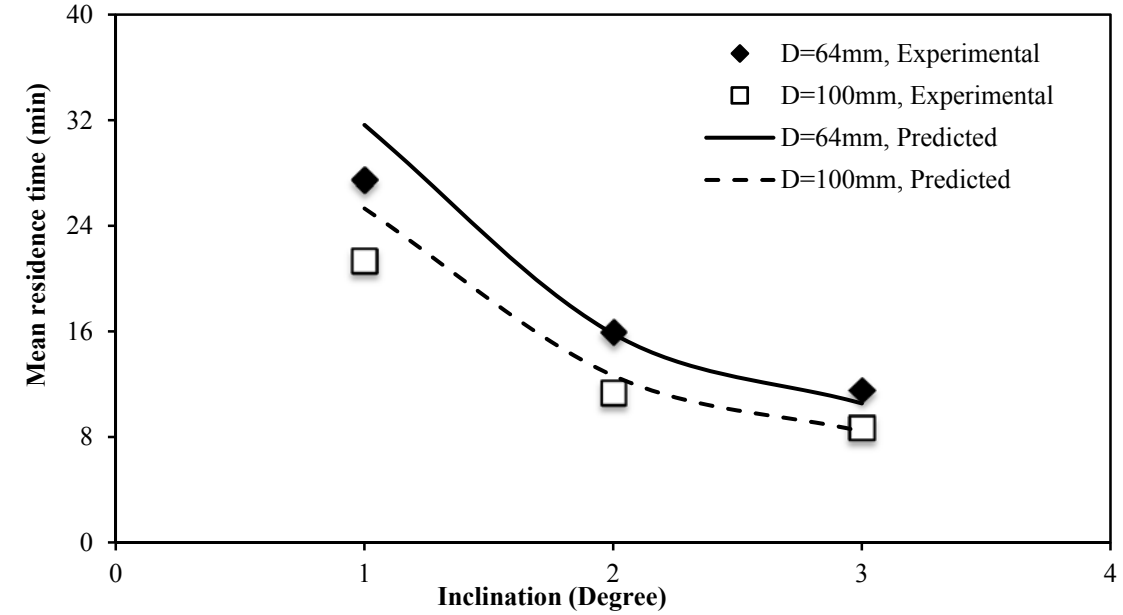

(a)

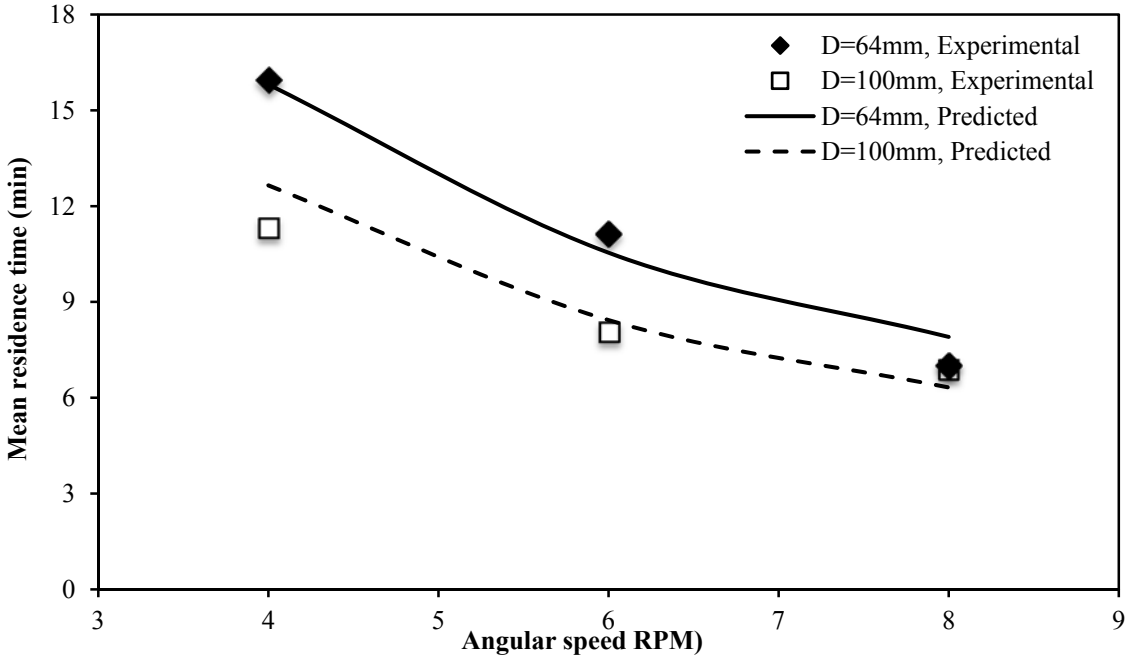

(b)

Figure 4.7: Effect of reactor diameter on mean residence time: (a) Variation with inclinations at 4RPM; and (b) Variation with angular speeds at 2°

Filling factor, therefore, increases when the reactor is operated at low inclination and angular speed. It will further increase when the diameter of the reactor is reduced. Such increase in filling factor in a small reactor is due to the decrease in the reactor volume.

In this study, filling factors were observed in the range of 3.0-14.3% in the dryer and 0.8-3.6% in the torrefier. The average dimensionless correction constant (K_{ccFf}) was found to be 0.564. So, the expression for the filling factor can be rewritten as:

$$F_f = 0.564 \frac{BFR}{\rho_b} \frac{1}{D^3 N \tan\beta} \frac{1}{\left(1 + \frac{2L_f}{D} + \left(1 - \frac{2L_f}{D}\right)\sin\theta\right)} \times 100(\%) \qquad (4.12)$$

This expression is now used to predict filling factors for the whole range of conditions studied. Figure 4.8 shows a strong correlation the measured and predicted values of filling factors, which supports the validity of the semi-empirical relationship presented in Eq. 4.12.

Figure 4.8 also shows how filling factor varies with the angular speed and inclination of the reactor, rising in conjunction with each of those two variables. For instance, the filling factor of the dryer with an inclination of 1° was reduced to 6.5 from 14.3% when angular speed was increased from 4 to 8 RPM. The filling factor was, however, decreased to 6.0% when the inclination of the dryer rotated at 4 RPM was increased from 1 to 3°. This decrease may be due to higher sliding and rolling possibilities of particles at high inclination compared with low inclination, causing only small solid inventory in the reactor. Decrease in the filling factor at high angular speed and inclination of the reactor was also reported by Sai et al (1990).

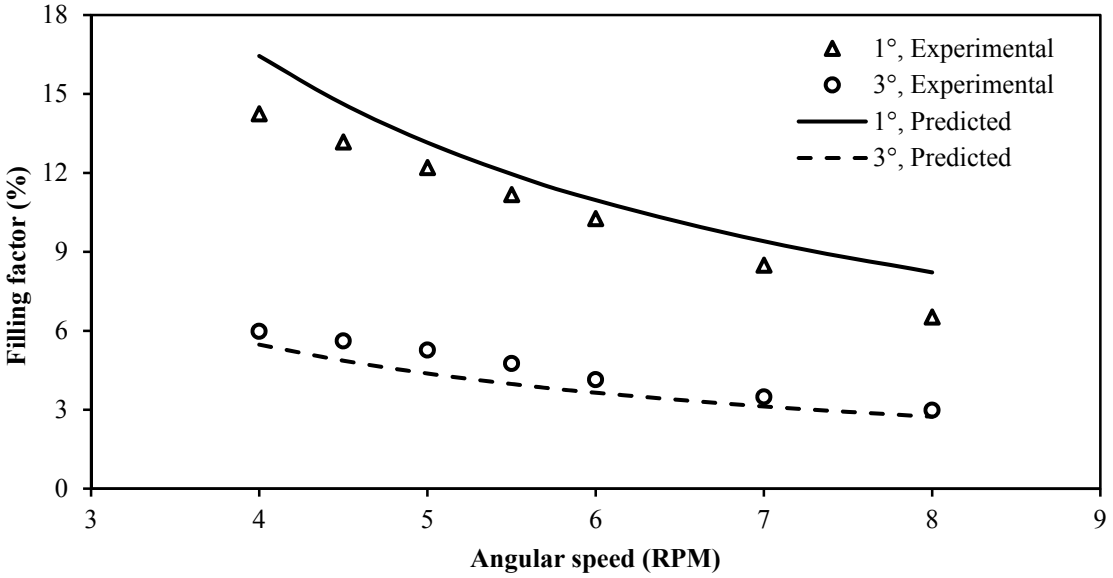

(a)

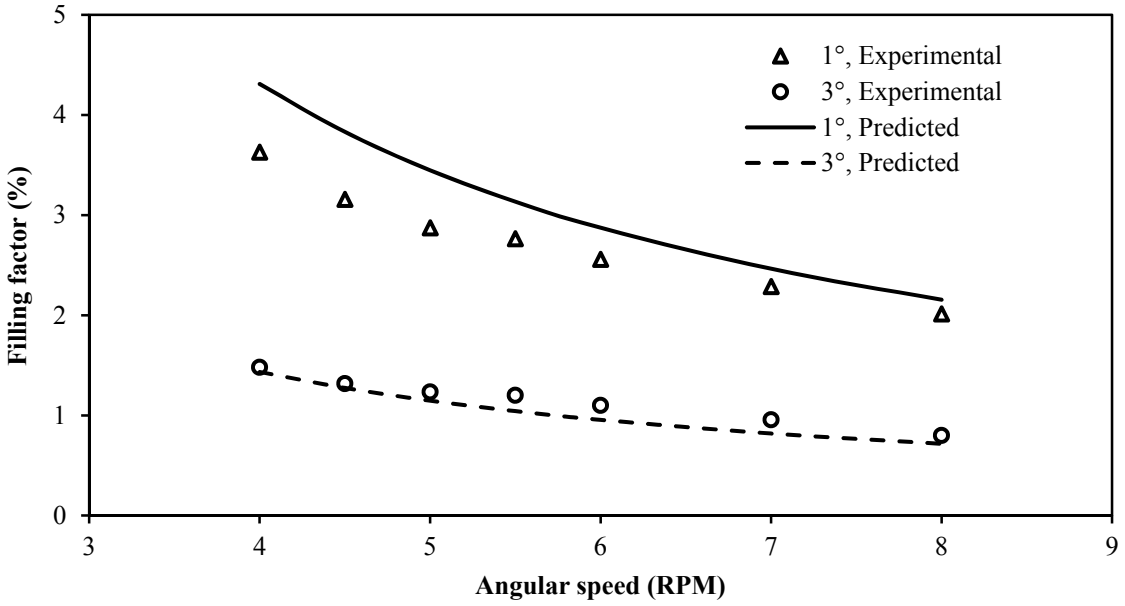

(b)

Figure 4.8: Variation of filling factor with different operating conditions in: (a) Dryer; and (b) Torrefier

4.5. SUB-CONCLUSIONS

In this study, the mean residence times and filling factors of two rotary reactors designed for a continuous two-stage indirectly heated rotary torrefier were investigated. Experimental data for different operating conditions showed that both mean residence time and filling factor of a rotary reactor supplied with a constant solid flow rate decrease with an increase in angular speed. An increase in the inclination of the reactor also decreases the mean residence time. Both of these also decrease when the diameter of the reactor increases. The proper selection of the angular speed, reactor inclination and reactor diameter are therefore vitally important when designing a rotary reactor to achieve a desired level of drying and devolatilization of biomass. In the case of the present reactor system, which comprises a dryer section followed by a torrefier section, the filling factor was found to be in the range of 3.0-14.3% in the dryer and 0.8-3.6% in the torrefier. The mean residence time of solid particles was found to be in the range of 5.8-27.5 minutes and 4.7-21.4 minutes in the dryer and the torrefier, respectively.

As the developed cascaded model for a single spherical particle does not account for axial movement of particles caused by bumping and sliding motions, the model overestimates the mean residence time. To address this, a semi-empirical expression using a dimensionless constant was developed for the mean residence time (minutes):

$$R_t = 0.435 \frac{\mathcal{L}}{DN tan\beta} \frac{1}{\left(1 + \frac{2L_f}{D} + \left(1 - \frac{2L_f}{D}\right) sin\theta\right)}$$

Considering the plug flow condition at steady operation of the reactor, a semi-empirical expression of the filling factor (%) was developed as:

$$F_f = 0.564 \frac{BFR}{\rho_b} \frac{1}{\tan(\beta)\, ND^3} \frac{1}{\left(1 + \frac{2L_f}{D} + \left(1 - \frac{2L_f}{D}\right) sin\theta\right)} \times 100\ (\%)$$

Though the empirical constants for the above two expressions were determined using a small amount of discrete experimental data, the model nonetheless predicted values that were close the measured experimental values, indicating a good accuracy of prediction. These proposed expressions, which account for different operating and geometrical parameters, may therefore be useful to scale up a rotary torrefier.

Prediction of both mean residence time and filling factor, which are the most useful parameters affecting equipment design and operation, could be enhanced by correlating them with the drying and devolatilization kinetics of biomass. This will further simplify the design and modeling of the rotary torrefier.

CHAPTER 5: INVESTIGATION INTO OVERALL HEAT TRANSFER COEFFICIENT IN INDIRECTLY HEATED ROTARY TORREFIER[§]

For externally heated torrefiers, heat transfer from the walls to the solids inside exerts critical influence on the torrefaction process. The heat transfer scenario in such reactors being different from that in conventional reactors, it is necessary to investigate into the process and examine how the heat transfer coefficient is influenced by different design and operating parameters. This chapter presents details of the investigation into the overall heat transfer coefficient and reports experimental data on how it is influenced by relevant parameters.

5.1. BACKGROUND

Major attraction of inclined rotary reactor lies in its mixing but is limited by heat transfer from external wall. To understand this it is necessary to develop a mechanistic model, which could evaluate the overall heat transfer coefficient of a cylindrical rotary reactor with flights operated with a constant wall temperature. Limited numbers of published experimental data, available at the time of writing, were used to validate effective wall to solid heat transfer coefficient (EHTC). On the other hand, an indirect experimental method was deployed to estimate and validate the overall heat transfer coefficient (OHTC). Experiments were conducted in a temperature range of 150-340°C, which could be used in the drying and devolatilization sections of a continuous two-stage indirectly, heated rotary torrefier. The inert test materials (brass particles) were used to avoid reaction terms as an undesirable influence on the heat transfer mechanism. The effects of the different operating parameters on the overall heat transfer coefficient were also discussed.

[§] This part of the work is being considered for publication in the International J. of Heat Mass Trasnsfer, 2016.

5.2. MODEL DEVELOPMENT

5.2.1 Heat Transfer Mechanism in Rotary Reactor

Heat transfer from the reactor wall to the granular mass of solids involves three parallel mechanisms such as particle convection, conduction at the solid-wall contact surface, and radiation (Malhotra, 1989). The radiation heat transfer is considered to be negligible at temperatures less than 527°C (Malhotra, 1989). A study by Canales et al. (2001) has reported that the heat transfers to the particles in the directly heated system is mainly from the convection mode. A detailed review of the wall to solid heat transfer in a rotary kiln thermo-reactor is presented in Li et al. (2005). A number of investigations to estimate the heat transfer coefficient between the reactor wall and the contact bed for the rotary kilns (Ferron and Singh, 1991; Tsheng and Watkinson, 1979; Wes et al., 1976) and the circulating fluidized bed (Basu, 1990) can be found in the literatures.

In an indirectly heated rotary reactor without through gas flow, the effective heat transfer coefficient from the reactor wall to solid can be determined using the penetration theory (Wes et al., 1976). However, the penetration model presented by Wes et al. (1976) overestimates the effective heat transfer coefficient. Schlunder (1981) has, therefore, presented a two-steps heat transfer mechanism from the hot wall to solid: (i) the wall-solid surface; and (ii) the solid surface-solid bed. According to this, the heat transfer rate depends on the surface contact resistance and the heat penetration (conduction) resistance of the solid bed. Similar two-steps heat transfer first through a thin layer of gas on the wall and then to rest of the body of solids in the circulating fluidized bed reactor was also studied in Basu (1990), and is known as cluster renewal theory.

A complete analysis of detailed heat transfer phenomenon in the rotary reactor involves a number of parameters and becomes a complex process. In a rotary inclined reactor, the solids fed at one end continuously move down to the opposite end of the reactor. No gas is blown through the rotary torrefier under consideration. Only the volatiles released

during torrefaction fills the void in the reactor. Here, the solids are swept up the rotating cylindrical wall by friction as well as by the flights attached to the wall, and then they drop down on the floor of the cylinder under the gravity force (Figure 5.1). Thus, the packets of solids come in periodic contact with a section of the wall. Such motion of the solids is very similar to that in fluidized beds where cluster or packets of solids randomly come in contact with the wall and leave after a certain period of residence on the wall. So, we could make use of the cluster renewal model developed by Basu and Subbarao (1988) to develop a mechanistic model for the effective wall to solids heat transfer in an indirectly heated rotary reactor.

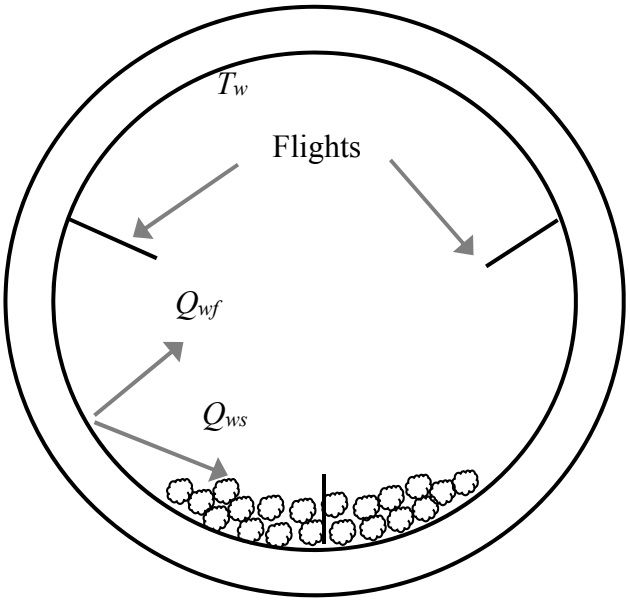

Figure 5.1: Cross-section of indirectly heater rotary reactor at wall temperature T_w showing different heat transfer pathways: (i) Q_{wf}= wall to gas; and (ii) Q_{ws} = wall to particle

A close examination of the heat transfers from wall to solid cluster or packets in a fluidized bed shows that the heat conduction through the actual contact area of solids on the wall is negligible. Major heat transfer occurs through conduction across thin layer gas trapped between the wall and the first layer of solids (Basu, 1990; Mahalingam and

Kolar, 1991). Further heat conduction from the first layer into the bulk solids occurs through transient heat conduction similar to that developed by Mickley and Fairbanks (1955) for fluidized beds. Since the heat transfer depends mainly on the area of the reactor covered by solids, this study also develops an expression to predict the fraction of surface area of the rotary reactor covered by the solid at different operating conditions.

5.2.2 Model Formulation

Figure 5.1 shows a reactor heated and insulated externally to maintain reactor wall temperature at T_w and no external gas is supplied into the reactor. The reactor wall is, thus, only responsible for the overall heat transfer (i) to the solid and (ii) to the gas inside the reactor.

Assumptions:

- The rotary reactor operated at steady state condition is considered to have a uniform solid filling fraction (F_{ff}) or solid filling factor (%) along the reactor length.
- Reactors are installed with three axial rectangular flights, which are placed at 120° apart from each other.
- These flights help to lift up the solid and maintain the cascaded motion of the particle. The solids stay in contact with the wall until the angle of the flight is too stiff when gravity force exceeds the flight to solid friction. So, the average solid contact time with the hot reactor wall is, therefore, assumed time the flight takes to travel from the solid pick up point (lowest point of the reactor) to the angular position where solid falls down from the flight.
- The surface area of the flight is very small compared that of the reactor, thus its effect on heat transfer can be neglected. Flights, however, increase solid mixing in the reactor.

- Rotary reactor is of indirectly heated type without any through flow of gas. So, it is assumed that the gas in the reactor remains stationary. Some portion of the lateral surface area of the reactor is, therefore, covered with solids and the rest of the area by gas inside the reactor.
- As there is very little flow of gas through the rotary reactor, one can neglect gas convection and assume that the major heat is transferred to the body of particles through particles contact with the wall.
- The temperature within the bulk solids is uniform at a given axial location of the reactor.
- Reactor surface is heated by an external heat source that maintains the wall temperature at a constant value (T_w). Therefore, the external heat losses from the reactor are not included.
- The maximum reactor wall temperature being only $T_w = 340°\mathrm{C}$, the radiation from the reactor wall is negligible (Basu and Fraser, 1991; Malhotra and Majumdar, 1991).

The heat from the reactor wall flows to the solid particles and the gas inside the reactor through the convection heat transfer. Therefore, the overall heat transfer coefficient (Basu and Fraser, 1991) can be expressed as:

$$h_o = \delta h_{ewb} + (1-\delta) h_{wf} \tag{5.1}$$

Where, h_{ewb} is the average effective heat transfer coefficient from wall to bulk solids, h_{wf} is the average heat transfer coefficient from wall to gas, and δ_d is the average fraction of the wall area covered by the solids.

Solids initially enter at an average initial volumetric temperature (T_{in}) and then receive heat from the hot reactor wall while they are being lifted up by the flight. The average thermal resistance across the solid pack being lifted is similar to that of particle packets in

a fluidized bed. So, following Mickley and Faribank (1955) and Wes, (1976), the thermal resistance of solid packs can be estimated as:

$$\frac{1}{h_{sb}} = \left(\frac{\pi t_c}{4 k_{bs} C_{pbs} \rho_{bs}} \right)^{0.5} \tag{5.2a}$$

The thermal resistance due to the thin gas film between the wall and the first layer of particles can be estimated as (Schlunder, 1981):

$$\frac{1}{h_{ws}} = \frac{\psi d_p}{k_f} \tag{5.2b}$$

Where, d_p is the effective diameter of the particle, k_f is the thermal conductivity of gas inside and ψ is the thickness of the gas film as the fraction of particle diameter.

The effective heat transfer coefficient from wall to bulk solids (EHTC) is combined effect of above two thermal resistances. So the EHTC from wall to bulk solids (h_{ewb}) can be written as:

$$h_{ewb} = \frac{1}{\frac{1}{h_{ws}} + \frac{1}{h_{sb}}} \tag{5.2}$$

$$h_{ewb} = \frac{1}{\frac{\psi d_p}{k_f} + \left(\frac{\pi t_c}{4 k_{bs} C_{pbs} \rho_{bs}} \right)^{0.5}} \tag{5.3}$$

Where, k_{bs} is the thermal conductivity of solids, C_{pbs} is the specific heat capacity of solid, ρ_{bs} is the bulk density of solid, and t_c is the average contact time of particle with the hot reactor surface in one cascaded cycle.

The solid packs comprise both solids and gas. So the effective properties of the solid packs viz, thermal conductivity, specific heat capacity, and bulk density of bed materials, can be written as (Basu and Fraser, 1991).

$$E_{eff} = (1 - e_{bs})E_s + e_{bs}E_f \tag{5.4}$$

Where, E_{eff} is the effective properties of solids, E_s is the properties of solid, E_f is the properties of the gas, and $e_{bs} = 0.47$ is the voidage fraction of the solids, which was measured by weighing the mass of solids in a container of known volume. The properties of gas are estimated at the mean gas temperature in the reactor.

The value of ψ in the Eq. (5.3) is reported 0.1 in Basu and Fraser (1991). Li et al. (2005) also reported that the optimum value of ψ is 0.1 though its value could lie in the range of 0.096-0.198. Therefore, in the present study, the value of ψ is taken 0.1.

Li et al. (2005) suggested that the contact time (t_c) depends on the half-filling angle (ϕ_s) of solid inside the reactor and angular speed (ω) of the reactor, and can be determined as:

$$t_c = \frac{\phi_s}{180\omega} \tag{5.5}$$

The half-filling angle depends mainly on the solid filling fraction. It increases when the solid filling fraction rises and vice-versa. The half-filling angle can be related to the solid filling fractions (F_{ff}) (Herz et al., 2012) as:

$$2\pi F_{ff} = \frac{2\pi\phi_s}{180} - \sin(2\phi_s)$$

This expression can be simplified (with ±3% percentage error) as:

$$\phi_s = 108.46 F_{ff}^{0.357} \tag{5.6}$$

To determine the solid filling fraction (F_{ff}), this study has used the expression (Eq. 5.7) presented in the Chapter 4. This expression has assumed the plug flow of solids inside the reactor with an average axial velocity. The average axial flow velocity of solid, however, depends on the different operating conditions and the geometry of the reactor. Therefore, the variations of the filling factor in a reactor operating at a constant solid feed rate at the inlet can be estimated by using Eq. (5.7). Because of the closed end at the reactor exit and solids leave reactor only in intermittent fashion, the solid bed height inside the reactor is assumed uniform throughout the reactor length. In addition to this, the installed rectangular flights assist to maintain the uniform distribution of solids along the reactor axis.

$$F_{ff} = 0.564 \frac{BFR}{\rho_{bs}} \frac{1}{\tan(\beta) N D^3} \frac{1}{\left(1 + \frac{2L_f}{D} + \left(1 - \frac{2L_f}{D}\right)\sin\theta_s\right)} \tag{5.7}$$

Unlike in the Li et al. (2005), this study proposes the lifting time, defined as the time taken by the flight to travel an angular displacement equivalent to the angle of friction, as an average residence time of particles on the hot wall or a contact period. Therefore, in this present study, the contact period of solid on the hot reactor surface can be estimated as:

$$t_c = \frac{(90 + \theta_s)\pi}{180\omega} \tag{5.8}$$

Where, θ_s is the angle made by the flight, from where solid starts falling. It is ideally equivalent to the angle of friction, with the horizontal plane.

Gas being nearly stationary inside the reactor, the heat transfer from the reactor wall to gas is assumed to be by natural convection inside a horizontal pipe. Thus, the average wall to gas heat transfer coefficient can be estimated using the Churchill and Chu equation (Incropera and De-Witt, 1985) as:

$$h_{wf} = \frac{k_f}{D}\left(0.60 + \frac{0.387 Ra_D^{1/6}}{\left(1+\left(\frac{0.559}{\mathrm{Pr}_f}\right)^{9/16}\right)^{8/27}}\right)^2 \tag{5.9}$$

Where, $Ra_D = g\beta_V\left(T_w - T_f\right)D^3/\upsilon_f\alpha_f$ is the Rayleigh Number ($10^{-5} < Ra_D < 10^{12}$), Pr_f is the Prandtl Number of gas, g is the acceleration due to gravity, β_V is the volumetric expansion coefficient of gas, T_f is the mean gas temperature, υ_f is the kinematic viscosity of gas, and α_f is the thermal diffusivity of gas.

The overall heat transfer coefficient (OHTC) of indirectly heated rotary reactor can be, thus, expressed as:

$$h_o = \delta\frac{1}{\frac{\psi d_p}{k_f} + \left(\frac{\pi t_c}{4k_{bs}C_{pbs}\rho_{bs}}\right)^{0.5}} + \left(1-\delta\right)\frac{k_f}{D}\left(0.60 + \frac{0.387 Ra_D^{1/6}}{\left(1+\left(\frac{0.559}{\mathrm{Pr}_f}\right)^{9/16}\right)^{8/27}}\right)^2 \tag{5.10}$$

2.3. Fraction of Cylindrical Wall Area Covered by Solids (δ_d)

The value of δ_d can be defined as the ratio of the lateral surface area of reactor wall covered by the solid packs to the total lateral surface of the reactor. By definition,

$$\delta_d = \frac{\text{Surface area of reactor covered by solid bed per unit length}}{\text{Total lateral surface area of reactor per unit length}} \tag{5.11}$$

The value of δ_d depends on the amount of solids in the reactor and their distribution. The solid filling fraction being the primary factor of the rotary reactor greatly affects the solid distribution with the time of rotation. This section discusses different cases of the solid filling fraction for a given reactor size. The loading of the rotary reactor can be categorized into three cases:

A. Overloaded case (Figure 5.2 (a))
B. Designated loading case (Figure 5.2 (b))
C. Under loaded case (Figure 5.2 (c))

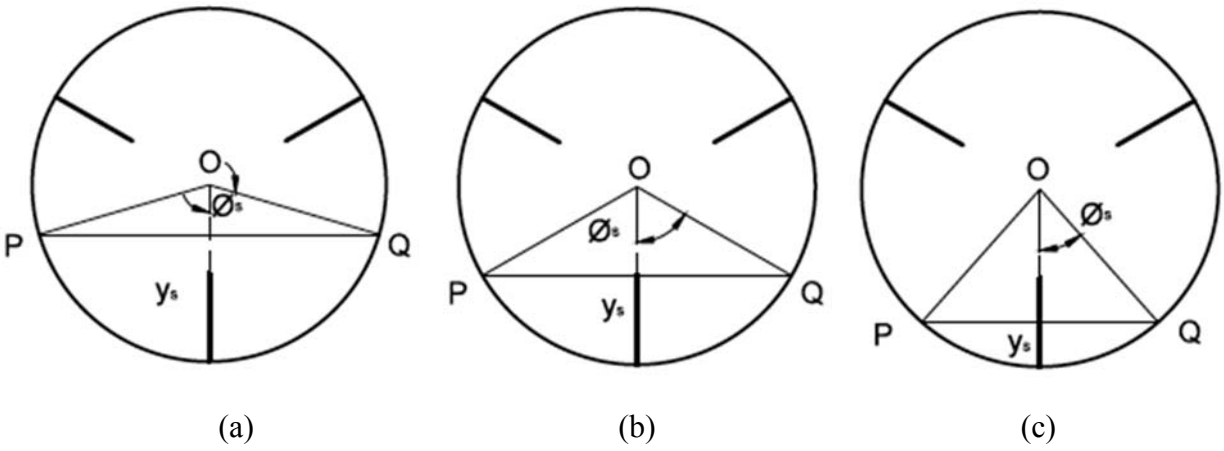

(a) (b) (c)

Figure 5.2: Different loading configuration (a) Overloading ($y_s > L_f$), (b) Designated loading ($y_s = L_f$), and (c) Under loading ($y_s < L_f$)

Designated loading is defined as the case of the solid filling when the solid level just balances the flight size. The vertical bed height at this condition would be equal to the width of the flight (L_f). This, then, defines the overloaded and under loaded as the cases when the vertical bed height $y_s > L_f$ and $y_s < L_f$, respectively.

The distribution of solid in the reactor filled with the low solid filling fraction may be different at stationary and rotating conditions. But, the distribution of solids would be same at both the stationary and rotating conditions when the reactor is filled above the designated loading of solids (Figure 5.3). Irrespective of the loading conditions, the stationary solid bed height can be related geometrically to the stationary half-angle ($\emptyset_s$) and reactor diameter (D) as:

$$y_s = D\left[\sin\left(\phi_s/2\right)\right]^2 \tag{5.12}$$

Figure 5.3: Reactor surface covered by solid at overloading case at different time

For a given reactor of diameter (D) installed with the flights of width (L_f), the designated solid filling ($at\ y_s = L_f$), which is the ratio of the cross-sectional area of solid at a steady plug flow condition and the cross-sectional area of the reactor, can be estimated as (see in the Appendix B.1):

$$F_{ff,\ designated} = \frac{\emptyset_s}{180} - \frac{2}{\pi}\frac{L_f}{D}\left(1 - 2\frac{L_f}{D}\right)\sqrt{\frac{D}{L_f} - 1}$$

Where, $L_f = D(\sin(\emptyset_s/2))^2$

The designated solid filling fraction of a reactor with $L_f/D = 0.25$ was observed to be 0.196 (19.6%). From the experimental observation, the lateral reactor surface covered by the solids operated at or above designated loading conditions is same for both at stationary and rotating conditions and equal to the fraction of reactor perimeter covered by solids at stationary condition (Figure 5.3).

Konidis (1984), however, recommended that the maximum allowable solid filling fraction would be only up to 0.16. In the present study, the solid filling fraction is, therefore, maintained well below the maximum allowable fraction. The area covered by the solid in such under loading condition may vary with the time of rotation. Although researchers have used the solid filling angle at stationary condition to estimate the area covered by the solid in the rotary reactors without flights (Thammavong et al., 2011), finding the value of δ becomes a complex process in the rotary reactor with the flights. Therefore, an approach to estimate δ, taking consideration of the experimental observations, is presented here.

Consider a rotating reactor with the solid moving along the reactor axial axis at a steady plug flow condition. A single particle ideally stays on the flight surface till the angle of inclination of flight with the horizontal plane (θ_1) is equal to the static frictional angle (θ_s). However, in a reactor with multi-particles, the corresponding inclination reduces significantly below the static frictional angle. From the number experimental tests in a clear plastic model as shown in Figure 5.4 (b), the flight inclination (θ_1) reduces close to a half of the static frictional angle. The solid distribution at this condition of each cascaded cycle can be represented as in Figure 5.4 (a). Solids remaining on the flight

make an angle of Ω with the flight surface. Rest of solids has already dropped back to the reactor surface to continue another cascaded cycle. This instant was adopted to estimate the approximate value of δ_d. It clearly shows that δ_d depends on the arc XY and the arc $P_d Q_d$.

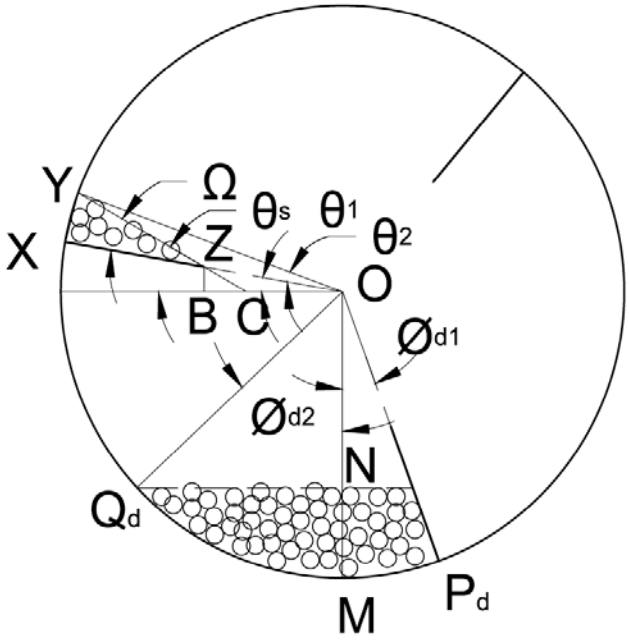

(a)

(b

Figure 5.4: Distribution of solids in the reactor

To determine δ_d, angles ($\phi_{d1} = \measuredangle P_d OM, \phi_{d2} = \measuredangle MOQ_d, and\ \theta_2 = \measuredangle XOY$) subtended by solid at the center of the reactor have to be determined. Referring to the appendix B.2, the solid filling angle ($\phi_d = \phi_{d1} + \phi_{d2}$) can be estimated (Eq. B.7) as:

$$\phi_d = 23.75 + 139.56 F_{ff}^{0.449} \tag{5.13}$$

The angle subtended by solids at flight (θ_2) can be estimated (Eq. B.8) as:

$$\cos\theta_2 = 1 - 2\left(\frac{L_f}{D}\right)^2 (tan\Omega)^2$$

The fraction of the reactor surface covered by solids, which is valid for the solid filling factor in the range of 0.0044-0.098 (0.44-9.80%), can be calculated as:

$$\delta_d = \frac{\phi_d + \theta_2}{360} \tag{5.14}$$

Figure 5.5 shows the variation of δ_d with the solid filling fraction. From here it is evident that the solid coverage increases with the amount of solid filling. The values of δ_d are slightly lesser compared with that of Thammavong et al. (2011), in which they have assumed the constant solid filling angle at both the stationary and rotating condition of the reactor.

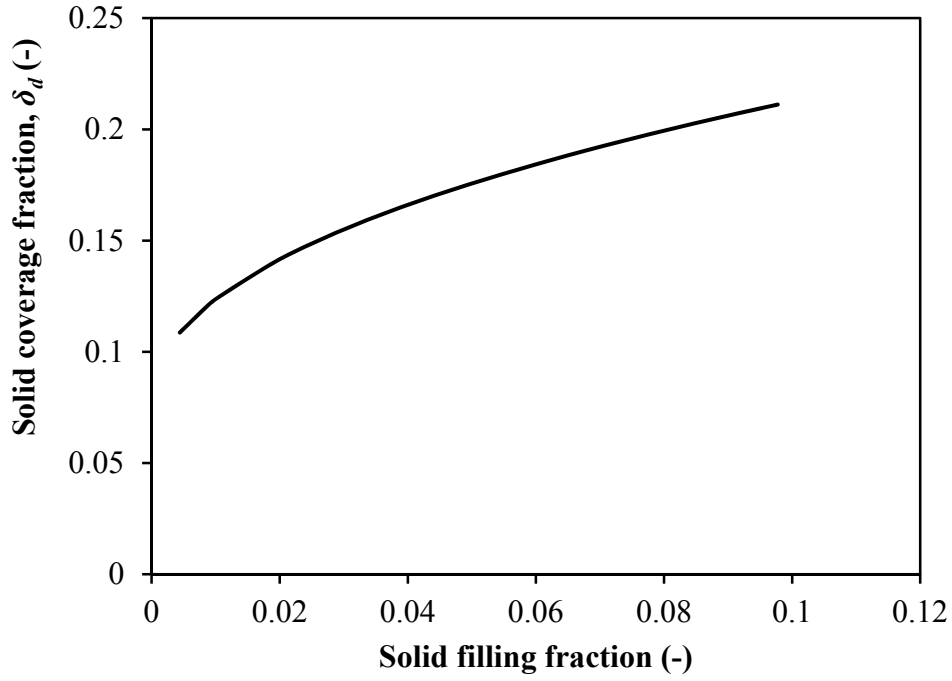

Figure 5.5: Variations of solid coverage fraction (δ_d) in stationary and rotating reactor

5.3. EXPERIMENTS

In this section, materials used and experimental methods deployed are discussed.

5.3.1 Material

This study uses pieces of cylindrical yellow-coated brass rod of diameter 4.76 mm (3/16 inch) and length 5 mm Use of unreactive solid particle avoided the influence of reactions on the heat transfer. Properties brass such as particle density, specific heat capacity, and thermal conductivity are considered as 8470 kg/m^3, 401.93 J/kgK, and 119.91 W/mK, respectively (Engineersedge, 2014). The bulk density of brass particles used in this study was determined experimentally and found to be 4523 kg/m^3.

5.3.2 Test Unit

General descriptions of reactors are presented in Chapter 4. The schematic diagram of a continuous two-stage indirectly heated rotary reactor torrefaction technology is shown in Figure 5.6. Two reactors designated as a dryer and a torrefier are fitted with three flights placed at 120° as shown in Figure 5.6. Each rotary reactor is inserted in a cylindrical shell with a small clearance. The shell is wrapped with the electrical tape heater that maintains the desired reactor wall temperature. Shells are insulated tightly using the Calcium-Magnesium-Silicate (CMS) wool. Major dimensions of reactors used in the developed two-stage rotary torrefier are listed in the Chapter 4.

5.3.3 Procedures

In this work, an indirect method for measuring the solid exit temperature (as shown in Figure 5.7) was used to estimate the overall heat transfer coefficient. The reactor is operated at steady state condition with a solid flow rate of 21.9 g min^{-1} (±3%). A container with a known amount of water is connected at the exit of the reactor to collect the heated brass materials coming out from the reactor. The initial and final temperatures of the container and water were measured using the K-type of thermocouples. The water container was insulated tightly using the CMS wool. Experiments only at selected operating conditions were repeated three times to ensure the reliability of the experimental data. Results of repeatability tests are shown in error bars, which are presented in the results and discussion section.

Measurement of wall temperature proved difficult as the wall was rotating. For this one K-type thermocouple was inserted through the outer stationery wall (Figure 5.7). The tip of this thermocouple was pressed against the inner rotating wall. The cylindrical rotor rotated at very low speed of few rpm. So the contact resistance between thermocouple and wall could be neglected.

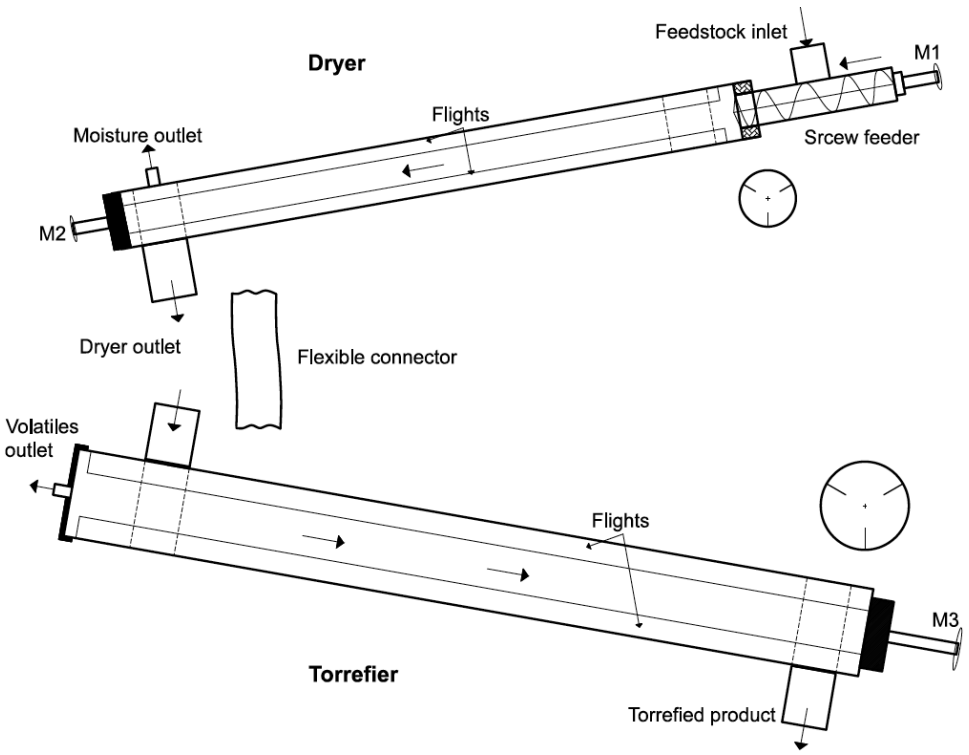

Figure 5.6: Schematic diagram of two-stage indirectly heated rotary reactors (M1, M2, and M3 are the DC gear motors)

The overall heat transfer coefficient is, then, estimated as:

$$h_o = \frac{Q_{gain}}{A_{lsr} LMTD} \tag{5.15}$$

Where, Q_{gain} is the rate of net heat gain by particles, $A_{lsr} = \pi D \mathcal{L}$ is the lateral surface area of the reactor, and $LMTD$ is the log mean temperature difference. The $LMTD$ is calculated as:

$$LMTD = \frac{(T_w - T_{ex}) - (T_w - T_{in})}{\ln\left(\frac{T_w - T_{ex}}{T_w - T_{in}}\right)}$$

Where, T_w, T_{ex}, and T_{in} are the temperatures of reactor wall, particles at the exit, and particles at the inlet, respectively. T_w and T_{in} were measured using the K-type of thermocouple connected to the data logger whereas T_{ex} was calculated by establishing thermal energy balance for the plastic container (insulated tightly) as:

$$\text{Heat gain by water} + \text{Heat gain by plastic container} = \text{Heat loss by brass particles}$$

$$m_w C_{Pw}\left(T_e - T_{iw}\right) + m_c C_{Pc}\left(T_{fc} - T_{ic}\right) = m_b C_{Pbs}\left(T_{ex} - T_e\right) \tag{5.16}$$

Where,

m_w is the mass of water inside the plastic container, kg

m_c is the mass of plastic container, kg

m_b is the mass of brass particles, kg

T_{iw} is the initial temperature of water in the container, °C

T_e is the final equilibrium temperature of water in the container, °C

T_{ic} is the initial temperature of plastic container, °C

T_{fc} is the final temperature of plastic container, °C

C_{pw} is the specific heat capacity of the water = 4.186, kJ/kg K

C_{pc} is the specific heat capacity of the plastic container = 1.670, kJ/kg K

C_{pb} is the specific heat capacity of the yellow coated brass = 0.402 , kJ/kg K

Assuming all solid particles will have uniform heating and leave at same exit temperature from the reactor, the heat gained by solids may be estimated as:

$$Q_{gain} = \dot{m}_b C_{Pbs}\left(T_{ex} - T_{in}\right) \tag{5.17}$$

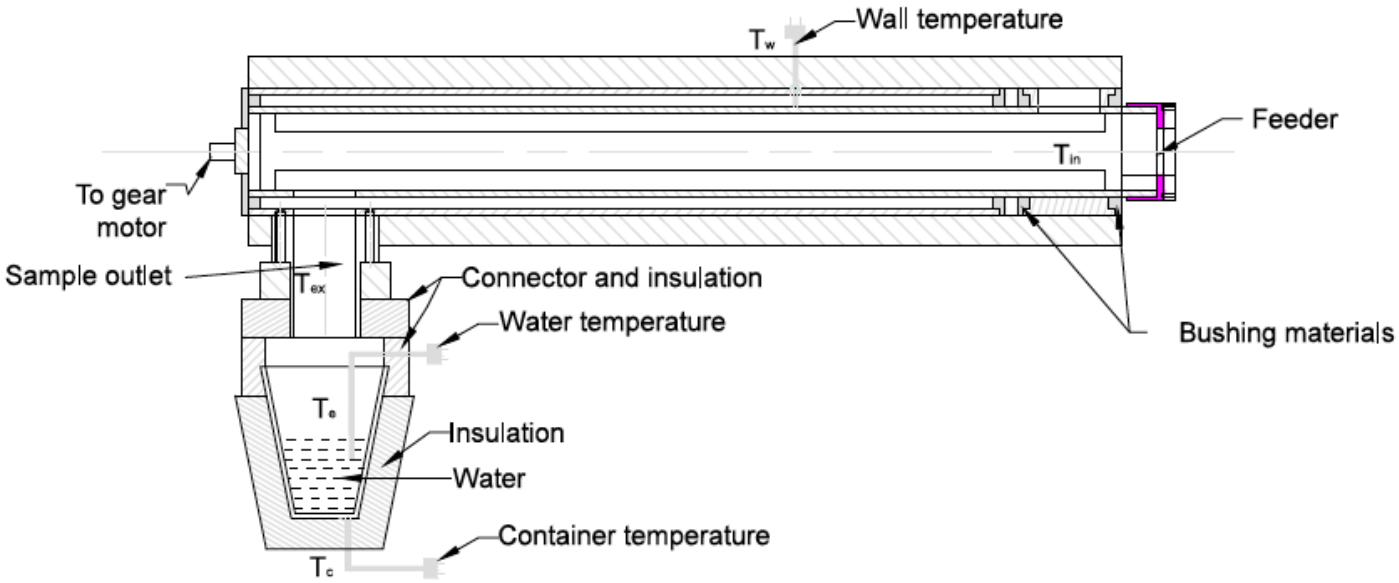

Figure 5.7: Schematic diagram of indirect method of solid exit temperature

5.4. RESULTS AND DISCUSSION

Experiments were conducted to validate the predicted overall heat transfer coefficients (OHTC). On the other hand, this study used the published experimental data points of Herz et al. (2012a) to verify the predicted values of the effective wall to solid heat transfer coefficient (EHTC). The predicted EHTC values were also compared with the existing models (Li et al., 2005; Schlunder 1981).

5.4.1 Validation and comparison of effective wall to solid heat transfer coefficient (EHTC)

Figure 5.8 shows the variation of the predicted values of the effective wall to solid heat transfer coefficient (EHTC) with angular speeds. It is also plotted against the experimental data reported by Herz et al. (2012a) and the model values predicted by earlier models of Li et al. (2005) and Schlunder (1981). Predicted EHTC was 231.3

W/m^{2}K at 1 RPM and 318.1 W/m^{2}K at 6 RPM as compared to the published experimental values Herz et al. (2012a) of 250 W/m^{2}K and 310 W/m^{2}K at respective conditions. The model predicted values are well within the range of 10% error of the experimental data. This shows that the present model has a good predictive power compared to other published models by Li et al. (2005) and Schlunder (1981).

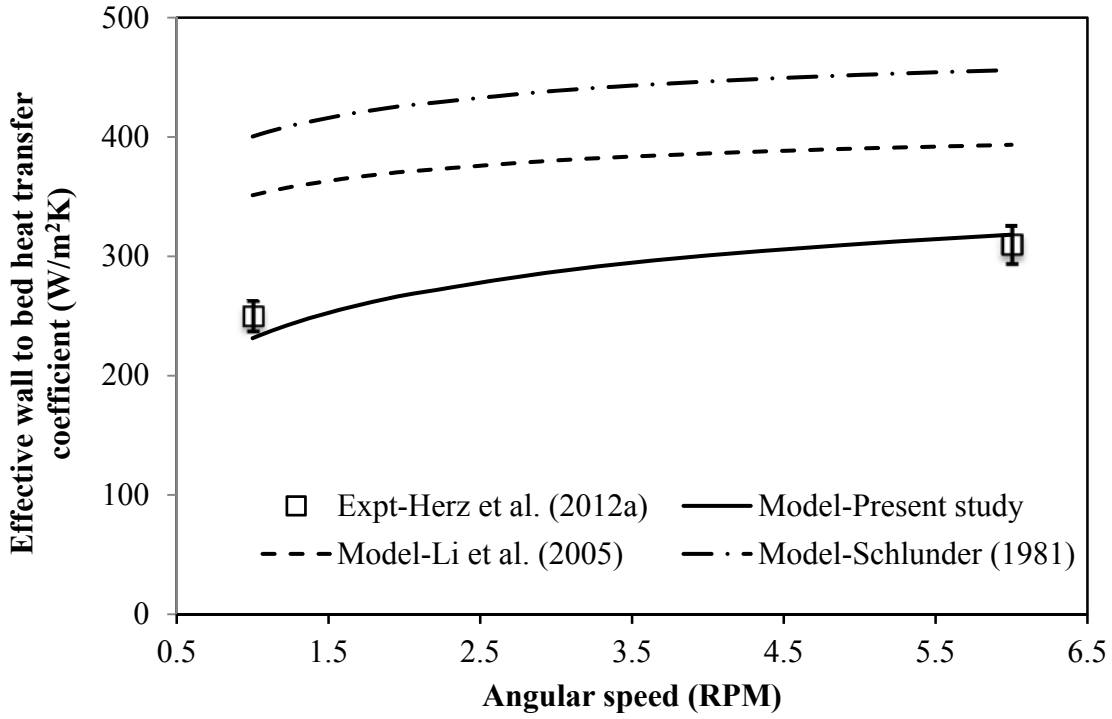

Figure 5.8: Validation and comparison of present EHTC (h_{ewb}) model with published literatures (Copper beads 0.8 mm and filling factor 10%)

An increase in the angular speed of the rotary reactor improves the solid mixing in one hand; on the other hand, it decreases the average contact time of particle (Eq. 5.8). This then decreases heat penetration resistance (Herz et al., 2012a) and then escalates the effective wall to solid heat transfer coefficient (Eq. 5.2a). Furthermore, the number of bed circulations rise with an increase in angular speed of the reactor, resulting in a better mixing in the solid bed (Herz et al. 2012a; Nafsun et al., 2015). However, the thermal

resistance due to the thin gas film for a larger particle size would be much higher compared to the thermal resistance due to the bulk solids. The effective thermal resistance is, therefore, close to the thermal resistance of the thin gas film. A similar observation is also reported in Basu and Fraser (Basu and Fraser, 1991). Therefore, in the present study, one can see only small variations on the effective heat transfer coefficient with the angular speed of the reactor. Such small variation of the effective heat transfer coefficient from wall to solid at a higher angular speed is also presented in Li et al. (2005). Li et al. (2005) have also shown that the variation of the effective heat transfer coefficient would be further low for a larger particle size.

5.4.2 Experimental verification of overall heat transfer coefficient (OHTC)

The overall heat transfer coefficients determined experimentally for two reactors of different diameter at different temperatures, angular speeds, and inclinations are presented in Tables 5.1 and 5.2. These data are validated with the values predicted by the developed model (Eq. 5.10).

Table 5.1: Overall heat transfer coefficient (W/m^2K) in dryer at different operating conditions

Angular speed (RPM)	Temperature (°C)								
	150			205			260		
	Inclination (Degree)								
	1.0	1.5	2.0	1.0	1.5	2.0	1.0	1.5	2.0
4.00	17.71	16.03	15.44	19.03	17.51	16.66	20.91	18.79	17.80
4.25	17.55	15.82	15.34	18.66	16.96	16.18	20.03	18.51	17.64
4.50	17.40	15.50	15.04	18.44	16.85	15.98	19.80	18.22	17.20
4.75	16.94	15.41	14.73	18.21	16.77	15.62	19.41	17.89	16.79
5.00	16.83	15.33	14.60	18.15	16.35	15.50	19.35	17.71	16.47
5.25	16.72			17.76			19.17		
5.50	16.47			17.50			18.85		
5.75	16.33			17.46			18.59		
6.00	16.11			17.33			18.29		

Table 5.2: Overall heat transfer coefficient (W/m^{2}K) in torrefier at different operating conditions

Angular speed (RPM)	Temperature (°C)								
	260			300			340		
	Inclination (Degree)								
	1.0	1.5	2.0	1.0	1.5	2.0	1.0	1.5	2.0
4.00	15.54	14.19	13.80	16.02	15.20	14.24	16.81	15.55	15.05
4.25	15.28	14.16	13.48	15.77	14.89	14.23	16.72	15.46	14.86
4.50	15.04	14.07	13.41	15.57	14.61	14.16	16.37	15.23	14.63
4.75	14.68	14.05	13.26	15.29	14.57	13.94	16.20	15.10	14.45
5.00	14.58	13.97	13.20	15.15	14.36	13.67	15.97	14.83	14.25
5.25	14.35			15.00			15.91		
5.50	14.20			14.94			15.86		
5.75	14.15			14.83			15.77		
6.00	14.09			14.74			15.42		

Figure 5.9 shows the variation of the overall heat transfer coefficient with the solid coverage fraction (δ_d). It shows that the overall heat transfer coefficient increases with the solid coverage fraction. For instance, the overall heat transfer coefficient of rotary reactor increases from 16.1 to 17.7 W/m^{2}K when the solid coverage fraction rises from 0.19 to 0.21. An increase in the solid coverage of the reactor increases the portion of heat transfer from the wall to particle compared to that from the wall to gas. In the Eq. (5.10), one can see that the reactor (of diameter 64 mm) wall to particle heat transfer coefficient is significantly higher (Eq. 5.3) compared to that with the wall to gas (Eq. 5.9). This results in a linear increase in the overall heat transfer coefficient when the solid coverage factor is increased. The model predicted values of the overall heat transfer coefficients, which fall within the estimated error level obtained from the repetition of experiments, indicate that they are in a good agreement with the experimentally calculated values.

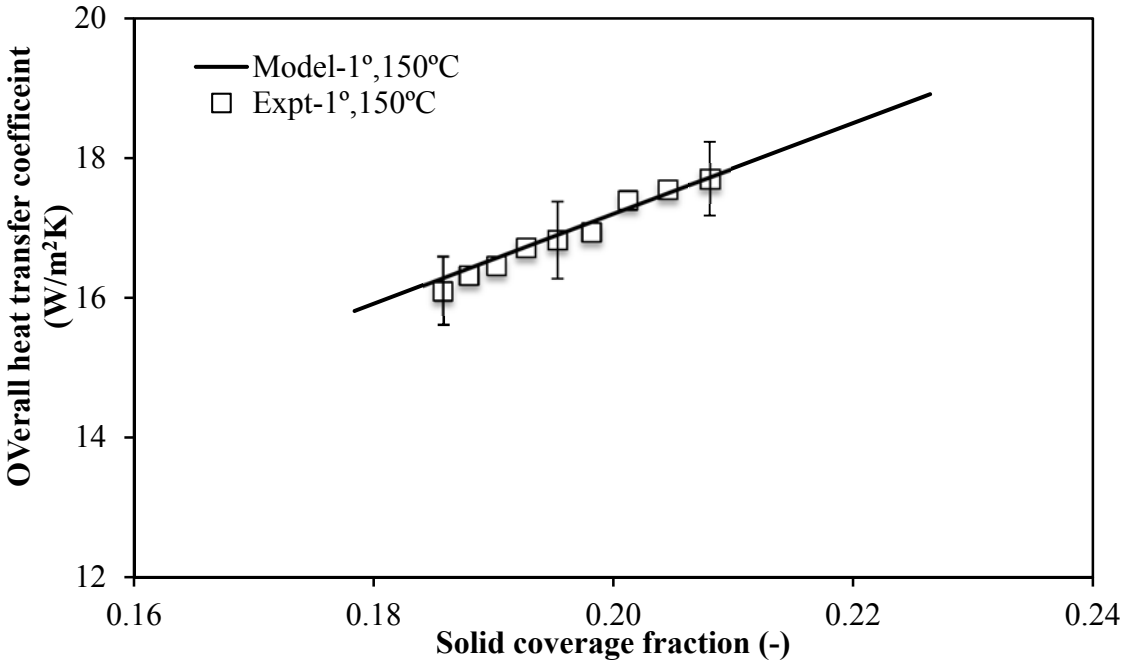

Figure 5.9: Effect of the solid coverage fraction on the overall heat transfer coefficient (Inclination 1º, temperature 150ºC, and diameter 64 mm)

5.4.2.1 Effect of Angular Speed

Figure 5.10 shows a decrease in overall heat transfer coefficient with an increase in angular speed of the reactor. The decrease is, however, modest. In a reactor operated at a constant inlet feed rate, the amount of solid in the reactor is reduced at high angular speed, which in turn decreases the solid wall coverage, and from Eq. (5.1) one notes that a decrease in solid wall coverage decreases the overall heat transfer coefficient. For instance, the overall heat transfer coefficient of the rotary reactor operated at inclination 1° and reactor temperature 150°C was decreased from 17.7 to 16.1 W/m^{2}K when the angular speed was increased from 4 to 6 RPM.

Figure 5.10 also compares the variation of the model predicted and experimentally calculated overall heat transfer coefficients of the reactor (of diameter 64 mm) with the angular speed. The overall heat transfer coefficient reduces further at a higher inclination of the reactor. However, one should note that existing models (Herz et al., 2012a; Li et al., 2005; Schlunder et al., 1984) for rotary reactor without flight showed that high solid filling factor reduces the wall to solid heat transfer. This is due to increase in the average contact time predicted by Eq. (5.5) in their models. A decrease in the number of bed circulations in a rotary reactor without flights operated at high solid filling factor also reduces wall to solid heat transfer (Herz et al, 2012a). However, in the present study, rotary reactors with flights will have a continuous solid mixing with the rotation of the reactor and also the average contact time is less affected by the solid filling factor (Eq. 5.8). Therefore, an increase in the solid filling factor at low angular speed increases solid coverage fraction. This then improves the overall heat transfer coefficient (Eq. 5.10).

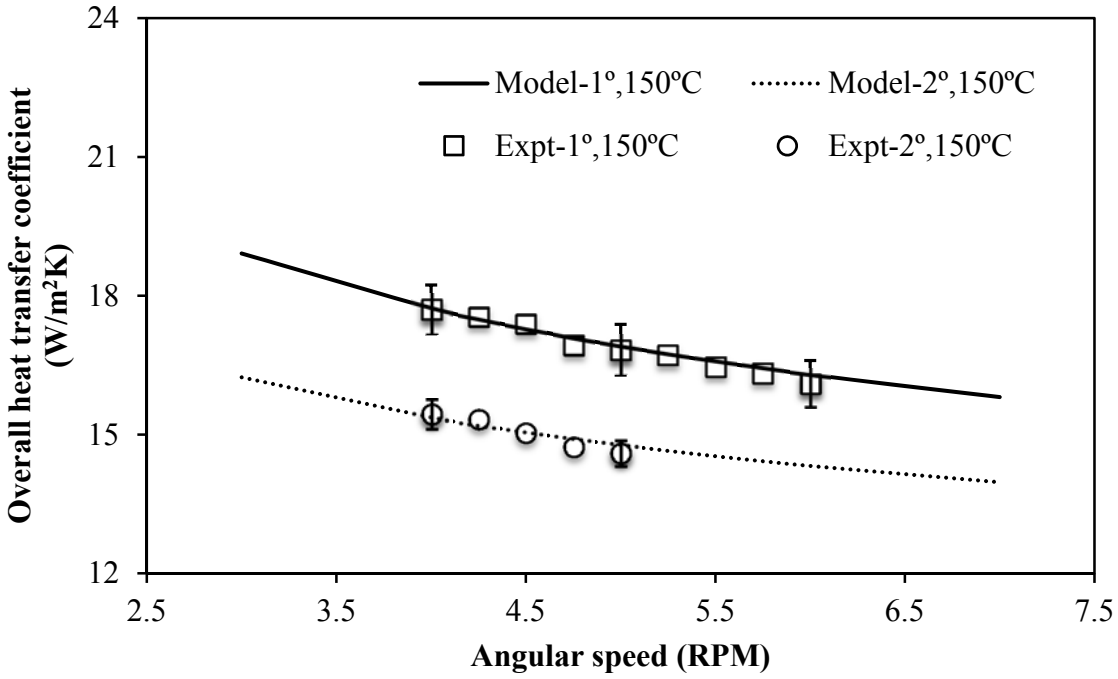

Figure 5.10: Effect of angular speed on overall heat transfer coefficient of reactor (64mm diameter) at 150°C, and inclinations 1° & 2°

5.4.2.2 Effect of Inclination

An increase in the inclination of the rotary reactor reduces the solid filling fraction and the mean residence time (discussed more in Chapter 4). This then reduces the solid coverage fraction in the rotary reactor, which decreases the overall heat transfer coefficient of the reactor.

Figure 5.11 shows the effect of inclination on both model predicted and the experimentally determined values of the overall heat transfer coefficient of the reactor maintained at 260°C and operated at 4 RPM and 5 RPM. For instance, the overall heat transfer coefficient decreased from 17.7 to 15.4 W/m^2K when the inclination of the reactor (of 64 mm diameter) was raised from 1 to 2º at 150ºC and rotating at 4 RPM. It also shows that the heat transfer coefficient decreases more at 5 RPM compared to that at 4 RPM when the inclination increases. This may be a more due to reduction in the solid filling fraction at high angular speed and high inclination of the reactor. One should also note that the variation of the overall heat transfer coefficient with the angular speed (Figure 5.10) is smaller compared that to the variation with the inclination (Figure 5.11).

Figure 5.11 also shows that the overall heat transfer coefficient may increase further when the reactor inclination is reduced to a horizontal position. However, authors aim to develop a continuous torrefier system that requires a smooth flow of solid inside the reactor. Because of this, no experiments were conducted keeping the reactor in the horizontal position. One should also note that the observed trend can not be extrapolated to a horizontal reactor because an increase in the solid filling factor for a given angular speed may decrease solid mixing, resulting in low heat transfer and even non-uniform torrefaction.

These results showing a decrease in the overall heat transfer coefficient at high angular speed and inclination conclude that any operating conditions reducing the solid coverage fraction reduce the overall heat transfer coefficient of the reactor.

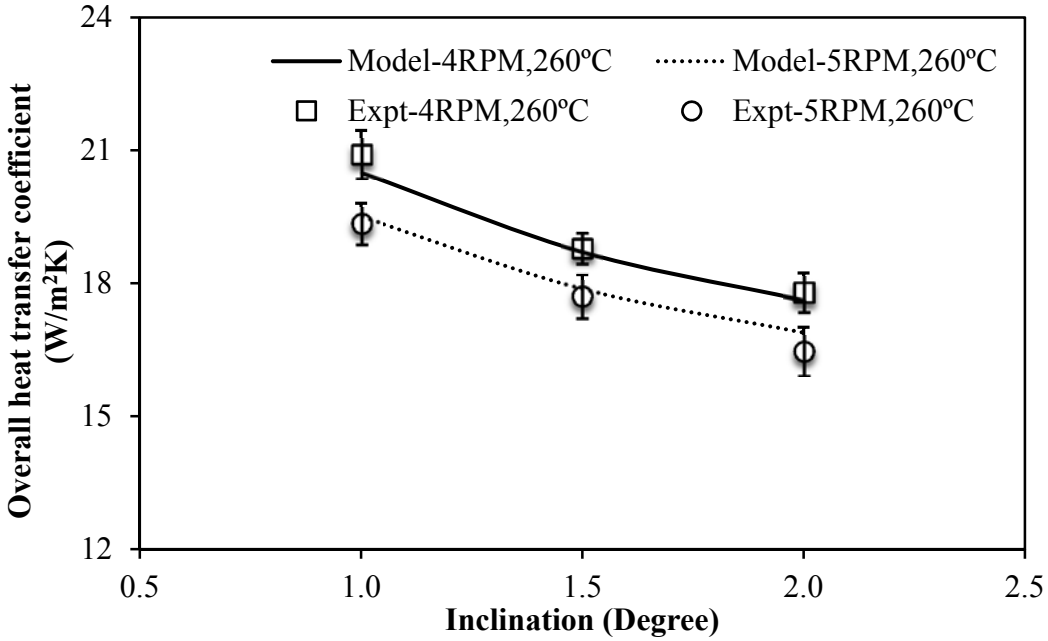

Figure 5.11: Effect of inclination of reactor (diameter 64 mm, operated at 4 and 5 RPM) on overall heat transfer coefficients

5.4.2.3 Effect of Reactor Temperature

Higher wall temperature gives a higher temperature of the gas-solid mixture inside the reactor. An increase in gas temperature increases the thermal conductivity of the gas. This decreases the thermal resistance due to the thin gas film between the reactor wall and the bed particle. This, thus, increases both the effective heat transfer coefficient from the wall to solid (Eq. 5.3) and the overall heat transfer coefficient (Eq. 5.10) of the rotary reactor. Figure 5.12 shows a variation of the overall heat transfer coefficient with the temperature of the two reactors. Here we note that the heat transfer coefficient increased from 17.7 to 20.9 W/m^2K when the temperature of the reactor (diameter 64 mm, inclination 1°, angular speed 4 RPM) was increased from 150 to 260°C (Figure 5.12a). Similarly, the overall heat transfer coefficient was increased from 15.5 to 16.8 W/m^2K when the temperature of the reactor of 100 mm diameter at same operating conditions was increased from 260 to 340°C (Figure 5.12b). Increased overall heat transfer coefficients with the reactor wall temperature were similar at both inclinations 1° and 2°.

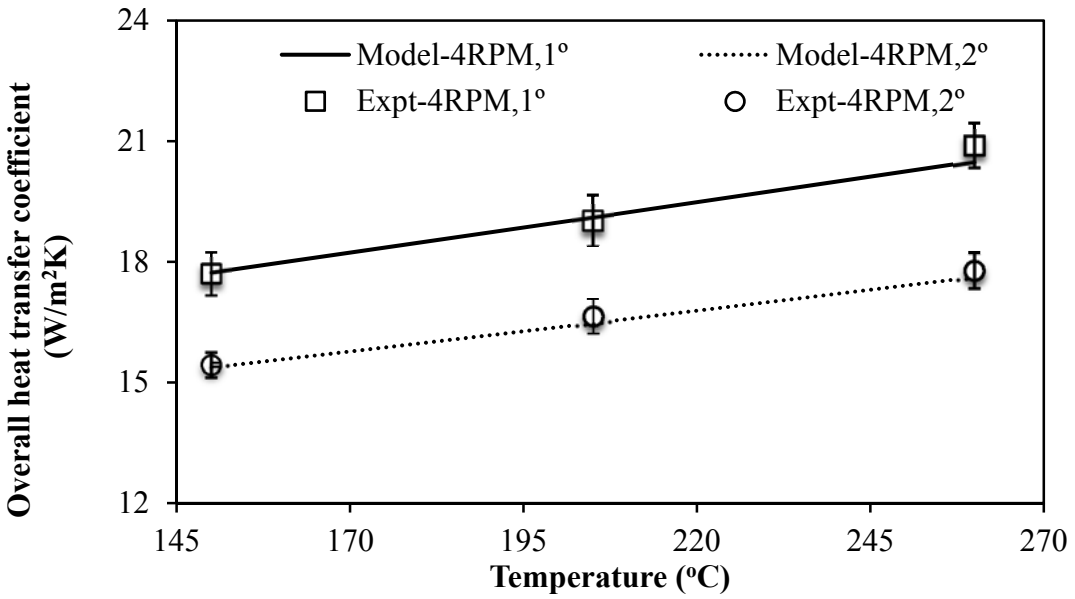

(a)

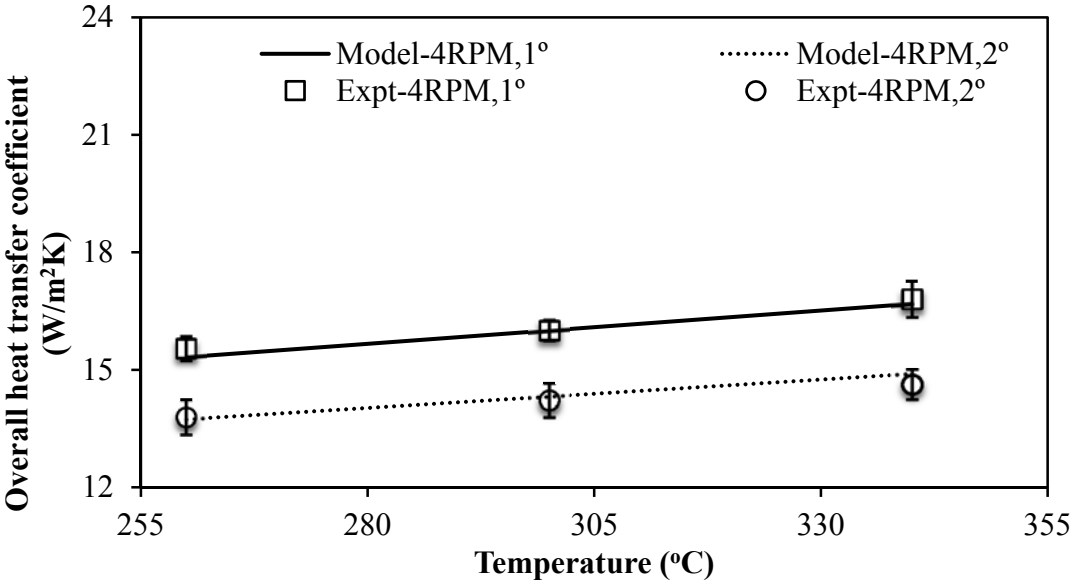

(b)

Figure 5.12: Effect of reactor temperature on overall heat transfer coefficient of reactor diameter: (a) 64 mm; and (b) 100 mm (Angular speed 4 RPM and inclinations 1º and 2º

5.4.2.4 Effect of Reactor Diameter

Figure 5.13 shows a typical variation of the overall heat transfer coefficient in two reactors at different angular speeds. Equation (5.10) clearly shows that the reactor diameter does not affect the first term of the expression, but the second term decreases with an increase in the reactor diameter. Since the first term (in Eq. 5.10) is dominant over the second term, only a small decrement in the overall heat transfer coefficient should be expected with the rise in the reactor diameter if the reactor was to be operated at a same solid filling factor. But, the present study is carried out at a constant inlet-feeding rate, the solid filling fraction reduces in a large diameter reactor compared to that in a small reactor. Therefore, the solid coverage fraction reduces significantly in the big reactor. The overall heat transfer coefficient was decreased significantly in a large reactor compared to that in a small reactor. For instance, reactors of diameter 64 and 100 mm operated at 260°C, 4 RPM and 1° have a solid coverage fraction 0.23 and 0.14, respectively. The overall heat transfer coefficient was found to be 20.9 W/m^{2}K in the small reactor and 15.5 W/m^{2}K in the big reactor.

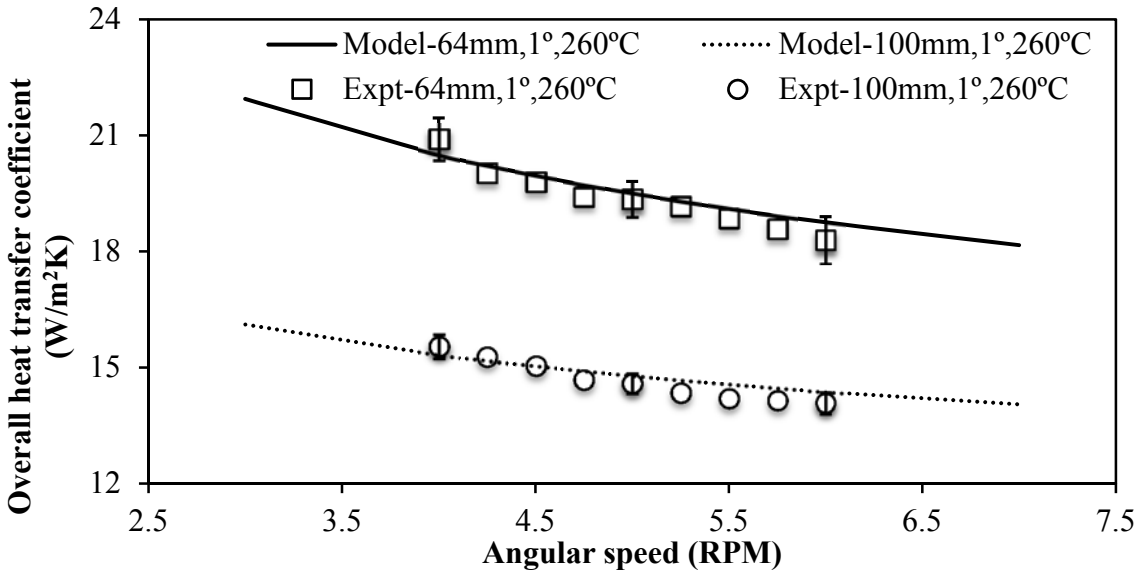

Figure 5.13: Variations of overall heat transfer coefficients in two reactors at 260°C and 1° with angular speeds (Reactor diameters 64 mm and 100 mm)

5.5. SUB-CONCLUSIONS

The cluster renewal model is adopted here to develop a mechanistic model of the overall heat transfer coefficient of an indirectly heated rotary torrefaction reactor. Assuming a steady and plug flow condition with a constant cross-sectional area of solid throughout the reactor length, an expression for the solid coverage fraction, which is valid for the solid filling factor in the range of 0.44-9.80%, was derived. For the current experimental conditions, the thermal resistance due to the gas film between the reactor wall surface and the solid bed surface had a dominant effect on the overall heat transfer coefficient. The overall heat transfer coefficients from the reactor wall surface to brass particles were found to be in the range of 14.6-20.9 W/m^2K and 13.2-16.8 W/m^2K for the dryer (64 mm diameter) and the torrefier (100 mm diameter), respectively.

The overall heat transfer coefficients are observed higher in a small reactor (dryer) compared to that in the big reactor (torrefier). The rise in the reactor wall temperature increases the overall heat transfer coefficient. The overall heat transfer coefficient decreases with a rise in the angular speed and inclination of the reactors due to a decrease in the solid wall coverage fraction. However, the effect of inclination was found higher compared to that of angular speed. The model predictions showed good agreement with experimentally measured values of overall heat transfer coefficient, which validates the model. Therefore, the developed model could be used to predict the overall heat transfer coefficient in an indirectly heated rotary torrefaction reactor with granular particles at different solid filling fractions.

CHAPTER 6: TORREFACTION OF POPLAR IN A CONTINUOUS TWO-STAGE, INDIRECTLY HEATED ROTARY TORREFIER[**]

Earlier two chapters (4 and 5) presented the bases of the important design parameters including mean residence time, filling factors, and heat transfers in rotary torrefier. The present chapter shows the effect of the developed two-stage novel rotary torrefier on torrefaction of woody biomass. It shows, by subjecting poplar wood to the developed unit of torrefaction, how operating parameters of such torrefaction affect the qualities of the torrefied solid product.

6.1. INTRODUCTION

Rotary reactors can be classified into directly and indirectly heated types. Due to direct contact of the heating source, mostly hot flue gas, the directly heated reactor poses the risk of spontaneous combustion – a phenomenon observed in the fixed bed torrefier. On the other hand, indirectly heated rotary reactors with a continuous solid movement are less likely to have such issues. Though many companies are working in their pilot units of rotary torrefiers, only limited number of research papers (Carrasco et al., 2014; Colin et al., 2014; Gil et al., 2015; Hilten et al., 2012; Kim et al., 2012; Mei et al., 2015; Repellin et al., 2010; Saleh et al., 2013; Strandberg et al., 2015) studied the effect of temperature and residence time on the torrefaction, but they all were for batch type reactors. Work on continuous torrefaction in rotary reactor is even few (Colin et al., 2014; Gil et al., 2015; Mei et al., 2015; Strandberg et al., 2015) but these reactors involved continuous supply of external inert gas through it. Thus none of the existing works are on two-stage continuous reactor with flights and without external gas flow

[**] This chapter is taken from the paper published by the candidate: Nhuchhen, D. R., Basu, P. and Acharya, B. (2016), "Torrefaction of Poplar in continuous two-stage indirectly heated rotary torrefier,"*Energy and Fuels*, 30(2), 1027-1038.

through the reactor. This leaves an important knowledge gap in the understanding of this novel promising process of torrefaction.

This chapter presents a complete parametric study of a continuous two-stage, indirectly heated rotary torrefier with flights where internally generated volatile gases serve as the torrefaction medium. This chapter aims at understanding the effect of operating parameters, like temperature, rotation, and inclination of the reactor on the properties of the torrefied solid product, including higher heating values, volumetric energy densities, elemental compositions, and proximate analyses. This work also examines the impact of process parameters on different product attributes such as fuel ratio, solid mass yield, energy density enhancement, and energy yield, and then prepares an overall energy balance of the system. Some tests at selected operating conditions were also conducted in a nitrogen medium to compare the quality of product that was obtained in a volatile medium.

6.1.1 Process Parameters

Process parameters used to define the quality of torrefied product are fuel ratio (*FR*), solid mass yield (*MY, %*), energy density enhancement (*EDE, %*), and energy yield (*EY, %*). Following equations are used for calculating them in dry and ash free basis.

$$FR = \frac{FC}{VM} \tag{6.1}$$

$$MY = \frac{\dot{M}_{T,daf}}{\dot{M}_{R,daf}} \times 100 \tag{6.2}$$

$$EDE = \frac{HHV_{T,daf} - HHV_{R,daf}}{HHV_{R,daf}} \times 100 \tag{6.3}$$

$$EY = \frac{\dot{M}_{T,daf}}{\dot{M}_{R,daf}} \frac{HHV_{T,daf}}{HHV_{R,daf}} \times 100 \quad (6.4)$$

Where, the subscripts *R* and *T* represent raw biomass and torrefied biomass, respectively. FC and VM are the fixed carbon and volatile matter contents of the solid fuel. $\dot{M}_{daf}$ and HHV_{daf} are the mass flow rate and higher heating value on dry and ash free basis, respectively.

6.2. EXPERIMENTAL METHODS

6.2.1 Materials

Chips of yellow cylindrical Poplar (dowels), which are initially chopped into small sizes ranging from 3 to 8 mm and stored in plastics bags to prevent changes in initial moisture content of raw biomass, were used for the experiments. Table 6.1 presents the properties of raw biomass.

Table 6.1: Properties of raw biomass (yellow poplar)

Properties	Parameters	Value
Proximate analysis	Moisture (M, % AR)	4.50
	Volatile matter (VM, % dry)	88.32
	Ash content (ASH, % dry)	0.28
	Fixed carbon (FC, % dry)	11.40
Ultimate analysis	Carbon (C, % daf)	45.97
	Nitrogen (N, % daf)	0.44
	Hydrogen (H, % daf)	6.12
	Oxygen (O, daf)	47.47
Higher heating value	HHV (MJ/kg, dry)	19.02

6.2.2 Experimental Setup

Schematic diagram of a continuous two-stage, rotating drum torrefier is shown in Figure 6.1. The rotary torrefier system consists of a dryer and a torrefier. The dryer is a cylindrical drum of 64mm ID and 610mm length. The torrefier has an ID of 100mm and is 762mm long. Both the rotary dryer and torrefier has axially inserted three flights (sized is given in Chapter 4) placed 120° apart from each other. Both the dryer and torrefier rotates inside a co-centric fixed cylindrical shell, which is wrapped with electric heaters and then tightly covered with insulation (Calcium-Magnesium-Silicate wool). Thermocouples (K-type) measure the surface temperatures of both the dryer and torrefier. The screw feeder at one end of the dryer, as shown in Figure 6.1, feeds biomass at a desired rate. The inclination and rotation of the drum assist in axial movement of biomass particles and maintain the desired level of mean residence time. No external gas is supplied to dryer or torrefier. Moisture released during drying comes out from the opening at the other end of the dryer. As the biomass reached other end of the dryer, it drops into the torrefier via a flexible aluminum pipe, where it is devolatilized under a volatile gases medium at a steady state condition. The torrefied biomass is finally collected at the other end of torrefier in a nitrogen-flushed container. Once the feeding is started, it takes 40-45 minutes to reach steady state operation in each reactor. The sample of torrefied biomass is therefore collected only after 120 minutes from initial operation. The collected torrefied biomass is first cooled in a desiccator. The proximate, ultimate, and heating value analyses are then conducted on the cooled torrefied biomass.

Proximate analysis is conducted in the Muffle Furnace as per ASTM standard method (ASTM D1762-84) (ASTM, 2013). An ultimate analysis is performed using an Elemental Analyzer (Organic Elemental Analyzer - Model EA1110) to determine carbon, nitrogen, and hydrogen compositions. The oxygen content is determined by the difference. The higher heating value (HHV) is determined using a semi-automatic Compensated Jacket Calorimeter (Model Parr-6100). The volatile released during torrefaction is removed through an opening as shown in Figure 6.1 and condensed to determine the rate of liquid product yield. The dried non-condensable gas is collected in

a gasbag. The rate of non-condensable gas released during the process is estimated by simple mass balance. Compositions of the non-condensable gas are measured using the SRI 8610C Gas Chromatograph.

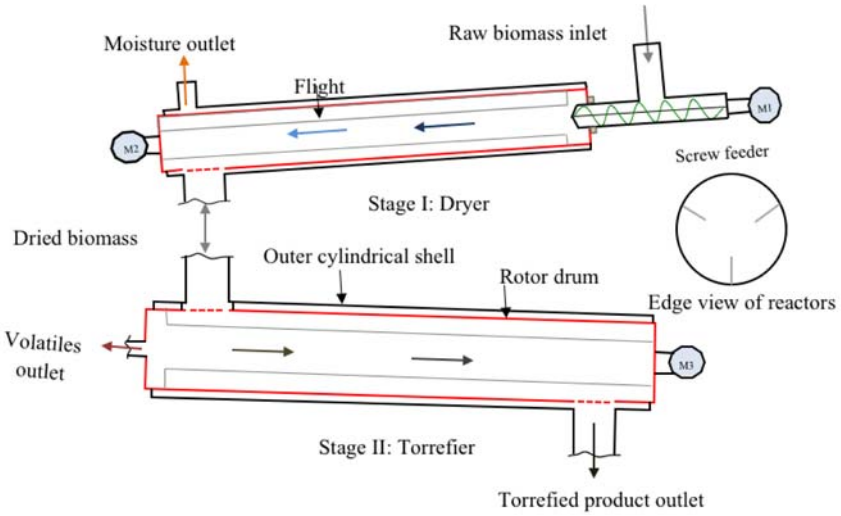

Figure 6.1: Schematic flow diagram of the two-stage indirectly heated rotary torrefier

From the preliminary experiments, it is found that when the dryer is operated at 150°C, 1°, and 4 RPM, the moisture content of biomass is reduced to less than 0.1%, so for the entire tests, the operating condition of dryer are set to those values. No literatures with specific criteria to select operating torrefaction temperature have been published so far. Some studies (Chen et al., 2011; Nhuchhen and Basu, 2014; Sabil et al., 2013) selected operating temperature based on the mode of torrefaction, whereas other adopted the temperature in the range of 200-350ºC (Carrasco et al., 2014; Pelaez-Samaniego et al., 2014; Strandberg et al., 2015; Zheng et al., 2012), which is based on the range of the thermal degradation of the polymeric compositions of biomass. In the present study, operating temperature was started at 260ºC to ensure a majority of hemicellulose (>58%) constituent of biomass gets devolatilized (Nhuchhen et al., 2014). Experiments were conducted mainly at three different torrefaction temperatures (260, 290, and 320°C), three angular speeds (4.0, 4.5, and 5.0 RPM), and three inclinations (1.0, 1.5, and 2.0°). Two more temperatures (275 and 310°C) of the torrefier at angular speed 4 RPM and inclination 2° were also selected to analyze the effect of torrefaction temperature on the

solid mass yield. Three additional angular speeds (4.25, 4.84, and 5.50 RPM) of the torrefier at 290°C and 1° and 2° inclinations were chosen to investigate the effect of rotation of the reactor on the torrefied solid products. The inclination of the reactor is measured using Master Craft Level of 0.1° accuracy. The angular speed is controlled by DC gear motor and determined manually by measuring the time taken to rotate a known number of rotations.

For the torrefaction tests in the fixed bed reactor, a muffle furnace was used. A K type thermocouple was installed to measure the temperature of torrefaction. Nitrogen gas was supplied continuously through a steel pipe inserted inside the muffle furnace to maintain an oxygen free environment. A detailed description of this reactor is presented in Dhungana (2011). Dried sample of poplar was used to conduct the test at 260ºC and 320ºC at different residence times equivalent to the mean residence time of the rotary torrefier. Torrefied samples were cooled inside the desiccator and then stored in the plastic bags.

6.3. RESULTS AND DISCUSSION

6.3.1 Changes in Color

A change in the color of biomass is a good indicator to show the degree of torrefaction. A number of factors such as losses in mass including surface moisture, bound moisture, and light volatile gases; types of wood; polymeric compositions content of biomass; changes in the surface properties of biomass that affect absorption, reflection, and scattering properties; formation of different chromophoric groups; and the movement of sugar molecules with low-molecular-weight to the surface of biomass may affect the color of the solid product after the thermal treatment (Nhuchhen et al., 2014). Among different parameters, the torrefaction temperature is considered to be the main operating parameter that affects the degree of torrefaction (Lin and Wu, 2013; Nhuchhen and Basu, 2014; Pimchuai et al., 2010). Figure 6.2 shows the effect of the torrefaction temperature

on the product color. The darkness of the torrefied product increases with temperature (Na et al., 2013). However, one could see that colors of the solid products are uniform, indicating a similar level of thermal degradation to all particles in the torrefier. The product color, however, may not be uniform in the fixed bed reactor, as reported by Nhuchhen et al. (2014).

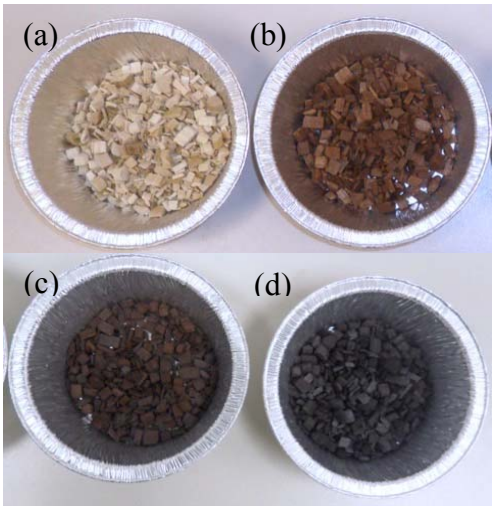

Figure 6.2: Variations in color of torrefied biomass with temperature compared with raw biomass (a) Raw poplar, (b) T = 260°C, (c) 290°C, and (d) 320°C (Angular speed 4 RPM and inclination 1°)

6.3.2 Proximate Analysis

As the volatile matter and fixed carbon contents quantify an improvement on the fuel ratio of the solid fuels (Nhuchhen and Basu, 2014), which helps in increasing biomass to coal blend ratio in the co-firing plants, it is therefore necessary to carry out the proximate analyses of the torrefied solid products. Table 6.2 gives the proximate analyses (% wt. daf) of the torrefied biomass produced at different operating conditions. With the change in the torrefaction conditions, the percentage decrease in the volatile matter content of the torrefied products compared to that of the raw biomass were found in the range of 0.1-13.7% whereas the fixed carbon content in the torrefied biomass was increased to more than double at 320°C, 4 RPM, and 1° compared to that in the raw biomass.

Table 6.2: Proximate analyses (% wt.), ultimate analyses (% wt.), and higher heating value (MJ/kg) (in dry and ash free basis-daf) of torrefied products at different operating conditions

Temperature (°C)	Inclination (Degree)	1.0			1.5			2.0		
	Angular speed (RPM)	4.0	4. 5	5.0	4.0	4. 5	5.0	4.0	4. 5	5.0
260	VM	86.74	87.64	87.92	87.65	87.88	88.15	88.13	88.29	88.52
	FC	13.26	12.37	12.09	12.36	12.14	11.87	11.88	11.73	11.50
	C	48.18	47.91	47.85	47.87	47.72	47.68	47.65	47.57	47.45
	N	0.45	0.46	0.47	0.48	0.46	0.47	0.48	0.46	0.46
	H	5.87	5.89	5.92	5.93	5.94	5.96	5.98	6.00	6.00
	O	45.49	45.74	45.76	45.71	45.88	45.89	45.88	45.97	46.08
	HHV	20.04	19.88	19.84	19.89	19.83	19.74	19.69	19.63	19.62
290	VM	81.94	83.88	84.97	83.29	84.99	85.41	84.01	85.92	86.63
	FC	18.06	16.13	15.05	16.71	15.03	14.61	16.01	14.10	13.40
	C	50.09	49.71	49.35	49.35	49.02	48.83	48.81	48.65	48.50
	N	0.45	0.47	0.45	0.44	0.46	0.47	0.46	0.45	0.44
	H	5.52	5.57	5.67	5.55	5.62	5.66	5.76	5.80	5.83
	O	43.94	44.25	44.53	44.65	44.90	45.03	44.96	45.10	45.23
	HHV	21.58	20.91	20.56	21.14	20.75	20.34	20.41	20.20	20.09
320	VM	76.42	78.48	80.37	78.77	80.30	81.34	80.59	81.69	82.22
	FC	23.58	21.61	19.81	21.34	19.87	18.88	19.60	18.55	18.04
	C	53.47	52.84	51.64	51.92	50.50	49.87	49.68	48.81	48.59
	N	0.44	0.44	0.44	0.44	0.45	0.43	0.43	0.45	0.44
	H	5.48	5.57	5.63	5.55	5.61	5.64	5.70	5.75	5.79
	O	40.62	41.15	42.29	42.09	43.44	44.05	44.19	44.99	45.18
	HHV	23.24	22.18	21.65	22.71	21.98	21.22	21.85	21.37	20.96

A decrease in the volatile matter content and an increase in the fixed carbon content of the torrefied biomass were observed when the torrefaction temperature was increased. For instance, the volatile matter content of the torrefied biomass obtained at angular speed of 4 RPM and inclination of 1° was decreased from 86.7 to 76.4%, when the torrefaction temperature was increased from 260 to 320°C. Increases in the angular speed and in the inclination, which both decrease the mean residence time of solid in the reactor, reduce the devolatilization reactions. This therefore produces the solid products with the high volatile matter content and low fixed carbon content when angular speed and inclination of the torrefier are high. For example, the volatile matter content decreased from 81.3 to 78.8% when the angular speed was decreased from 5 to 4 RPM at 1.5° and 320°C. Likewise, the volatile matter content of the torrefied solid product obtained at 4 RPM and 320°C decreased from 80.6 to 76.4% when the inclination of the reactor was reduced from 2 to 1°. However, the effects of angular speed and inclination were found significant only at high torrefaction temperature (320°C).

Changes in the volatile matter and fixed carbon contents after torrefaction are proven beneficial in biomass co-firing plants. These changes usually measure using the fuel ratio, which is defined as the ratio of fixed carbon content to volatile matter content of the solid fuel. Though increases in the fuel ratios are small at studied operating conditions, they can produce a profound benefit in co-firing power plants. For instance, co-firing of biomass with a low fuel ratio increases CO and hydrocarbon emissions if the co-firing ratio is increased (Casaca and Costa, 2003). Biomass with a low fuel ratio produces a high amount of volatile gases, which will travel faster to the low temperature region of the combustor and then have only limited oxidation reactions. Low temperature oxidation of volatiles can increase the reduction reaction of N_2 content of the biomass, forming nitric oxide. Therefore, the level of NO_x emissions increases significantly when the co-firing blend ratio rises. Co-firing of biomass would further emit more NO_x if biomass with high N_2 content had to be cofired (Narayanan and Natarajan, 2007). To avoid such emissions, biomass co-firing plants usually require a modification of the reactor system such as an increase in reactor height or secondary airports so that the

reactor can provide sufficient gas residence time for complete oxidation of volatiles in the combustor. Such modification in existing pulverized coal facilities to mix biomass up to 15% by mass will require a considerably big investment. It may be close to that of a new wood-firing facility (Benjamin, 1997). Therefore, a torrefaction process, which can substantially increase the fuel ratio (up to 139% compared that with raw biomass – in the present study), could increase the share of biomass in co-firing plants and reduce the level of emissions. Figure 6.3 shows the fuel ratios of the torrefied solid products at selected operating conditions and compares them with that of raw biomass. The figure indicates that the fuel ratio decreases at high angular speed and inclination of the reactor, whereas it increases at high torrefaction temperature. For instance, fuel ratio of the torrefied poplar obtained at 290ºC and 1º inclination decreases from 0.22 to 0.19 when the angular speed increases from 4 to 4.5 RPM. In similar manner, the fuel ratio of the torrefied poplar produced at 320ºC and 4 RPM decreases from 0.31 to 0.24 when the inclination of the reactor rises from 1º to 2º. However, the fuel ratio of the torrefied product obtained at 4.5 RPM and 1º inclination was double (from 0.14 to 0.28) when the torrefaction temperature was increased from 260 to 320ºC.

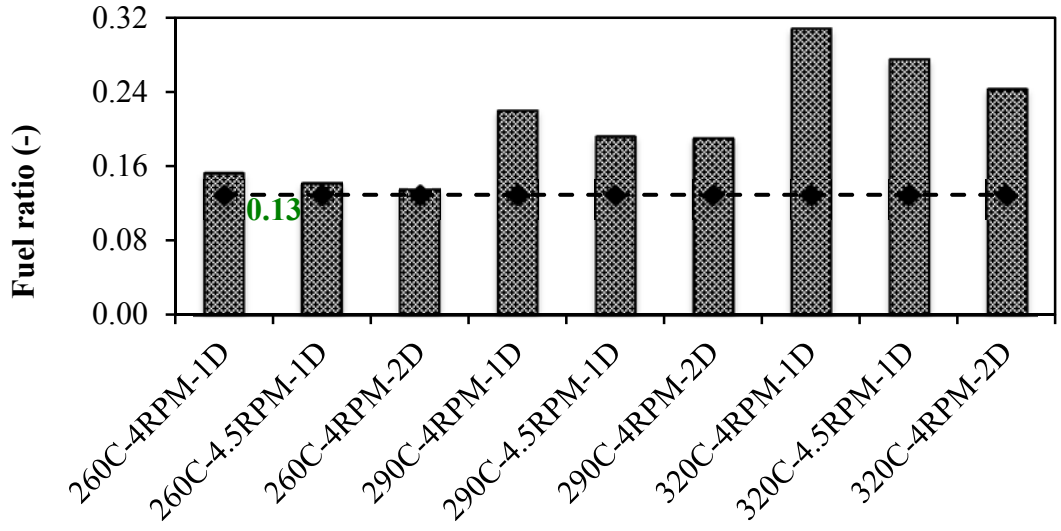

Figure 6.3: Fuel ratios of torrefied solid products at selected torrefaction conditions and raw biomass (0.13)

6.3.3 Ultimate Analysis

Table 6.2 presents the ultimate analyses of the torrefied biomass produced under different operating conditions. An increase in the carbon content and a decrease in the hydrogen and oxygen contents were observed after the torrefaction process. The decreased hydrogen and oxygen contents are caused mainly by the removal of hydrogen and oxygen based compounds such as water vapor and carbon dioxide. At high torrefaction temperature, the decarboxylation reactions will be more, and the torrefied biomass becomes a more carbon dense product compared to that at a low temperature. A case at 4 RPM and 1° inclination shows that the carbon content in the torrefied biomass increased from 48.2 to 53.5% when the torrefaction temperature was raised from 260 to 320°C. This increment is equivalent to 4.8% and 16.3% compared to the carbon content of the raw poplar. Hydrogen content, on the other hand, decreased from 5.9 to 5.5% when the torrefaction temperature was increased in a similar range. This decrease could be due to the increase in the formation of condensable volatiles gases containing higher number of hydrogen atoms such as acetic acids, methanol, and lactic acids (Prins et al., 2006). Oxygen content of biomass also decreases more at high torrefaction temperature as it could transform oxygen-containing compounds into light volatile gases such as CO and CO_2. A high temperature torrefaction, which is also suitable for releasing more carboxylic compounds (Shoulaifar et al., 2012), can therefore significantly enhance the deoxygenation of biomass.

As explained earlier, biomass undergoes more devolatilization reactions at the low angular speed and inclination. One can, therefore, expect an increase in the share of carbon and a decrease in the share of hydrogen and oxygen in the torrefied biomass when angular speed and inclination decrease. For example, the carbon content of the torrefied biomass obtained under the torrefaction temperature 320°C and inclination 1° decreased gradually from 53.5 to 51.6% when angular speed was increased from 4 to 5 RPM. Similar trends were also found when the inclination of the reactor was increased. For instance, the carbon content of the torrefied biomass obtained at 320ºC and angular

speed 4 RPM decreased from 53.6 to 49.7% when the reactor inclination was increased from 1 to 2°.

The advantages of deoxygenating biomass can be explained from the Van Krevelen diagram as shown in Figure 6.4. It clearly indicates the positions of different torrefied biomass at various operating conditions compared to that of a low quality coal (lignite). The O/C and H/C ratios of the torrefied biomass were observed in the range of 0.760-0.971 and 0.102-0.127, respectively. The reduction in the H/C increases the product stability due to the increased number of aromatic structures (Kloss et al., 2012; Schimmelpfennig and Glaser, 2012) whereas the decrease in the O/C improves the hydrophobicity due to the elimination of the hydrophilic functional groups (Schimmelpfennig and Glaser, 2012). The use of improved torrefied biomass with low O/C ratio shows a higher cold gas efficiency of the gasification process compared to that with the biomass with high O/C ratio (Ghassemi and Shahsavan-Markadeh, 2014). Deoxygenating biomass also helps in producing the liquid oil product with the concentrated phenols and the gas with the concentrated H_2 and CH_4 from a pyrolysis process (Chen et al., 2014).

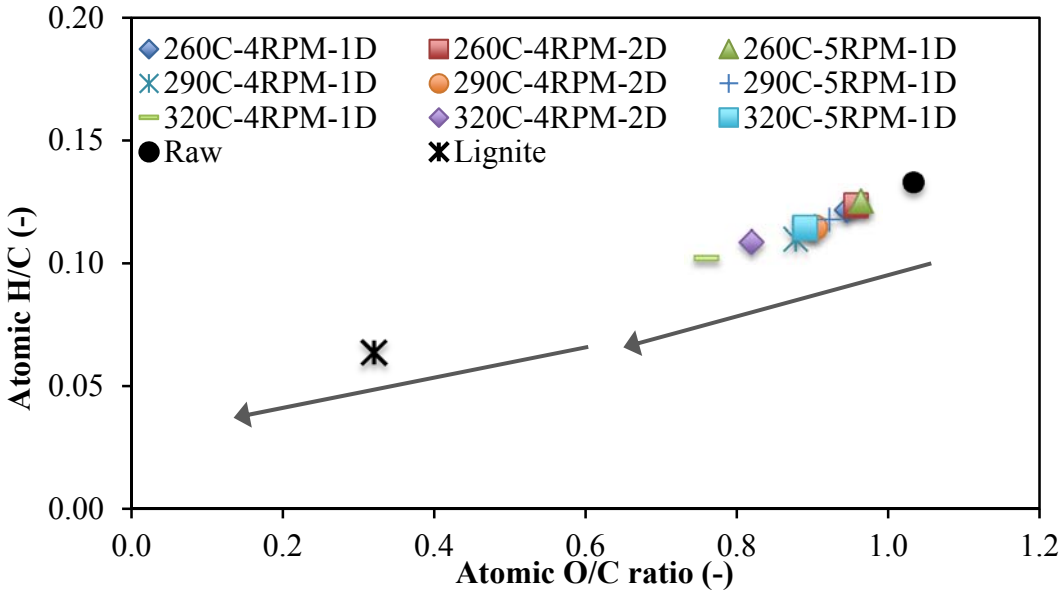

Figure 6.4: Van Krevelen diagram showing H/C and O/C of different torrefied biomass

6.3.4 Mass Yield

The performance of the torrefaction process is often measured quantitatively using the solid mass yield, which can be used as an indicator to examine the economic viability of the overall process. A decrease in the mass of the raw sample is the result of losses in the volatile matter of biomass during the process. This then reduces the density of the torrefied solid products; on the other hand, it increases the energy density of the solid products. As the main product of interest of torrefaction is solid mass yield, the condensable and non-condensable liquid products were measured only at selected operating conditions. Figure 6.5 shows a typical variation of product yield distributions including non-condensable liquid, condensable liquid, and solid products of torrefaction in three different operating cases. The solid mass yield (which will be discussed more later) decreases substantially at higher temperature because an increase in the torrefaction temperature is more suitable for devolatilization reactions. Liquid and gas products yield were increased with the rise in torrefaction temperature. Chen et al. (2015) and Giijun et al. (2011) have also reported similar results. An increase in condensable products such as acetic acid, formic acids, and lactic acids at high temperature torrefaction is responsible for the rise in the share of liquid product.

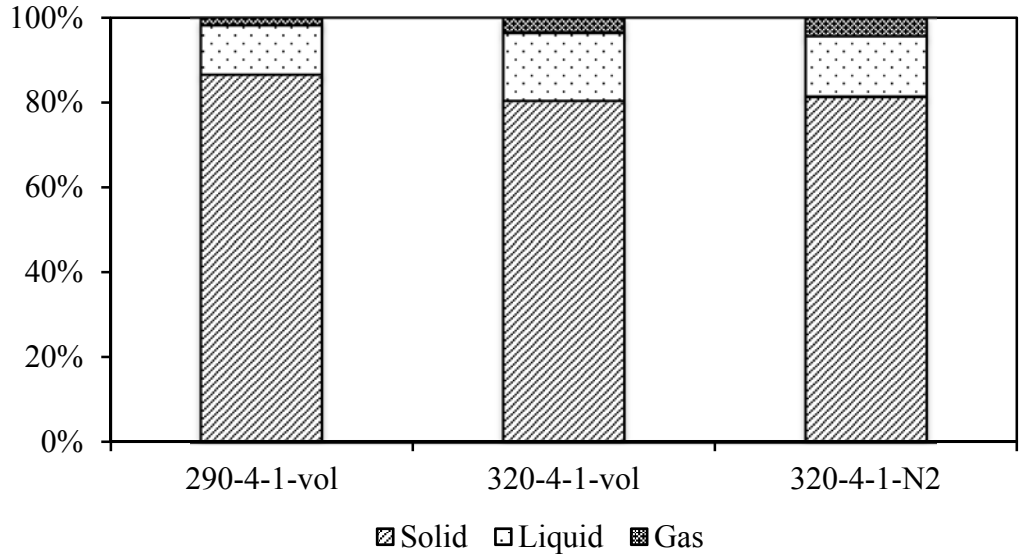

Figure 6.5: Products yield distribution at selected operating conditions of torrefaction (Temperature-RPM-Inclination-Medium)

Figure 6.6 shows the major gas compositions of the non-condensable gaseous products of torrefaction. As the high temperature is more suitable for heterogeneous reaction between CO_2 and solid (Duan et al., 2009), the CO concentration was found to be higher at 320°C compared to that at 290°C. The share of CO was, however, found lesser in a nitrogen-flushed torrefaction compared to that in a slowly moving volatile gases medium based torrefaction at the same operating conditions.

As a low angular speed, a small inclination of the reactor, and a high torrefaction temperature are suitable operating conditions for more devolatilization reactions, the solid mass yield decreases accordingly (Table 6.3). The lowest solid mass yield of 80.2% was found at 320°C, 4 RPM, and 1°. Figure 6.7 shows a surface plot of solid mass yields at 290°C, showing the variation of the solid mass yield with angular speed and inclination of the reactor. One can see that the solid mass yield rises gradually with increase in both angular speed and inclination of the reactor. However, the increment of the solid mass yield per unit change in angular speed was found to be more as compared to per unit change in inclination.

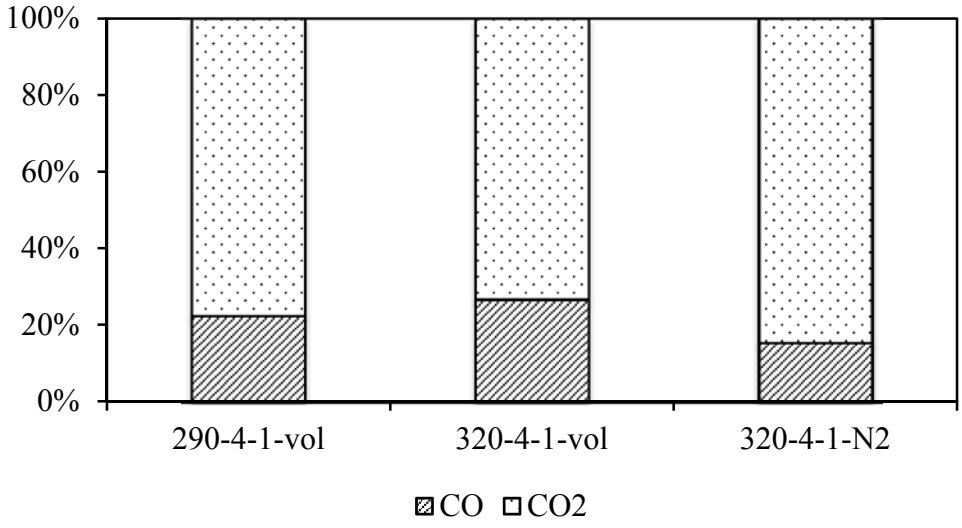

Figure 6.6: Compositions of non-condensable gas products of torrefaction at selected operating conditions (Temperature-RPM-Inclination-Medium)

Table 6.3: Process parameters fuel ratio (-), energy density enhancement (%), mass yield (%), and energy yield (%) in dry and ash free basis (daf) at different operating conditions

Temperature (°C)	Inclination (Degree)	1.0			1.5			2.0		
	Angular speed (RPM)	4.0	4. 5	5.0	4.0	4. 5	5.0	4.0	4. 5	5.0
260	FR	0.15	0.14	0.14	0.14	0.14	0.13	0.13	0.13	0.13
	EDE	5.02	4.23	4.00	4.25	3.97	3.49	3.26	2.94	2.91
	MY	92.34	93.10	94.26	93.20	94.11	95.16	93.53	94.45	95.47
	EY	97.24	97.27	98.27	97.40	98.08	98.71	96.80	97.43	98.46
290	FR	0.22	0.19	0.18	0.20	0.18	0.17	0.19	0.16	0.15
	EDE	13.14	9.70	7.92	10.88	8.91	6.81	7.16	6.09	5.54
	MY	85.94	88.43	90.28	87.41	89.69	90.92	89.20	90.89	92.13
	EY	97.71	97.40	97.78	97.35	98.05	97.42	95.90	96.72	97.51
320	FR	0.31	0.28	0.25	0.27	0.25	0.23	0.24	0.23	0.22
	EDE	21.82	16.48	13.86	19.14	15.51	11.66	14.83	12.45	10.40
	MY	80.19	81.17	82.87	80.78	82.51	84.45	82.12	83.85	85.60
	EY	99.31	95.92	95.62	97.74	96.65	95.47	95.60	95.50	95.62

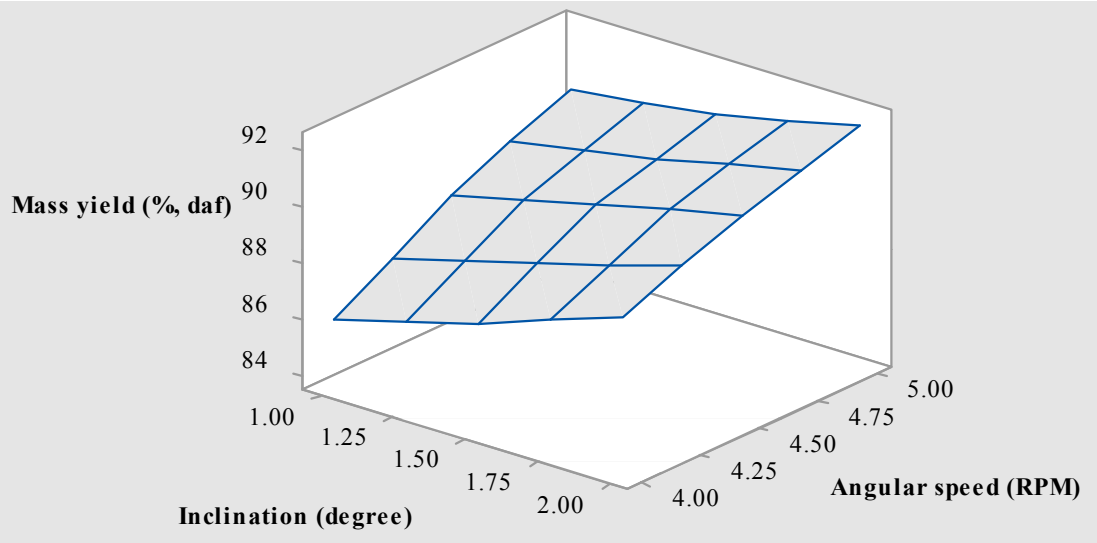

Figure 6.7: Surface plot of solid mass yields (% dry and ash free basis) with inclination and angular speed of reactor

As the mean residence time and the torrefaction temperature are the two primary factors of a torrefaction process, Figures 6.8 (a) and 6.8 (b) are shown separately to examine their effects. The expression for estimating the mean residence time at a given operating condition was presented in Chapter 4. Increase in the mean residence time from 18 to 25 minutes reduces the solid mass yield from 91.4% to 85.9%. The solid mass yield also decreases substantially with the torrefaction temperature. A typical variation of the solid mass yield at 4 RPM and 2° is shown in Figure 6.8(b). The variation ranges from 93.5 to 82.1% (daf) when the torrefaction temperature increases from 260 to 320°C.

The reduction in the solid mass yield is due to a decrease in volatile matter caused by a complete devolatilization of hemicellulose and a partial degradation of cellulose. This produces the porous solid product. A decrease in hemicellulose fraction in biomass weakens the fibrous structure of biomass, which improves the grindability of biomass (Peng et al., 2013; Phanphanich and Mani, 2011). A torrefaction process therefore makes biomass suitable to be milled in the existing pulverized co-firing facilities, with a minor technical retrofit. In addition to this, the porous solid produced after a torrefaction

process becomes more brittle. This not only reduces the grinding energy consumption by 70-90% (Bergman, 2005) but also reduces the average particle size distribution (Repellin et al., 2010a). A decrease in the average particle size then enhances the combustion process in the co-firing plants, reducing the level of emissions (Casaca and Costa, 2003).

6.3.5 Higher Heating Value, Energy Density Enhancement, and Energy Yield

An increase in the higher heating value of the torrefied biomass is considered to be a qualitative improvement on biomass fuel properties. As increased HHV only could compensate all necessary expenses required for a torrefaction process, it is always desirable to have all torrefied products analyzed for their heating values. Table 6.2 presents the HHV of the torrefied solid products obtained at different operating conditions. It is apparent from the Table 6.2 that only a small increase in the HHV of torrefied products is seen at low torrefaction temperature. For instance, a typical increment of 0.55 MJ/kg in the torrefied biomass compared to the HHV of raw biomass was found at 260°C, 5 RPM, and 2°. This increment was found nearly 3.5 times more at 320°C compared to that at 260°C. Increase in the HHV of biomass escalates the share of biomass energy in co-firing power plants.

Since the gain in the HHV is often compared with the HHV of raw biomass, energy density enhancement (EDE) is determined. Table 6.3 presents the energy density enhancement (%, daf) at different operating conditions. The EDE was found in the range 2.9-21.7% at different studied operating conditions. Unquestionably the EDE increases sharply with the torrefaction temperature. For example, the EDE of the torrefied biomass produced at 4 RPM and 1° was increased from 5.0% at 260°C to 13.1% at 290°C, and then to 21.7% at 320°C. The EDE at same angular speed was decreased to 3.2%, 7.0%, and 14.4%, respectively, when the inclination was increased from 1 to 2°. The EDE, however, decreases with an increase in the angular speed and inclination.

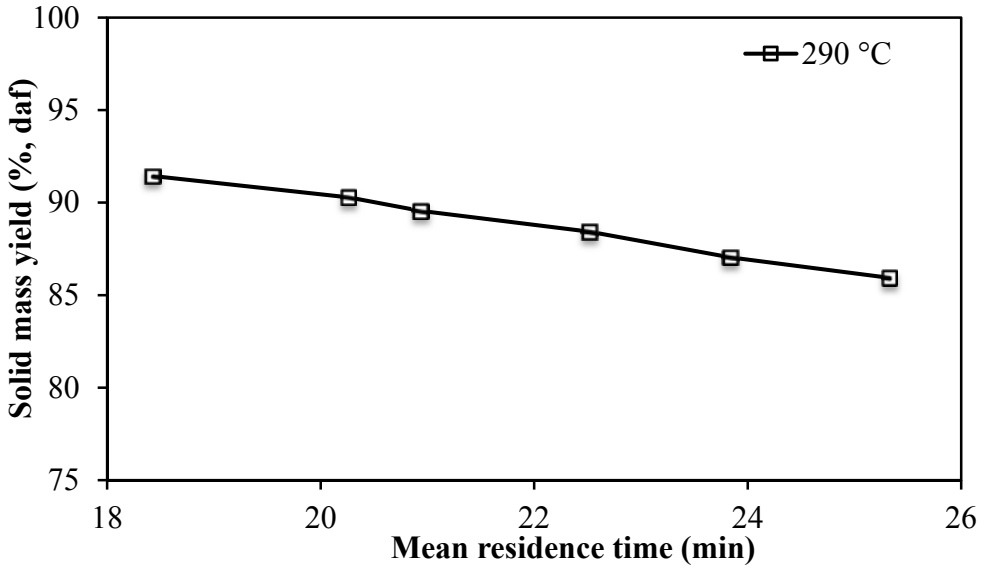

(a)

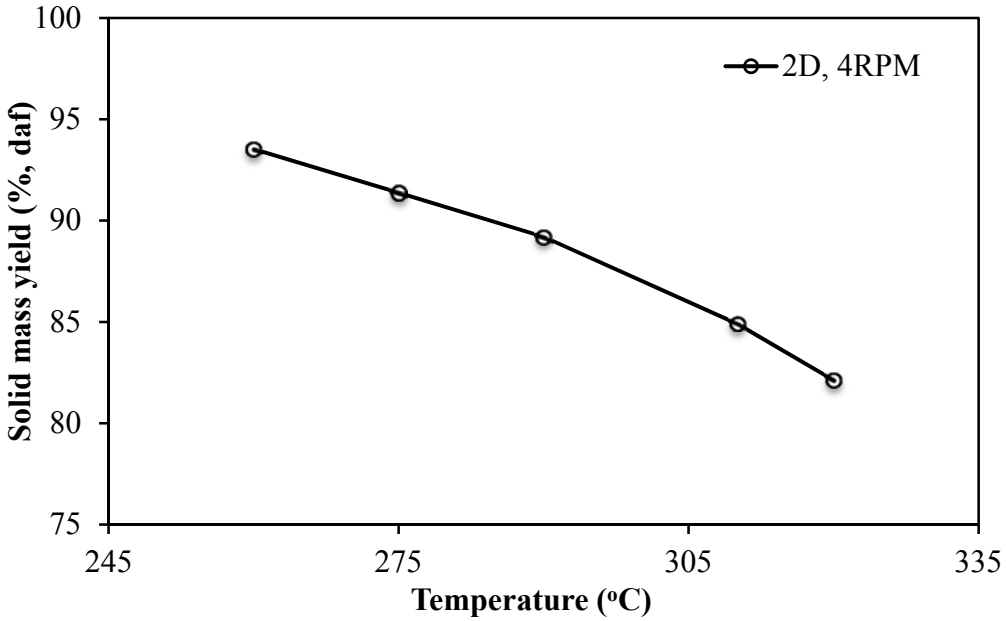

(b)

Figure 6.8: Variations in the solid mass yields: (a) Effect of mean residence time at 290°C; and (b) Effect of temperature at 4RPM and 2°

Energy yield measures the combined effect of the solid mass yield and the HHV of the solid products of torrefaction. As discussed before, the deoxygenation of biomass after a torrefaction process reduces the O-H and O-C based compounds and increases the C-C based compounds, improving the energy content of the torrefied biomass. As the losses in mass and the gain in the HHV have a good relation with the operating conditions, their selection can be trade off, accordingly, to achieve a reasonable level of energy yield. Without the energy yield, which is a qualitative measure of the torrefaction process, it would be difficult to have a techno-economic evaluation of the technology. Energy yield is thus seen as a primary parameter of interest.

Table 6.3 provides the energy yield (% daf) obtained under different operating conditions studied in the present study. Energy yields were observed in the range 93.9-98.5%. Though the gain in the HHV has a strong direct relation with the mass losses (R^2=0.93), as shown in Figure 6.9, the increase in the mass losses does not always raise the energy yield. As a high mass loss could be prone to loosing more carbon, such high mass loss may increase the energy loss (Shang et al., 2012) and reduce the energy yield.

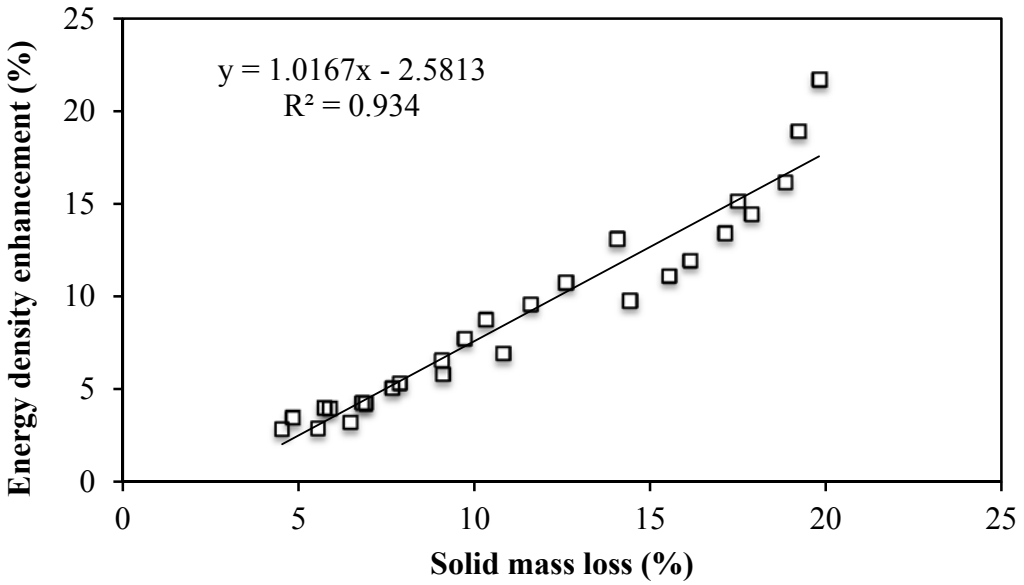

Figure 6.9: Relationship between solid mass loss and energy density enhancement

6.3.6 Bulk Densities and Volumetric Energy Densities

Table 6.4 presents the bulk densities and the volumetric energy densities of the torrefied biomass obtained under different operating conditions. A torrefaction process, which releases light volatile gases leaving the solid product more porous, decreases the bulk density of solid. For instance, the bulk density of the torrefied biomass produced at angular speed 4 RPM and inclination 1° was reduced to 3.6%, 5.9%, and 10.6% when the torrefaction process was conducted at 260°C, 290°C, and 320°C, respectively. The effect of the torrefaction temperature on the bulk density is shown in Figure 6.10.

On the other hand, the volumetric energy density of biomass increases significantly after the torrefaction process. The volumetric energy densities of the torrefied biomass and their percentage increase compared to raw biomass under various operating conditions are also presented in Table 6.4. The increase in volumetric energy density was found in the range 0.8-8.9%. Increased volumetric density not only reduces the transportation cost of biomass per unit energy transfer, but also makes possible to be used in the existing facility of co-firing plants with the least or no modifications. The effect of the torrefaction temperature on the percentage increase in the volumetric energy density is also illustrated in Figure 6.10. It shows that the increase in the volumetric energy density is not significant at low torrefaction temperature, but rises sharply at high torrefaction temperature, at which the gain in the HHV and the reduction in the bulk densities were higher.

Table 6.4: Bulk densities (BD, kg/m^3) and volumetric energy densities (VEN, MJ/m^3) of the torrefied biomass at different operating conditions

Temperature (°C)	Inclination (Degree)	1.0			1.5			2.0		
	Angular speed (RPM)	4.0	4.5	5.0	4.0	4.5	5.0	4.0	4.5	5.0
260	BD	233.56	235.10	236.09	234.54	236.24	237.52	236.54	239.06	240.94
	VEN	4685.65	4679.81	4689.01	4669.92	4690.60	4693.91	4663.88	4698.25	4734.00
	% Decrease in BD	3.61	2.98	2.57	3.21	2.51	1.98	2.38	1.34	0.56
	% Increase in VEN	1.36	1.24	1.43	1.02	1.47	1.54	0.89	1.63	2.41
290	BD	228.04	230.01	231.22	229.06	231.05	232.46	230.01	231.97	233.48
	VEN	4941.15	4827.85	4772.11	4861.24	4813.69	4746.57	4712.57	4703.88	4709.05
	% Decrease in BD	5.89	5.08	4.58	5.47	4.65	4.07	5.08	4.27	3.64
	% Increase in VEN	6.89	4.44	3.23	5.16	4.13	2.68	1.94	1.76	1.87
320	BD	216.70	219.90	221.20	221.35	224.59	225.71	226.37	227.90	228.64
	VEN	5085.71	4924.62	4837.07	5075.67	4985.60	4835.70	4994.05	4918.91	4840.30
	% Decrease in BD	10.57	9.25	8.71	8.65	7.31	6.85	6.58	5.95	5.64
	% Increase in VEN	10.02	6.53	4.64	9.80	7.85	4.61	8.03	6.41	4.71

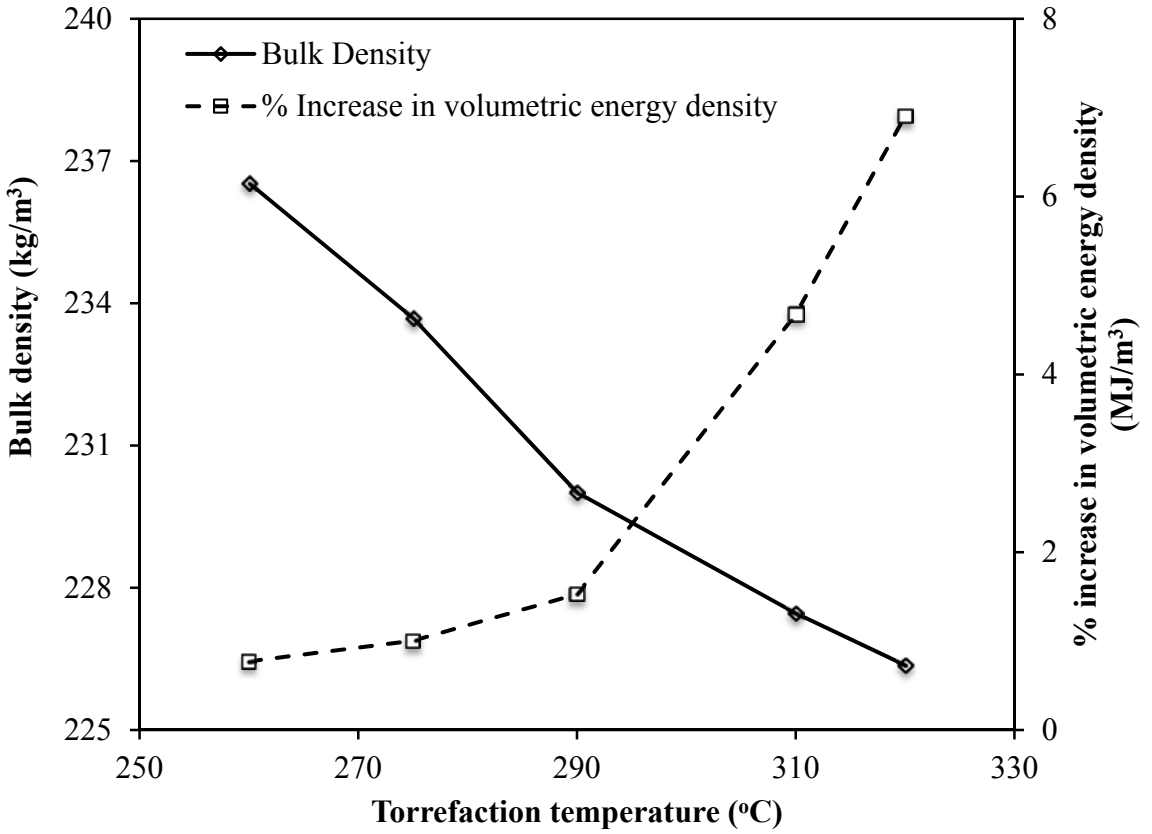

Figure 6.10: Effect of torrefaction temperature on bulk density and volumetric energy density of torrefied biomass (at angular speed 4 RPM and inclination 2°)

6.3.7 Torrefaction under Nitrogen Medium in Rotary and Fixed Bed Reactors

The continuous solid mixing characteristic is the main motivation of using a rotary reactor over a fixed bed reactor. Lack of solid mixing in the fixed bed reactors not only causes the formation of such hot heat spots, causing a spontaneous combustion of particles, but also produces non-uniform solid products. The possibility of such spontaneous combustion in the fixed bed reactor if a sophisticated control system is not installed may cause operational difficulties. In addition to this, the rotary reactors, as it operates with the limited solid load, can also use volatile gases as a torrefying medium.

In this section, results of some additional tests, which were conducted in the rotary reactor and the fixed bed reactor (the Muffle furnace) in a nitrogen medium keeping same mean residence time, are discussed.

Two different observations were observed from the experimental results. At the low torrefaction temperature (260°C), the solid mass yields were observed more than 90% in both fixed and rotating reactors, but the color of the torrefied biomass is not uniform in the fixed bed reactor, which may be due to the poor solid mixing. But, at high torrefaction temperature (320°C), the solid mass yields were found in the range 56.5-62.9% in the fixed bed reactor and the range 77.2-84.7% in the rotary reactor. The torrefied biomass products produced at such high torrefaction temperature in the fixed bed reactor were more like a char. Some of the analyzed properties of the torrefied solid are listed in Table 6.5.

Table 6.5: Comparison of the characteristics of solid product obtained from rotary and fixed bed reactor in nitrogen medium

Temperature (°C)	Reactor	Fixed bed reactor					Rotary reactor				
	Mean residence time (Minutes)	29	25	23	20	18	29	25	23	20	18
260	VM (%, daf)	87.20	87.41	87.94	88.42	88.48	86.48	87.07	87.75	87.98	88.13
	FC (%, daf)	12.80	12.59	12.06	11.58	11.52	13.52	12.93	12.25	12.02	11.87
	HHV (MJ/kg, daf)	19.61	19.49	19.47	19.44	19.41	20.11	19.84	19.64	19.45	19.37
	MY (%, daf)	91.03	92.85	94.48	95.32	96.89	90.28	92.63	94.11	94.92	95.66
	EDE (%, daf)	2.82	2.16	2.07	1.90	1.72	5.41	4.01	2.97	1.95	1.51
	EY (%, daf)	93.59	94.86	96.44	97.13	98.56	95.17	96.34	96.90	96.77	97.11
320	VM (%, daf)	53.00	55.51	57.17	59.51	61.89	75.63	77.28	79.07	80.24	81.44
	FC (%, daf)	47.00	44.49	42.83	40.49	38.11	24.37	22.72	20.93	19.76	18.56
	HHV (MJ/kg, daf)	25.54	25.34	24.87	24.42	24.22	23.56	22.75	22.02	21.29	20.83
	MY (%, daf)	56.54	58.05	60.93	61.65	62.99	77.24	79.76	82.82	83.86	84.70
	EDE (%, daf)	33.86	32.80	30.36	28.00	26.95	23.51	19.27	15.43	11.62	9.20
	EY (%, daf)	75.69	77.09	79.43	78.91	79.97	95.40	95.13	95.60	93.61	92.50

Note: Mean residence time was estimated at inclination 1° and varying angular speed from 3.5 to 5.5 RPM

One of the observed benefits of the rotary reactor over the fixed bed reactor at low temperature torrefaction was the uniformity in the solid product. However, the

significant reduction in the solid mass yield at the high torrefaction temperature lessens the energy yield in the fixed bed reactor (75.7-80%) compared to that in the rotary reactor (92.5-95.6%). This concludes that the rotary reactor has a good control over the torrefaction at high temperature compared to the fixed reactor, and maintains a reasonable level of energy recovery.

Tables 6.2, 6.3, and 6.5 can also be used to compare different parameters of torrefaction in nitrogen and volatile gases media. The solid mass yields, the gain in the HHV, and the energy yields obtained at similar operating conditions were observed to be similar in both working media. For instance, the solid mass yields at 260°C, 4 RPM, and 1° in nitrogen and volatile gases medium were found to be 92.6% and 92.3%, respectively. Similar results, such as the solid mass yield of 79.8% in nitrogen and 80.2% in volatile gases medium, were also found at 320°C. Therefore, it can be concluded that the nitrogen supply can be substituted by the volatiles gases based torrefaction with the negligible effects on the solid products.

6.3.8 Process Energy Flows and System Efficiencies

As shown in the Figure 6.1, the overall torrefaction process can be divided into two phases: (a) drying and (b) devolatilization. The overall torrefaction process thus requires thermal power for the drying and heating in the first phase (Dryer) and for the post-drying heating and heat of devolatilization reactions in the second phase (Torrefier). Figure 6.11 shows a typical schematic process layout and power flow in and out for the torrefaction process at 260°C, 4 RPM, and 1°. It also shows the process powers available at different sections and the efficiencies of the overall torrefaction process. A detailed explanation on the methodology of the energy balance is provided in the Appendix C.

Table 6.6 presents the mass and energy flows at various sections of the two-stage torrefaction process conducted at different torrefaction temperatures. The dryer that was kept at the reactor temperature of 150°C produces a superheated steam at atmospheric

pressure and a dried biomass; and the torrefier produces volatile gases and the torrefied biomass. The power required for the drying process and the heat of devolatilization process are two main heat loads of the overall torrefaction process.

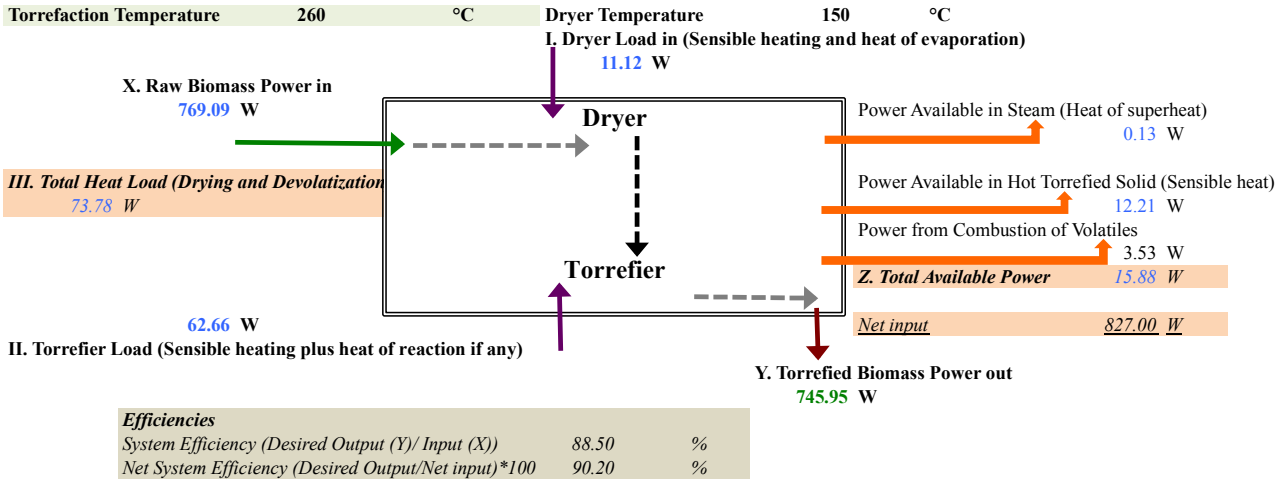

Figure 6.11: Schematic process layout showing power flows at torrefaction temperature 260°C

The drying heat load depends mainly on the initial moisture contents of the raw biomass whereas the devolatilization heat load depends on the type of reactions. Different studies have reported a wide range of data on the heat of reaction of the torrefaction process with a high degree of variation. For instance, Bates and Ghoniem (2013) have reported a range of heat of reaction from 300 kJ/kg endothermic to -200 kJ/kg exothermic at 200°C and from -50 kJ/kg exothermic to -550 kJ/kg exothermic at 300°C. While Peduzzi et al. (2014) have estimated the heat of torrefaction of -170 kJ/kg for the woody biomass torrefied at 250°C, Ohliger et al. (2013) have found in the range from -150 to 150 kJ/kg for beech wood. Van der Stelt (2011) has also reported a further wider range of the heat of reaction from 1500 to -1200 kJ/kg. Thus, in the present study, an extreme endothermic heat of reaction (1500 kJ/kg) was used to determine the lowest efficiency of the torrefaction process. The sensitivity analysis, however, shows that the system efficiency increases to more than 94% when the heat of reaction reduces to 0 kJ/kg, keeping all the other parameters same. The heating value of the combustible volatile gases, though, depends on the gas composition of volatiles; this study has adopted the heating values of

1184 kJ/kg reported in Van der Stelt (2011). In addition to this, the overall energy balance also includes the sensible heat in the torrefied biomass and the amount of superheat available in the steam released from the dryer. Considering the overall energy flows diagram, we have defined two efficiencies (a) system efficiency (η_s), and (b) net system efficiency (η_n) as:

$$\eta_s = \frac{HHV_{td}\,\dot{m}_{td}}{HHV_{rd}\,\dot{m}_{rd} + THL} \times 100\% \tag{6.4}$$

$$\eta_n = \frac{HHV_{td}\,\dot{m}_{td}}{HHV_{rd}\,\dot{m}_{rd} + THL - TAP} \times 100\% \tag{6.5}$$

Where, $\dot{m}_{rd}$ is the raw biomass mass flow rate in dry basis at the dryer inlet, $\dot{m}_{td}$ is the torrefied biomass flow rate at the torrefier exit, HHV_{td} and HHV_{rd} are the higher heating values of the torrefied and raw biomass in dry basis, THL is the total heat loads, which is the sum of the devolatilization and drying heat loads, and TAP is the total available process heats, which is sum of the heat available in the superheated steam, the heat of combustion of the volatile gases, and the sensible heat of the hot torrefied solid. The system efficiency was found to be around 88.5% at 260°C and increased to 89.5% at 320°C. The net system efficiency depending upon the torrefaction temperature also increased from 90.2 to 92.0%. The overall process energy recovery was found to be around 90%, which is as good as the cold gas efficiency of biomass gasification. Therefore, the biomass torrefaction process could be as good as any other intermediate biomass thermochemical conversion technologies, such as a biomass gasification process.

Table 6.6: Mass and energy flows at different sections of a two-stage torrefaction process

Temperature (°C)	260	290	320
Inlet (Raw biomass)			
Moisture content (%)		4.50	
Solid feed rate (g/min)		2.54	
HHV (MJ/kg, dry)		19.02	
Feed rate g/min (dry)		2.43	
Feed inlet temperature (°C)		25.00	
Specific heat capacity dry wood (kJ/kgK)		1.46	
Specific heat capacity water (kJ/kgK)		4.19	
Enthalpy of moisture at inlet (kJ/kg)		104.88	
P. Heat of combustion solid in (W)		769.09	
Dryer			
Reactor wall temperature (°C)		150	
Fluid temperature (°C)		135	
Average solid exit temperature (°C)		130	
Moisture in solid at dryer exit (%)		0.10	
Solid feed rate at dryer exit (g/min)		2.43	
Water vapour (g/min)		0.11	
Enthalpy of steam at dryer (kJ/kg)		2746.21	
A. Drying Load			
A1. Sensible heat of biomass (W)	6.19	6.19	6.19
A2. Heat of evaporation	4.92	4.92	4.92
B. Available process heat from the dryer			
B.1 Sensible heat in steam (heat of superheat only) (W)	0.13	0.13	0.13
Torrefier			
Reactor wall temperature (°C)	260	290	320
Fluid temperature (°C)	245	275	305
Average solid exit temperature (°C)	240	270	300
Heat of torrefaction (kJ/kg, dry)	1500	1500	1500
Solid mass yield (%, dry)	92.62	86.58	81.27
Torrefied product rate (g/min, dry)	2.25	2.10	1.97
Energy yield (%, dry)	96.99	97.21	97.62
HHV of torrefied biomass (MJ/kg, dry)	19.92	21.36	22.85
Volatiles (g/min)	0.18	0.33	0.45
Specific heat capacity of char (kJ/kgK)	1.57	1.59	1.60
Specific heat capacity of torrefied biomass (kJ/kgK)	1.52	1.52	1.53
Heating value of volatiles (MJ/kg)	1.18	1.18	1.18
Q. Heat of combustion of torrefied product (W)	745.95	747.60	750.82
C. Torrefier load			
C1. Sensible heat of biomass (W)	6.50	8.04	9.52
C2. Heat of torrefaction (W)	56.17	52.51	49.29
D. Available process heat from torrefier			
D1. Heat of combustion of volatiles (W)	3.53	6.42	8.96
D2. Heat of cooling torrefied product (W)	12.21	13.06	13.80
E. Total Heat Load (W) (E=A+C), W	73.78	71.66	69.92
F. Total Available Power (F=D+B), W	15.88	19.61	22.90
System efficiency (%) (Q/(P+E)*100%	88.5	88.9	89.5
Net System efficiency (%), (Q)/(P+E-F)*100%	90.2	91.04	92.0

6.4. SUB-CONCLUSIONS

Torrefaction of poplar in a continuous two-stage indirectly heated rotary torrefier is investigated. Different operating parameters are varied to analyze the effect of operating parameters on the torrefied biomass. Results showed that the torrefaction temperature has a more significant effect compared to the angular speed and the inclination. Both quantitative and qualitative assessment was established conducting the proximate analysis, the ultimate analysis, the higher heating values, the solid mass yield, the bulk density, the volumetric energy density, the energy density enhancement, and the energy yields. Increased torrefaction temperature increases carbon content, mass loss, and energy density enhancement, whereas the angular speed and inclination shows an opposite trend. The elemental carbon content and the fixed carbon content in the torrefied biomass were found up to 53.5% (daf) and 23.6% (daf) compared to 46.0% (daf) and 11.4% (daf) in the raw poplar, respectively. The least solid mass yield of 80.2% (daf) was observed at 320°C, 4 RPM, and 1°. Plausibly, the energy density enhancement was observed up to 21.7% with a solid mass loss of 19.8% (daf). The volumetric energy density of the torrefied biomass was increased up to 8.9% as compared to the raw biomass. Although it produces similar torrefied solid products as in the fixed bed reactor at the low torrefaction temperature, the rotary reactor has a greater operational control over the fixed bed reactor at the high torrefaction temperature. The overall process energy balance shows that the system efficiency is found to be above 88%. Results of different characteristics of the torrefied biomass and process parameters indicate that the torrefaction process in a volatile gases medium could also substitute the nitrogen gas.

CHAPTER 7: CONCLUSIONS AND RECOMMENDATIONS

This chapter summarizes the overall conclusions of different chapters of this thesis and provides recommendations for future works. Conclusions of individual chapters are also presented in the respective chapters.

7.1. CONCLUSIONS

This study investigated into two innovative means of torrefaction of biomass: (i) batch torrefaction in mildly pressurized reactor (PBR); and (ii) continuous torrefaction in two-stage indirectly heated inclined rotary reactor with flights (TIR). Torrefaction in PBR using air medium is a viable option for production of torrefied products with comparable product qualities without nitrogen medium. TIR also produces torrefied products in volatile gas medium with superior mass and energy yields to that by the conventional fixed bed reactor with good energy efficiency; it provides an option for the use of released volatiles for heating or for chemical extractions. Therefore, this study concludes that above two methods of torrefaction can obviate the need of expensive nitrogen supply as in other conventional methods without a significant degradation of product quality and produce more uniform torrefied products.

More specific outcomes of the studies are presented below:

I. Mildly pressurized (200-600 kPa) batch reactor provides an option for torrefying biomass at lower pressure without going into the expensive means needed for high-pressure hydrothermal torrefaction.

1. Torrefaction temperature exerts a greater influence on the solid product than that exerted by other operating parameters like reactor pressure and residence time.
2. The mass yield in this system without nitrogen is much higher (~49%) than that in conventional air torrefaction at atmospheric pressure (~26.1% at 300ºC, 35

minutes), but no further improvement was noted when the pressure was increased in the range of 200-600 kPa.

3. Energy density enhancement factor is higher in a mildly pressurized air reactor than that in nitrogen fed atmospheric pressure reactor.
4. The energy and mass yield is higher in nitrogen compared to that in air medium, but this difference is very small at low temperature (220ºC).
5. Fuel ratio and energy density enhancement can be predicted using mass loss in the pressurized torrefier.

II. Two-stage continuous indirectly heated inclined rotary (TIR) torrefier allowed separation of drying from the torrefaction stage and thereby allowing better utilization of the undiluted volatile for the provision of process heat or chemical extractions.

1. Mean residence time in a rotary reactor operated at a constant feed rate decreases with increase in angular speed, inclination and diameter of the reactor. For example, residence time of solid was 5.8 minutes at 8 RPM and 3º inclination, and 27.5 minutes at 4 RPM at 1º inclination in the dryer (dia. 64 mm and 610 mm long), whereas they were 4.7 and 21.4 minutes respectively in the torrefier (dia. 100 mm, 762 mm long) at respective operating conditions.
2. Solid filling factor decreases with increase in angular speed, inclination and diameter of the reactor. For example, it was 3.0 % at 8 RPM and 3º and 14.3 % at 4 RPM and 1º was found in the dryer, whereas they were 0.8 % and 3.6 % in the torrefier at the corresponding angular speed and inclination.
3. A cascaded model is developed considering the motion of a particle in a cycle, but the model overestimates the mean residence time because the model does not account for the axial movement of particles due to potential particle-particle interaction and their sliding motions. Semi-empirical expressions are proposed for mean residence time and filling factor introducing an average value of dimensionless correction factor. These expressions showed good agreement with the full range of experimental data.

4. A mechanistic model of heat transfers in indirectly heated rotary reactors is developed by combining the wall-to-solid and wall-to-gas heat transfer coefficients. The proposed model was validated conducting experiments in the TIR reactor.
5. Cluster renewal approach of fluidized bed was used to derive an expression of the effective wall to solid heat transfer coefficient for reactor with flights. The model was validated against published experimental data. This model has better accuracy of prediction than shown by other existing models.
6. An expression is developed for the average solid coverage fraction for a range of solid filling factor 0.44-9.80 % in a rotary reactor. It has major influence on the heat transfer to solids.
7. As the particle size used for the experimental verification is large, the thermal resistance due to the fluid film showed a dominant effect on the overall heat transfer coefficient. A small increase in the overall heat transfer coefficient was also found with the rise in the reactor temperature. However, the overall heat transfer coefficient in the reactor decreases with increase in angular speed, inclination, and diameter of the reactor.
8. Poplar wood successfully torrefied in the TIR torrefier under volatile gas medium. Torrefaction temperature showed significantly higher effect on the solid products of the torrefaction compared to that shown by angular speed and inclination of the reactor.
9. Increase in torrefaction temperature increases the carbon content of solid product, solid mass loss, and energy density enhancement.
10. Beside temperature and residence time, the inclination and angular rotation of the reactor also affect the product qualities.
11. Measured characteristics of the torrefied biomass and process parameters indicate that the torrefaction in volatiles medium in the TIR could substitute the expensive nitrogen gas for provision of an inert ambient.
12. Additional experiments conducted in a fixed bed reactor showed that the mass and energy yields were similar between rotary and fixed bed reactors at low

temperature, but they were higher in rotary reactors at higher temperature torrefaction under the identical conditions.

13. The process energy balance of the TIR torrefier shows the system efficiency is above 88%. This indicates that biomass torrefaction can be as energy efficient as the biomass gasification.

7.2. RECOMMENDATIONS FOR FUTURE STUDY

This study presents two different means and some parametric studies of torrefaction. However, this study has some limitations, which could be investigated further to help better understand the overall processes. Following section presents a list of recommended future works:

1. Layers of condensed volatiles were observed on the solid product of torrefaction in the PBR when the residence time is longer. A detailed study on the surface morphology of solid products under different pressures is recommended to examine the effect of such condensation on the HHV.
2. Condensation of heavy volatiles produced from the PBR may reduce the porosity of the torrefied biomass, affecting its reactivity. Therefore, effect of reactor pressure on the reactivity of torrefied biomass produced from the PBR can be established in future.
3. The present model for estimating the overall heat transfer coefficients can be verified with data for different materials to widen the validity of model.
4. This study uncovered the potential of improving system efficiency by resuing heat from volatiles and sensible heat of torrefied solids. Thus, the current reactor could be either scaled up or modified by adding a heat exchanger and a volatile burner.
5. An overall performance predictive model needs to be developed using the heat transfer and kinematic models developed in the present work.

REFERENCES

Abbasi, T. and Abbasi, S.A. (2007), "Dust Explosions–Cases, Causes, Consequences, and Control," *Journal of Hazardous Materials*, 140 (1-2), 7-44.

Acharjee, T. C., Coronella, C. J. and Vasquez, V. R. (2011), "Effect of thermal pretreatment on equilibrium moisture content of lignocellulosic biomass," *Bioresource Technology*, 102(7), 4849-4854.

Acharya, B. (2013), Torrefaction and pelletization of different forms of biomass, M.Sc Thesis, School of Engineering, University of Guelph, Ontario, Canada, 2013.

Acharya, B., Sule, I. and Dutta, A. (2012), "A review on advances of torrefaction technologies for biomass processing," *Biomass Conversion and Refinery*, 2, 349-369.

Agar, D. and Wihersaari, M. (2012), "Torrefaction technology for solid fuel production," *Opinion, Global Change Biology Bioenergy*, 4, 475-478.

Agbor, E., Zhang, X. and Kumar, A. (2014), "A review of biomass co-firing in North America," *Renewable and Sustainable Energy Reviews*, 40, 930-943.

Agbor, V. B., Cicek, N., Sparling, R., Berlin, A. and Levin, D. B. (2011), "Biomass pretreatment: Fundamentals toward application," *Biotechnology Advances,* 29, 675-685.

Akin, D. E., Rigsby, L. L., Sethuraman, A., Morrison, W. H., Gamble, G. R. and Eriksson, K. E. (1995), "Alterations in structure, chemistry, and biodegradability of grass lignocellulose treated with the white rot fungi Ceriporiopsis subvermispora and Cyathus sterocoreus," *Applied and Environmental Microbiology*, 61(4), 1591-1598.

Almeida, G., Brito, J. O. and Perre, P. (2010), "Alterations in energy properties of eucalyptus wood and bark subjected to torrefaction: The potential of mass loss as a synthetic indicator," *Bioresource Technology*, 101, 9778-9784.

Alvarez, P. I. and Shene, C. (1994), "Experimental study of residence time in a direct rotary dryer," *Drying Technology*, 12, 1629-1651.

Andrej, B., Basu, P. and Amyotte, P. (2013), "An exploratory study of explosion potential of dust from torrefied biomass," Not published.

Aravindhakshan, S. C., Epplin, E. M. and Taliaferro, C. M. (2010), "Economics of switchgrass and miscanthus relative to coal as a feedstock for generating electricity," *Biomass and Bioenergy*, 34, 1375-1383.

Arias, B., Pevida, C., Fermoso, J., Plaza, M. G., Rubiera, F. and Pis, J. J. (2008), "Influence of torrefaction on the grindability and reactivity of woody biomass," *Fuel Processing Technology,* 89, 169-175.

ASTM (2013), "Standard test method for bulk density of densified particulate biomass fuels," American Society for Testing and Materials, 2013. Retrieved online at http://www.astm.org/Standards/E873.htm, 15 January 2015.

ASTM (2013), "Standard test method for chemical analysis of wood charcoal," The American Society for Testing and Materials, D1762-84 (Reapproved 2013), Retrieved online at http://enterprise1.astm.org/DOWNLOAD/D1762.000132808-1.pdf, 16 September 2014.

ASTM. (2007), "The American Society for Testing and Materials, D1762-84 (Reapproved 2007), 2007. Retrieved at http://enterprise1.astm.org/DOWNLOAD/D1762.000132808-1.pdf, 15 November 2012

Aydemir, D., Gunduz, G. and Ozden, S. (2010), "The influence of thermal treatment on color response of wood materials," *Color Research and Application*, Wiley Periodicals Inc., 148-153. Retrieved at http://onlinelibrary.wiley.com/store/10.1002/col.20655/asset/20655_ftp.pdf?v=1andt=hg2vaya4ands=4dc95dab957f27b7a1c4b72b31533dd9ced61a3f, 29 April 2013.

Bach, Q., Tran, K., Khalil, R. A., Skreiberg, O. and Seisenbaeva, G. (2013), "Comparative assessment of wet torrefaction," *Energy and Fuels*, 27(11), 6743-6753.

Basu, P. (1990), "Heat transfer in fast fluidized combustors", *Chemical Engineering Science,* 45 (10), 3123-3136.

Basu, P. (2010), Biomass gasification and pyrolysis: Practical Design and Theory, ISBN 978-0-12-37488-8, Elsevier Inc., Burlington, 2010.

Basu, P. (2013), Biomass gasification, pyrolysis and Torrefaction: Practical Design and Theory, ISBN 978-0-12-396488-5, Academic Press, London, 2013.

Basu, P. and Fraser, S. A. (1991), "Circulating Fluidized Bed Boilers: Design and Operations," Butterworth-Heinemann, Reed Publishing Inc., USA, 1991.

Basu, P. and Kaushal, P. (2009), "Modeling of pyrolysis and gasification of biomass in fluidized beds: A review," *Chemical Product and Process Modeling,* 4(1), 1934-2659. Article 21. DOI: 10.2202/1934-2659.1338

Basu, P., Butler, J. and Leon, M. A. (2011), "Biomass co-firing options on the emission reduction and electricity generation costs in coal-fired power plants," *Renewable Energy*, 36, 282-288.

Basu, P., Dhungana, A., Rao, S. and Acharya, B. (2013), "Effect of oxygen presence in torrefier," *Journal of the Energy Institute*, 86(3), 171-176.

Basu, P., Rao, S. and Dhungana, A. (2013a), "An investigation into the effect of biomass particle size on its torrefaction," *The Canadian Journal of Chemical Engineering,* 91(3), 466-474.

Bates, R. B. and Ghoniem, A. F. (2012), "Biomass torrefaction: Modeling of volatile and solid product evolution kinetics," *Bioresource Technology*, 124, 460-469.

Bates, R. B. and Ghoniem, A. F. (2013), "Biomass torrefaction: Modeling of reaction thermochemistry," *Bioresource Technology*, 134, 331-340.

Batidzirai, B., Mignot, A. P. R., Schakel, W. B., Junginger, H. M. and Faaij, A. P. C. (2013), "Biomass torrefaction technology: Techno-economic status and future prospects," *Energy*, 62, 196-214.

BCBN (2014), "British Columbia Bioenergy Network," Retrieved online at http://www.marketwired.com/press-release/bc-based-diacarbon-energy-incs-pilot-torrefaction-project-be-supported-bc-bioenergy-1893670.htm, 17 November 2014.

Belosevic, S. (2010), "Modeling approaches to predict biomass co-firing with pulverized coal," *The Open Thermodynamics Journal,* 4, 50-70.

Ben, H. and Ragauskas, A. J. (2012), "Torrefaction of loblolly pine," *Green Chemistry,* 14, 72-76.

Benjamin, W. (1997), "Biomass development and waste wood co-firing," *Energy Conversion Management*, 38, S545-S549.

Bensmann, S. Subagyo, A. and Walzel, P. (2010), "Residence time distribution of segregating sand particles in a rotary drum," *Particulate Science and Technology: An International Journal*, 28, 319-331.

Bergman, P. C. A. (2005), "Combined torrefaction and pelletization the TOP Process," Energy Research Center of the Netherlands, Netherland, 2005, Report ECN-C-05-073.

Bergman, P. C. A. and Kiel, J. H. A. (2005), "Torrefaction for biomass upgrading," Conference Proceedings of 14th European Biomass Conference and Exhibition, Paris, France, 17-21 October, (2005), Energy Research Center of the Netherlands (ECN), Netherland. Retrieved at http://www.ecn.nl/docs/library/report/2005/rx05180.pdf, 30 April 2013.

Bergman, P. C. A., Boersma, A. R., Kiel, J. H. A., Prins, M. J., Ptasinski, K. J. and Janseen, F. J. J. G. (2005), "Torrefaction for entrained-flow gasification of biomass," A research carried out in collaboration between the Technical University of Eindhoven and the Energy Research Center of the Netherlands (ECN), Petten, Netherlands.

Bergman, P. C. A., Boersma, A. R., Kiel, J. H. A., Prins, M. J., Ptasinski, K. J. and Janseen, F. J. J. G. (2005a), "Torrefaction for biomass co-firing in existing coal-fired power stations-Biocoal," A research carried out in collaboration between the DEN Programs of SenterNovem, and the Energy Research Center of the Netherlands (ECN), Petten, Netherlands.

Bi, T. (2012), "Torrefaction and densification of biomass," Presentation, Biomass and Bioenergy Research Group, Clean Energy Research Center, University of British Columbia, 20 March 2012.

Boateng, A. A. (1993), "Rotary kiln transport phenomena: Study of the bed motion and heat transfer," Doctoral Thesis, University of British Columbia, British Columbia, Canada, 1993.

Bourgois, J. and Guyonnet, R. (1988), "Characterization and analysis of torrefied wood," *Wood Science Technology*, 22(2), 143-155.

Bourgois, P. J., Janin, G. and Guyonment, R. (1991), "The color measurement: A fast method to study and to optimize the chemical transformations undergone in the thermally treated wood," *Holzforschung,* 45 377-382. In: Sundqvist, B. (2004), Color changes and acid formation in wood during heating, Doctoral Thesis, Division of Wood and Material Science, Lulea University of Technology. Retrieved at http://epubl.luth.se/1402-1544/2004/10/LTU-DT-0410-SE.pdf, 29 April 2013.

Brebu, M. and Vasile, C. (2009), "Thermal degradation of lignin-A review," *Cellulose Chemistry and Technology*, 44 (9), 353-363.

Bridgeman, T. G., Jones, J. M., Shield, I. and Williams, P. T. (2008), "Torrefaction of reed canary grass, wheat straw and willow to enhance solid fuel qualities and combustion properties," *Fuel*, 87, 844-856.

Bridgeman, T. G., Jones, J. M., Williams, A. and Waldron, D. J. (2010), "An investigation of the grindability of the torrefied of energy crops," *Fuel*, 89, 3911-3918.

Buranov, A. U. and Mazza, G. (2008), "Lignin in straw of herbaceous crops," *Industrial Crops and Products*, 28, 237-259.

Cannales, E. R., Borquez, R. M. and Melo, D. L. (2001), "Steady state modeling and simulation of an indirect rotary dryer," *Food Control,* 12, 77-83.

Carrasco, J. C., Oporto, G. S., Zondlo, J. and Wang J. (2014), "Observed kinetics parameters during the torrefaction of red oak (Quercus rubra) in a pilot rotary kiln reactor," *Bioresources,* 9(3), 5417-5437.

Carter, C. L. (2012), Physicochemical properties and thermal decomposition of torrefied woody biomass and energy crops, Master Thesis, University of Auburn, USA, 2012.

Casaca, C. and Costa, C. (2003), "Co-combustion of biomass in a natural gas-fired furnace," *Combustion and Science and Technology*, 175(11), 1953-1977.

Cashdollar, K. L. (2000), "Overview of dust explosibility characteristics," *Journal of Loss Prevention in the Process Industries*, 13, 183-199.

Cashdollar, K. L. and Hertzberg, M. (1987), "Industrial Dust Explosions," *ASTM,* 1987.

Cashdollar, K.L. (1996), "Coal Dust Explosibility," *Journal of Loss Prevention in the Process Industries*, 9(1), 65-76.

CCPC (2011), "Biomass Co-firing," A Final Phase III Report, Canadian Clean Power Coalition, Technical Committee, November 2011, Appendix C. Retrieved online at http://www.canadiancleanpowercoalition.com/files/7813/2621/8340/Appendix%20C.pdf , 12 November 2014.

CG (2011), "Financing New Coal-Fired Power Plants," The Climate Group, Guidance Note 2011. Retrieved online at http://www.theclimategroup.org/_assets/files/Guidance-for-Financing-New-CFPP-TCG-2011_1.pdf, 11 November 2014.

Chan, M. L., Jones, J. M., Pourkashanian, M., Williams, A. (1999), "The oxidative reactivity of coal chars in relation to their structure," *Fuel*, 78, 1539-1552.

Chaouch, M., Petrissans, M., Petrissans, A. and Gerardin P. (2010), "Use of wood elemental composition to predict heat treatment intensity and decay resistance different softwood and hardwood species," *Polymer Degradation and Stability,* 95 (12), 2255-2259.

Chaturvedi, V. and Verma, P. (2013), "An overview of key preatreatment processes employed for bioconversion of lignocellulosic biomass into biofuels and value added products," *Biotech*, 3(5), 415-431.

Chen, W. H. and Kuo, P. C. (2010), "A study on torrefaction of various biomass materials and its impact on lignocellulosic structure simulated by a thermogravimetry," *Energy*, 35, 2580-2586.

Chen, W. H. and Kuo, P. C. (2011), "Torrefaction and co-torrefaction characterization of hemicellulose, cellulose and lignin as well as torrefaction of some basic constituents in biomass," *Energy*, 36 803-811.

Chen, W. H., Du, S. W., Tsai, C. H. and Wang, Z. Y. (2012), "Torrefied biomasses in a drop tube furnace to evaluate their utility in blast furnaces," *Bioresource Technology,* 111, 433-438.

Chen, W. H., Hsu, H. C., Lu, K. M., Lee, W. J. and Lin, T. C. (2011), " Thermal pretreatment of wood (Lauan) block by torrefaction and its influence on the properties of the biomass," *Energy,* 36, 3012-3021.

Chen, W. H., Liu, S. H., Juang, T. T., Tsai, C. M. and Zhunag, Y. Q. (2015), "Charecterization of solid and liquid products from bamboo torrefaction," *Applied Energy*, 160, 829-835.

Chen, W. Z., Wang, C. H., Liu, T., Zuo, C. Y., Tian, Y. H., Gao, T. T. (2009), "Residence time and mass flow rate of particles in carbon rotary kilns," *Chemical Engineering and Processing: Process Intensification*, 48, 955-960.

Chen, Y., Yang, H., Yang, Q., Lao, H., Zhu, B. and Chen, H. (2014), "Torrefaction of agriculture straws and its application on biomass pyrolysis poly-generation," Bioresource Technology, 156, 70-77.

Chew, J. J. and Doshi, V. (2011), "Recent advances in biomass pretreatment – Torrefaction fundamentals and technology," *Renewable and Sustainable Energy Reviews*, 15, 4212-4222.

Chiueh, P. T., Lee, K. C., Syu, F. S. and Lo, S. L. (2012), "Implications of biomass pretreatment to cost and carbon emissions: Case study of rice straw and Pennisetum in Taiwan," *Bioresource Technology,* 108, 285-294.

Chouchene, A., Jeguirim, M., Khiari, B., Zagrouba, F. and Trouve, G. (2010), "Thermal degradation of olive solid waste: influence of particle size and oxygen concentration," *Resources, Conservation and Recycling*, 54, 271-277.

Clausen, L. R., Elmegaard, B. and Houbak, N. (2010), "Techno-economic analysis of a low CO_2 emission dimethyl ether (DME) plant based on gasification of torrefied biomass," *Energy,* 35, 4831-4842.

Colin, B., Dirion, J. L., Arlabosse, P. and Salvador, S. (2014), "Experimental study of wood chips torrefaction in a pilot scale rotary kiln," *Chemical Engineering* Transactions, 37, 505-509.

Coronella, C. J., Yan, W., Reza, M. T. and Vasquez, V. R. (2012), "Method for wet torrefaction of biomass," Patent Application Number 20120110896, Publication Date 2012-05-10.

Couhert, C., Salvador, S. and Commandre, J-M. (2009), "Impact of torrefaction on syngas production from wood," *Fuel*, 88 (11), 2286-2290.

Demirbas, A. (2008), "Biofuels sources, biofuel policy, biofuel economy and global biofuel projections," *Energy Conversion and Management,* 49, 2106-2116.

Deng, J., Wang, G., Kuang, J., Zhang, Y. and Luo, Y. (2009), "Pretreatment of agriculture residues for co-gasification via torrefaction," *Journal of Analytical and Applied Pyrolysis,* 86 (2), 331-337.

Descoins, N., Dirion J. L. and Howes, T. (2005), "Solid transport in a pyrolysis pilot scale rotary kiln: Preliminary results- stationary and dynamic results," *Chemical Engineering and Processing*, 44, 315-321.

Deutmeyer, M., Bradley, D., Hektor, B., Tumuluru, J. S., Hess, R., Nikolaisen, L. and Wild, M. (2012), "Possible effect of torrefaction on biomass trade," IEA Bioenergy, Task: 40 Sustainable International Bioenergy Trade. Retrieved at http://www.bioenergytrade.org/downloads/t40-torrefaction-2012.pdf, 13th May 2013.

Dhungana, A. (2011), "Biomass torrefaction," Master Thesis, Dalhousie University, Halifax, Canada, 2011.

Dhungana, A. Basu, P. and Dutta, A. (2012), "Effects of reactor design on the torrefaction of biomass," *Journal of Energy Resources Technology*, 134(4), 041801-1-041801-11.

Doelle, H. W. (2012), "Biomass and organic waste conversion to food, feed, fuel, fertilizer, energy and commodity products," Biotechnology X. Encyclopedia of Life Support Systems (EOLSS). Retrieved at http://www.eolss.net/Sample-Chapters/C17/E6-58-09-04.pdf, 28th April 2013.

Duan, L., Zhao, C., Zhou, W., Qu, C. and Chen, X. (2009), "Investigation on coal pyrolysis in CO_2 atmosphere," *Energy and Fuels*, 23, 3826-3830.

Duncan, A., Pollard, A. and Fellouah, H. (2013), "Torrefied, spherical biomass pellets through the use of experimental design," *Applied Energy*, 101, 237-243.

Dutta, A. (2013), University of Guelph, *Personal communication*, October 19, 2013.

ecoTech Energy Group (2010), Torrefaction Technology. Retrieved at http://www.ecotechenergygroup.com/index.php/alternative-energy, 7 July 2012.

ECPI (2012), Dust explosion and fire: Torrefied biomass Vs. non-torrefied biomass. Earth Care Products Incorporated. Retrieved at http://ecpisystems.com/documents/, 25 May 2013.

Emsley, A. M. and Stevens, G. C. (1994), "Review: Kinetics and mechanisms of the low-temperature degradation of cellulose," *Cellulose*, 1, 26-56.

Engineersedge (2014), "Thermal conductivity, heat transfer review, Metal Products Distributor Supplier: Engineering Metals and Materials, 2014," Retrieved online at http://www.engineersedge.com/properties_of_metals.htm, 8 October 2014.

Enting, I. G., Etheridge, D. M. and Fielding M. J. (2008), "A perturbation analysis of the climate benefit from geo-sequestration of carbon dioxide," *International Journal of Greenhouse Gas Control*, 29, 1383-92.

Erlach, B., Harder, B. and Tsatsaronis, G. (2012), "Combined hydrothermal carbonization and gasification of biomass with carbon capture," *Energy*, 45(1), 329-338.

Eseltine, D., Thanapal, S. S., Annamalai, K. and Ranjan, D. (2013), "Torrefaction of woody biomass (Juniper and Mesquite) using inert and non-inert gases," *Fuel*, 113, 379-388.

EUBIA (2007), Biomass characteristics. European Biomass Industry Association (EUBIA). Retrieved at http://www.eubia.org/115.0.html, 15 May 2012.

EUBIONET (2003), "Biomass co-firing: An efficient way to reduce greenhouse gas emissions," European Bioenergy Networks, VTT Processes, Finland. Retrieved online at http://ec.europa.eu/energy/renewables/studies/doc/bioenergy/2003_cofiring_eu_bionet.pdf, 15 November 2014.

Fang, M. X., She, D. K., Li, Y. X., Yu, C. J., Luo, Z. Y. and Cen, K. F. (2006), "Kinetic study on pyrolysis and combustion of wood under different oxygen concentrations by using TG-FTIR analysis," *Journal of Analytical and Applied Pyrolysis,* 77, 22-29.

Felfli, F. F., Luengo, C. A., Suarez, J. A. and Beaton, P. A. (2005), "Wood briquette torrefaction," *Energy for Sustainable Development*, 9 (3), 19-22.

FEMP (2004), "Biomass co-firing in coal-fired boilers," Federal Technology Alert, Federal Energy Management Program, Energy Efficiency and Renewable Energy, US Department of Energy. Retrieved online at http://www.nrel.gov/docs/fy04osti/33811.pdf, 16 November 2014.

Ferron, J. R. and Singh, D. K. (1991), "Rotary kiln transport processes," *AIChE Journal*, 37, 7147-758.

Fick, G., Mirgaux, O., Neau, P. and Patisson, F. (2012), "Using biomass for Pig Iron production: A technical environmental and economical assessment," *Waste Biomass Valorisation*, 5, 43-55. Springer, DOI 10.1007/s12649-013-9223-1.

Fisher, E. M., Dupont, C., Darvell, L. I., Commandre, J. M., Saddawi, A., Jones, J. M., Grateau, M., Nocquet, T. and Salvador, S. (2012), "Combustion and gasification characteristics of chars from raw and torrefied biomass," *Bioresource Technology,* 119, 157-165.

Foster, C. E., Martin, T. M. and Pauly, M. (2010), "Comprehensive compositional analysis of plant cell walls lignocellulosic biomass part II: Carbohydrates," *Journal of Visualized Experiments,* 37. Retrieved at http://paulylab.berkeley.edu/Publications/JoVE_Protocol_1837.pdf , 27 February 2013. DOI: 10.3791/1837.

Friedman, S. J. and Marshall, W. R. (1949), "Studies in rotary drying: Part I – Holdup and dusting.,"*Chemical Engineering Progress*, 45, 482-493.

Fullerton, D. G., Bruce, N. and Gordon, S. B. (2008), "Indoor air pollution from biomass fuel smoke is a major health concern in the developing world," *Transaction of the Royal Society of Tropical Medicine and Hygiene,* 102(9), 843-851.

Funke, A. and Zeigler, F. (2010), "Hydrothermal carbonization of biomass: A summary and discussion of chemical mechanisms for process engineering," *Biofuel, Bioproducts and Biorefining*, 4 (2), 160-177.

Gani, A., Morishita, K., Nishikawa, K. and Naruse, I. (2005), "Characteristics of co-combustion of low-rank coal with biomass," *Energy and Fuels*, 19, 1652-1659.

Ge, L., Zhang, Y., Wang, Z., Zhou, J., Cen, K. (2013), "Effects of microwave irradiation treatment on physicochemical characteristics of Chinese low-rank coals," *Energy Conversion and Management*, 71, 84-91.

Ghassemi, H. and Shahsavan-Markadeh, R. (2014), "Effects of various operational parameters on biomass gasification process; a modified equilibrium model," *Energy Conversion and Management,* 79, 18-24.

Gil, M. V., Garcia, R., Pevida, C. and Rubera, F. (2015), "Grindability and combustion behavior of coal and torrefied biomass blends," *Bioresource Technology*, 191, 205-212.

Gilbert, P., Ryu, C., Sharifi, V. and Swithenbank, J. (2009), "Effects of process parameters on pelletisation of herbaceous crops," *Fuel,* 88 (8), 1491-1497.

Giudicianni, P., Cardone, G. and Ragucci, R. (2013), "Cellulose, hemicellulose and lignin slow steam pyrolysis: Thermal decomposition of biomass components mixtures," *Journal of Analytical and Applied Pyrolysis,* 100, 213-222.

Glaser, B., Haumaier, L., Guggenberger, G. and Zech, W. (2001), "The 'Terra Preta' phenomenon: a model for sustainable agriculture in the humid tropics," *Naturwissenschaften*, 88, 37-41.

Glaser, B., Lehmann, J. and Zech, W. (2002), "Ameliorating physical and chemical properties of highly weathered soils in the tropics with charcoal – a review," *Biol Fertil Soils*, 35, 219-230.

Gonzalez-Fernandez, C., Sialve, B., Bernet, N. and Steyer, J. P. (2012), "Thermal pretreatment to improve methane production of Scenedesmus biomass," *Biomass and Bioenergy,* 40, 105-111.

Grajales, L. M., Xavier, N. M., Henrique, J. P. and Thomeo, J. C. (2012), "Mixing and motion of rice particles in a rotating drum," *Powder Technology*, 222, 167-175.

Guerrero, M., Ruiz, M. P., Millera, A., Alzueta, M. U. and Bilbao, R. (2008), "Characterization of biomass chars formed under different devolatilization conditions: Differences between rice husk and Eucalyptus," *Energy and Fuels*, 22, 1275-1284.

GuiJun, W., YongHao, L., Jian, D., JiangHong, K. and YunLiang, Z. (2011), "Pretreatment of biomass by torrefaction," Special Topic: Bioenergy and Energy Science & Technology, *Chinese Science Bulletin*, 56(14), 1442-1448.

Gupta, R. B. and Demirbas, A. (2010), Gasoline, diesel, and ethanol biofuels from grasses and plants. Cambridge University Press, Technology and Engineering, 2010.

Harmsen, P. F. H., Huijgen, W. J. J., Lopez, L. M. B. and Baker, R. R. C. (2010), "Literature review of physical and chemical pretreatment processes for lignocellulosic biomass," Energy Research Center of the Netherlands, ECN-E-10-013. Retrieved at http://www.ecn.nl/docs/library/report/2010/e10013.pdf, 26 May 2012.

Henrich, E., Dinjus, E., Rumpel, S. and Stahl, R. (2008), "A two-stage pyrolysis/gasification process for herbaceous waste biomass from agriculture," In the Book: Progress in Thermochemical Biomass Conversion, 221-236, Online ISBN, 9780470694954 Retrieved at http://s3.amazonaws.com/zanran_storage/www.fzk.de/ContentPages/849605316.pdf, 1 May 2013. DOI:10.1002/9780470694954.

Herz, F., Mitov, I., Specht, E. and Stanev, R. (2012), "Experimental study of the contact heat transfer coefficient between the covered wall and solid bed in rotary drums," *Chemical Engineering Science*, 82, 312-318.

Herz, F., Mitove, I., Specht, E., Stanev, R. (2012a), "Influence of operational parameters and material properties on the contact heat transfer in rotary kilns", International Journal of Heat and Mass Transfer, 55, 7941-7948.

Hilten, R. N., Speir, R. A., Kastner, J. R., Mani, S. and Das, K. C. (2012), "Effect of torrefaction on bio-oil upgrading over HZSM-5. Part 2: Byproduct formation and catalyst properties and function," *Energy and Fuels*, 27, 844-856.

Hoekman, S. K., Broch, A., Robbins, C., Zielinska, B. and Felix, L. (2013), "Hydrothermal carbonization of selected woody and herbaceous biomass feedstock," *Biomass Conversion and Biorefineries*, 3, 113-126.

Hoffmann, S. Bartlett, M., Finkenrath, M., Evulet, A. and Ursin, T. P. (2009), "Performance and cost analysis of advanced combined cycles with pre-combustion CO_2 Capture," *Journal of Engineering for Gas Turbines and Power*, 131, 0217011-0217017.

Homan, W., Tjeerdsma, B., Beckers, E. and Jorissen, A. (2012), "Structural and other properties of modified wood," Retrieved at http://woodwestwood.com/Researches/3-5-1.pdf, 30th April 2013.

Hoogwijk, M., Faaij, A., Eickhout, B., Vries, B. and Turkenburg, W. (2005), "Potential of biomass energy out to 2100, for four IPCC SRES land-use scenarios," *Biomass and Energy,* 29, 225-257.

Huang, Y. F., Chen, W. R., Chiueh, P. T., Kuan, W. H. and Lo, S. L. (2012), "Microwave torrefaction of rice straw and Pennisetum," *Bioresource Technology*, 123, 1-7.

Huescar, C., Phylaktou, H. N., Andrews, G. E. and Gibbs, B. M. (2013), "The development of an experimental method for the determination of the minimum explosible concentration of biomass powders," *Biomass and Bioenergy*, 53, 95-104.

IEA (2009), Energy balance of the World: 2009. International Energy Agency. Retrieved at http://www.iea.org/stats/balancetable.asp?COUNTRY_CODE=29, 15 May 2012.

IEA (2014), "Key world energy statistics," International Energy Agency 2014. Retrieved online at http://www.iea.org/publications/freepublications/publication/KeyWorld2014.pdf, 15 June 2015.

IEO (2011), International energy outlook 2011. U. S. Energy Information Administration 2011. Retrieved at www.eia.gov/ieo/pdf/0484(2011).pdf, 24 October 2011.

Incropera, F. P. and De-Witt, D. P. (1985), "Introduction to Heat Transfer," John Willey & Sons Inc., Canada, 1985.

IPCC (2000), Land use, Land-use change, and forestry. Watson, R.T., Noble, R., Bolin, B., Ravindranath, N.H., Verardo, D.J. and Dokken, D.J. (eds.). Intergovernmental Panel on Climatic Change Special Report, Cambridge, Cambridge University Press, 2000.

IRENA (2013), "Biomass co-firing: Technology brief 2013," International Renewable Energy Agency, Energy Technology Systems Analysis Programme (ETSAP). Retrieved online at https://www.irena.org/DocumentDownloads/Publications/IRENA-ETSAP%20Tech%20Brief%20E21%20Biomass%20Co-firing.pdf, 15 June 2015.

Iroba, K. L., Tabil, L. G., Sokhansanj, S. and Dumonceaux, T. (2014), "Pretreatment and fractionation of barely straw using steam explosion at low severity factor," *Biomass and Bioenergy,* 66, 286-300.

Jena, U., Vaidyanathan, N., Chinnasamy, S. and Das, K. C. (2011), "Evaluation of microalgae cultivation using recovered aqueous co-product from thermochemical liquefaction of algal biomass," *Bioresource Technology,* 102(3), 3380–3387.

Jones, J. M., Bridgeman, T. G., Dravell, L. I., Gudka, B., Saddawi, A. and Williams, A. (2012), "Combustion properties of torrefied willow compared with bituminous coals," *Fuel Processing Technology*, 101, 1-9.

Kelly, J. J. and O'Donnell, J. P. (1968), "Dynamics of granular material in rotary dryers and coolers. *I." Chemical Engineering Symposium Series*, 29, 34-44.

Kelly, J. J. and O'Donnell, J. P. (1977), "Residence time model for rotary drum," *Trans. IchemE*, 55, 243-252.

Kiel, J. (2011), "ECN's torrefaction based BO_2 technology from pilot to demo," PowerPoint presented in International Energy Agency Workshop: Torrefaction, 28 January 2011, Energy research Center of the Netherland, Netherland. Retrieved online at http://www.bioenergytrade.org/downloads/grazkiel2011.pdf, 17 November 2014.

Kim, Y. H., Lee, S. M., Lee, H. W. and Lee, J. W. (2012), "Physical and chemical characteristics of products from the torrefaction of yellow poplar," *Bioresource Technology*, 116, 120-125.

Klinger, J., Klemetsrud, B., Bar-Ziv, E. and Shonnard, D. (2014), "Temperature dependence of aspen torrefaction kinetics," *Journal of Analytical and Applied Pyrolysis*, 110, 424-429.

Klose, W. and Wiest, W. (1999), "Experiments and mathematical modeling of maize pyrolysis in a rotary kiln," *Fuel*, 78, 65-72.

Kloss, S., Zehetner, F., Dellantonio, A., Hamid, R., Ottner, F., Liedke, V., Schwanninger, M., Gerzabek, M. H. and Soja, G. (2012), "Characterization of slow pyrolysis biochars: Effect of feedstocks and pyrolysis temperature on biochar properties," *Journal of Environment Quality*, 41, 990-1000.

Koh, M. P. and Hoi, W. K. (2003), "Sustainable biomass production for energy in Malaysia," *Biomass and Bioenergy*, 25, 517-529.

Kokko, L., Tolvanen, H., Hamalainen, K. and Raiko, R. (2012), "Comparing the energy required for fine grinding torrefied and fast heat-treated pine," *Biomass and Bioenergy*, 42, 219-223.

Konidis, J. (1984), "Design of direct heated rotary dryers," A Technical Report-Master Thesis, Mechanical Engineering Department, Concordia University, Montreal, Quebec, Canada, 1984.

Konisia, J. (1984), "Design of direct heated rotary dryers. Master Thesis, Mechanical Engineering Department, Concordia University, Montreal, Canada, 1984.

Koppajan, J., Sokhansanj, S., Melin, S. and Madrali, S. (2012), "Status of overview of torrefaction technologies," Report on IEA Bioenergy Task 32, 2012, International Energy Agency, France. Retrieved online at http://www.ieabcc.nl/publications/IEA_Bioenergy_T32_Torrefaction_review.pdf, 13 June 2015.

Koppejan, J., Sokhansanj, S., Melin, S. and Madrali, S. (2012), "Status overview of torrefaction technologies," IEA Bioenergy Task 32 Report. International Energy Agency, France.

Krokida, M., Kouris, D. M., Mujumdar, A. S. (2006), Rotary drying. In *Handbook of Industrial Drying*, 4th ed.; Mujumdar, A. S. Editor; CRC Press, Taylor & Francis Group, LLC, 6000 Broken Sound Parkway NW, Suite 3000, Boca Raton, FL 33487-2742, USA, 2006, Chapter 7, pp. 139-159.

Kuai, N., Huang, W., Du, B., Yuan, J., Li, Z., Gan, Y. and Tan, J. (2013), "Experiment-based investigations on the effect of ignition energy on dust explosion behaviors," *Journal of Loss Prevention in the Process Industries*, 26, 869-877.

Lamsal, B., Yoo, J., Brijwani, K. and Alavi, S. (2010), "Extrusion as a thermo-mechanical pretreatment for lignocellulosic ethanol," *Biomass and Bioenergy*, 34 (12), 1703-1710.

Lebas, E., Hanrot, F., Ablitzer, D., Houzelot, J. L. (1995), "Experimental study of residence time, particle movement and bed depth profile in rotary kilns," *The Canadian Journal of Chemical Engineering*, 73, 173-180.

Lehmann, J., Gaunt, J. and Rondon, M. (2006), "Bio-char sequestration in terrestrial ecosystems – A review," *Mitigation and Adaptation Strategies for Global Change*, 11, 403-427.

Lempp, P. (2013), "Biomass co-firing: Technology brief," IEA-ETSAP and IRENA, Technology Brief E2. Retrieved online at https://www.irena.org/DocumentDownloads/Publications/IRENA-ETSAP%20Tech%20Brief%20E21%20Biomass%20Co-firing.pdf, 18 January 2016.

Leung, D. Y. C., Garamanna, G. and Maroto-Valer, M. M. (2014), "An overview of current status of carbon dioxide and storage technologies," *Renewable and Sustainable Energy Reviews,* 39, 426-443.

Li, H., Liu, X., Legros, R., Bi, X. T., Lim, C. J. and Sokhansanj, S. (2012), "Pelletization of torrefied sawdust and properties of torrefied pellets," *Applied Energy*, 93, 680-685.

Li, Q., Lin, B., Dai, H. and Zhao, S. (2012a), "Explosion characteristics of H_2/CH_4/air and CH_4/coal dust/air mixtures," *Powder Technology*, 229, 222-228.

Li, S. Q., Ma, L. B., Wan, W. and Yao, Q. (2005), "A mathematical model of heat transfer in rotary a rotary kiln thermo-reactor," *Chemical Engineering Technology*, 28 (12), 1480-1489.

Li, S. Q., Yan, J. H., Li, R. D., Chi, Y. and Cen, K. F. (2002), "Axial transport and residence time of MSW in rotary kilns Part I. Experimental," *Powder Technology*, 126, 217-227.

Li, S. Q., Yan, J. H., Li, R. D., Chi, Y., Cen, K. F. (2002a), "Axial transport and residence time of MSW in rotary kilns Part II. Theoretical and optimal analyses," *Powder Technology*, 126, 228-240.

Libra, J. A., Ro, K. S., Kammann, C., Funke, A., Berge, N. D., Neubauer, Y., et al. (2011), "Hydrothermal carbonization of biomass residuals: a comparative review of the chemistry, process, and applications of wet and dry pyrolysis," *Future Science Group, Biofuels*, 2 (1), 89-124.

Lin, Y. L. and Wu, C. W. (2013), "Impact of torrefaction on the physicochemical properties of woody biomass," International Conference on Frontiers, *Energy and Bioscience* (ICFEEB 2013), ISBN: 978-1-60595-133-1.

Lipinsky, E. S., Arcate, J. R. and Reed T. B. (2002), "Enhanced wood fuels via. Torrefaction," *Fuel Chemical Division Pre-prints,* 47 (1), 408-410.

Liu, Q., Bai, C., Li, X., Jiang, L. and Dai, W. (2010), "Coal dust/air explosions in a large-scale tube," *Fuel*, 89, 329-335.

Liu, X. Y. and Specht, E. (2006), "Mean residence time and hold-up of solids in rotary kilns," *Chemical Engineering Science*, 61, 5176-5181.

Liu, Z., Quek, A., Hoekman, S. K. and Balasubramanian, R. (2013), "Production of solid biochar fuel from waste biomass by hydrothermal carbonization," *Fuel*, 103, 943-949.

Lu, G., Yan, Y., Cornwell, S., Whitehouse, M. and Riley, G. (2008), "Impact of co-firing coal and biomass on flame characteristics and stability," *Fuel*, 87(7), 1133-1140.

Lu, J. J. and Chen, W. H. (2014), "Product yields and characteristics of corncob waste under various torrefaction atmospheres," *Energies*, 7, 13-27.

Lu, K. M., Lee, W. J., Chen, W. H., Liu, S. H. and Lin, T. C. (2012), "Torrefaction and low temperature carbonization of oil palm fiber and eucalyptus in nitrogen and air atmospheres," *Bioresource Technology*, 123, 98-105.

Lynman, J. G., Coronella, C. J., Yan, W., Reza, M. T. and Vasquez, V. R. (2011), "Acetic acid and lithium chloride effects on the hydrothermal carbonization of lignocellulosic biomass," *Bioresource Technology*, 102, 6192-6199.

Madrali, S. (2008), "Canadian experience in Co-firing biomass in coal-fired power plants," CANMET Energy Technology Center, 2008. Retrieved on http://www.ieabcc.nl/workshops/task32_Beijing_WS/A2%20Cofiring%202%20in%20Canada%20IEA%20TAsk%2032%20Apr%202008.pdf, 13 November 2014.

Mahalingam, M. and Kolar, A.K. (1991), "Heat transfer model for the membrane wall of a high temperature circulating fluidized bed," In Circulating Fluidized Bed Technology III, Edited by Basu, P., Horio, M. and Hasatani, M., Pergamon Press, Oxford, 239-246.

Mahinpey, N., Murugan, P., Mani, T. and Raina, R. (2009), "Analysis of bio-oil, biogas, and biochar from pressurized pyrolysis of wheat straw using a tubular reactor," *Energy and Fuels*, 23, 2736-2742.

Malhotra K. (1989), "Particle flow and contact heat transfer characteristics of stirred granular beds," Doctoral Thesis, Department of Chemical Engineering, McGrill University, Montreal Canada, 1989.

Malhotra, K. and Mujumdar, A. S. (1991), "Model for contact heat transfer in mechanically stirred granular beds," *International Journal of Heat and Mass Transfer*, 34(2), 415-425.

Mani, T., Mahinpey, N. and Murugan, P. (2011), "Reaction kinetics and mass transfer studies of biomass char gasification with CO_2," *Chemical Engineering Science,* 66, 36–41.

Mckendry, P. (2002), "Energy production from biomass (part 1): Overview of biomass," *Bioresource Technology*, 83, 37-46.

Medic, D., Darr, M., Shah, A., Potter, B. and Zimmerman, J. (2011), "Effects of torrefaction process parameters on biomass feedstock upgrading," *Fuel*, 91(1), 147-154.

Mei, Y., Liu, R., Yang, Q., Yang, H., Shao, J., Draper, C., Zhang, S. and Chen, H. (2015), "Torrefaction of cedarwood in a pilot scale rotary reactor kiln and the influence of industrial flue gas," *Bioresource Technology*, 177, 355-360.

Melin, S. (2011), "Torrefied wood: A new emerging energy carrier," Presentation, Presented on Clean Coal Power Coalition, Wood Pellet Association of Canada. http://www.pellet.org/linked/2011-03 09%20ccpc%20presentation%20(2).pdf, 20th December 2013.

Melkior, T., Jacob, S., Gerbaud, G., Hediger, S., Le, Pape, L., Bonnefios, L. and Bardet, M. (2011), "NMR analysis of the transformation of wood constituents by torrefaction," *Fuel*, 92 (1), 271-280.

Meng, J., Park, J, Tilotta, D. and Park, S. (2012), "The effect of torrefaction on the chemistry of fast pyrolysis bio-oil," *Bioresource Technology*, 111, 439-446.

Mickley, H. S. and Fairbanks, D. F. (1955), "Mechanism of heat transfer to fluidized beds," *AIChE Journal*, 1, 374-384.

Moghtaderi, B. (2006), "The state-of-the-art in pyrolysis modeling of lignocellulosic solid fuels," *Fire and Materials*, 30, 1-34.

Mok, W. S. L. and Antal, Jr. M. J. (1983), "Effects of pressure on biomass pyrolysis II: Heats of reaction of cellulose pyrolysis," *Thermochimica Acta*, 68, 165-186.

Na, B. I., Kim, Y. H., Lim, W. S., Lee, S. M., Lee, H. W. and Lee, J. W. (2013), "Torrefaction of oil palm mesocarp fiber and their effect on pelletizing," *Biomass and Bioenergy,* 52, 159-165.

Na, B. L., Kim, Y. H., Lim, W. S., Lee, S. M. and Sokhansanj, S. (2013), "Torrefaction of sawdust in a fluidized bed reactor," *Biomass and Bioenergy*, 52, 195-165.

Nafsun, A. I., Herz, F., Specht, E., Scherer, V. and Wirtz S. (2016), "Heat transfer experiments in a rotary drum for a variety of granular materials," *Experimental Heat Transfer*, 29, 1-16.

Narayanan, K. V. and Natarajan, E. (2007), "Experimental studies on co-firing of coal and biomass blends in India," *Renewable Energy*, 32, 2548-2558.

Nasr-EI-Din, H. A., Afacan, A. and Masliyah, J. H. (1996), "Flow of solids and slurries in rotary drums," In *Advances in Engineering Fluid Mechanics: Multiphase Reactor and Polymerization System Hydrodynamics*, Advances in Engineering Fluid Mechanics Series 1996; Cheremisinoff, N. P., Editor; Gulf Publishing Company, P. O. Box 2608, Houston, Texas, 1996, Chapter 9, . 193-253.

Nhuchhen, D. R. and Basu, P. (2014), "Experimental investigation of mildly pressurized torrefaction in air and nitrogen," *Energy and Fuels*, 28, 3110-3121.

Nhuchhen, D. R. and Salam, P. A. (2012), "Estimation of higher heating value of biomass from proximate analysis: A new Approach," *Fuel*, 99, 55-63.

Nhuchhen, D. R., Basu, P. and Acharya, B. (2014), "A comprehensive review on biomass torrefaction," *International Journal of Renewable Energy & Biofuels*, 2014, 1-56, Doi: 10.5171/2014.506376.

NSWDPI (2013), "Biochar," Primary Industries Science and Research, NSW Department of Primary Industries, Australia. Retrieved at http://www.dpi.nsw.gov.au/research/topics/biochar, 27 September 2013.

Odeh, N. A. and Cockerill, T. T. (2008), "Life cycle GHG assessment of fossil fuel power plants with carbon capture and storage," *Energy Policy*, 36, 367-380.

Ohliger, A., Forster, M. and Kneer, R. (2013), "Torrefaction of beechwood: a parametric study including heat of reaction and grindability," *Fuel,* 104, 607-613.

Olajire, A. A. (2010), "CO_2 capture and separation technologies for end-of-pipe application – a review," *Energy*, 35, 2610-2628.

Oliveira, I., Blohse, D. and Ramke, H. G. (2013), "Hydrothermal carbonization of agriculture residues," *Bioresource Technology*, 142, 138-146. DOI: http://dx.doi.org/10.1016/j.biortech.2013.04.125

Pach, M., Zanzi, R. and Bjornbom, E. (2002), "Torrefied biomass a substitute for wood and charcoal," 6th Asia-Pacific International Symposium on Combustion and Energy Utilization, 20-22 May 2002, Kuala Lumpur, Malaysia.

Pandey, M. P. and Kim, C. S. (2011) "Lignin depolymerization and conversion: A review of thermochemical methods," *Chemical Engineering Technology*, 34, 29-41.

Pasangulapati, V., Ramachandriya, K. D., Kumar, A., Wilkins, M. R., Jones, C. L. and Huhnke, R. L. (2012), "Effects of cellulose, hemicellulose and lignin on thermochemical conversion characteristics of the selected biomass," *Bioresource Technology*, 114, 663–669.

PCSB (2011), "Commercialization summary," *PCS Biofuels Incorporated*, Presentation slides, June 2011, Not Published.

PCSB (2013), "The PCS biofuel technology," *PCS Biofuels*, Retrieved at http://www.pcsbiofuels.com/technology.php#htp, 29th May 2013.

Peduzzi, E., Boissonnet, G., Haarlemmer, G., Dupont, X. and Marechal, F. (2014), "Torrefaction modeling for lignocellulosic biomass conversion processes," *Energy*, 70(1), 58-67.

Pehnt, M. and Henkel, J. (2009), "Life cycle assessment of carbon dioxide capture and storage from lignite power plants," *International Journal of Greenhouse Gas Control*, 3, 49-66.

Pelaez-Samaniego, M. R., Yadama, V., Garcia-Perez, M., Lowell, E. and McDonald, A. G. (2014), "Effect of temperature during wood torrefaction on the formation of lignin liquid intermediates," *Journal of Analytical and Applied Pyrolysis*, 109: 222-233.

Peng, J. H., Bi, H. T., Lim, C. J. and Sokhansanj, S. (2013), "Study on density, hardness, and moisture uptake of torrefied wood pellets," *Energy and Fuels*, 27, 967-974.

Peng, J.H., Bi, H. T., Sokhansanj, S. and Lim, J. C. (2012), "A study of particle size effect on biomass torrefaction and densification," *Energy and Fuels,* 26, 3826-3839.

Pentananunt, R., Rahman, A. N. M. M. and Bhattacharya, S. C. (1990), "Upgrading of biomass by means of torrefaction," *Energy*, 15 (12), 1175-1179.

Perry, R. and Green, D. (1984), Chemical Engineer's Handbook, 6th Eds.; McGraw-Hill: New York, USA, 1984.

Phanphanich, M. and Mani, S. (2011), "Impact of torrefaction on the grindability and fuel characteristics of forest biomass," *Bioresource Technology,* 102, 1246-1253.

Pimchuai, A., Dutta, A. and Basu, P. (2010), "Torrefaction of agriculture residue to enhance combustible properties," *Energy and Fuels*, 24-9, 4638-4645.

Pirraglia, A., Gonalez, R., Denig, J. and Saloni, D. (2013), "Technical and economic modeling for the production of torrefied lignocellulosic biomass for the U. S. densified fuel industry," *Bioenergy Resources*, 6, 263-275. DOI 10.1007/s12155-012-9255-6

Prando, D., Patuzzi, F., Baggio, P. and Baratieri, M. (2013), "CHP gasification system fed by torrefied biomass: Assessment of the energy performance," *Waste Biomass Valorization*, 5, 147-155. DOI 10.1007/s12649-013-9227-x.

Prins, M, J., Ptasinski, K. J. and Janssen, F. J. J. G. (2006a), "Torrefaction of wood part 2. Analysis of products," *Journal of Analytical and Applied Pyrolysis,* 77, 35-40.

Prins, M. J., Ptasinski, K. J. and Janssen, F. J. J. G. (2007), "From coal to biomass gasification: Comparison of thermodynamic efficiency," *Energy*, 32(7), 1248-1259.

Prins, M. J., Ptasninski, K. J. and Janssen, F. J. J. G. (2006), "More efficient biomass gasification via torrefaction," *Energy*, 31(15), 3458-347. DOI: http://dx.doi.org/10.1016/j.energy.2006.03.008

Ptasinski, K. J. (2008), "Thermodynamic efficiency of biomass gasification and biofuels conversion," *Biofuels Bioproducts and Biorefining,* 2, 239-253.

Qing, C., JinSong, Z., BingJun, L., QinFeng, M. and ZhngYang, L. (2011), "Influence of torrefaction pretreatment on biomass gasification technology," Special Topic: Bioenergy Energy Science & Technology, *Chinese Science Bulletin*, 56(14), 1449-1456.

Ragland, K. W., Aerts, D. J. and Baker, A. J. (1991), "Properties of wood for combustion analysis," *Bioresource Technology,* 37, 161-168.

Ratte, J., Fardet, E., Mateos, D. and Hery, J. S. (2011), "Mathematical modeling of a continuous biomass torrefaction reactor: TORSPYDTM column," *Biomass and Bioenergy*, 35, 3481-3495.

Raut, M. K., Basu, P. and Acharya, B. (2013), "Effect of torrefaction pretreatment on the Gasification of Biomass," *CSChE Conference*, 20-23 October, Fredericton, 2013.

Raut, M. K. (2014), "Studies into the effect of torrefaction on gasification of biomass," Master Thesis, Dalhousie University, Halifax, Canada, 2014.

Rautiainen, M., Havimo, M. and Gruduls, K. (2012), "Biocoal production, properties and uses," *Baltic Bioenergy and Industrial Charcoal*, Report 1/2012, Production and Logistics.

Raveendran, K., Ganesh, A. and Khilar, K. C. (1996), "Pyrolysis characteristics of biomass and biomass components," *Fuel*, 75(8), 987-998.

Rawls, J., Stromberg, B., Weston, J., Jiang, X. and Hunt, T. (2011), "Method and system for the torrefaction of lignocellulosic material," US Patent, US 2012/0042567 A1. Retrieved online at http://www.google.com/patents/US20120042567, 15 January 2014.

Ren, S., Lei, H., Wang, L., Bu, Q., Wei, Y., Liang, J., Liu, Y., et al. (2012), "Microwave torrefaction of Douglas fir sawdust pellets," *Energy Fuels*, 26, 5936-5943.

Renaud, M., Thibault, C. O., and Schutte W. H. (2000), "Solid transport model of an industrial rotary dryer," *Drying Technology*, 18(4-5), 843-865.

Repellin, V., Govin, A., Rolland, M. and Guyonnet, R. (2010), "Modeling anhydrous weight loss of wood chips during torrefaction in a pilot kiln." *Biomass and Bioenergy*, 34, 602-609.

Repellin, V., Govin, A., Rolland, M. and Guyonnet, R. (2010a), "Energy requirement for fine grinding of torrefied wood," *Biomass and Energy*, 34, 923-930.

Richard, N. and Thumann, H. (2002), "General equations for biomass properties," Chalmer University of Technology, Sweden, 2002. Retrieved at http://www.unece.lsu.edu/biofuels/documents/2003-2006/bf03_011.pdf, 18 February 2013.

Roman, S., Nabais, J. M. V., Laginhas, C., Ladesma, B. and Gonzalez, J. F. (2012), "Hydrothermal carbonization as an effective way of densifying the energy content of biomass," *Fuel Processing Technology*, 103, 78-83.

Rousset, P., Davrieux, F., Macedo, L. and Perre, P. (2011), "Characterization of the torrefaction of beech wood using NIRS: Combined effects of temperature and duration," *Biomass and Bioenergy*, 35, 1219-1226.

Rousset, P., Macedo, L., Commandre, J-M. and Moreira, A. (2012), "Biomass torrefaction under different oxygen concentrations and its effect on the composition of the solid by-products," *Journal of Analytical and Applied Pyrolysis,* 96, 86-91.

Rousset, P., Macedo, L., Commandre, J. M. and Moreira, A. (2012), "Biomass torrefaction under different oxygen concentrations and its effect on the composition of the solid by-product," *Journal of Analytical and Applied Pyrolysis*, 96, 86-91.

Rowell, R. M. (2005), Handbook of wood chemistry and wood composites. Taylor and Francis, CRC press, USA.

Saadon, S., Uemura, Y. and Mansor, N. (2014), "Torrefaction in the presence of oxygen and carbon dioxide: The effect on yield of oil palm kernel shell," Procedia Chemistry, 9, 194-201, International Conference and Workshop on Chemical Engineering UNPAR 2013, ICCE UNPAR 2013.

Sabil, K. M., Aziz, M. A., Lal, B. and Uemura, Y. (2013), "Effects of torrefaction on the physiochemical properties of oil palm empty fruit bunches, mesocrap fiber and kernel shell," *Biomass and Bioenergy*, 56, 351-360.

Sai, P. S. T., Surender, G. D., Damodaran, A. D., Suresh, V. and Philip, Z. G., (1990), "Residence time distribution and material flow studies in a rotary kiln," *Metallurgical Transaction*, 21B, 1005 -1011.

Saleh, S. B., Hansen, B. B., Jensen, P. A. and Dam-Johansen, K. (2013), "Efficient fuel pretreatment: Simultaneous torrefaction and grinding of biomass," *Energy and Fuels*, 27, 7531-7540.

Scheller, H. V. and Ulvskov, P. (2010), "Hemicelluloses: Annual review of plant biology," *Plant Biology*, 61 263-289, DOI: 10.1146/annurev-arplant-042809-112315.

Schimmelpfennig, S. and Glaser, B. (2012), "One step forward toward characterization: Some important material properties to distinguish biochars," *Journal of Environmental Quality*, 41(4), 1001-1013.

Schlesinger, W.H. and Lichter, J. (2001), "Limited carbon storage in soil and litter of experimental forest plots under increased atmospheric CO_2," *Nature,* 411, 466–469.

Schlunder, E. U. (1981), "Heat transfer between packed, agitated and fluidized beds and submerged surfaces," *Chemical Engineering Communications*, 9(1-6), 273-302.

Seaman, W. C. (1951), "Passage of solids through rotary kilns: Factors affecting time of passage," *Chemical Engineering Progress*, 47, 508-514.

Seebauer, V. P. J. and Staudinger, G. (1997), "Effects of particle size, heating rate, and pressure on measurement of pyrolysis kinetics by thermogravimetric analysis," *Fuel,* 76, 1277-1282.

Shafizadeh, F. (1985), "Pyrolytic reactions and products of biomass, in: Prins, M. J., Ptasinski, K. J., Janssen, F. J. J. G., 2006. Torrefaction of wood: Part 1. Weight loss kinetics," *Journal of Applied Pyrolysis*, 77, 28-34.

Shah, A., Darr, M. J., Medic, D., Anex, R. P., Khanal, S. and Maski, D. (2011), "Techno-economic analysis of a production-scale torrefaction system for cellulosic biomass upgrading," *Biofuels Bioproducts and Biorefining*, 6, 45-57.

Shang, L., Nielsen, N. P. K., Dahl, J., Stelte, W., Ahrenfeldt, J., Holm, J. K., Thomsen, T. and Henriksen, U. B. (2012), "Quality effect caused by torrefaction of pellets made from Scot Pine," *Fuel Processing Technology*, 101, 23-28.

Shone, C. and Bravo, S. (2007), "Mathematical modeling of indirect contact rotary DRTHRS," *Drying Technology: An International Journal*, 16, 1567-1583.

Shoulaifar, T. K., DeMartini, N., Ivaska, A., Fardim, P. and Hupa, M. (2012), "Measuring the concentration of carboxylic acid groups in torrefied spruce wood," *Bioresource Technology*, 123, 338-343.

Song, Y. (2003), "Solid transportation, heat and mass transfer in rotary dryers", Master Thesis, University of Ottawa, Ottawa, Canada.

Sorum, L., Groni, M. G. and Hustad, J. E. (2001), "Pyrolysis characteristics and kinetics of municipal solid wastes," *Fuel*, 80 (9), 1217-1227.

Stelte, W. (2012), "Torrefaction of unutilized biomass resources and characterization of torrefaction gases," Resultat Kontrakt (RK) Report, Biomass Section, Center for Renewable Energy and Transport, Energy and Climate Danish Technological Institute, Denmark, 2012.

Stelte, W., Clemons, C., Holms, J. K., Sanadi, A. R., Ahrenfeldt, J., Shang, L., and Henriksen, U. B. (2011), "Pelletizing properties of torrefied spruce," *Biomass and Bioenergy,* 35 (11), 4690-4698.

Stephan, C. R. (2012), "Coal dust explosion hazards," *Mine Safety and Health Administration Pittsburgh*, Pennsylvania, U. S. A. Retrieved at http://www.msha.gov/SandHINFO/TECHRPT/PandT/COALDUST.pdf, 31 May 2013.

Strandberg, M., Olofsson, I., Pommer, L., Wiklund-Lindstrom, S., Aberg, K. and Nordin, A. (2015), "Effects of temperature and residence time on continuous torrefaction of spruce wood," *Fuel Processing Technology*, 134, 387-398.

Subbarao, D. and Basu, P. (1988), "A model for heat transfer in circulating fluidized beds," *International Journal of Heat and Mass Transfer*, 39(3), 487-489.

Sule, I.O. (2012), Torrefaction behavior of agricultural biomass, M.Sc Thesis, School of Engineering, University of Guelph, Ontario, Canada.

Sullivan, J. D., Maier, C. G. and Ralston, O. C. (1927), "Passage of solid particles through rotary cylindrical kilns", Technical Papers, 384, pp.1-42, US Bureu of Mines, USA.

Sun, C. L., Xiong, Y. Q., Liu, Q. X. and Zhang, M. Y. (1997), " Thermogravimetric study of the pyrolysis of two Chinese coals under pressure," *Fuel*, 76, 639-644.

Sun, Y. and Cheng, J. (2002), "Hydrolysis of lignocellulosic materials for ethanol production: A review," *Bioresource Technology,* 83, 1-11.

Sun, Y., Jiang, J., Zhao, S., Hu, Y. and Zheng, Z. (2011), "Review of torrefaction reactor technology," Conference Paper, International Conference on Energy, Environment and Sustainable Development (ICEESD 2011), October 21-23, 2011, Shanghai, China.

Sundqvist, B. (2004), Color changes and acid formation in wood during heating, Doctoral Thesis, Division of Wood and Material Science, Lulea University of Technology. Retrieved at http://epubl.luth.se/1402-1544/2004/10/LTU-DT-0410-SE.pdf, 29th April 2013.

Svanberg, M., Olofsson, I., Floden, J. and Nordin, A. (2013), "Analysis biomass torrefaction supply chain costs," *Bioresource Technology*, 142, 287-296.

Svoboda, K., Pohorely, M., Hartman, M. and Martinec, J. (2009), "Pretreatment and feeding of biomass for pressurized entrained flow gasification," *Fuel Processing Technology*, 90, 629-635.

Tapasvi, D., Khalil, R., Varhegyi, G., Skreiberg, O., Tran, K. and Gronli, M. (2013), "Kinetic behavior of torrefied biomass in an oxidative environment," *Energy and Fuels,* 27(2), 1050-1060.

Tapasvi, D., Tran, K. Q., Gronli, M., Khalil, R., Skreiberg, O. and Varhegyi, G. (2013), "Thermal decomposition kinetics of woods with an emphasis on torrefaction," *Energy and Fuels*, 27(10), 6134-6145.

Thammavong, P., Debacq, M., Vitu, S. and Dupoizat, M. (2011), "Experimental apparatus for studying heat transfer in externally heated rotary kilns," *Chemical Engineering Technology*, 34 (5), 707-717.

Thanapal, S. S., Chen, W., Annamalai, K., Carlin, N. and Ansley, J. R. (2014), "Carbon dioxide torrefaction of woody biomass," *Energy and Fuels*, 28(2), 1147-1157.

Tomme, P., Warren, R. A. J., and Gilkes, N. R. (1995), "Cellulose hydrolysis by bacteria and fungi," In: Advances in Microbial Physiology, Vol. 37, Poole, R. K., pp. 1-81, Academic Press, ISBN 0-12-027737-9, London, UK, 1995.

Tooyserkani, Z., Sokhansanj, S., Bi, X., Lim, J., Lau, A., Saddler, J., Kumar, L., Lam, P. S. and Melin, S. (2013), "Steam treatment of four softwood species and bark to produce torrefied wood," *Applied Energy*, 103, 514-521.

Topell (2012), "Torrefied biomass: Advantages over untreated biomass," *Topell Energy*, Updated in 11th June 2012. Retrieved at http://www.topellenergy.com/product/torrefied-biomass/, 13 May 2013.

Topell (2014), "Topell Energy: Co-firing," Retrieved online at http://www.topellenergy.com/applications/co-firing/, 17 November 2014.

Torrent, J. (2011), "Test report on characterization of flammable solids, torrefied wood fuel," *Laboratorio Official J.M. Madariaga,* (October 2011), Not published.

Torres, S. S., Jomaa, W., Marc, F. and Puiggali, J. R. (2010), "Causes of color changes in wood during drying," *Forestry Studies in China,* 12(4), 167-175. DOI 10.1007/s11632-010-0404-8.

Tremel, A., Spemann, J., Herrmann, M., Erlach, B. and Spliethoff, H. (2012), "Entrained flow gasification of biocoal from hydrothermal carbonization," *Fuel*, 102, 396-403.

Tscheng, S. H. (1978), "Convective heat transfer in a rotary kiln", Doctoral Thesis, University of British Columbia, British Columbia, Canada, 1978.

Tscheng, S. H. and Watkinson, A. P. (1979), "Convective heat transfer in a rotary kiln," *The Canadian Journal of Chemical Engineering*, 57, 433-443.

Tumuluru, J. S., Sokhansanj, S., Hess, J. R., Wright, C. T. and Boardman, R. D. (2011), "A review on biomass torrefaction process and product properties for energy applications," *Industrial Biotechnology,* 7, 384-401.

Tumuluru, J. S., Sokhansanj, S., Hess, J. R., Wright, C. T. and Kremer, T. (2012), "GC analysis of volatiles and other products from biomass torrefaction process," *Advanced Gas Chromatography-Progress in Agricultural, Biomedical and Industrial Applications*. Retrieved at http://cdn.intechopen.com/pdfs/32823/InTech-Gc_analysis_of_volatiles_and_other_products_from_biomass_torrefaction_process.pdf, 27 April 2013.

Turner, I., Rousset, P., Remond, R. and Perre, P. (2010), "An experimental and theoretical investigation of the thermal treatment of wood (Fagus Sylvatica L.) in the range 200-260°C," *International Journal of Heat and Mass Transfer,* 53 (4), 715-725.

Uemura, Y., Omar, W. N., Othman, N. A. B., Yusup, S. B. and Tsutsui, T. (2011), "Effect of atmosphere on torrefaction of oil palm wastes," Bioenergy Technology, World Renewable Energy Congress 8-13 May 2011, Linkoping, Sweden.

Uemura, Y., Omar, W. N., Tsutsui, T. and Yusup, S. B. (2011), "Torrefaction of oil palm wastes," *Fuel,* 90, 2585-2591.

Uemura, Y., Omar, W., Othman, N. A., Yusup, S. and Tsutsui, T. (2013), "Torrefaction of oil palm EFB in the presence of oxygen," *Fuel*, 103, 156-160.

Uemura, Y., Saadon, S., Osman, N., Mansor, N. and Tanoue, K. (2015), "Torrefaction of oil plam kernel shell in the presence of oxygen and carbon dioxide," *Fuel*, 144, 171-179.

Van de Weerdhof, M. W. (2010), "Modeling of the pyrolysis process of biomass particles," Master Thesis, WVT 2010.07, Eindhoven University of Technology, Department of Mechanical Engineering, Netherlands, 2010.

Van der Stelt, M. J. C. (2011), "Chemistry and reaction kinetics of bio-waste torrefaction," Dissertation, Technical University of Eindhoven, Eindhoven, Netherland, 2011.

Van der Stelt, M. J. C., Gerhauser, H., Kiel, J. H. A. and Ptasinski, K. J. (2011), "Biomass upgrading by torrefaction for the production of biofuels: A review," *Biomass and Bioenergy*, 35, 3748-3762.

Vanholme, R., Demedts, B., Morreel, K., Ralph, J., and Boerjan, W. (2010), "Lignin biosynthesis and structure," *Plant Physiology*, 153(3) 895-905.

Vincent, R., Alexandre, G., Mathieu, R. and Rene, G. (2010), "Modelling anhydrous weight loss of wood chips during torrefaction in a pilot kiln," *Biomass and Bioenergy*, 34(5), 602-609.

Wang, C., Peng, J., Li, H., Bi, X. T., Legros, R., Lim, C. J. and Sokhansanj, S. (2012), "Oxidative torrefaction of biomass residues and densification of torrefied sawdust to pellets," *Bioresource Technology*, 127, 318-325.

Wang, G., Luo, Y., Deng, J., Kuang, J. and Zhang, Y. (2011), "Pretreatment of biomass torrefaction," *Special Topic: Bioenergy, Energy Science and Technology, Chinese Science Bulletin,* 56, 1442-1448. DOI: 10.1007/s11434-010-4143-y

Wang, M. J., Huang, Y. F., Chiueh, P. T., Kuan, W. H. and Lo, S. L. (2012a), "Microwave- induced torrefaction of rice husk and sugarcane residues," *Energy*, 37, 177-184.

Wang, W., Peng, J., Li, H., Bi, X. T., Legros, R., Lim, C. J.and Sokhansanj, S. (2013), "Oxidative torrefaction of biomass residues and densification of torrefied sawdust to pellets," *Bioresource Technology*, 127, 318-325.

Wannapeera, J. and Worasuwannarak, N. (2012), "Upgrading of woody biomass by torrefaction under pressure," *Journal of Analytical and Applied Pyrolysis*, 96, 173-180.

Wannapeera, J., Fungtammasan, B., and Worasuwannarak, N. (2011), "Effects of temperature and holding time during torrefaction on the pyrolysis behaviors of woody biomass," *Journal of Analytical and Applied Pyrolysis*, 92(1), 99-105.

Weigo, C., Liyuan, H., Jianxin, Z., Sen, X., Shanshan, Q. and Feng, P. (2012), "Research on characteristics parameters of coal-dust explosion," 2012 International Symposium on Safety Science and Technology, *Procedia Engineering* (2012), 45, 442-447.

Wes, G. W. J., Drinkenburg, A. A. H. and Stemerding, S. (1976), "Heat transfer in a horizontal rotary drum reactor," *Power Technology*, 13, 185-192.

White, R. H. and Dietenberger, M. A. (2001), "Wood products: thermal degradation and fire," In Torres, S. S., Jomaa, W., Marc, F., Puiggali, J. R. (2010), "Causes of color changes in wood during drying," *Forestry Studies in China,* 12(4), 167-175. DOI 10.1007/s11632-010-0404-8.

Wingreini, A., Galbe, M., Roslander, C., Rudolf, A., and Zacchi, G. (2005), " Effect of reduction in yeast and enzyme concentrations in a simultaneous-saccharification-and-fermentation- based bioethanol process," *Biotechnology for Fuels and Chemicals*, 26 ABAB Symposium 2005, 485-499.

Wu, K. T., Tsai, C. J., Chen, C. S. and Chen, H. W. (2012), "The characteristics of torrefied microalgae," *Applied Energy*, 100, 52-57.

Yan, W., Acharjee, T. C., Coronella, C. J. and Vasquez, V. R. (2009), "Thermal pretreatment of lignocellulosic biomass," *Environmental Progress & Sustainable Energy*, 28(3), 435-440.

Yan, W., Hastings, J. T., Acharjee, T. C., Coronella, C. J. and Vasquez, V. R. (2010), "Mass and energy balance of wet torrefaction of lignocellulosic biomass," *Energy and Fuels,* 24, 4738-4742.

Yang, H., Yan, R., Chen, H., Lee, D. H. and Zheng C. (2007), "Characteristics of hemicellulose, cellulose and lignin pyrolysis," *Fuel*, 86, 1781-1788.

Yusup, S., Ahmad, M. M., Uemura, Y., Ali, R. M., Azmi, A. S., Mohamad, M. F. and Lay, S. L. (2013), "Pretreatment of Malaysian agricultural wastes towards biofuel production," Book Chapter 17. Pretreatment Techniques for Biofuels and Biorefineries, *Green Energy and Technology*, 393-416. DOI 10.1007/978-3-642-32735-3_17.

Zakri, B., Saari, J., Sermyagina, E. and Vakkilainen, E. (2013), "Integration of torrefaction with steam power plant," Research Reports 8, LUT Scientific and Expertise Publications Tutkimusraportit, LUT Energy, Lappeenranta University of Technology, Finland. Retrieved online at https://www.doria.fi/bitstream/handle/10024/94111/Biotuli_torrefiointi_tutkimusraportti.pdf?sequence=2, 19 November 2014.

Zeng, D. (2005), "Effects of pressure on coal pyrolysis at higher heating rates and char combustion," Doctoral Dissertation, Department of Chemical Engineering, Brigham Young University, 2005.

Zheng, A., Zhao, Z., Chang, S., Huang, Z., He, F. and Li, H. (2012), "Effect of torrefaction temperature on product distribution from two-staged pyrolysis of biomass," *Energy and Fuels*, 26, 2968-2974.

Zheng, Y., Pan, Z. and Zhang, R. (2009), "Overview of biomass pretreatment for cellulosic ethanol production," *International Journal of Agriculture and Biological Engineering*, 2(3), 51-66.

APPENDIX A: SUPPLEMENTARY INFORMATION FOR CHAPTER 4

A.1. Mean Residence Time of a Single Particle

Consider a spherical particle of diameter d and mass m in a rotary drum reactor of effective length $\mathcal{L}$ rotated at angular speed N (angular velocity $\omega = 2\pi N/60$ rad/s), inner diameter $D = 2R$, and axial rectangular flights of width L_f. Figure 4.2 shows the forces acting on the particle and their variations at any instant of the flight position with the rotation of the reactor. The particle moves up from position 1, where the particle is subjected to centrifugal force ($F_c = mD\omega^2/2$) and gravity force ($F_g = mg$) in an outward direction.

At position 1, the weight of the particle due to the inclination of the reactor can be resolved into two directions: along the axis of rotation ($F_a = F_g sin\beta$), and normal to the reactor axis or parallel to the transverse direction of the flight surface ($F_r = F_g cos\beta$). Note that the directions of these two force components must remain the same at any point of time or for any location of the flight. The force diagram clearly indicates that the particle will be motionless at flight position 1. The net outward force on the particle can be thus estimated as:

$$F_{net,1} = F_c + F_r$$

For a position with the flight at 1' with an angle $\measuredangle 1'C1 = \emptyset$, the normal force component of the weight of the particle (F_r) can be resolved into two perpendicular directions: along the transverse direction of the flight surface ($F_{r,1',i} = F_r cos\emptyset$) and normal to the flight surface ($F_{r,1',n} = F_r sin\emptyset$). The net outward force along the flight surface can be now estimated as:

$$F_{net,1'} = F_c + F_{r,1',i}$$

At one instant, the flight will be horizontal at $1''$ and the angle will be $\measuredangle 1'C1 = \emptyset = 90^{\circ}$. Therefore, the components of force may be written as:

$$F_{r,1'',i} = 0$$

$$F_{r,1'',n} = F_r$$

The net outward force on the particle at 1'' will be vertically downward and equivalent to only the centrifugal force acting on the particle:

$$F_{net,1''} = F_c$$

Further rotation of the reactor will establish a force towards the center of the reactor, which increases with the angle of inclination of the flight (θ). This means that the direction of the force component $F_{r,1',i}$ becomes opposite to the direction of the centrifugal force. In addition to this, the particle will exert frictional force that acts along the same direction as the centrifugal force. At a certain point ($1'''$), one component of the weight (along the transverse direction of the flight surface) will balance the centrifugal and frictional forces acting on the particle. At this point, the particle will start moving down. The force balance equation can be expressed as:

$$F_{r,1''',i} = \mu_{\theta s} F_{r,1''',n} + F_c$$

$$F_r sin\theta = \mu_{\theta s} F_r cos\theta + F_c$$

$$mgcos\beta sin\theta = \mu_{\theta s} mgcos\beta cos\theta + \frac{mD\omega^2}{2}$$

$$\sin\theta = \mu_{\theta s}\cos\theta + \frac{D\omega^2}{2g\cos\beta} \tag{A.1}$$

Above, $\mu_{\theta s}$ is the static friction coefficient between particle and flight surface. This equation can be used to estimate the angular displacement of a particle before it falls back to the reactor. The rotary reactors usually operate at low angular speeds to maintain a desired residence time. The effect of the centrifugal force on the angular displacement (θ) is thus not significant, such that the angular displacement can be assumed to be the angle equivalent to the static friction coefficient.

The total angular displacement made by the particle when it moves from flight position 1 to 1''' can be then estimated as:

$$\theta_d = \frac{(90+\theta)\pi}{180} \tag{A.2}$$

The uplifting time (t_u) may be then estimated as:

$$t_u = \frac{(90+\theta)\pi}{180\omega} \tag{A.3}$$

As the reactor is inclined at angle β, it is assumed that the particle rolls at a constant velocity on the flight surface at an angle equivalent to the angle of inclination of the reactor, as shown in the Figure 4.2f. The velocity of the particle at the tip of flight, before it leaves the flight, can be estimated by using the principle of energy conservation as:

$$\text{Loss in the elevation energy} + \text{Loss due to friction} = \text{Gain in kinetic energy} + \text{Gain in rotational energy}$$

$$mg\frac{L_f}{\cos\beta}\sin\theta+\mu_k mg\cos\beta\sin\theta\frac{L_f}{\cos\beta}=\frac{mv_r^2}{2}+\frac{2Iv_r^2}{d^2} \tag{A.4}$$

Above, I represents the moment of inertia of the particle and μ_k is the coefficient of rolling friction. For a spherical particle, the moment of inertia can be considered as $I = md^2/10$. This gives an expression for the rolling velocity of particle as:

$$g\frac{L_f}{cos\beta}sin\theta+\mu_k L_f g sin\theta=\frac{{v_r}^2}{2}+\frac{{v_r}^2}{5}$$

$$L_f g sin\theta\left(\frac{1}{cos\beta}+\mu_k\right)=\frac{7{v_r}^2}{10}$$

$$v_r=\sqrt{\frac{10L_f g\sin\theta}{7}\left(\frac{1}{\cos\beta}+\mu_k\right)} \tag{A.5}$$

Rolling time, which is the time taken by the particle to travel the projected width of the flight, can be expressed as:

$$t_r=\frac{\frac{L_f}{cos\beta}}{v_r}$$

$$t_r=\frac{\frac{L_f}{cos\beta}}{\sqrt{\frac{10L_f g sin\theta}{7}\left(\frac{1}{cos\beta}+\mu_k\right)}}$$

$$t_r=\sqrt{\frac{7}{10gL_f sin\theta\left(\frac{1}{cos\beta}+\mu_k\right)}\left(\frac{L_f}{cos\beta}\right)^2}$$

$$t_r = \frac{1}{\cos\beta}\sqrt{\frac{7L_f}{10g\sin\theta\left(\frac{1}{\cos\beta}+\mu_k\right)}} \tag{A.6}$$

As the reactor is rotating at a constant angular velocity, the new flight position ($1''''$) before particle falls off from the edge of the flight (A) may be determined as:

$$\theta_f = \theta + t_r\omega \times \frac{180}{\pi} \tag{A.7}$$

The particle velocity at the edge of the flight (v_r) can further be resolved into vertical, horizontal, and axial components:

$$Axial\ component, v_a = v_r sin\beta$$

$$Vertical\ component, v_{s,v} = v_r cos\beta sin\theta_f$$

$$Horizontal\ component, v_{s,h} = v_r cos\beta cos\theta_f$$

As shown in Figs. 4.2e and 4.2g, there may be two possible trajectories depending on the horizontal distance h_h travelled by the particle: (a) Path AP'P_i (if BC > h_h), (b) Path AP''P_i (if BC < h_h). Falling time (flight time) is considered to be the time taken by the particle to move from A (edge of the flight) to P_i (the position of the particle on the reactor surface). Assuming an angle $\measuredangle P_i C1 = \alpha$, the vertical height may be estimated as:

$$h_v = radius\ of\ particle + AB\ (A'B') + BD(B'D''')$$

$$h_v = \frac{d}{2} + \left(R - L_f\right)\sin\theta_f + \left(R - \frac{d}{2}\right)\cos\alpha \tag{A.8}$$

The falling time (t_f) can be estimated by solving the quadratic equation as:

$$\frac{d}{2} + (R - L_f) sin\theta_f + \left(R - \frac{d}{2}\right) cos\alpha = v_r cos\beta sin\theta_f t_f + \frac{1}{2} g {t_f}^2$$

$$t_f = \frac{-v_r \cos\beta \sin\theta_f + \sqrt{\left(v_r \cos\beta \sin\theta_f\right)^2 + 2g\left(\frac{d}{2} + \left(R - L_f\right)\sin\theta_f + \left(R - \frac{d}{2}\right)\cos\alpha\right)}}{g}$$

(A.9)

The horizontal distance travelled by the particle ($DP\ or\ AA'$) may be calculated as:

$$h_h = v_r \cos\beta \cos\theta_f t_f \tag{A.10}$$

The assumed value of angle $\measuredangle P_i C1 = \alpha$ (for both trajectories) can be reiterated to obtain the converge solution as:

$$sin\alpha = \pm \frac{BC - h_h}{R - \frac{d}{2}}$$

$$\sin\alpha = \pm \frac{\left(R - L_f - v_r t_f \cos\beta\right)\cos\theta_f}{R - \frac{d}{2}} \tag{A.11}$$

A.2. Critical Falling Time

As we can see from the Figure 4.2, the positions of the particle and the flight vary with time. Therefore, it is necessary to introduce a new term, critical falling time, that can

indicate which flight will continue during the next cascaded cycle. The critical falling time may be defined as the time taken by the particle to travel from the flight edge (A) to just above the horizontal line ($C'D'$). When the particle reaches this level, it will be picked up by the light blue flight if that flight is approaching towards the particle. Otherwise, only the next dark green flight will continue the cycle.

The critical falling time can be determined using the vertical distance ($AD'\ or\ A'D''$) travelled by the particle. The vertical distance can be geometrically expressed using different design parameters as:

$$AD' = Radius\ of\ particle + A(A'B') + BD'(B'D'')$$

$$AD' = \frac{d}{2} + \left(R - L_f\right)\sin\theta_f + \left(R - L_f\right) \tag{A.12}$$

The critical falling time (t_{cft}) can be obtained by solving the quadratic equation as:

$$\frac{d}{2} + \left(R - L_f\right)sin\theta_f + (R - L_f) = v_r cos\beta sin\theta_f t_{cft} + \frac{g t_{cft}^2}{2}$$

$$t_{cft} = \frac{-v_r \cos\beta\sin\theta_f + \sqrt{\left(v_r \cos\beta\sin\theta_f\right)^2 + 2g\left(\frac{d}{2} + \left(R - L_f\right)\sin\theta_f + \left(R - L_f\right)\right)}}{g}$$

(A.13)

The critical horizontal distance travelled by the particle ($D'P'or\ D'P''$) is then determined as:

$$h_{hhc} = v_r \cos\beta \cos\theta_f t_{cft} \tag{A.14}$$

This critical horizontal distance will help to determine the position of the particle at that particular instant. The critical angle (θ_{crp}) defining the particle location at that instant can be expressed as:

$$\theta_{crp} = \measuredangle P'C5 = \measuredangle 1C5 + \measuredangle P'C1$$

$$\theta_{crp} = \measuredangle P''C5 = \measuredangle 1C5 - \measuredangle P''C1$$

$$\theta_{crp} = 120 + tan^{-1}\left(\pm\frac{BC - h_{hhc}}{R - L_f}\right)$$

$$\theta_{crp} = 120 + tan^{-1}\left(\pm\frac{(R - L_f)cos\theta_f - v_r cos\beta cos\theta_f t_{cft}}{R - L_f}\right)$$

$$\theta_{crp} = 120 + \tan^{-1}\left(\pm\left(1 - \frac{v_r \cos\beta t_{cft}}{R - L_f}\right)\cos\theta_f\right) \tag{A.15}$$

After knowing the position of the particle, the position of the flight is also required in order to identify the flight that will continue during the cascaded cycle. In order to do this, the angular displacement of the flight, known as the critical angular displacement defining the flight location (θ_{crf}), has to be determined as:

$$\theta_{crf} = \omega t_{cr} \times \frac{180}{\pi} \tag{A.16}$$

Above, t_{cr} is the total critical time, which can be defined as the total time taken by the particle to travel from position 1 to P' or P'' (Figs. 4.2e and 4.2g). It can be determined as:

$$t_{cr} = t_u + t_r + t_{cft} \tag{A.17}$$

A.3. Cascaded Cycle Time

CASE I. When $\theta_{crf} > \theta_{crp}$

This is the case in which the light blue flight has already crossed the particle location. The particle falls at point P_i and moves down very quickly to the lowest position of the reactor (i.e., the location of the first flight at 1). At this moment, it can be assumed, because of the small inclination of the reactor, that the particle will not produce any axial displacement. Finally, the particle will reestablish the cascaded cycle with the help of the dark green flight.

The position of the flight when the particle lands on the reactor surface can be determined as:

$$\theta_{Pi} = \omega t_{Pi} \times \frac{180}{\pi} \tag{A.18}$$

Where, t_{Pi} is the total time taken by the particle to reach the position P_i and can be estimated as:

$$t_{Pi} = t_u + t_r + t_f \tag{A.19}$$

The dark green flight, therefore, has to travel though a certain angular displacement before picking up the particle, which can be estimated as:

$$\theta_{Pick} = 240 - \theta_{Pi} \tag{A.20}$$

The pick-up time (t_{pu}) can be thus determined as:

$$t_{pu} = \frac{(240 - \theta_{Pi})\,\pi}{180\omega} \tag{A.21}$$

Therefore, the total time taken by particle to complete one cascaded cycle can be estimated as:

$$t_{cas} = t_u + t_r + t_f + t_{pu} \tag{A.22}$$

$$t_{cas} = \frac{(90 + \theta)\,\pi}{180\omega} + \frac{1}{\cos\beta}\sqrt{\frac{7L_f}{10g\sin\theta\left(\frac{1}{\cos\beta} + \mu_k\right)}} + t_f + \frac{(240 - \theta_{Pi})\,\pi}{180\omega} \tag{A.23}$$

CASE II. When $\theta_{crf} < \theta_{crp}$

In this case, the light blue color flight helps to continue the cascaded cycle. The angular displacement and the pick up time can be estimated as:

$$\theta_{Pick} = 120 - \theta_{Pi} \tag{A.24}$$

$$t_{pu} = \frac{(120 - \theta_{Pi})\pi}{180\omega} \tag{A.25}$$

The cascaded time per cycle can be then estimated as:

$$t_{cas} = \frac{(90 + \theta)\pi}{180\omega} + \frac{1}{\cos\beta}\sqrt{\frac{7L_f}{10g\sin\theta\left(\frac{1}{\cos\beta} + \mu_k\right)}} + t_f + \frac{(120 - \theta_{Pi})\pi}{180\omega} \tag{A.26}$$

In Eqs. A.23 and A.26, the rolling and falling times are much smaller than the picking and uplifting times, and contribute a very small fraction (< 1%) of the total cascaded cycle time. Neglecting the rolling and falling times, we can write $\theta_f = \theta$, and $t_{Pi} \approx t_u$. This gives

$$\theta_{Pi} = \omega t_u \times \frac{180}{\pi}$$

Substituting the value of t_u from the Eq. A.3,

$$\theta_{Pi} = 90 + \theta \tag{A.27}$$

The selection of the expressions (Eqs. A.23 and A.26) for the cascaded cycle time in the two cases discussed above can also be simplified by knowing the angular displacement (θ). With a particle that has an angular displacement higher than 30°, the cascaded time per cycle can be determined using Eq. A. 23.

APPENDIX B: SUPPLEMENTARY INFORMATION FOR CHAPTER 5

B.1. Estimation of Designated Solid Filling Fraction

Assuming the steady plug flow of solids with a uniform cross-section of solid throughout the reactor length (Figure 5.2(b)), the filling factor in the designated loading condition ($y_s = L_f$) can be written (Herz et al., 2012) as:

$$F_{\text{ff, designated}} = \frac{\text{Area of cross-section of solid (Area under PQ)}}{\text{Area of cross-section of reactor (Area of circle)}} \tag{B.1}$$

$$\mathrm{F}_{ff,\ designated} = \frac{2\left(\frac{\pi D^2}{4}\frac{\emptyset_s}{360} - \frac{1}{2}\sqrt{\left(\frac{D}{2}\right)^2 - \left(\frac{D}{2} - y_s\right)^2} \times \left(\frac{D}{2} - y_s\right)\right)}{\frac{\pi D^2}{4}}$$

$$\mathrm{F}_{ff,\ designated} = \frac{2\left(\frac{\pi D^2}{4}\frac{\emptyset_s}{360} - \frac{1}{2}\sqrt{\left(\frac{D}{2}\right)^2 - \left(\frac{D}{2} - \mathrm{L}_f\right)^2} \times \left(\frac{D}{2} - \mathrm{L}_f\right)\right)}{\frac{\pi D^2}{4}}$$

$$\mathrm{F}_{ff,\ designated} = \frac{\emptyset_s}{180} - \frac{4}{\pi D^2}\sqrt{\left(\frac{D}{2}\right)^2 - \left(\frac{D}{2} - \mathrm{L}_f\right)^2} \times \left(\frac{D}{2} - \mathrm{L}_f\right)$$

$$\mathrm{F}_{ff,\ designated} = \frac{\emptyset_s}{180} - \frac{1}{\pi}\sqrt{\left(1 - \left(1 - 2\frac{\mathrm{L}_f}{D}\right)^2\right)} \times \left(1 - 2\frac{\mathrm{L}_f}{D}\right)$$

$$\mathrm{F}_{ff,\ designated} = \frac{\emptyset_s}{180} - \frac{1}{\pi}\sqrt{\left(1 - 1 + 4\frac{\mathrm{L}_f}{D} - 4\left(\frac{\mathrm{L}_f}{D}\right)^2\right)} \times \left(1 - 2\frac{\mathrm{L}_f}{D}\right)$$

$$\mathrm{F}_{ff,\ designated} = \frac{\emptyset_s}{180} - \frac{2}{\pi}\sqrt{\left(\frac{\mathrm{L}_f}{D}\left(1 - \frac{\mathrm{L}_f}{D}\right)\right)} \times \left(1 - 2\frac{\mathrm{L}_f}{D}\right)$$

$$F_{\mathrm{ff,\ designated}} = \frac{\phi_s}{180} - \frac{2}{\pi}\frac{L_f}{D}\left(1 - 2\frac{L_f}{D}\right)\sqrt{\frac{D}{L_f} - 1} \tag{B.2}$$

B.2. Estimation of Solid Coverage Fraction

From the Figure 5.4, different solid filling angles can be related geometrically and determined accordingly. Assuming the cross-sectional area of the solid remains constant throughout the operation, the cross-sectional area of the solids forming arc $P_d Q_d$ can be estimated by simple cross-sectional area balance as:

$$\frac{F_{ff}\pi D^2}{4} - \frac{1}{2}L_f L_f tan\Omega = \frac{\phi_{d2}}{360}\frac{\pi D^2}{4} - \frac{1}{2}\frac{D}{2}\sin\phi_{d2}\frac{D}{2}cos\phi_{d2} + \frac{\phi_{d1}}{360}\frac{\pi D^2}{4} - \frac{1}{2}\frac{D}{2}cos\phi_{d2}tan\phi_{d1}\frac{D}{2}cos\phi_{d2}$$

$$\frac{F_{ff}\pi D^2}{4} - \frac{1}{2}L_f L_f tan\Omega = \frac{\phi_{d2}}{360}\frac{\pi D^2}{4} - \frac{D^2}{8}\sin\phi_{d2}cos\phi_{d2} + \frac{\phi_{d1}}{360}\frac{\pi D^2}{4} - \frac{D^2}{8}cos\phi_{d2}tan\phi_{d1}cos\phi_{d2}$$

$$2F_{\mathrm{ff}}\pi - 4\left(\frac{L_f}{D}\right)^2 \tan\Omega = \frac{\pi}{180}\left(\phi_{d2} + \phi_{d1}\right) - \sin\phi_{d2}\cos\phi_{d2} - \left(\cos\phi_{d2}\right)^2 \tan\phi_{d1} \tag{B.3}$$

This expression is valid for a certain range of the critical solid filling fraction. The lower critical solid filling fraction is defined as the case when the entire solid in the reactor remains on the flight surface before the end of the cascaded cycle (no solids under arc $P_d Q_d$). The solid filling fraction at such condition can be determined as:

$$\frac{F_{ff,cr,lo}\pi D^2}{4} - \frac{1}{2} L_f L_f tan\Omega = 0$$

$$F_{ff,\,cf,\,lo} = \frac{2}{\pi}\left(\frac{L_f}{D}\right)^2 \tan\Omega \qquad \text{(B.4)}$$

This indicates that the lower critical solid filling fraction depends only on the geometric features and properties of the bed (brass particles) materials. For a design with $L_f/D = 0.25$, and $\Omega = 6.25$, the lower critical solid filling fraction is $F_{ff,cr,lo} = 0.0044$. Similarly, the upper critical value of the solid filling fractions, which is defined as the case at which the amount of solid just balances one side of the flight (Figure 5.2(b)). The upper critical value of the solid filling fraction is, therefore, considered to be 50% of the total designated loading size. This leads to the upper solid filling fraction of 0.098 (9.8%).

From the Figure 5.4 (a), it is also clear that the angle ϕ_{d1} depends only on the flight position. As the angle between two flights is $120°$ and the flight travels angle θ_1 with horizontal line before particles drop back to the reactor, the angle ϕ_{d1} can, therefore, be expressed as:

$$\phi_{d1} = 120 - 90 - \theta_1$$

$$\phi_{d1} = 30 - \theta_1 \qquad \text{(B.5)}$$

The filling angle ϕ_{d2}, however, depends on the amount of solid inside the reactor and their properties. For the brass particles with $\theta_1 = 6.25°$, the variation of the filling angle ϕ_{d2} with the solid filling fraction can be calculated using the Eq. (B.3) and represented graphically as shown in Figure B.1. The curve can also be fitted as:

$$\phi_{d2} = 139.56 F_{ff}^{0.449} \tag{B.6}$$

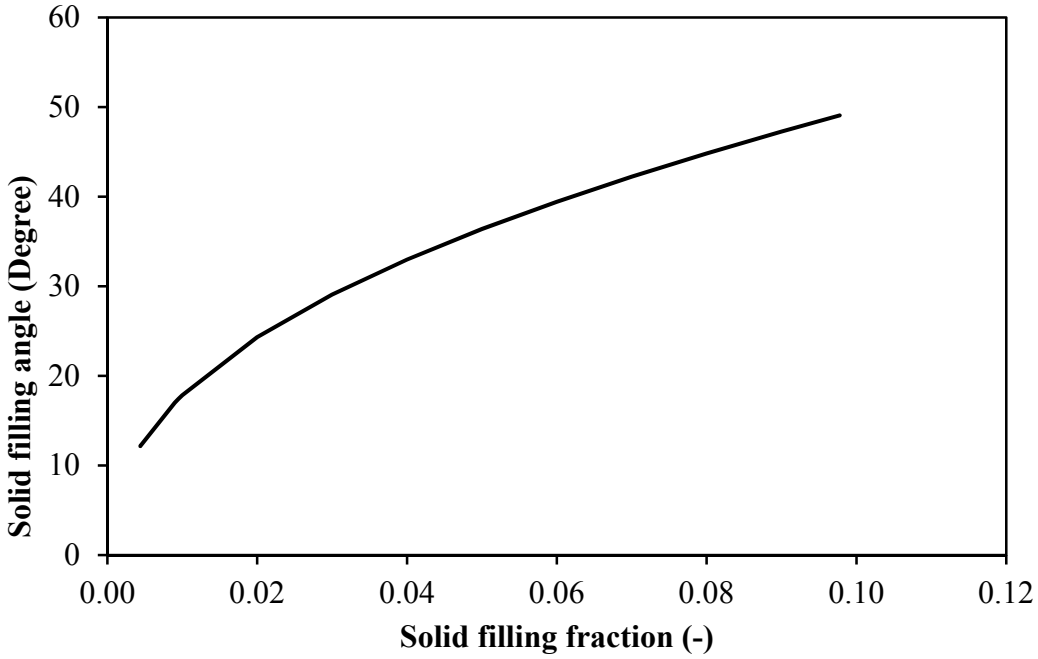

Figure B.1 Variation of the solid filling angle (ϕ_{d2}) with the solid filling fraction

This leads to the expression for the total solid filling angle as a function of property of solid and the solid filling fraction as:

$$\phi_d = 23.75 + 139.56 F_{ff}^{0.449} \tag{B.7}$$

To determine the arc XY formed by the solids at the flight surface, Figure 5.4(a) can be used. In a right angled triangle ΔXYZ,

$$XY = L_f tan\Omega$$

In triangle ΔXYO, the cosine law gives,

$$\cos\theta_2 = \frac{OX^2 + OY^2 - XY^2}{2\,OX\,OY}$$

$$\cos\theta_2 = \frac{\frac{D^2}{4} + \frac{D^2}{4} - {L_f}^2(tan\Omega)^2}{2\frac{D}{2}\frac{D}{2}}$$

$$\cos\theta_2 = 1 - 2\left(\frac{L_f}{D}\right)^2 \left(\tan\Omega\right)^2 \tag{B.8}$$

APPENDIX C: SUPPLEMENTARY INFORMATION FOR CHAPTER 6

C.1. Methodology for the Energy Balance

All the equations involved in analyzing the energy balance of the overall system are presented below:

The rate of energy entering into the system through the solid biomass (dry basis) can be estimated as:

$$\dot{Q}_{in} = HHV_{rd}\,\dot{m}_{rd} \tag{C.2}$$

The rate of energy leaving the system through the torrefied biomass can be determined as:

$$\dot{Q}_{out} = HHV_{td}\,\dot{m}_{td} \tag{C.3}$$

The total heat load (THL) is the sum of the drying and devolatilization heat loads. Drying heat load is the sum of the sensible heat required ($\dot{Q}_{sen-D}$) to heat biomass to the particle exit temperature in the dryer and the rate of heat available in steam leaving dryer ($\dot{Q}_{steam-D}$).

$$\dot{Q}_{sen-D} = \dot{m}_{rd}\,C_{pdb}\left(T_{ex-D} - T_{in-D}\right) \tag{C.4}$$

$$\dot{Q}_{steam-D} = M_C\,\dot{m}_{rd}\left(h_{ex-D} - h_{in-D}\right) \tag{C.5}$$

Where, $\dot{m_{rd}}$ is the mass flow rate of biomass in dry basis, C_{pdb} is the specific heat capacity of dried biomass, T_{ex-D} is the biomass temperature at dryer exit, T_{in-D} is the biomass temperature at dryer inlet, M_c is the moisture content of the raw biomass in (%) dry basis, h_{ex-D} is the enthalpy of steam leaving dryer, and h_{in-D} is the enthalpy of the moisture at the inlet temperature of the dryer.

Devolatilization heat load is the sum of the sensible heat required ($\dot{Q}_{sen-T}$) to heat the dried biomass to the particle exit temperature in the torrefier and the heat of torrefaction ($\dot{Q}_{torr-T}$) (heat of endothermic reactions).

$$\dot{Q}_{sen-T} = \dot{m}_{avg}\, C_{pavg} \left(T_{ex-T} - T_{ex-D}\right) \tag{C.6}$$

$$\dot{Q}_{torr-T} = \dot{m}_{td}\, HT_{endo} \tag{C.7}$$

Where, $\dot{m_{avg}}$ is the average mass flow rate in the torrefier, C_{pavg} is the average specific heat capacity of dried and torrefied biomass, and HT_{endo} is the heat of torrefaction.

$$\dot{m_{avg}} = \frac{\dot{m_{rd}} + \dot{m}_{td}}{2}$$

$$C_{pavg} = \frac{C_{pdb} + C_{ptb}}{2}$$

Therefore, the total heat load can be estimated as:

$$THL = \dot{Q}_{sen-D} + \dot{Q}_{steam-D} + \dot{Q}_{sen-T} + \dot{Q}_{torr-T} \tag{C.8}$$

The total available process heat (TAP) is the sum of the heat available in the superheated steam ($\dot{Q}_{sup-steam}$), the heat of combustion of the volatile gases ($\dot{Q}_{comb-vol}$), and the sensible heat of the hot torrefied solid ($\dot{Q}_{sen-tor}$).

The heat available in the superheated steam (only above saturated steam) coming out from the dryer can be estimated as:

$$\dot{Q}_{\text{sup}-steam} = M_C \dot{m}_{rd} \left(h_{ex-D} - h_g \right) \tag{C.9}$$

Where, h_g is the enthalpy of the saturated steam. The heat of combustion of the volatile gases ($\dot{Q}_{comb-vol}$) can be estimated as:

$$\dot{Q}_{comb-vol} = \left(\dot{m}_{rd} - \dot{m}_{td} \right) H_{comb-vol} \tag{C.10}$$

Where, $H_{comb-vol}$ is the heat of combustion of the volatile gases released from the torrefier. The sensible heat in the hot torrefied solid ($\dot{Q}_{sen-tor}$) can be expressed as:

$$\dot{Q}_{sen-torr} = \dot{m}_{td} C_{ptb} \left(T_{ex-T} - T_{in-D} \right) \tag{C.11}$$

The specific heat capacity of the torrefied biomass estimated as the average specific heat capacity of dry wood and the specific heat capacity of char. The specific heat capacity dried biomass (J/kgK) was calculated average particle temperature (in Kelvin) using following expression (Ragland et al., 1991):

$$C_{pdb} = 103.1 + 3.867T$$

No literatures so far have been published to estimate the specific heat capacities of torrefied biomass, this study, therefore, assumed that the specific heat capacity of torrefied biomass is the average of specific heat capacity of dried biomass and the specific heat capacity of the char. The specific heat capacity of the char (J/kgK) at the particle temperature at the torrefier exit (in Kelvin) was estimated using the expression (Ragland et al., 1991):

$$C_{pc} = 1390 + 0.36T$$

Therefore, the average specific heat capacity of torrefied biomass can be estimated as:

$$C_{ptb} = \frac{C_{pdb} + C_{pc}}{2}$$

The total available process heat can be estimated as:

$$TAP = \dot{Q}_{\sup-steam} + \dot{Q}_{comb-vol} + \dot{Q}_{sen-torr} \quad \text{(C.12)}$$

Combining Equations C.2, C.3, C.8, and C.12, the system efficiency and net system efficiency can be determined.

APPENDIX D: COPYRIGHT PERMISSION LETTERS

D.1. Chapter 2: A Comprehensive Review on Biomass Torrefaction

May 25, 2015

Daya Ram Nhuchhen
Mechanical Engineering,
Dalhousie University, Morris Street,
Halifax, Canada

Dear Daya Ram Nhuchhen,

This is to let you know that your article entitled "A Comprehensive Review on Biomass Torrefaction," has been accepted for publication at "International Journal of Renewable Energy & Biofuels," Published by IBIMA Publishing, USA, The article was published on April 2014.

The article is published under Distributed under Creative Commons CC-BY 3.0, which mean authors retain copyright of the article as their intellectual property.

Sincerely

Managing Editor
IBIMA publishing

D.2. Chapter 3: Experimental Investigation of Mildly Pressurized Torrefaction in Air and Nitrogen

1/8/2016 Rightslink® by Copyright Clearance Center

Copyright Clearance Center RightsLink® Home Create Account Help Live Chat

ACS Publications Most Trusted. Most Cited. Most Read.

Title: Experimental Investigation of Mildly Pressurized Torrefaction in Air and Nitrogen
Author: Daya Ram Nhuchhen, Prabir Basu
Publication: Energy & Fuels
Publisher: American Chemical Society
Date: May 1, 2014
Copyright © 2014, American Chemical Society

LOGIN
If you're a copyright.com user, you can login to RightsLink using your copyright.com credentials. Already a RightsLink user or want to learn more?

Quick Price Estimate

Permission for this particular request is granted for print and electronic formats, and translations, at no charge. Figures and tables may be modified. Appropriate credit should be given. Please print this page for your records and provide a copy to your publisher. Requests for up to 4 figures require only this record. Five or more figures will generate a printout of additional terms and conditions. Appropriate credit should read: "Reprinted with permission from {COMPLETE REFERENCE CITATION}. Copyright {YEAR} American Chemical Society." Insert appropriate information in place of the capitalized words.

I would like to... reuse in a Thesis/Dissertation
Requestor Type Author (original work)
Portion Full article
Format Print
Will you be translating? No
Select your currency USD - $
Quick Price Click Quick Price

QUICK PRICE CONTINUE

This service provides permission for reuse only. If you do not have a copy of the article you are using, you may copy and paste the content and reuse according to the terms of your agreement. Please be advised that obtaining the content you license is a separate transaction not involving Rightslink.

To request permission for a type of use not listed, please contact the publisher directly.

Copyright © 2016 Copyright Clearance Center, Inc. All Rights Reserved. Privacy statement. Terms and Conditions.
Comments? We would like to hear from you. E-mail us at customercare@copyright.com

D.3. Chapter 6: Torrefaction of Poplar in a Continuous Two-stage Indirectly, Heated Rotary Torrefier

Rightslink® by Copyright Clearance Center 2016-01-26, 6:12 AM

Copyright Clearance Center RightsLink® Home Create Account Help Live Chat

ACS Publications Most Trusted. Most Cited. Most Read.

Title: Torrefaction of Poplar in a Continuous Two-Stage, Indirectly Heated Rotary Torrefier

Author: Daya Ram Nhuchhen, Prabir Basu, Bishnu Acharya

Publication: Energy & Fuels

Publisher: American Chemical Society

Date: Jan 1, 2016

Copyright © 2016, American Chemical Society

LOGIN

If you're a copyright.com user, you can login to RightsLink using your copyright.com credentials. Already a RightsLink user or want to learn more?

Quick Price Estimate

Permission for this particular request is granted for print and electronic formats, and translations, at no charge. Figures and tables may be modified. Appropriate credit should be given. Please print this page for your records and provide a copy to your publisher. Requests for up to 4 figures require only this record. Five or more figures will generate a printout of additional terms and conditions. Appropriate credit should read: "Reprinted with permission from {COMPLETE REFERENCE CITATION}. Copyright {YEAR} American Chemical Society." Insert appropriate information in place of the capitalized words.

I would like to... reuse in a Thesis/Dissertation

Requestor Type Author (original work)

Portion Full article

Format Print and Electronic

Will you be translating? No

Select your currency USD - $

Quick Price Click Quick Price

QUICK PRICE CONTINUE

This service provides permission for reuse only. If you do not have a copy of the article you are using, you may copy and paste the content and reuse according to the terms of your agreement. Please be advised that obtaining the content you license is a separate transaction not involving Rightslink.

To request permission for a type of use not listed, please contact the publisher directly.

APPENDIX E: PHOTOGRAPHS

E.1. Pressurized Batch Reactor

E.2. Bomb Calorimeter: Parr 6100

E.3. Muffle Furnace

E.4. Ultimate Analyzer: EA 1110

E.5. SRI 8610C Gas Chromatograph

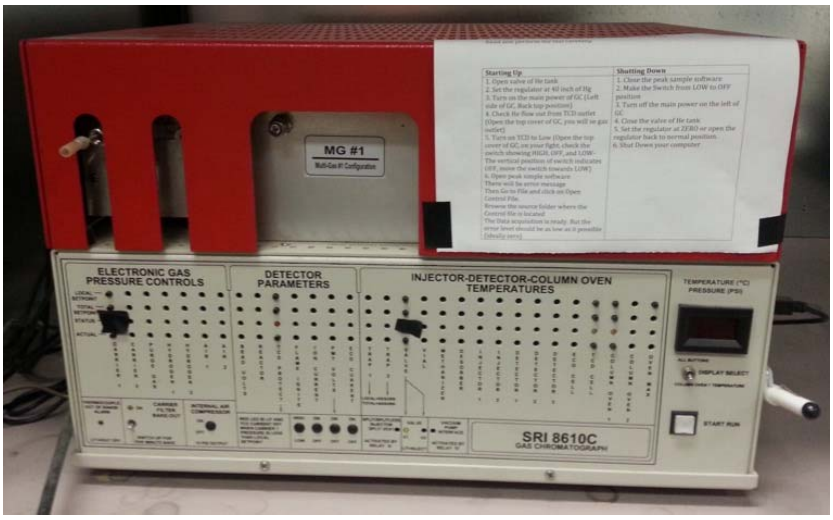

E.6. Two-Stage Continuous Indirectly Heated Inclined Rotary Reactor

E.7. Continuous Two-Stage Indirectly Heated Rotary Torrefier: Dryer Section

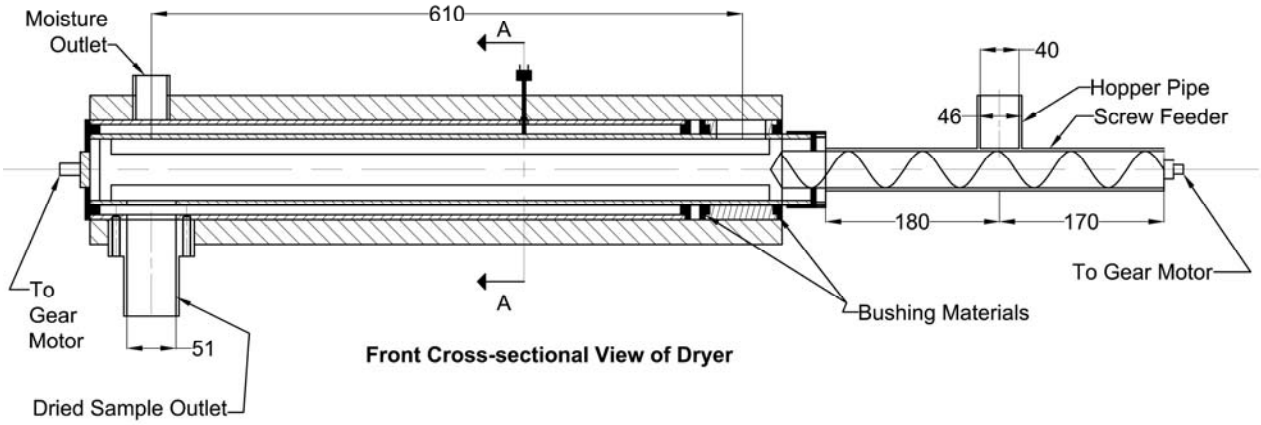

Front Cross-sectional View of Dryer

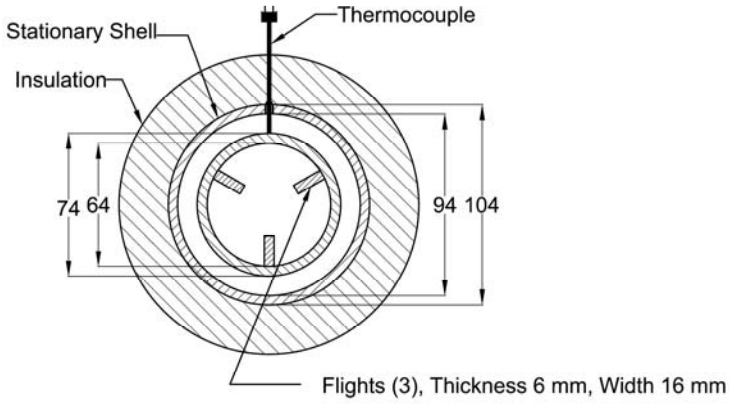

Section A-A

E.8. Continuous Two-Stage Indirectly Heated Rotary Torrefier: Torrefier Section

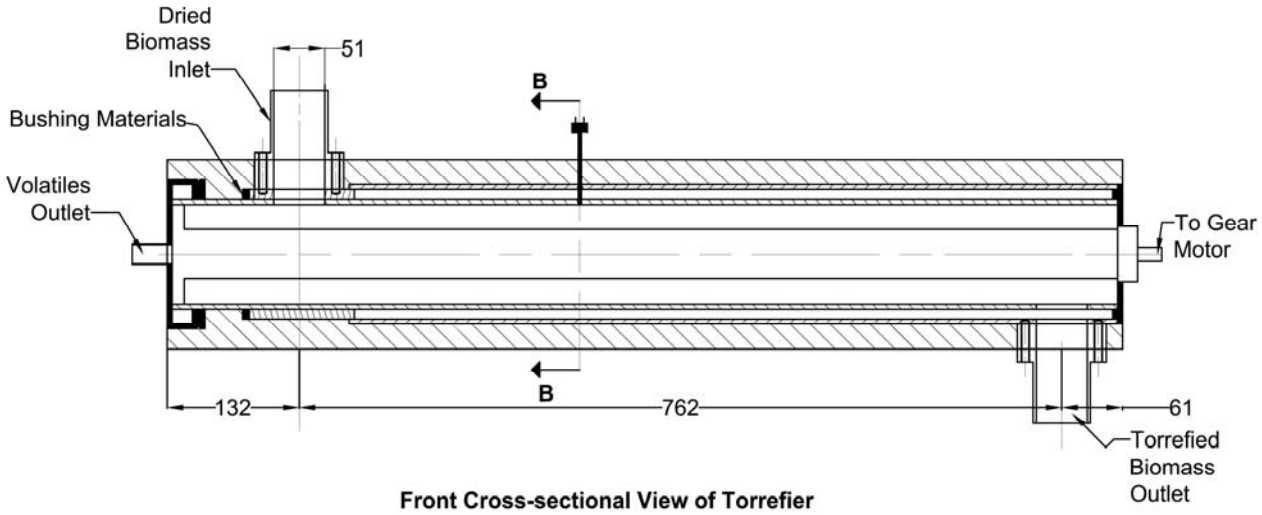

Front Cross-sectional View of Torrefier

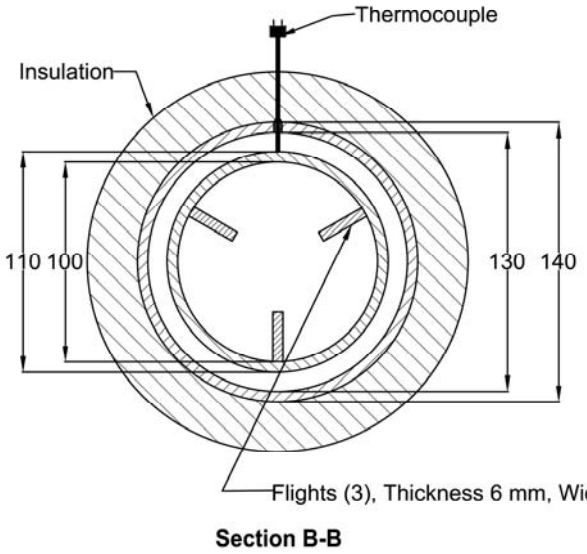

Section B-B

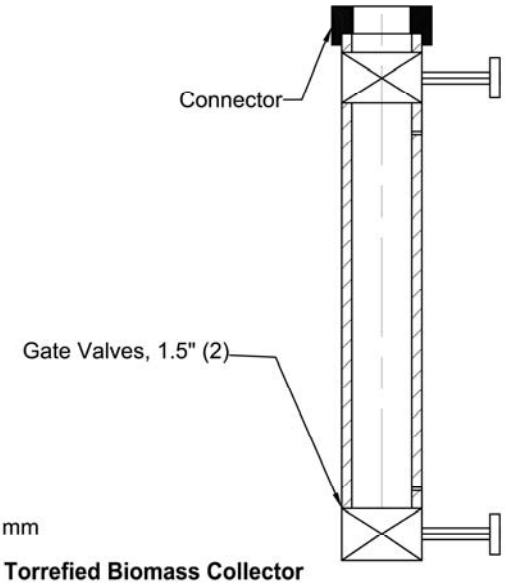

Torrefied Biomass Collector

E.9. Muffle Furnace Reactor

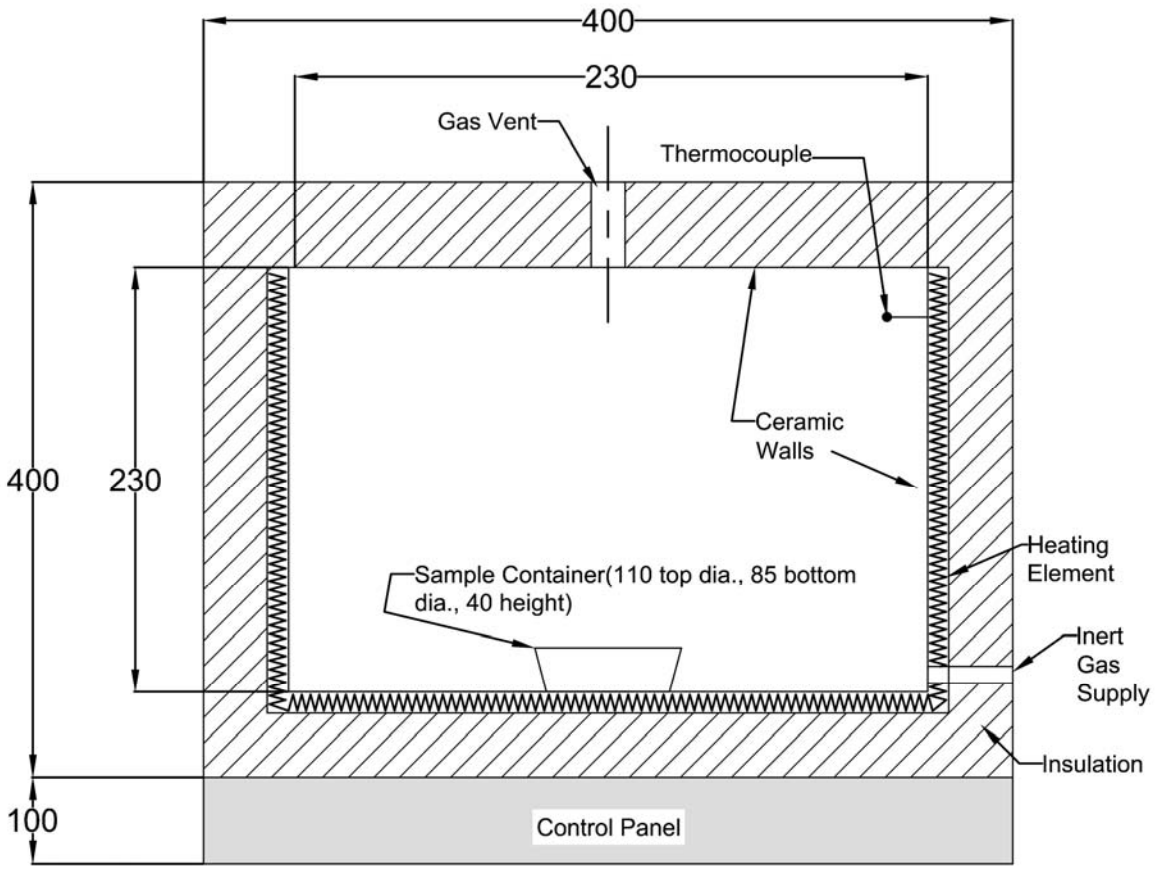

APPENDIX F: REPEATABILITY TESTS RESULTS

In the following sections, repeatability tests of experimental studies for different works of this study are presented.

F.1. Mildly Pressurized Reactor

Table III.1: Repeatability tests on the proximate analyses

Raw poplar	Test 1	Test 2	Absolute % error
Empty Crucible (g)	19.7820	21.5928	
Crucible with sample (g)	20.8082	22.6399	
Crucible wt after 105 °C (g)	20.7595	22.5909	
Crucible wt after 950 °C (g)	19.8834	21.7012	
Crucible wt after 750 °C (g)	19.7831	21.5939	
Wet sample wt (g)	1.0262	1.0471	
Dry sample wt (g)	0.9775	0.9981	
Moisture wet basis (g)	0.0487	0.0490	
Volatiles (g)	0.8761	0.8897	
Ash (g)	0.0011	0.0011	
Moisture content (%, AR)	4.75	4.68	1.39
Volatile matter content (%, AR)	85.37	84.97	0.47
Ash content (%, AR)	0.11	0.10	2.89
Fixed carbon content (%, AR)	9.77	10.25	4.85

Table F.2: Repeatability tests and process parameters (dry and ash free basis, daf) at 300°C and 600kPa in Air and N_2 media

Medium	Air			N_2		
Parameters	Test 1	Test 2	Absolute % error	Test 1	Test 2	Absolute % error
VM (%, daf)	51.11	50.12	1.47	58.54	59.42	1.50
FC (%, daf)	48.89	49.65	2.17	41.46	40.58	2.12
FR	0.957	0.991	3.55	0.708	0.683	3.58
HHV (%, daf)	27.12	26.96	0.61	26.00	26.16	0.61
EDEF	1.40	1.39	0.57	1.34	1.35	0.61
MY (%, daf)	49.08	48.55	1.07	55.55	54.13	2.55
EY (%, daf)	68.51	67.38	1.64	74.33	72.88	1.95

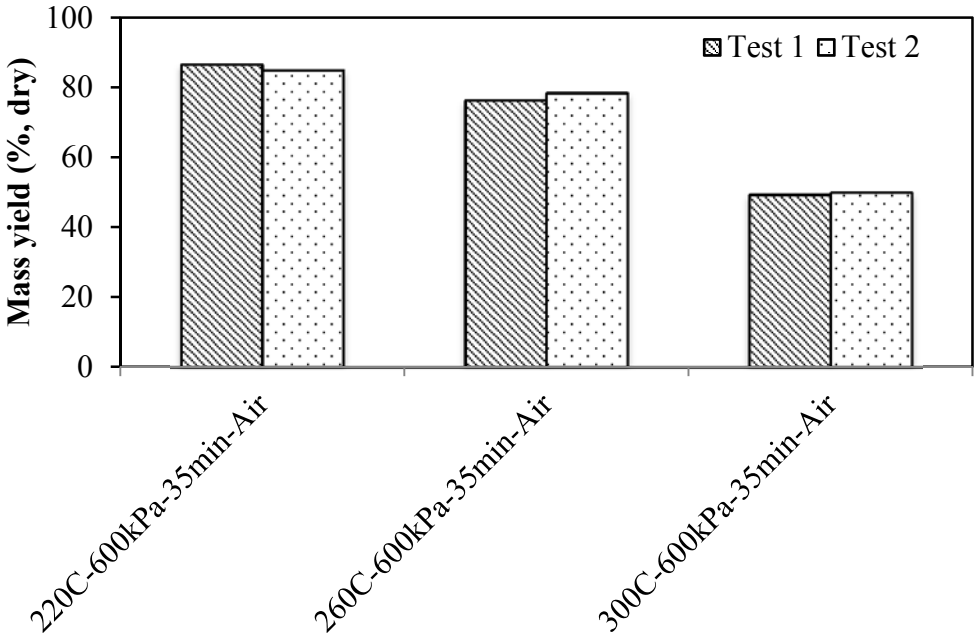

(a)

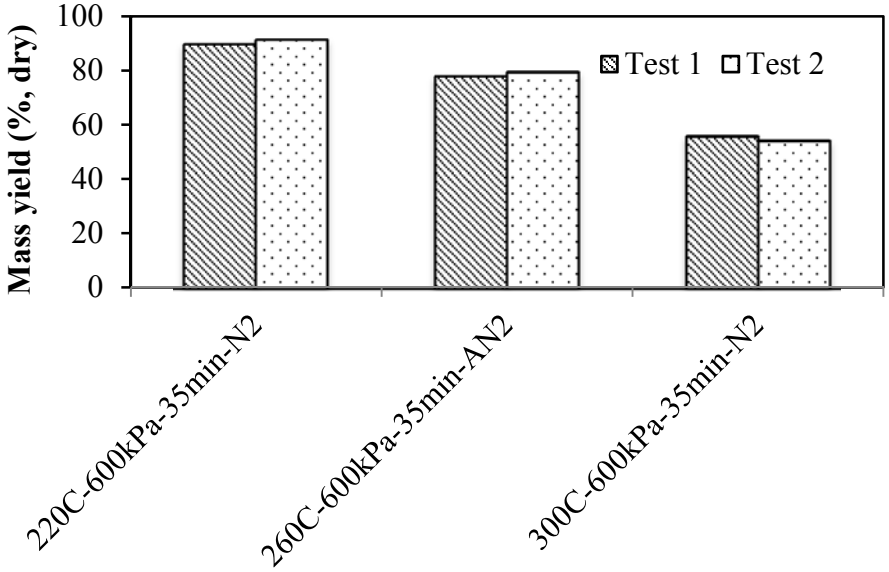

(b)

Figure F.1: Repeatability tests at 300°C and 600 kPa for mass yields (%, dry): (a) air medium; and (b) Nitrogen medium

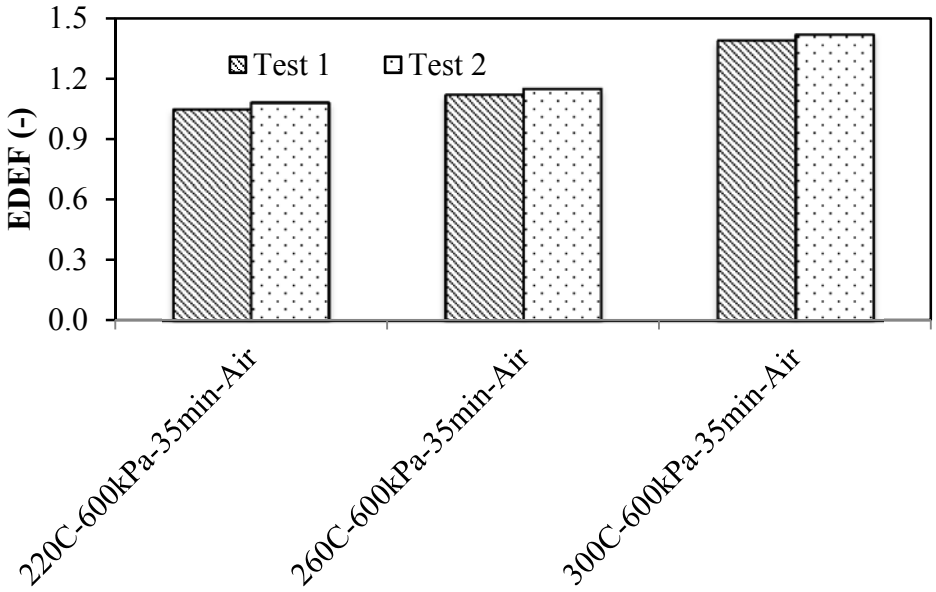

(a)

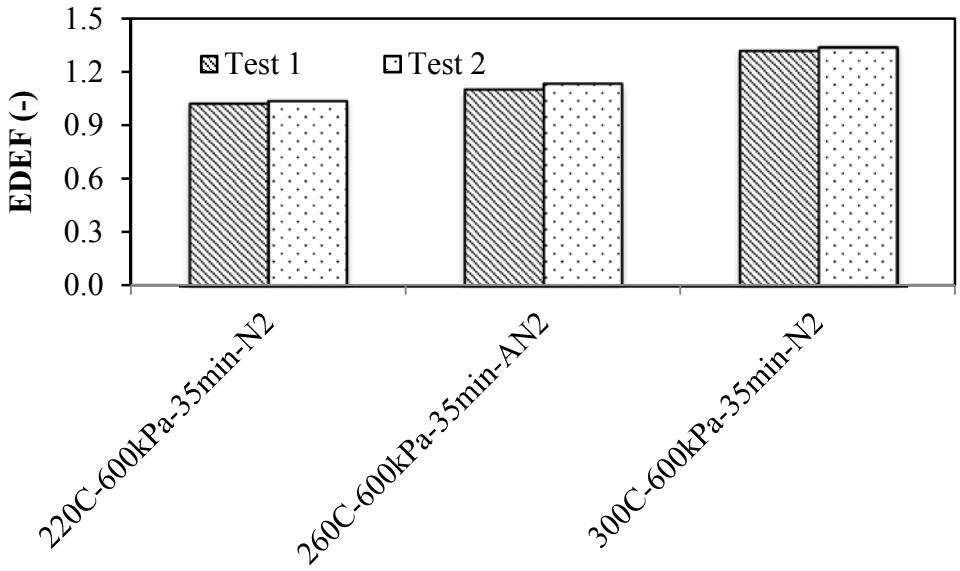

(b)

Figure F.2: Repeatability tests at 300°C and 600 kPa for energy density enhancement factor: (a) Air medium; and (b) Nitrogen medium

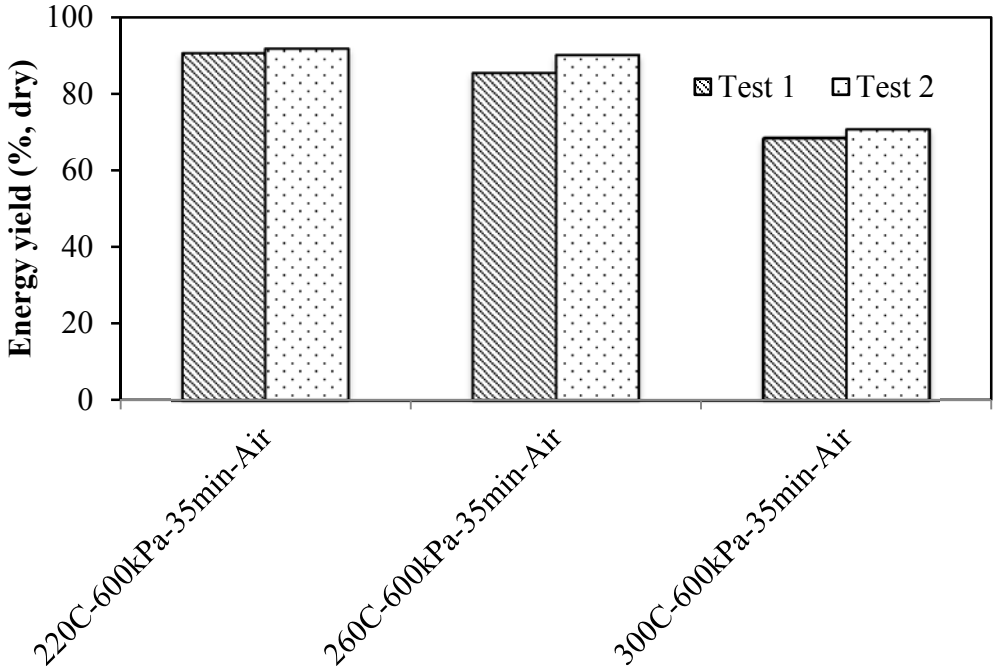

(a)

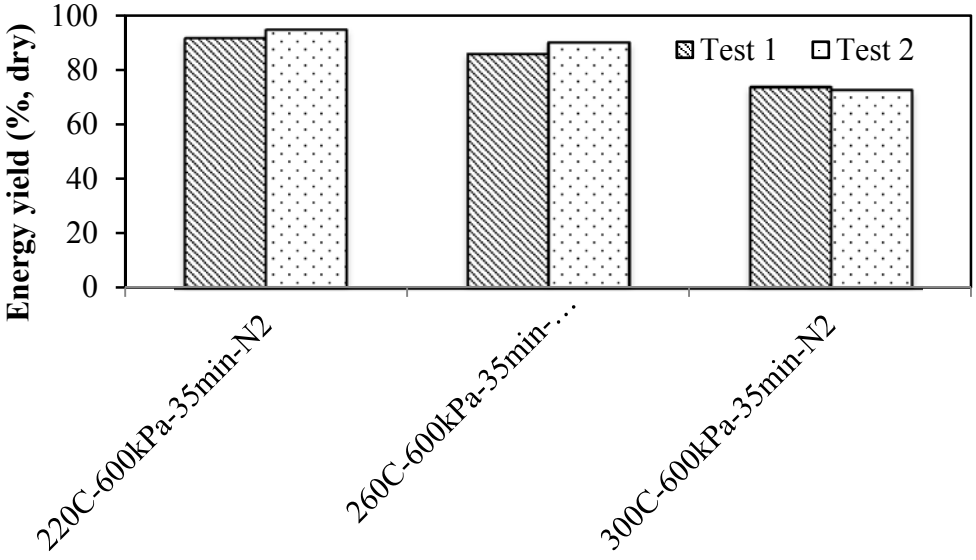

(b)

Figure F.3: Repeatability tests at 300°C and 600 kPa for energy yield (% dry): (a) Air medium; and (b) Nitrogen medium

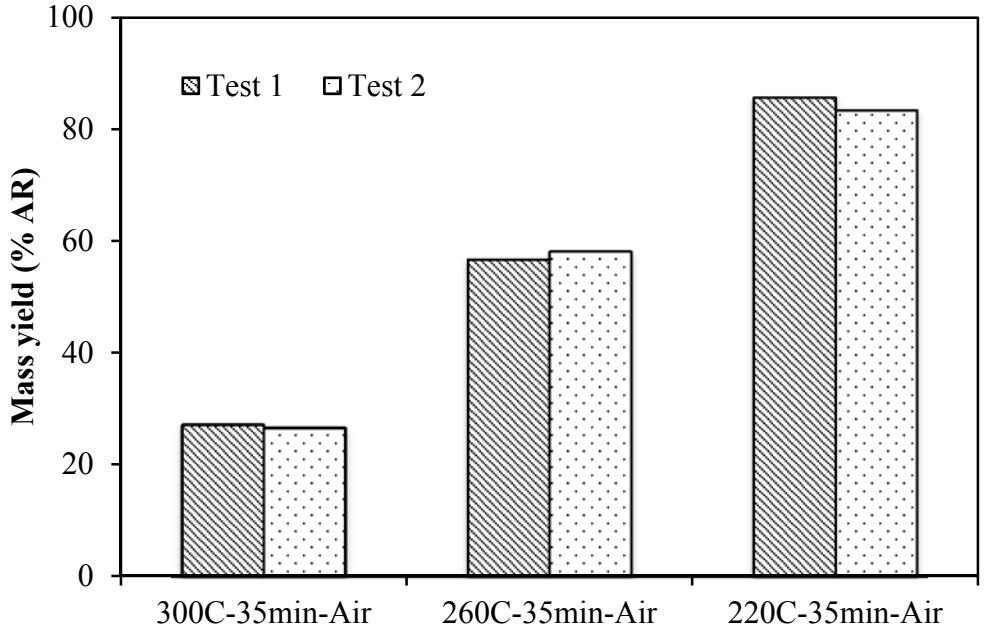

(a)

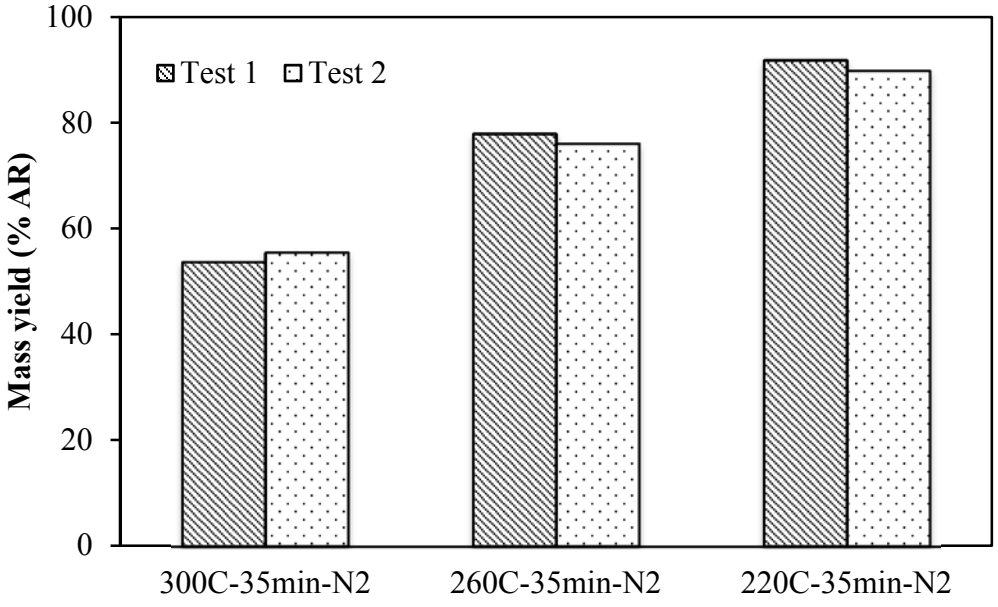

(b)

Figure F.4: Repeatability tests for mass yield at atmospheric pressure condition (% as received basis): (a) Air medium; and (b) Nitrogen medium.

F.2. Mean Residence Time and Filling Factor in Rotary Reactor

Table F.3: Repeatability tests for measuring mean residence time

RPM-Inclination-Reactor	Test 1	Test 2	Absolute % Error
4-1-D	27.49	28.72	4.48
6-3-D	8.00	8.46	5.75
8-3-D	5.75	5.45	5.32
6-1-D	19.81	19.22	2.94
6-2-D	11.15	10.52	5.65
5-1-D	23.14	22.62	2.28
4-1-T	21.36	20.11	5.85
6-3-T	6.48	6.19	4.44
8-3-T	4.72	4.58	2.93
6-1-T	15.07	14.26	5.35
6-2-T	8.08	7.81	3.30
5-1-T	17.51	16.91	3.43

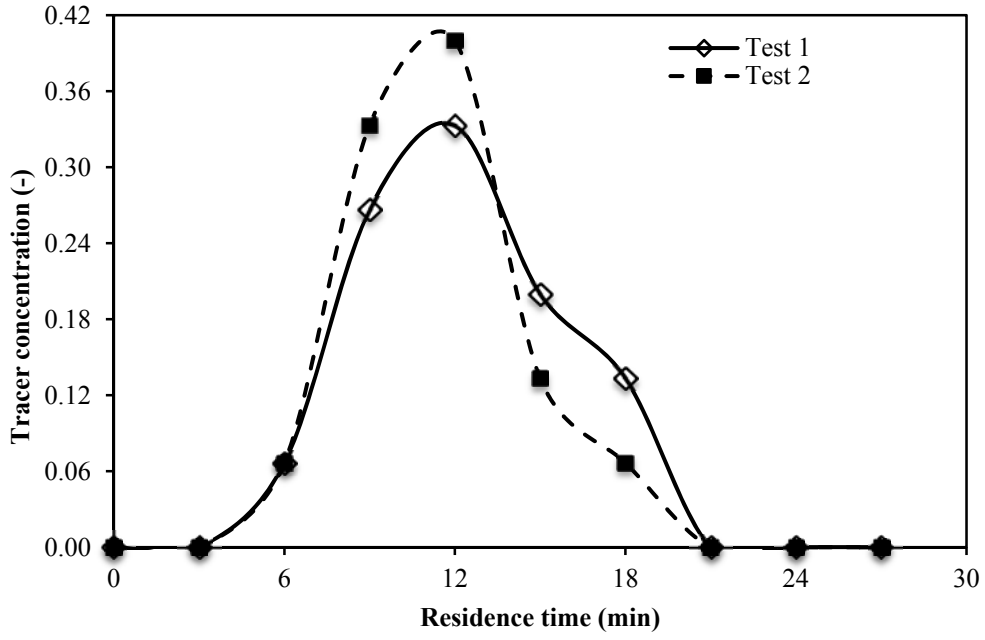

Figure F.5: Repeatability tests of tracer concentration distribution in the rotary dryer (absolute % error for the calculated average residence time =3.08%)

F.3. Overall Heat Transfer Coefficient of Rotary Reactor

Table F.4: Repeatability tests at selected operating conditions for estimating the overall heat transfer coefficient in dryer

Temperature-RPM-Inclination	Test 1	Test 2	Absolute % error
150C-4RPM-1D	17.71	18.64	5.29
150C-4RPM-2D	15.44	16.11	4.34
205C-4RPM-1D	19.03	19.64	3.18
205C-4RPM-2D	16.66	17.30	3.87
260C-4RPM-1D	20.91	19.64	6.09
260C-4RPM-2D	17.80	18.63	4.65
150C-5RPM-1D	16.83	18.18	7.98
150C-5RPM-2D	14.60	14.95	2.39
205C-5RPM-1D	18.15	19.24	5.99
205C-5RPM-2D	15.50	14.83	4.29
260C-5RPM-1D	19.35	20.20	4.37
260C-5RPM-2D	16.47	16.10	2.24
150C-6RPM-1D	16.11	16.89	4.84
205C-6RPM-1D	17.33	18.36	5.94
260C-6RPM-1D	18.29	16.84	7.93

Table F.5: Repeatability tests at selected operating conditions for estimating the overall heat transfer coefficient in torrefier

Temperature-RPM-Inclination	Test 1	Test 2	Absolute % error
260C-4RPM-1D	15.54	16.05	3.25
260C-4RPM-2D	13.80	13.97	1.20
300C-4RPM-1D	16.02	16.49	2.92
300C-4RPM-2D	14.24	14.49	1.76
340C-4RPM-1D	16.81	16.12	4.12
340C-4RPM-2D	15.05	15.57	3.44
260C-5RPM-1D	14.58	14.00	4.04
260C-5RPM-2D	13.20	13.23	0.29
300C-5RPM-1D	15.15	14.53	4.06
300C-5RPM-2D	13.67	13.08	4.27
340C-5RPM-1D	15.97	15.17	5.04
340C-5RPM-2D	14.25	15.17	6.42
260C-6RPM-1D	14.09	13.59	3.58
300C-6RPM-1D	14.74	13.63	7.54
340C-6RPM-1D	15.42	14.85	3.71

F.4. Solid Product Characterization of Torrefied Poplar in Rotary Reactor

Table F.6: Test results of proximate analyses of raw sample at different period of time (MC-Moisture content; VM-Volatile content; ASH-Ash content; and FC-Fixed carbon content)

Test	MC (%, AR)	VM (%, dry)	ASH (%, dry)	FC (%, dry)
15-Jan-14	4.36	87.98	0.29	11.73
22-Mar-14	4.45	87.04	0.23	12.73
17-Jun-14	4.56	88.02	0.30	11.68
22-Feb-15	4.59	88.61	0.21	11.18
15-Mar-15	4.27	88.45	0.26	11.30
22-May-15	4.47	86.85	0.19	12.96
05-Jun-15	4.38	87.79	0.11	12.10
Average	4.44	87.82	0.23	11.95
Standard deviation	0.11	0.61	0.06	0.63

Table F.7: Repeatability tests biomass torrefaction at selected operating conditions of torrefier (absolute % error)

Parameter	260C-4RPM-1D			290C-4RPM-1D			320C-4RPM-1D		
	Test 1	Test 2	% Error	Test 1	Test 2	% Error	Test 1	Test 2	% Error
Volatile content (%, daf)	86.74	88.18	1.66	81.95	80.76	1.46	75.66	74.07	2.11
Fixed carbon (%, daf)	13.26	11.83	10.76	18.00	19.19	6.58	24.23	25.81	6.52
Fuel ratio (-)	0.15	0.13	12.22	0.22	0.24	8.15	0.32	0.35	8.82
Energy density enhancement (%)	5.04	4.89	2.91	13.11	13.26	1.14	21.74	21.59	0.71
Mass yield (%, daf)	92.34	90.65	1.83	85.94	87.93	2.31	80.19	81.25	1.32
Energy yield (%, daf)	96.99	95.08	1.97	97.21	99.59	2.45	97.62	98.79	1.20
Carbon content (%, daf)	48.18	48.58	0.83	50.09	49.44	1.30	53.47	54.06	1.11
Nitrogen (%, daf)	0.45	0.46	2.62	0.45	0.47	2.31	0.44	0.43	2.24
Hydrogen (%, daf)	5.87	5.98	1.77	5.52	5.55	0.54	5.48	5.58	1.91
Oxygen (%, daf)	45.49	44.98	1.13	43.94	44.55	1.39	40.62	39.93	1.70

APPENDIX G: UNCERTAINTY ANALYSIS

Following instruments were used for the measurement and their measurement errors are:

1. Analytical Balance (1), Δm_1 = 0.0001 gm
2. Analytical Balance (2), Δm_2 = 0.00001 gm
3. Stopwatch, Δt = 0.01 sec
4. Length, ΔL = 1 mm
5. Diameter, ΔD = 0.01 mm
6. Thermocouple, ΔT = 1ºC
7. Bomb Calorimeter, (Parr 6100), $\Delta \mathrm{HHV}/\mathrm{HHV}$ = 0.002 (0.2%)

Table G.1: Procedure to calculate uncertainty errors (*D*=dependent parameter, *A* and *B*=independent parameters, *n*=power constant)

SN	Relation, $Z = f(A, B)$	Relation, $\Delta Z = f(\Delta A, \Delta B)$
1	$Z = A + B$	$\Delta Z^2 = \Delta A^2 + \Delta B^2$
2	$Z = A - B$	$\Delta Z^2 = \Delta A^2 + \Delta B^2$
3	$Z = A \times B$	$\left(\frac{\Delta Z}{Z}\right)^2 = \left(\frac{\Delta A}{A}\right)^2 + \left(\frac{\Delta B}{B}\right)^2$
4	$Z = A/\mathrm{B}$	$\left(\frac{\Delta Z}{Z}\right)^2 = \left(\frac{\Delta A}{A}\right)^2 + \left(\frac{\Delta B}{B}\right)^2$
5	$Z = A^n$	$\frac{\Delta Z}{Z} = n\frac{\Delta A}{A}$
6	$Z = e^A$	$\frac{\Delta Z}{Z} = \Delta A$

Results of uncertainty analysis are presented below:

Table G.2: Measurement errors

SN	Parameter	Errors
1	Proximate analysis	
	Moisture content	±0.21%
	Volatile matter content	±0.02%
	Ash content	±9.09%[a]
	Fixed carbon content	±0.19%
2	Biomas mass flow rate (BFR = mass/time), $\Delta BFR/BFR$	±0.83%
3	Rate of energy entering/leaving to the TIR $d\dot{Q}/\dot{Q}$	±0.86%
4	Mass yield, $\Delta MY/MY$	±1.18%
5	Energy density enhancement factor, , $\Delta EDEF/EDEF$	±0.28%
6	Energy yield, $\Delta EY/EY$	±1.21%

Note: [a] High measurement error is due to a very small ash content in the used biomass